Palaeoclimatic and palaeoceanographic studies on the sediment cores of the northwestern continental margin of India

Thesis submitted for the Degree of

Doctor of Philosophy

in

Marine Sciences

to the

Goa University

by

Anil Kumar A
Department of Marine Sciences
Goa University

Work carried out at:

National Institute of Oceanography, Dona Paula, Goa

October 2005

To my Parents

STATEMENT

As required under the University ordinance 0.19.8 (vi), I state that the present thesis entitled **"Palaeoclimatic and palaeoceanographic studies on the sediment cores of the northwestern continental margin of India"** is original contribution and the same has not been submitted on any previous occasion. To the best of my knowledge, the present study is the first of its kind for the area mentioned.

The literature related to the problem investigated has been cited. Due acknowledgement have been made whenever facilities and suggestions have been availed of.

Anil Kumar A.

CERTIFICATE

This is to certify that the thesis entitled **"Palaeoclimatic and palaeoceanographic studies on the sediment cores of the northwestern continental margin of India"**, submitted by **Mr. Anil Kumar A.** for the award of the degree of Doctor of Philosophy in Marine Sciences is based on his original studies carried out by him under my supervision. The thesis or any part thereof has not been previously submitted for any other degree or diploma in any universities or institution.

V. Purnachandra Rao

Place: Dona Paula
Date: 19-10-05

Dr. V. Purnachandra Rao, F. A. Sc

Research Guide
Geological Oceanography Division
National Institute of Oceanography
Dona Paula, Goa – 403 004.

All the corrections suggested by the examiners have been incorporated.

17/01/2007.

R. SHANKAR
External Examiner.

CONTENTS

LIST OF TABLES

LIST OF FIGURES

Synopsis

Arabian Sea is a semi- enclosed basin surrounded by landmasses to the north, east and west and characterized by seasonal reversal of circulation patterns in response to the strong seasonal monsoon wind patterns. The reversal of monsoonal winds results in large seasonal variations in physics, chemistry and biology of the seas and transportation of terrigenous material onto the continental margins and deep seas. The terrigenous sediments on the continental margins are the ultimate products of weathering and erosion of rocks and denudational processes controlled by climatic conditions on land and transported by fluvial and/or aeolian processes. On the other hand, seasonal changes in monsoons induce variations in upwelling and related productivity and a stable and permanent oxygen minimum zone at intermediate depths, impinging the continental margins. As a consequence, a variety of organic-rich, biogenic and chemogenic sediment components are deposited on the sea floor, either as distinct facies or intermixed with terrigenous sediments. The sediments thus deposited on the continental margins act as an ideal archive to better understand the past variations in climate and oceanography.

The surficial sediments of the northwestern margin of India exhibit distinct lateral variations. The inner continental shelf is characterized by predominant terrigenous sediments and outer shelf by relict sandy sediments. The continental slope consists of a mixture of terrigenous and biogenous sediment components, including lime muds. The gravity cores recovered at depths between 31 and 1900 m from the northwestern margin of India were investigated. The objectives of the present study are to (a) trace the climatic history and provenance of sediments during the late Quaternary, (b) resolve the issues related to the genesis of late Quaternary lime muds and influence of sea level changes and neo-tectonic activity on its distribution and 3) report the sources of organic

carbon (OC), productivity changes and factors controlling OC distribution during the late Quaternary.

In order to achieve the objectives, multi-proxy data were generated on the sediments of the gravity cores. The proxies investigated include detailed analyses of rock-magnetic parameters for magnetic concentration, magnetic grain size and magnetic mineralogy, clay, $CaCO_3$ and organic carbon content, median grain size of mud fraction, mineralogy of the fine-grained (<2 μm) sediments (clay mineralogy, illite crystallinity, illite chemistry), Sr content, oxygen and carbon isotopes and morphology of the lime muds and radiocarbon ages of the sediments. The results obtained from the multi-proxy data and inferences drawn form the thesis and are presented in 7 chapters.

In Chapter 1, a general introduction, the scope and scientific importance of the study with special reference to the study area and objectives of the study are given. This is followed by the description of the physiographic and geologic features of the study area. The tectonic framework and neo-tectonic history of the area are briefly mentioned. The climatic and oceanographic setup of the area and previous studies with reference to the topics concerned are also presented.

Chapter 2 is on the materials and methods used for the present study. The location of the gravity cores and core descriptions are presented in the first section. The methods followed for analyzing different properties of the sediments are described in the next section. Analytical instruments such as Magnetic Susceptibility meter, AF Demagnetizer, Pulse Magnetizer, Spinner Magnetometer, Laser particle analyzer, Carbon-nitrogen and sulfur (CNS) analyzer, Inductively-coupled plasma atomic emission spectrometer (ICP-AES), Isotope-ratio mass spectrometer (IRMS), Scanning electron microscope (SEM) and X-ray Diffractometer were used.

The rock magnetic records of 15 gravity cores collected along the western margin of India at depths between 31 m and 1940 m are presented in **Chapter 3**. Of the 15 cores, eight are located off the Gulf of Kachchh - Saurashtra and seven are off the Gulf of Khambat - Cape Comorin. Down-core variations of magnetic concentration (Magnetic Susceptibility - MS, Anhysteritic Remanent Magnetization – ARM, Saturation Isothermal Remanent Magnetization - SIRM), magnetic grain size (inter-parametric ratios) and magnetic mineral composition (Hard Isothermal Remanent Magnetization-HIRM and S-ratio%) parameters are analysed in relation to the variations in Acid-insoluble Residue (AIR), organic carbon (OC), carbonate and sand content and median grain size of the terrigenous mud fraction. The magnetic properties are largely controlled by the detrital magnetite content of the sediments. Magnetic signal is enhanced at certain intervals by the presence of authigenic iron-rich minerals and biogenic magnetites, and reduced at certain other intervals by reductive diagenesis. The glacial sediments off the Indus exhibit low MS/S-ratio% associated with high AIR content, while those off the southwestern (SW) margin of India exhibit low MS/high S-ratio% associated with low AIR content. The early Holocene sediments of all cores are characterized by high MS/S-ratio% associated with high AIR content. The results imply that during the Last Glacial Maximum (LGM), the NW margin India received abundant continental supply through eolian/fluvial processes than that of the SW margin India. Increased intensity of the SW monsoon during the early Holocene contributed high MS/AIR content on the continental margin sediments. Rock-magnetic properties are modified by early diagenesis in the late Holocene organic-rich sediments.

Chapter 4 deals with the genesis of late Quaternary lime muds in 6 sediment cores collected off northwestern India. Lime muds occur as distinct facies in the lower sections of each core and are admixed with 30-50% terrigenous sediments on the continental shelf and <5% of terrigenous material on the continental slope. Aragonite is the dominant mineral. Grain size of the lime muds varies from 6 μm to 27 μm. The age of lime mud ranges from ~17 ka BP to

12 ka BP in the shelf cores. The lime mud deposition ceased after 14 ka BP in deeper water cores and after 12 ka BP in shallow water cores. Comparative studies on Sr content, oxygen ($\delta^{18}O$) and carbon ($\delta^{13}C$) isotopes and morphology of the lime muds with that of modern ones from other regions suggest that the lime muds in the shallow shelf are detrital and probably reworked from the Gulf of Kachchh / carbonate platform. The lime muds from the shelf break/slope are largely derived from the disintegration of codiacean algae. The late Quaternary neo-tectonic activity in the Gulf of Kachchh, the influence of global events such as Melt Water Pulse (MWP)-1A, MWP-1B and Younger Dryas and regional climatic conditions on the formation and distribution of lime muds were discussed.

The down-core distributions of organic carbon (OC), $CaCO_3$, AIR, sand and planktonic foraminifers and median grain size of terrigenous mud in 6 sediment cores are presented in **Chapter 5**. In the shelf cores, the OC content is low (0.15-0.47%) and most probably reworked along with terrigenous sediments. Within the slope cores, the cores from the oxygen minimum zone contain more OC (2-5%) than those above (0.06-1.14%) and below oxygen minimum zone (0.28-0.88%). The OC content is low in early deglacial sediments and increases progressively from ~12-11 ka BP to ~7-6 ka BP and remains high in the mid- and late Holocene sediments. There exist a mismatch between OC record in the cores studied and the past monsoon intensity record. The high OC coincides with high rates of sedimentation. Fine-grained sediments preserved more OC. Comparative study of OC data suggests that high OC is not always associated with high productivity areas. This study emphasizes that the spatial and temporal distribution of OC is controlled by a combination of several factors such as surface productivity, oxygen concentration at the sea floor, sediment texture, sedimentation rate and physiography of the sea floor.

Chapter 6 comprises the down-core variations in mineralogy of the fine-grained sediments (clay mineralogy, illite crystallinity and illite chemistry), clay

content and median grain size of the terrigenous mud fraction of five gravity cores. The Late Pleistocene sediments on the continental shelf off the Gulf of Kachchh and continental slope contain abundant Indus-derived clay minerals (illite and chlorite), while the core on the shelf off Saurashtra contains an admixture of clays derived from the Indus and hinterland (smectite and kaolinite). A gradual increase in smectite and kaolinite and decrease in illite and chlorite since early Holocene indicates a distinct change in sediment source from Indus-dominated to hinterland-dominated clays in the slope cores. Illite crystallinity and illite chemistry are in accord with the changing sedimentary environment. The intervals of high smectite and poor-crystalline illites coincide with that of the past monsoonal intensity record. The Influence of tides at the Gulf of Kachchh on long-shore sediment transport, cross-shelf transport processes with reference to the sea level changes, winnowing of finer sediments at the shelf edge and contribution of eolian dust to the study area were discussed.

Finally, the summary and conclusions of the Thesis are outlined in **Chapter 7**.

ACKNOWLEDGEMENTS

I am greatly indebted to **Dr. V. Purnachandra Rao**, my research supervisor, for his sustained interest and valued guidance in my work. He introduced and inspired me to the field of research and provided an ideal atmosphere to think, experiment and work. I am greatly obliged to him for his encouragement, support, motivation and critical assessment of the thesis with utmost care and patience.

My sincere thanks to **Dr. E. Desa**, former Director, NIO, Goa and **Dr. S.R. Shetye**, Director, NIO, Goa, for providing necessary research facilities and encouragement.

I am obliged to my co-guide, **Dr. V. M. Matta**, Lecturer, Department of Marine Sciences, Goa University for encouragement and administrative support for my thesis work.

I thank **Prof. G.N. Nayak**, Head, Department of Marine Sciences, Goa University, for his valuable advises, encouragement and administrative support.

Financial support for sample analysis and radiocarbon dating was from the funds of the PMN Project. I wish to express my sincere thanks to **Dr. V. N. Kodagali** and **Dr. M. Shyam Prasad**, Project Leaders of the PMN Project for their generous financial support and encouragement.

I thank **Council of Scientific and Industrial Research (CSIR), New Delhi** for awarding me Junior Research Fellowship.

I wish to place on record my indebtedness to the **AAS 42 cruise team** and the ship crew for helping me in sample collection, onboard investigations and sub-sampling of the sediment cores.

I am very thankful to **Dr. Shiva K. Patil**, Indian Institute of Geomagnetism, Alibagh, Raigarh, Maharashtra for teaching me the techniques of environmental magnetic measurements and giving free access to all the instruments in his laboratory. I also extend my sincere thanks to **Prof. R. Shankar**, Mangalore University, for providing facilities for magnetic susceptibility measurements in his laboratory on some of the sediments.

My sincere thanks to **Dr. V. Ramaswamy** for grain size analysis of the sediments and helping me with Malvern Laser Particle Size Analyser (Mastersizer 2000), **Dr. P.S. Rao** and **Dr. Prakash Babu** for organic carbon analysis using CNS analyzer.

I extend my sincere thanks to **Prof. Allan R. Chivas** and **Mr. David Wheeler**, University of Wollongong, Australia for stable isotope analysis of lime muds. **Dr. P. V. Narvekar, Ms. Witty D'souza** and **Dr. Anjali Chodankar** are thanked for ICP-AES analysis. **Dr. B. Sekar**, BSIP, Lucknow carried out radiocarbon ages of the samples.

I thank **Mr. Girish Prabhu** for XRD analysis and **Mr. V. D. Khedekar** for SEM studies.

My sincere thanks to **Mr. Arun Mahale** and his team, Drawing section NIO for their help in preparing of illustrations.

I thank **Dr. M. Tapaswi**, Documentation Officer, NIO and library staff for their help.

I am very thankful to **Shri. B. K. Saha**, Deputy Director General, Marine Wing, Geological Survey of India (GSI), **Dr. B. L. Narasayya**, Director CT and **Shri. B. L. Rao**, Director CGT, OP: EC-II, Marine Wing, GSI for granting permission to continue my Ph. D. work at GSI.

My special thanks to **Dr. Thamban Meloth,** my teacher for directing me to the National Institute of Oceanography, Goa and to the 'right research guide'. He has been a source of inspiration and support through out my research career.

The keen interest and help rendered by **Dr. Pratima M. Kessarkar** is greatly acknowledged.

It is my pleasure to record my particular obligation to my friends **Sudheesh, Yatheesh, Aparna, Shoby, Sumesh, Sreejith, Swapna, Sreekumar, Ramesh, Nuncio, Krishnan, Rajani, Vineesh and Ajay** for being with me and keeping my spirits high all the time.

Finally, I thank my parents, brothers and sister for their loving support, patience and encouragement towards my work.

Chapter 1

Chapter 1

INTRODUCTION

1.1. General introduction

Climate is a major component of earth system and has a direct control over the various physical, chemical and biological processes of the earth. There is increasing scientific evidence that natural processes combined with the anthropogenic activities are changing the Earth's climate. Greenhouse gas emissions from fossil fuel use are altering the atmosphere, creating an uncertain future of global warming, altered pattern of precipitation and sea-level rise for the generation to come. The potential threat of global climate change is a very serious problem to the entire Earth and its ecosystems. Climatic system of the Earth underwent several episodes of yearly to millennial scale variations in the past and knowledge on the past variations is necessary for understanding and prediction of regional and global climate (Kutzbach, 1981; Duplessy, 1982; Prell and Kutzbach, 1987; Fontugne and Duplessy, 1986; Gasse et al., 1991; Clemens et al., 1991; Sirocko et al., 1993; Reichart et al., 1997; Overpeck et al., 1996; Lamy et al., 1998; von Rad et al., 1998a; Naidu and Shankar, 1999; Gupta and Anderson, 2005). Firstly, the weathering and erosional products of the rocks and denudational processes on land vary with the changing climatic conditions and one can able to decipher climate by studying the properties of sediments through time. As these sediments transport and deposit on the continental margins, the terrigenous sediments deposited offer continuous record of information about the climate of the landmasses. Secondly, the terrigenous flux that has been transported to the continental margins together with changing seasonal monsoonal conditions induce several changes in the physics, chemistry and biology of the oceans that in turn leads to the varying upwelling and related changes in the primary productivity of the oceans. As a consequence the organic carbon (OC) deposited on the sea floor varies. By studying the OC distribution

one can able to decipher the productivity changes. Therefore, the sediments deposited on the continental margins of the World Ocean act as natural laboratories for studying the past climatic and oceanographic variations both regionally and globally.

1.2. Scope and scientific importance of the study

The continental margin off western India is an ideal site to study the past climatic and oceanographic conditions, especially for four reasons. Firstly, the terrigenous sediments are from diverse sources. The nature of terrigenous sediments and their rate of deposition vary from north to south along the continental margin. For example, the sediments in the extreme north are derived from the River Indus, one of the largest Rivers of the World, supplying sediments from the Himalayas. As the northwestern margin of India is bordered by alluvial soils of Pakistan and arid landmasses such as Iran-Makran-Thar regions, aeolian sediment supply is also an important terrigenous flux in this part of the margin (Kolla et al., 1981a; Chester et al., 1985; Reichart et al., 1997; von Rad et al., 1999; Prins et al., 2000). The sediment input from the Narmada-Tapti Rivers, discharged through the Gulf of Khambat, forms the second largest source of sediment. Further south the moderate and minor seasonal rivers supply sediments on the central and southwestern margin of India. Although broad understanding has been achieved on the provenance of the sediments based on mineralogy (Nair et al., 1982a; Rao and Rao, 1995) of the surficial sediments and Sr-Nd isotopes (Kessarkar et al., 2003), palaeoclimatic studies using exclusively terrigenous sediments have not been attempted. On the other hand, environmental magnetism or rock-magnetic properties of the terrigenous sediments deposited on the margins depend on magnetic concentration, magnetic minerals and magnetic grain size of the sediments, which in turn is modified by the climatic conditions on land.

Secondly, the lateral distribution of sediments on the northwestern margin of India shows distinct sediment types. For example, the inner continental shelf is characterized by predominant terrigenous sediments, followed by relict sandy sediments on the outer shelf and a mixture of terrigenous and biogenous sediments on the continental slope (Rao and Rao, 1995; Rao and Wagle, 1997). The relic sandy sediments on the outer shelf are largely carbonate-dominated in the northwestern part and terrigenous sand-dominated in the southwestern margin of India (Rao and Wagle, 1997). The sediment cores recovered from the NW margin of India also exhibit the occurrence of relic lime muds in the lower sections of each core. Although extensive studies have been carried out on modern lime muds from the Bahamas and the Persian Gulf (Cloud, 1962; Wells and Illing, 1964; Neuman and Land, 1975; Steinen et al., 1988; Robbins and Blackwelder, 1992), their origin is still a subject of debate. Some argue that the lime muds are inorganic in origin (Cloud, 1962; Wells and Illing, 1964; De Groot, 1965, Milliman et al., 1993; Dix, 2001), and others propose disaggregation of codiacean algae as a source for lime muds (Lowenstam and Epstein, 1957; Matthews, 1966; Stockman et al., 1967; Neuman and Land, 1975). Identifying the sources of lime muds is important to quantify the sediment carbonate budgets and in estimating carbon cycles. The relic lime muds of the northwestern margin of India provide opportunity to understand their genesis and the influence of late Quaternary sea level changes on their distribution. The northwestern margin of India is furthermore influenced by late Quaternary neo-tectonic activity (Rao et al., 1996; Rao and Veerayya, 1996; Rao and Wagle, 1997; Rao et al., 2003; Merh, 2005). The radiocarbon dating of different sediment intervals in the cores off Kachchh may provide better understanding on the precise timing of neo-tectonic activity and flooding of the Gulf after the Last Glacial Maximum (~18,000 yrs BP).

Thirdly, upwelling associated productivity is largely seasonal on the western margin of India. Widespread upwelling and high surface productivity

occurs during the SW monsoon and results in permanent oxygen minimum zone on the continental slope between 150 m and 1200 m water depth (Wyrtki, 1971) and high organic carbon in the underlying sediments. Factors controlling the enrichment of organic matter in marine sediments are a matter of debate for several years. Two different hypotheses exist. Some argue productivity is the main controlling factor (Pederson and Calvert, 1990; Pederson et al., 1992; Calvert et al., 1995; Thompson et al., 1997), whereas others propose preservation in poor-oxygenated conditions is responsible for enrichment of organic carbon (Canfield, 1989; Demaison, 1991; Paropkari et al., 1992, 1993). Since the sediments cores were recovered at different depths on the continental margin off Saurashtra, a moderate productivity region, the down-core distribution of OC together with other sedimentological parameters are helpful in verifying both hypothesis and understanding the palaeoceanography of the region.

Fourthly, despite two major rivers (the Indus and Narmada -Tapti Rivers) debouching enormous sediments in the vicinity of the Gulf of Kachchh and Saurashtra peninsula, the relic sediments on the outer continental shelf of the northwestern India are not buried by recent clastic sediments. Where are the river-borne sediments deposited? The macro-tides operating at the Gulf of Kachchh act as a natural barrier for the alongshore sediment transport in this region (Nair et al., 1982b; Chauhan, 1994). Did the Indus-borne sediments deposited in the shelf south of the Gulf of Kachchh during low sea level conditions in the late Pleistocene/ early Holocene? What is the role of neo-tectonic activity in transporting and diverting river-borne sediments? In order to address these questions a better understanding is required on the provenance and transport pathways of fine-grained sediments deposited on the NW margin of India during the late Quaternary. Studies on clay mineralogy of the sediments in the gravity cores would be the most straightforward tool for identifying their provenance.

1.3. Objectives of the study

Keeping in view of the above, detailed investigations were carried out on the sediment cores collected along the northwestern margin of India. I have focused on the down-core variations in the (a) grain size, mineralogy and rock-magnetic properties of the terrigenous sediments, (b) sedimentological, mineralogical, geochemical and stable isotope characteristics of the lime muds and (c) organic carbon and carbonate content of the sediments.

The objectives of the present study are to

1) trace the climatic history and provenance of the sediments during the late Quaternary,

2) resolve the issues related to the genesis of lime muds and influence of late Quaternary sea level changes and neo-tectonic activity on their distribution and

3) report the nature of organic carbon (OC), productivity changes and factors controlling the OC distribution in the late Quaternary.

1.4. Physiography and Geologic set up of the study area

Arabian Sea is a semi-enclosed basin forming the northern arm of the Indian Ocean, surrounded by the dry land masses of Africa, Arabia, the Iran-Makran-Thar regions towards west and north and by the coastal highlands of western India towards east (Kolla et al., 1981a; Fig. 1.1). Indus, the sixth major river in the world in terms of sediment discharge brings enormous sediments to the Arabian Sea (~400 million tons of suspended and bed load before the construction of dams - Mangala dam in the year 1967 and Tarbela dam in 1976

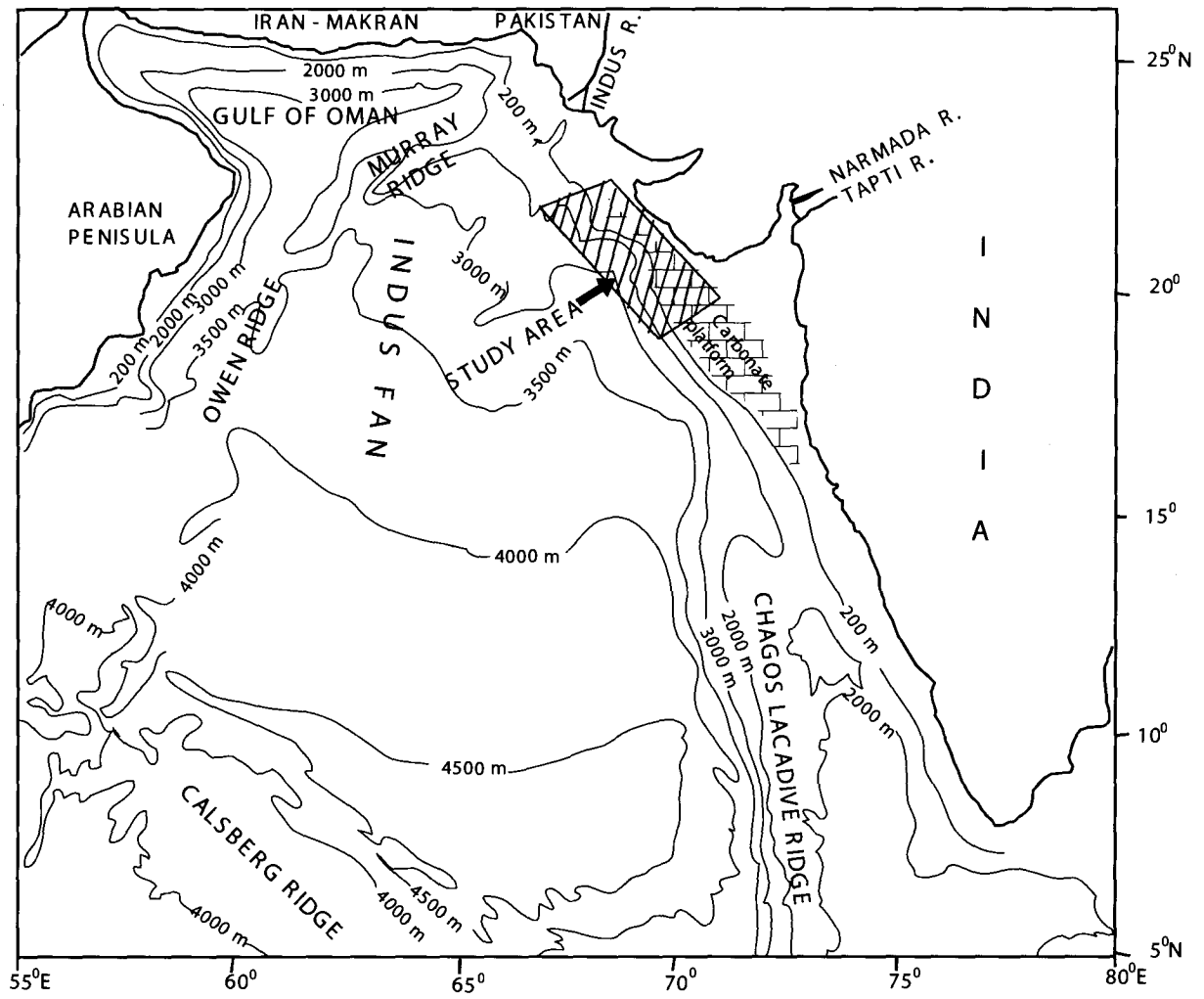

Fig. 1.1. Physiographic provinces of the Arabian Sea (modified after Kolla et al., 1981a) The hatched area represents the study area. (The cores used for rock magnetic studies extends beyond the hatched area -see Fig. 3.1).

that reduced to ~45 million tons at present – Milliman et al., 1984). The Narmada and Tapti rivers debouch 58.7 million cu. m. of water and several tons of suspended and bed load annually through the Gulf of Khambat (Rao, 1975). Besides, many small rivers and streams drain into the Arabian Sea from western India. The arid regions in the north and west of Arabian Sea (Arabian Peninsula and Iran-Makran area) contribute negligible riverine flux, but abundant aeolian material (~100 million tons annually - Sirocko and Sarnthein, 1989) to the Arabian Sea by transporting through the dry, northwesterly Shamal winds (Kolla et al., 1981a). The heavy sediment load from the Indus forms an extensive physiographic feature in the Arabian Sea called the 'Indus Fan'. The Indus-borne sediments extend as far as 1500 km away from its mouth (Lisitzin, 1972). The Indus and its tributaries drain the glaciers and the mountain slopes of the Himalayas and the Indo-Gangetic basin. The lithologic units in the Indus drainage area include slates, phyllites, quartzites, mica-schists, carbonaceous and graphitic schists, crystalline lime stones, dolomites, biotite-gneiss, granulites, intrusive igneous rocks like granite, pegmatite and dolerite and the various lithologic units of Siwalik and Salt Range formations (Krishnan, 1982). The Narmada and Tapti Rivers drain the Vindhyan, Satpura systems and the Deccan Traps. The tributaries of the Narmada and Tapti and some minor rivers like Mahi and Sabarmati drain the Aravalli mountain ranges and the younger formations of Gujarat and Rajasthan and discharge their sediment load in to the Arabian Sea through the Gulf of Khambat (Krishnan, 1982). The Gulf of Kachchh and Gulf of Khambat are two prominent embayments along the northwestern margin of India and are also the most prominent macro-tidal (average tidal range of ~4 m, Babu et al, 2005) sites of India. The Gulf of Kachchh receives little runoff from the land, whereas the Gulf of Khambat receives abundant run off from the land.

The hinterland region of Saurashtra is located astride the Tropic of Cancer and forms an important part of dry lands of western India. The monsoon rains are restricted to June - September and the rest of the months are dry. The geology of

the Saurashtra region is the result of complex interaction between tectonism and sea level changes during the Cenozoic (Chamyal et al., 2003). The basic framework was formed due to sequential fragmentation of the western continental margin of the Indian plate during the late Mesozoic as it collided with the Eurasian plate in the north (Biswas, 1987). The break up of the margin resulted in the formation of Kachchh, Khambat and Narmada rift basins (Biswas, 1987). The coastline of Saurashtra is highly varied and characterized by the presence of narrow belt of low ridges and cliffs of miliolite limestones and other shore deposits (Chamyal et al., 2003). The Saurashtra peninsula is largely covered by Deccan Trap basaltic flows. Cretaceous sediments crop out in the northeastern part and a thin veneer of Tertiary and Quaternary sediments occur along the coast (Bhattacharya and Subrahmanyam, 1986). Sedimentary sequences ranging in age from Jurassic to Pleistocene are found in the interior of Saurashtra and in the coastal regions in the northern part of the Gulf of Kachchh (Fig.1.2).

The physiography of the continental shelf is a result of the depositional and erosional processes that occurred during the glacio-eustatic sea level fluctuations (Wagle et al., 1994). The tectonic movements and the isostatic adjustments might have further modified the physiography. Except in the Gulf of Kachchh and Gulf of Khambat, the topography of the inner shelf is smooth with no major undulations. The physiographic features of the order of 5-10 m high occur on the outer shelf. Submarine terraces and notches are observed on the continental slope off Saurashtra. A carbonate platform, also called as 'Fifty Fathom Flat' is the largest topographic feature on the outer continental shelf of the northwestern margin of India. The water depth on the platform ranges between 60 and 110 m. The width of the continental shelf varies from about 100 km south of the mouth of Indus to 160 km southwest of the Gulf of Kachchh. The width of the continental shelf is only 70 km off Saurashtra. The shelf width is greatest (~345 km) off Mumbai and decreases southwards (Rao and Wagle, 1997). The shelf break

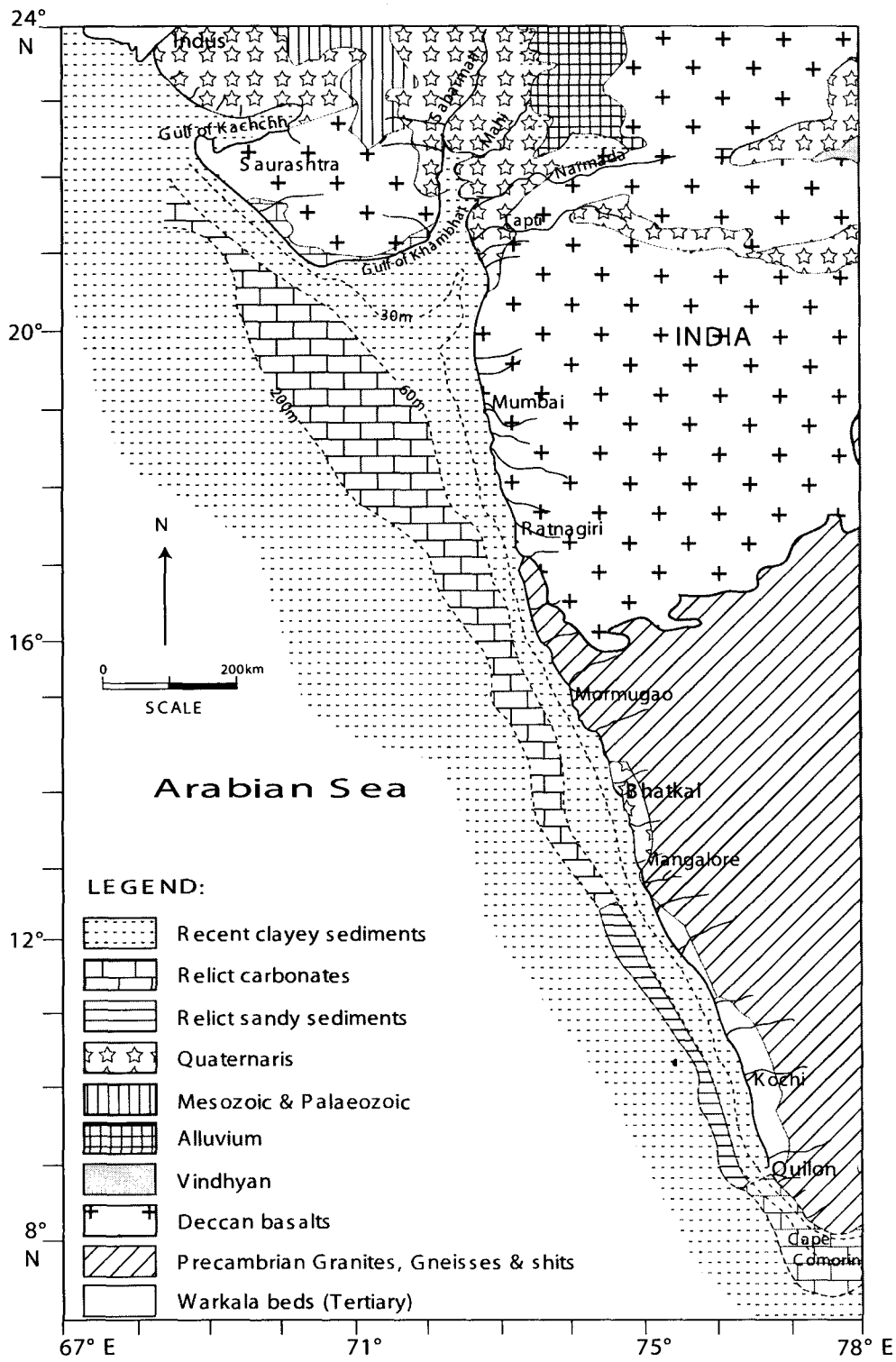

Fig. 1.2. Geology of the western margin of India. Onshore geology after Anonymous (1965) and offshore geology after Rao and Wagle (1996)

occurs at about 80-140 m off Saurashtra and at about 90 m off the platform (Rao and Wagle, 1997). Two distinct sediment types occur on the continental shelf: modern clastic clays on the inner shelf and relict sandy sediments on the outer shelf. Relic deposits on the outer shelf and carbonate platform comprise abundant aragonite faecal pellets, oolites, *Halimeda* grains and a few bivalves, benthic and planktic foraminifers. The platform also contains indurated aragonite muds, *Halimeda*- and pelletal limestones, coralline algal nodules, a few coral fragments, oyster shells and dolomite encrustations (Nair, 1971; Nair et al., 1979; Rao et al., 1994, 2003a&b). *Halimeda* bioherms of early Holocene age were also reported on the platform (Rao et al., 1994). Continental slope comprises silty clays that are an admixture of dominant terrigenous and biogenic components (Rao and Rao, 1995).

1.5. Tectonic framework and neo-tectonic history of the region

The northwestern continental margin and inland region exhibit a number of faults and horsts and graben structures. Notable amongst the tectonic elements are the Kachchh rift, the Cambay rift, the Narmada rift and the Kathiawar rift (Fig.1.3). The Kachchh region is controlled by numerous E-W faults and falls in the seismically active zone V. It is located quite close to the junction of the western continental margin and the geosynclinal belt of Sindh-Baluchistan (Merh, 2005). The Saurashtra peninsula is bordered by major faults and rift basins to its north, south and east and forms a horst block in relation to its surrounding area. It is the uplifted part of the WSW plunging basement arch and is a divide between the northern Kachchh-Saurashtra shelf and the southern Bombay-Kerala shelf. Bhattacharya and Subrahmanyam (1986) identified WNW-ESE trending fault that extend across the Saurashtra continental margin between Porbandar and Varaval and considered it as a major linear tectonic feature in this area. The Saurashtra arch, which is an extension of the Aravalli range subsided along the eastern margin fault of Cambay Basin during Early Cretaceous forming

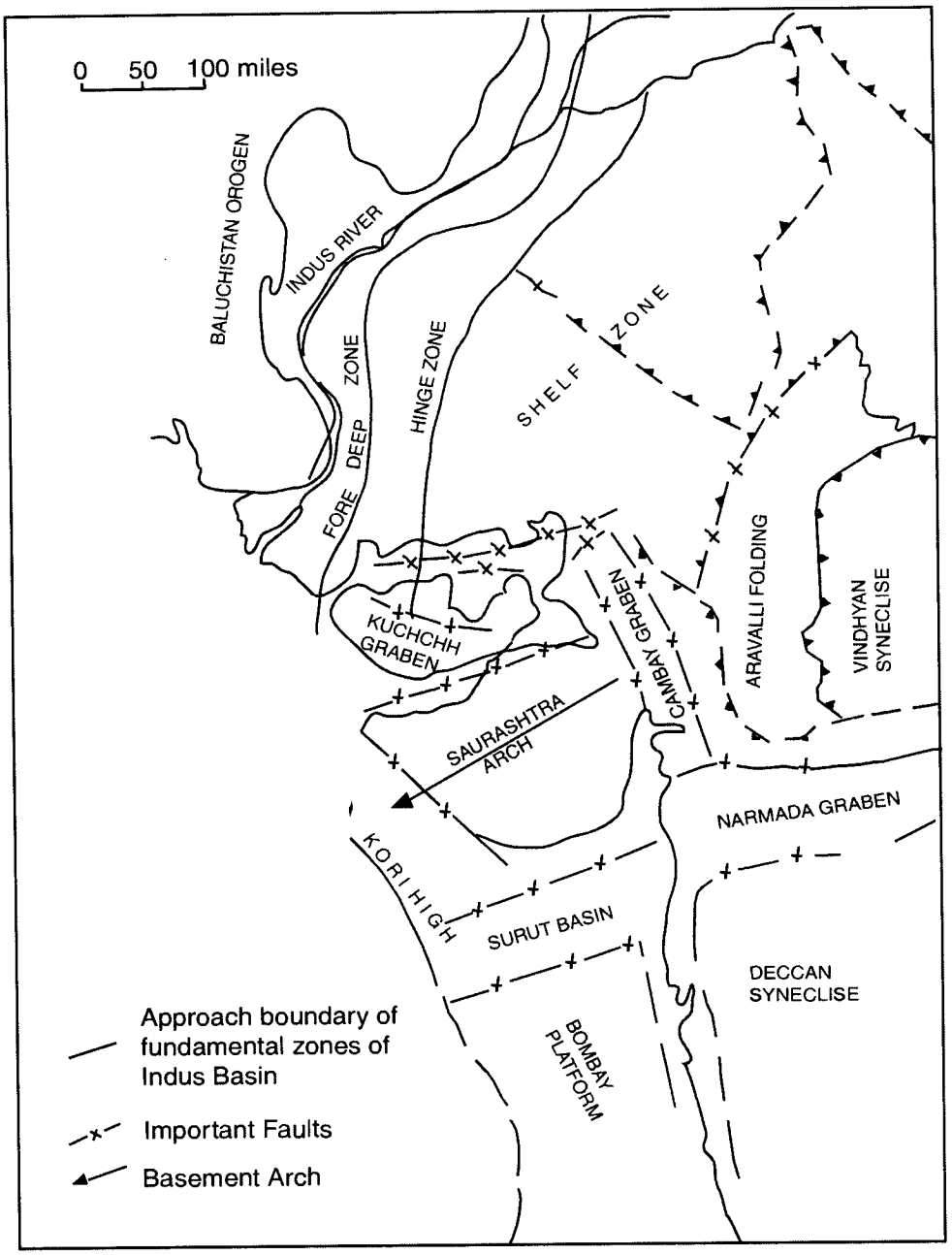

Fig. 1.3. Tectonic map of Western India (After Biswas, 1988)

an extensive depositional platform continuous with the Kachchh shelf and a part of the arch was uplifted in the late Quaternary (Mahadevan, 1994). The Saurashtra Arch separates the Saurashtra offshore basin from the Kachchh offshore basin. The Saurashtra Peninsula in the east and Narmada Graben in south mark the limits of the Saurashtra offshore basin (Fig. 1.3).

Historic events like disruption of River Saraswati, westward migration of Sutlej around 5ka BP and the decline of Harappan civilization around 4 ka BP (1900 BC) are attributed to the tectonic activity in the region (see Merh, 2005 and references therein). Imprints of severe tectonic and eustatic movements in the NW margin of India are also preserved in the Great Rann, the landmass lying north of the Gulf of Kachchh. Marine conditions existed in the Great Rann in the past and with gradual recession of sea, the area changed over to an estuary, that received sediments from Saraswati and Sutlej and today it is an area of high aridity. A massive earthquake around 1000 years back (1030 AD) is believed to be responsible for the uplift of the Great Rann and westward migration of the River Indus (see Merh, 2005). Presence of submarine terraces off Saurashtra-Bombay at 130, 145 and 170 m water depths that lie well below the glacio-eustatic sea-level low of –120 m, occurrence of inter-tidal limestones dated 11,980 yrs BP at 130 m depth, the mismatch between the depth and radiocarbon ages of oolite samples from the Fifty Fathom Flat (Rao et al., 1996; Rao and Veerayya, 1996; Rao and Wagle, 1997) and the corresponding glacio-eustatic sea level position (Fairbanks, 1989) and relic deposits dated 12550 yr BP at 35 m depth in the Gulf of Kachchh are evidences in favour of late Quaternary of neo-tectonic activity (Rao et al., 2003a).

1.6. Climatic and oceanographic set up

The Indian monsoon system is one of the major climatic systems of the world and showed drastic variations ever since its origin from late Miocene (cf.

Gupta and Anderson, 2005). The Indian monsoon system is controlled by seasonal reversal of wind system wherein during summer (June – September) the South Asian landmass is warmer than the ocean, driving winds from SW to NE towards the continents resulting in southwest monsoon or summer monsoon. During winter (November – February) the pressure cells reverse and thus the winds blow from NE to SW forming the northeast monsoon or winter monsoon. During the northern winter, when the snow cover increases the albedo, atmospheric pressures are high over Central Asia and this sets up a pressure gradient between Central Asia and the Inter Tropical Convergence Zone at about 10°S, forcing the dry and cold northeasterly winds of the winter monsoon (Reichart et al., 1997). Snow and ice melt at the end of the winter diminishes the albedo over Central Asia, causing a reversal of pressure gradient. This seasonal reversal of the Indian monsoons is one of the most spectacular features of Earth's climate system (Webster, 1987). The summer monsoon brings heavy rains over the Indian land mass whereas during winter monsoon season the precipitation is low.

Studies have shown that the cyclic variability in the obliquity and precession of earth's orbit that affected the intensity of solar insolation controlled the intensity of summer monsoon in the past (Prell and Kutzbach, 1987; Clemens et al., 1991). Marine records of past climatic changes from Arabian sea showed that the monsoon was significantly weaker than present during glacial times, much stronger than present during the early to mid-Holocene and weaker up to the present day (Duplessy 1982; Van Campo et al., 1982; Prell, 1984; Prell et al., 1990; Sirocko et al., 1991).

The northern Arabian Sea is a unique environment characterized by strong seasonal variability of monsoonal upwelling and high primary productivity that favor an exceptionally broad and stable mid-water oxygen-minimum zone (OMZ). During the northeast monsoon, biological productivity is low (289 mg C

m^{-2} day^{-1} – Sarupriya and Bhargava, 1993) and the monsoonal winds of the southwest monsoon cause widespread upwelling and high surface productivity (720 mg C m^{-2} day^{-1}- Sarupriya and Bhargava, 1993) in the western Indian margin.

1.7. Previous studies

Marine geological investigations in the Arabian Sea started with the *HMS Challenger* Expedition during 1872-76. This is followed by Vityaz (1889), *Valdivia* (1889-99), *Mabahiss - John Murray* (1933-34) and *Albatros* (1947-48) Expeditions. Topography and Sediment distribution in the Arabian Sea was first reported by Sewell (1935). Wiseman and Bennett (1940) presented organic carbon and nitrogen distribution in the Arabian Sea sediments by using the samples collected during John-Murray Expedition (1933-1934). The International Indian Ocean Expedition (IIOE- 1961-1965) sediment samples and oceanographic data were collected from the west coast of India. During IIOE, *INS Krishna* surveyed the western continental shelf of India between Bombay and Cochin, whereas *R/V Meteor* collected samples in different traverses across the shelf and slope region off Bombay – Cochin. *Oceanographer* studied northern Arabian Sea and focused on the shelf and slope off Bombay-Saurashtra. *Requisite* studied the northern Arabian Sea and *Vladimir Vorobyeo* the western continental shelf of India. *Vityaz* studied the deep Arabian Basin. R/V Vema of the Lamont-Doherty Geological Observatory and *USNS Wilkes* also carried out investigations along several transects in the Arabian Sea (Kolla et al., 1981a). The continental margin off Pakistan and western India was studied for the first time by the cruises of R/V *Meteor* and M/V *Machhera* during the International Indian Ocean Expedition (IIOE; Dietrich et al., 1966). The Indian research vessels such as *INS Darshak, RV Gaveshini, ORV Sagar Kanya, Samudra Manthan and Samudra Saudhikama* carried out subsequently detailed studies and collected sediments along the western continental margin of India.

Magnetic susceptibility (χ_{lf}, hereafter discussed as MS) is related to total magnetic mineral concentrations in the sediments. The MS signal is largely controlled by magnetic mineral concentration, grain size, carbonate dilution and the presence of dia- and paramagnetic minerals (Bloemendal et al., 1988). Magnetic susceptibility studies on the sediments of the Arabian Sea are few and include studies from the sediment cores collected during the Ocean Drilling Program (ODP) and deep Arabian Sea (Bloemendal and de Menocal, 1989; Shankar et al., 1994a; Sykes and Kidd, 1994; Meynadier et al., 1995; Hounslow and Maher, 1999). These workers used magnetic susceptibility as a proxy to study the source of the lithogenic and aeolian flux and the magnetic responses to climatic changes. Meynadier et al. (1995) used the magnetite/hematite ratio to study the influence of Antarctic Bottom Water Current in transporting fine-grained magnetic minerals to the Somali Basin. Prins et al. (2000) used magnetic susceptibility to identify the aeolian and Indus-borne sediments in turbidites of the Indus Fan. Karbassi and Shankar (1994) applied rock magnetic techniques locally to the riverine and estuarine sediments of Mulki (minor) River, for stream-bed load sediments (Shankar et al., 1994b) and off-shore placers of the SW coast of India (Shankar et al., 1996). There are no detailed studies on the sediments of the western margin of India. In this thesis, magnetic susceptibility and other remanent magnetic parameters were measured for the first time for the sediments in gravity cores collected along the western margin of India and inferred that provenance of the sediments controls on the rock-magnetic parameters and climatic conditions prevailed during the late Quaternary.

Lime muds are potentially produced by several mechanisms; mechanical disintegration of biological skeletal components, disaggregation of calcareous green algae, inorganic precipitation, bioerosion, erosion of tidal flat mud deposits, organic and bio-geochemical processes (Bathurst, 1971). Modern lime muds have been reported from the carbonate banks and platforms off Florida,

Bahamas, Southern Belize and the Persian Gulf (Ginsburg, 1956; Lowenstam and Epstein, 1957; Cloud, 1962; Wells and Illing, 1964; DeGroot, 1965; Matthews, 1966; Stockman et al., 1967; Mitterer, 1972; Neuman and Land, 1975; Steinen et al., 1988; Boardman and Carney, 1991; Macintyre and Reid, 1992; Robbins and Blackwelder, 1992; Milliman et al., 1993; Dix, 2001). Despite numerous detailed investigations on these modern lime muds there are no consensus on the origin of the lime muds. Inorganic origin and disintegration of codiacean algae as a primary source for the lime muds have gained popularity over other mechanisms of lime mud formation. The lime muds from the continental slope off the Gulf of Kachchh at depths between 150 and 500 m were reported (Vaz et al., 1993) and no further detailed studies were conducted to understand the genesis of lime muds. In this thesis detailed sedimentological, geochemical and stable isotope (oxygen and carbon) studies of the lime muds together with their radiocarbon age measurements were carried out in five sediment cores collected at water depths between 56 and 121 m and reported their origin and relevance of late Quaternary sea level changes and neo-tectonic activity on their distribution.

Wiseman and Bennett (1940) were the first to report the distribution of organic matter in the sediments of the Arabian Sea. Subsequently several workers reported the distribution and characteristics of organic matter in the sediments off western India (Kidwai and Nair, 1972; Rajamanickam and Setty, 1973; Paropkari, 1979; Rao and Rao, 1989; Ramamurty and Murty, 1989; Paropkari et al., 1992, 1993; Calvert et al., 1995; Thamban et al., 1997; Nagendranath et al., 1997; Babu et al., 1999; Rao and Veerayya, 2000; Bhushan et al., 2001; Thamban et al., 2001; Agnihotri et al., 2002, 2003; Pattan et al., 2003; Prabhu et al., 2004; Prabhu and Shankar, 2005). Organic carbon studies from the continental shelf and slope off Pakistan were also reported (von Rad et al., 1995; Cowie et al., 1999; Keil and Cowie, 1999; von Rad et al., 1999; Schulte et al., 2000; Suthhof et al., 2000). Kolla et al. (1981b) prepared a map on the distribution of organic carbon for the entire

Arabian Sea. Organic carbon in the sediment cores of the deep Arabian Sea was also reported (Reichart et al., 1997). Rixen et al. (2000a) studied the organic carbon flux in the Arabian Sea using data from the sediment trap experiments. In this thesis organic carbon distribution in the sediment cores collected across the continental shelf and slope of the northwestern India at depth between 56 m and 420 m is reported and discussed the factors controlling its distribution.

Several workers reported the mineralogy of the fine-grained (<2 μm) surficial sediments in the Arabian Sea, Bay of Bengal and Indian Ocean in general (Gorbunova, 1966; Griffin et al., 1968; Rateev et al., 1969; Goldberg and Griffin, 1970). Stewart et al. (1965) were the first to report the clay mineralogy of the northwestern margin of India. Subsequently Mattait et al. (1973), Nair et al. (1982a and b) and Rao and Rao (1995) reported regional studies on mineralogy of the <2μm fraction of the sediments covering the entire western margin and provenance of the sediments. Clay mineral distribution in different parts of the western margin was also reported (Bhattacharya, 1984; Rao et al., 1983; Guptha and Hashimi, 1985; Rao, 1991). Thamban et al. (2002) studied a few sediments cores on the SW margin of India and reported climatic variations during the late Quaternary. Kessarkar et al. (2003) studied clay mineralogy together with Sr-Nd isotopes of the few selected cores and reported their provenance. In this thesis I have studied the clay mineralogy of the sediments in five gravity cores collected at depths between 56 and 420 m depth and report their provenance during the late Quaternary and the influence of neo-tectonic activity in their distribution.

Chapter 2

Chapter 2

MATERIALS AND METHODS

2.1. Materials

Fifteen sediment gravity cores recovered during different cruises of M/V *AA. Sidorenko* and *ORV Sagar Kanya*, at water depths between 31 m and 1940 m, along the western margin of India are used for the present study. Sediments recovered in different gravity cores are in general 3 m to 5 m long. Gravity cores GC-1 to GC-8 are located on the continental margin off the Gulf of Kachchh - Saurashtra, GC-9 to GC-11 off Mumbai and GC-12 to GC-15 are from the central and southwestern margin of India between Goa and Cape Comorin (see Fig. 2.1). The location of the cores, water depth at which they were collected and length of the sediment recovered in each core are given in Table. 2.1. The colour of the sediments using rock-colour chart was noted during sub-sampling the sediment cores onboard immediately after their recovery. The cores were sub-sampled at 2 cm intervals for the first 2 m and at 5 cm intervals for the remaining potion of the cores. Part of the sub-sample was dried at <50°C and used for sedimentological, geochemical and stable isotope analyses.

Table 2.1. Details of the sediment cores

Serial Number	Core Number	Cruise Number	Water Depth (m)	Latitude (Deg)	Longitude (Deg)	Core Length (m)
1	GC-1	SK148/22	56	22.46 N	68.15 E	7.02
2	GC-2	SK148/21	1900	21.48 N	67.02 E	3.58
3	GC-3	SK148/31	65	21.02 N	69.35 E	5.98
4	GC-4	SK148/32	111	20.42 N	69.43 E	4.37
5	GC-5	SK148/30	121	21.12 N	68.95 E	5.49
6	GC-6	AAS42/22	330	20.37 N	69.32 E	5.21
7	GC-7	AAS42/20	430	21.73 N	67.95 E	5.95
8	GC-8	AAS42/21	333	21.03 N	69.02 E	5.43
9	GC-9	SK148/43	115	18.96 N	70.10 E	2.83
10	GC-10	SK148/55	500	17.75 N	70.86 E	6.13
11	GC-11	SK148/38	31	19.98 N	71.48 E	4.56
12	GC-12	SK126/39	1940	12.63 N	73.46 E	4.90
13	GC-13	AAS 6/5	280	10.22 N	75.33 E	3.33
14	GC-14	SK148/4	1380	8.20 N	75.96 E	2.84
15	GC-15	SK126/16	1420	8.03 N	76.05 E	4.80

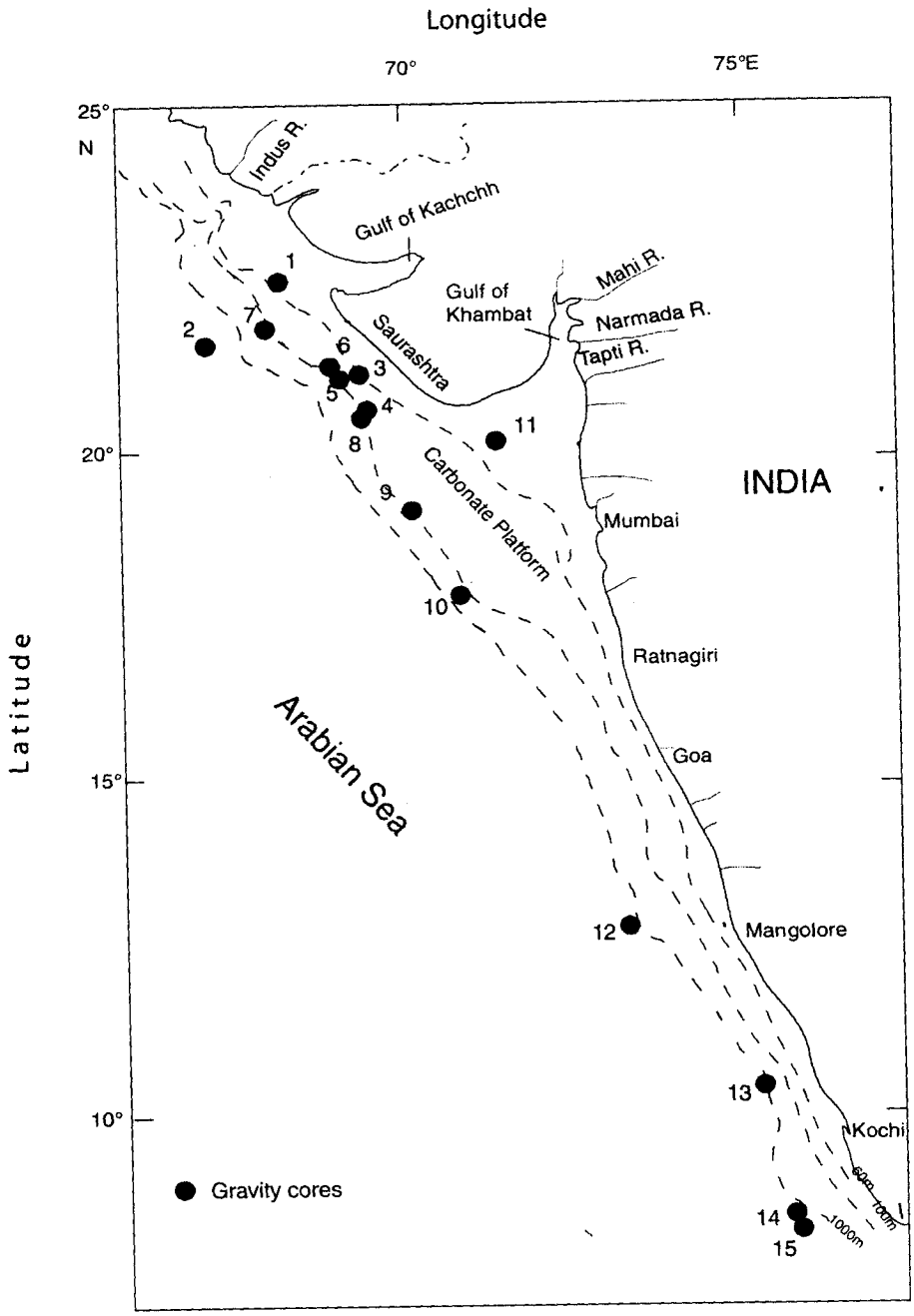

Fig. 2.1. Location of gravity cores on the western margin of India

2.2. Methods

2.2.1. Sedimentology

i. Grain size measurements

Grain size measurements of the sediments were carried out using a Malvern Laser Particle Sizer (Master Sizer 2000) that uses the principle of Low Angle Laser Light Scattering (LALLS). The Laser Particle Sizer comprises a Helium-Neon laser beam, which has been spatially filtered and collimated to produce a clean parallel beam of light. This is then focused down by a fourier or reverse fourier lens to a point at the center of a detector. The laser beam passes through a pinhole at the center of the detector array and falls on a detector known as an obscuration detector. If no particle pass through the laser beam, all the light falls on the obscuration detector. However, as soon as the particle enters the beam, it scatters light at an angle inversely proportional to its size. The particular property of the fourier lens is that it collects the scattering from an ensemble of particles and overlays the common angle of scattering on the detector array. This overlaid data known as the light energy distribution is used for the measurement of particle size distribution.

Grain size measurements were carried out on both bulk and $CaCO_3$ free fractions of the sediments. About 5 g of the dried sediment sample was used. Soluble salts were removed by repeated washing with distilled water. Organic matter was destroyed by treating with hydrogen peroxide. The sample was then wet sieved using a 63 μm sieve and the +63 μm fraction remained in the sieve was collected, dried and weighed accurately. The <63 μm fraction was used for size analyses using a Laser Particle Size Analyzer. For the size analysis of the carbonate free fraction, the sample is made free of carbonate by treating with 10% HCl, prior to removal of organic matter by hydrogen peroxide. Coarse fraction was separated and <63 μm fraction was used for particle size analyses

as described above. The ultrasonic dispersant provided with the instrument was used for sample dispersal. Grain size measurements were carried out on 332 bulk sediment samples and 253 carbonate free samples.

ii. Carbonate mineralogy

Carbonate-dominated fine-grained sediments (lime muds) occur in lower portions of several cores of the northwestern margin of India. These sediments were washed with distilled water, dried and powdered to fine size. Bulk mineralogy of all these samples was carried out by scanning sample powders from 25° 2θ to 35° 2θ at 1° 2θ/min on a Philips powder X-ray diffractometer using nickel-filtered Cu Kα radiation. Carbonate minerals were identified. The peak heights of the principal reflections of calcite and aragonite above the background were measured and the ratio of aragonite to calcite was plotted on a standard graph, prepared based on the known mixtures of aragonite and calcite. From the plot the weight percentage of aragonite and calcite in each sample was estimated. A total of 112 samples were analysed for carbonate mineralogy.

iii. Clay mineralogy

Representative samples were made free of salt by repeated washing with distilled water. The <2 μm fraction of the sediment was separated based on Stoke's settling velocity principle. The separated clay aliquots were made free of carbonate and organic matter by treating with 5 ml acetic acid and 10 ml hydrogen peroxide, respectively. The aliquots were washed several times with de-ionized water to remove excess reagents. Oriented slides were prepared by pipetting 1 ml of the concentrated clay suspension onto glass slides and allowed them to dry in air. A few samples were scanned from 2° to 30° 2θ but all the slides were treated with ethylene glycol for one and half hour at 100° C and then scanned from 2° to 22° 2θ at 1.2° 2θ min-1 on a Philips X-ray diffractometer (PW 1840 model) using nickel-filtered Cu Kα radiation, equipped with an automatic divergent slit. All the samples were rescanned from 24° to 26° 2θ at 0.5° 2θ min-1 to differentiate kaolinite and chlorite peaks (Biscaye, 1965). The weighted peak

area percentages of the major clay minerals were calculated from the X-ray diffractograms following the semi-quantitative method of Biscaye (1965). Accordingly, the peak areas of 17 Å reflection of smectite were multiplied by 1, 10 Å of illite by 4 and 7 Å of chlorite and kaolinite by 2. The kaolinite (3.54 Å) and chlorite (3.58 Å) peak areas were used to calculate the individual percentages of kaolinite and chlorite. Crystallinity of illite was measured as the half height width (HHW) of the 10 Å peak where the HHW is inversely proportional to the crystallinity and structural order of illite (Singer, 1984; Chamley, 1989). More humid and warmer climate leads to hydrolysis and open illite structure leading to poor crystallinity. In contrast the colder or dryer climate leads to preservation of illite structure representing better crystalline illites. Illite chemistry is expressed by the ratio of illite 5 Å /10 Å peak area, where ratio below 0.5 represents Fe, Mg-rich illite, which are characteristic of physically eroded, unweathered rocks, and ratios above 0.5 are characteristic of Al-rich illites, formed by strong hydrolysis (Gingele, 1996). A total of 242 sub-samples from 5 gravity cores were studied for clay mineralogy.

iv. Scanning Electron Microscope (SEM) studies

SEM studies were carried out on lime muds, which contain >95% carbonate. About 10 g of the sediment sample was made free of salts by repeated washing with distilled water. Organic matter was removed by treating with hydrogen peroxide for 24 hours. These sediments were then wet sieved using a 63 μm sieve and the coarse fraction (>63 μm) was separated, dried and weighed. The <63 μm fraction of the sediment was collected into a graduated 1 l cylinder. Using Stoke's settling velocity principle, different size fractions (< 4 μm, 4-8 μm, 8-16 μm, 16-32 μm and 32-63 μm) were separated, by carrying ou repeated settling for 8 times for each fraction. These separated fractions wa pipetted onto stubs and allowed them to dry in air. These stubs were examin under a JEOL 5800 LV Scanning Electron Microscope (SEM) with an Oxf EDS micro-analyzer.

2. 2.2. Geochemistry

i. Organic carbon analysis

A. Using CNS (Carbon, Nitrogen and Sulfur) Analyzer

Organic carbon and nitrogen were analysed using a Carlo Erba elemental analyzer (NCS-2500 model). The representative samples were made free of carbonate by treating with 10% HCl, washed and dried at <50°C. In this method, a weighed amount of powdered sample in a tin capsule, placed in a auto-sampler drum where it is de-aerated (to remove any atmospheric nitrogen), introduced into a vertical quartz tube heated at 1000°C with a constant flow of helium (carrier gas) stream. A few seconds before the sample drops into the combustion tube, the helium stream is enriched with a measured amount of high purity oxygen to achieve a strong oxidizing environment which guarantees almost complete combustion / oxidation of even thermally resistant substances. To achieve quantitative oxidation, the combustion gas mixture is driven through an oxidation catalyst (WO_3) zone, then through a subsequent one of copper which reduces nitrogen oxides and sulphuric anhydride (SO_3) formed during combustion or catalyst oxidation, to elemental nitrogen and sulphurous anhydride (SO_2) and retains the oxygen excess. At the outlet of the reaction tube, the gas mixture (N_2, CO_2, H_2O, SO_2) meets a trap containing anhydrone that absorbs water. The resulting three components of the combustion mixture are eluted and separated by a porapack PQSW column and subsequently determined by a thermal conductivity detector that generates an electrical signal proportional to the amount of eluted gas. Such a signal is fed into an automatic work station (Eager 200) that provides the sample elemental composition. The accuracy of the measurements was determined by using SBC-1 and TWTUC standards and the error was found to be <1%. A total of 144 samples from 3 cores were analysed by this method.

B. *Using titration method*

This method is based on the oxidation of organic carbon with chromic acid and titrimetric determination of the oxidant consumed (el Wakeel and Riley, 1957). The samples were made free of $CaCO_3$ by treating with 10% HCl and washed with de-ionized water to remove the excess acid and dried at <60°C and powdered. About 0.15-0.3 g of the powdered sample is accurately weighed and transferred to a boiling tube and 10 ml chromic acid is added. The tube was covered with aluminum foil and heated in a water bath for 15 minutes. The tube was allowed to cool and the contents of the tube were transferred into a 250 ml conical flask containing 200 ml distilled water. About 2-3 drops of Ferrous-Phenanthroline indicator was added and titrated with 0.2N Ferrous Ammonium sulphate. A blank determination was also carried out by the same method.

1 ml of 0.2N ferrous ammonium sulphate = 1.15 X 0.6 mg of carbon

OC content in the sample = 0.6 (X-Y) 1.15 x 100/weight of sample (mg), where X represents titration value for blank and Y - titration value for the sample.

Accuracy of the measurement was determined by analyzing duplicate samples and the error was found to be <5%. A total of 97 samples from 3 cores were analysed by this method.

ii. $CaCO_3$ determination

$CaCO_3$ content of the sediment was determined using titration method following Herrin et al. (1958). About 1 gram of powdered sample was weighed in 250 ml beaker, 50 ml of 0.5 N HCl was added to the sample and heated to about 90°C for 20 minutes. The pH was tested using indicator paper, and if pH was found to be greater than 2, another 50 ml HCl was added and heated for 20 minutes. When pH remains <2, distilled water was added till the beaker becomes half-full and phenolphthalein indicator was added (2 to 3 drops) and stirred constantly and back titrated with 0.25N of NaOH to phenolphthalein endpoint. The $CaCO_3$ percent was calculated using the formula

$CaCO_3\%$ = 100 x 0.05 x (ml of HCl x normality of HCl) – ml of NaOH x normality of NaOH.

Reproducibility of the result was checked by analyzing duplicate samples and it was found to be better than ±10 %. A total of 593 samples were analysed for $CaCO_3$ determination.

iii. Determination of Sr content

0.1 to 0.2 g of bulk sample powders were weighted and dissolved in 1N HCl. The acid-insoluble residue was filtered out and total volume of the solutions was made to 100 ml. These solutions together with the standards prepared in the laboratory were analysed for Sr content by using Inductively Coupled Plasma-Atomic Emission Spectrometer (ICP-AES). The accuracy and reproducibility of the results were found to be <5%. A total of 212 samples from 5 cores were analysed for Sr content.

2.2.3. Stable isotope studies

Thirty lime mud samples from different cores were treated with 5.3% aqueous solution of sodium hypochlorite for 24 hours to remove the organic matter and was subsequently washed and dried. These powders were analysed for stable isotope (oxygen and carbon) analyses at the University of Wollongong, using Micromass PRISM III mass spectrometer with a Multiprep acid-on-individual-carbonate device with analytical conditions as described by Chivas et al. (2002). The precision of the results for $\delta^{13}C$ and $\delta^{18}O$ are found to vary from 0.002‰ to 0.007‰ and 0.004‰ to 0.012‰, respectively.

2.2.4. Magnetic studies

Magnetic susceptibility (MS) for sediment samples was determined on dried samples using a Bartington MS-2 magnetic susceptibility meter (with an AC magnetic field amplitude of 80 A/m) linked to a MS2B dual frequency sensor (470 Hz and 4700 Hz). Representative samples were air-dried and packed into 8 cm^3 styren cubic pots. The following magnetic parameters were measured: (a) Low

frequency, χ_{lf}, (0.47 kHz) and high frequency χ_{hf}, (4.7 kHz) magnetic susceptibilities are measured 3 times on each sample and the average of 3 measurements are presented as mass specific values in 10^{-8} m^3/kg SI units; (b) Frequency dependent susceptibility (χ_{fd}%) is determined using a formula: $\chi_{fd}\%=(\chi_{lf} - \chi_{hf})/\chi_{lf}$ x 100 (Mullins and Tite, 1973). After measuring magnetic susceptibility, the samples are demagnetised in a Molspin AF demagnetiser. All remanences are measured using a Molspin fluxgate spinner magnetometer; (c) Anhysteritic Remanent Magnetization (ARM) was imparted to the samples by superposing a DC biasing field of 0.05 mT on a smoothly decreasing alternating field with a peak of 100 mT. It is customary to express ARM as an anhysteritic susceptibility χ_{ARM} (mass specific ARM / strength of the biasing field); (d) Isothermal Remanent Magnetizations (IRM) acquisition was carried out using a Molspin Pulse Magnetizer. Saturation Isothermal Remanent Magnetization (SIRM) was imparted using a maximum field of 1T. SIRM responds primarily to ferromagnetic material concentration, but unlike low field susceptibility (χ_{lf}) it is not affected by dia-magnetic and paramagnetic minerals. After acquisition of SIRM, the samples were subjected to reverse DC fields of 0.3T and the remanence was measured by using the Molspin magnetometer. To investigate the magnetic mineral composition, (e) HIRM (hard IRM) and (f) S-ratio ($S_{0.3T}$) are calculated using the definitions of Robinson (1986) and Bloemendal et al. (1992), respectively, where HIRM = $(IRM_{1T}+IRM_{-0.3T})/2$ and S-ratio% = $((1-IRM_{-0..3T}/IRM_{1T})/2)$ *100. The ratios of (g) χ_{ARM}/SIRM and χ_{ARM}/χ_{lf} are calculated to identify the presence of stable single domain magnetic grain sizes (0.03 to 0.06 μm) unambiguously in the sediment cores.

The Magnetic parameters for 12 cores (GC-1, GC-2, GC-3, GC-4, GC-5, GC-6, GC-7, GC-8, GC-11, GC-12, GC-14 and GC-15) were determined at Indian Institute of Geomagnetism (IIGM, Alibagh) and the MS of the sediments of three cores (GC-9, GC1-0 and GC-13) was determined at the Department of Marine Geology, Mangalore University, using the same instrument and the same

instrumental settings as at IIGM. A total of 1715 samples were subjected to the measurements of rock-magnetic parameters.

2.2.5. Radiocarbon dating

Representative bulk sediment samples at different intervals from each core were sent to the Birbal Sahni Institute of Palaeobotany (BSIP), Lucknow for radiocarbon age measurements. Measured ^{14}C ages obtained from BSIP were calibrated using CALIB rev. 4.3 of Stuiver et al. (1998) and are given in Table 2.2. During calibration a local deviation in ΔR - 163±30 for the northern Arabian Sea was used (Dutta et al., 2001). Corrected ages were obtained by subtracting surface ocean reservoir age 400 years and 163 years in local deviation in ΔR. Age was determined for 35 samples. Accelerator Mass Spectrometer (AMS) ages of the sediment cores of the southwestern margin of India (GC-12, GC-15- Kessarkar et al., 2003; GC-13- Thamban et al., 2001) were also utilised in Chapter 3. A total of 50 radiocarbon ages were used. The radiocarbon ages discussed in this thesis are calibrated ages (ka BP).

Table 2.2. Details of radiocarbon analyses on different sediment sections of the cores

Sl. No.	Core No.	Water depth (m)	Depth Interval dated (cm)	Lab. Code	Measured age (yr BP)	Calibrated age (ka BP)
1	GC-1 / SK-148/22	56	70-74	2020#	8990 ± 100	9.38
2	‘		105-110	2000#	12670 ± 200	14.05
3	‘		140-145	2019#	12230 ± 140	13.54
4	‘		200-205	1804#	11330 ± 140	12.76
5	‘		305-310	2001#	13250 ± 120	14.52
6	‘		400-405	1780#	15370 ± 550	17.60
7	GC- 2 /SK 148/21	1900	21-22	2079#	5210 ± 120	5.40
8	‘		54-55	2082#	16140 ± 290	18.48
9	‘		156-158	2106#	17510 ± 270	20.06
10	GC-3 / SK-148/31	65	20-22	1891#	7810 ± 100	8.07
11	‘		60-62	1792#	9950 ± 290	10.55
12	‘		74-82	2004#	11130 ± 140	12.46
13	‘		148-150	2032#	10910 ± 220	12.00
14	‘		220-235	2030#	11610 ± 280	12.98
15	‘		560-565	2017#	11340 ± 160	12.78
16	GC-4 / SK-148/32	111	26-28	1959#	6380 ± 70	6.64
17	‘		96-100	1979#	8240 ± 120	8.53
18	‘		178-180	2028#	10840 ± 160	11.91
19	‘		210-215	1984#	11430 ± 150	12.81
	‘		370-375	1975#	11060 ± 200	12.29
20	GC-5 / SK-148/30	121	26-30	1985#	5220 ± 100	5.41
21	‘		98-102	1963#	10230 ± 100	10.74
22	‘		136-138	1973#	12700 ± 140	13.99
23	‘		360-365	1980#	14070 ± 130	16.10
24	GC-6 / AAS 42/22	330	32-38	2139#	3200 ± 100	2.80
25			52-54	2147#	3470 ± 100	3.10
26			190-195	2168#	6770 ± 100	6.05
27			230-235	2160#	10440 ± 140	11.20

Continued...

Continuation of table 2.2

Sl. No.	Core No.	Water depth (m)	Depth Interval dated (cm)	Lab. Code	Measured age (yr BP)	Calibrated age (ka BP)
28	GC- 7 /AAS 42/20	420	52-54	2137#	11000 ± 130	12.15
29	‘		190-195	2135#	13700 ± 150	15.70
30			280-285	2110#	13880 ± 160	15.88
31			420-425	2149#	21590 ± 290	--
32	GC-9 / SK-148/43	115	26-28	2015#	11780 ± 120	13.05
33	‘		95-100	2034#	12800 ± 180	14.09
34	‘		210-215	2035#	12720 ± 120	13.99
35	‘		270-275	2022#	12760 ± 180	14.08
36	GC-12 /SK126/39	1940	25-30	KIA15267*	6720 ±30	7.1
37	‘		55-60	KIA14567*	9275 ±45	9.7
38	‘		120-130	KIA14568*	15120 ±70	17.3
39	‘		150-160	1573#	18790 ±680	21.6
40	‘		230-240	1570#	22230 ±360	
41	GC-13 / AAS VI/5	280	45-50	KIA5215*	2670 ± 30	2.33
42	‘		100-105	KIA5216*	5270 ± 50	5.62
43	‘		145-150	KIA5217*	11340 ± 60	12.86
44	‘		195-200	KIA5218*	13270 ±70	15.53
45	‘		245-250	KIA5219*	13920 ±70	16.20
46	GC-15 /SK126/16	1420	20-25	KIA14563*	6875 ±40	7.3
47	‘		45-50	KIA14564*	10090 ±55	10.7
48	‘		75-80	KIA14565*	16000 ±80	18.4
49	‘		95-100	1583#	20630 ±220	23.7
50	‘		190-200	1581#	32470 ±580	

*- AMS ^{14}C ages. Samples measured: *G. ruber, Lab:* Leibniz Labour für Altersbestimmung und Isotopenforschung, Christian-Alberchts-Universität, Kiel, Germany.

- Samples measured: Bulk samples analysed at BSIP, Lucknow, India.

Chapter 3

Chapter 3

ROCK MAGNETIC RECORDS OF THE SEDIMENTS ALONG THE WESTERN MARGIN OF INDIA: EVIDENCE FOR LATE QUATERNARY CLIMATIC CHANGE

3.1. Introduction

The Arabian Sea is characterised by the reversal of monsoonal winds that results in large seasonal variations in upwelling and related primary productivity. Of the two monsoons (SW and NE monsoons), the SW monsoon is dominant in the Arabian Sea and surface winds associated with this season (June-September) blow from the southwest direction leading to the increase in continental humidity and precipitation over the Indian peninsula. As a consequence, the northeastern Arabian Sea receives eolian sediments transported from the Arabian coasts and high riverine input through the Indus River. The hinterland of the SE Arabian Sea (SW margin of India) also receives heavy rainfall (more than 3000 mm/yr) and upwelling waters in this region are capped by a thin lens (5-10 m thick) of warm, low-salinity water, which in part forms from local precipitation and in part from runoff from the narrow coastal plain (Jayakumar, 1999; Naqvi et al., 2000). During the SW monsoon, biological productivity increases and results in a permanent Oxygen Minimum Zone (OMZ) that impinges the continental margins at depths between 150 and 1200 m (Wyrtki, 1971; von Stackelberg, 1972). Intensity of the monsoons has varied through time during the Quaternary and this variability can be traced by measuring independent proxies from sediments of the continental margins. Relative changes in biological productivity can be determined from variations in the organic carbon (OC) and carbonate content of the sediment. Runoff from the land brings enormous terrigenous supply and variations in the composition and sources of terrigenous material deposited offshore can be investigated through the study of the rock-magnetic properties of the sediments. Runoff also influences the isotopic composition of the seawater. The oxygen isotope composition of the

planktonic foraminifers that lived in the near surface waters is influenced by both the changes in the global ice volume and variations in regional precipitation and river discharge.

The purpose of the chapter is to report the rock-magnetic properties of the sediment cores collected along the western margin of India and compare the results with other parameters such as acid-insoluble residue (AIR), OC, carbonate content and oxygen isotopes. Such a comparison will provide better understanding of the utility of rock magnetic properties for extracting the late Quaternary palaeoclimatic signal recorded in these sediments.

3.2. Previous studies

A few studies have reported magnetic susceptibility variations in sediments of the northern Indian Ocean, especially the ODP cores (721and 722) from the northwestern Arabian Sea and/or sediments of the deep Arabian Sea (Bloemendal and de Menocal, 1989; Shankar et al., 1994a; Sykes and Kidd, 1994; Meynadier et al., 1995; Hounslow and Maher, 1999). These workers identified the sources of lithogenic flux, the influence of aeolian sediment deposition from the Asian monsoon during different phases of the late Quaternary, controls on magnetic susceptibility (carbonate dilution, diagenetic changes, paramagnetic minerals) and magnetic responses to climatic changes. The influence of the Antarctic bottom water current responsible for the transportation of fine-grained magnetic minerals during warmer episodes was traced by reporting the magnetite / hematite ratio in the Somali Basin (Meynadier et al., 1995). Sykes and Kidd (1994) used magnetic susceptibility along with spectral gamma rays to trace volcanic-rich sediments in the Indian Ocean. Prins et al. (2000) used magnetic susceptibility to identify eolian and Indus-borne sediments in the turbidites of the Indus Fan. Karbassi and Shankar (1994) applied rock magnetic techniques locally to the riverine and estuarine sediments of Mulki River, for stream-bed load sediments of Bhadra river to assess the influence of Kudremukh iron ore effluents (Shankar et al., 1994b) and off-shore placers of the SW coast of India (Shankar et al., 1996). Several workers used magnetic susceptibility data in correlation with

terrigenous content to extract high-resolution sedimentological data (Radhakrishnamurty et al., 1968; Somayajulu et al., 1975; Thompson et al., 1980; Bloemendal and de Menocal, 1989; Bloemendal et al., 1992, 1995; Yamazaki and Katsura, 1990; Robinson et al., 1995; Reichart et al., 1997; Rolph et al., 2004; Kessarkar et al., 2005). Here, detailed rock-magnetic studies along with other proxy records for the sediment cores along the western margin of India are reported for the first time.

3.3. Rock magnetic parameters

Magnetic susceptibility (MS) is related to total magnetic mineral concentrations in the sediments and, in general, is an expression of detrital input and the dilution by dia- and other paramagnetic minerals. The basic parameters that indicate variations in magnetic mineral concentrations are χlf, χARM and SIRM. These parameters increase in value as the concentrations of magnetic material in the sediment increase. χlf represents the total contribution from Fe-bearing minerals in the mineral assemblage (Thompson and Oldfield, 1986). It shows the least grain size dependence and is therefore possibly the best parameter for assessing concentrations (Peters and Dekkers, 2003). The χARM is controlled by the concentration of SSD and PSD ferrimagnetic grains (King et al., 1982). SIRM increases in value with an increase in the concentration of fine magnetic grain sizes (single domain) (Bloemendal et al., 1992). The interparametric ratios (χARM /χlf and χARM / SIRM) vary inversely with magnetic grain size and can be used to assess the relative change in concentrations of finer magnetic grain sizes. SIRM/χlf and χARM/χlf ratios are low for multidomain (MD>1 μm) and superparamagnetic (SP<0.03 μm) grains and high for single domain (SD- 0.03 to 1 μm) grains (Maher and Taylor, 1988). The S-ratio% and HIRM reflect variations in the coercivity spectrum of the magnetic mineral assemblage and therefore in mineralogy. The S ratio% is a ratio of high coercivity minerals (e.g. hematite/goethite) to low coercivity magnetic minerals (titano-magnetite and maghemite). Values of S-ratio% of ~100 indicate a high proportion of magnetite, whereas lower values indicate an increasing

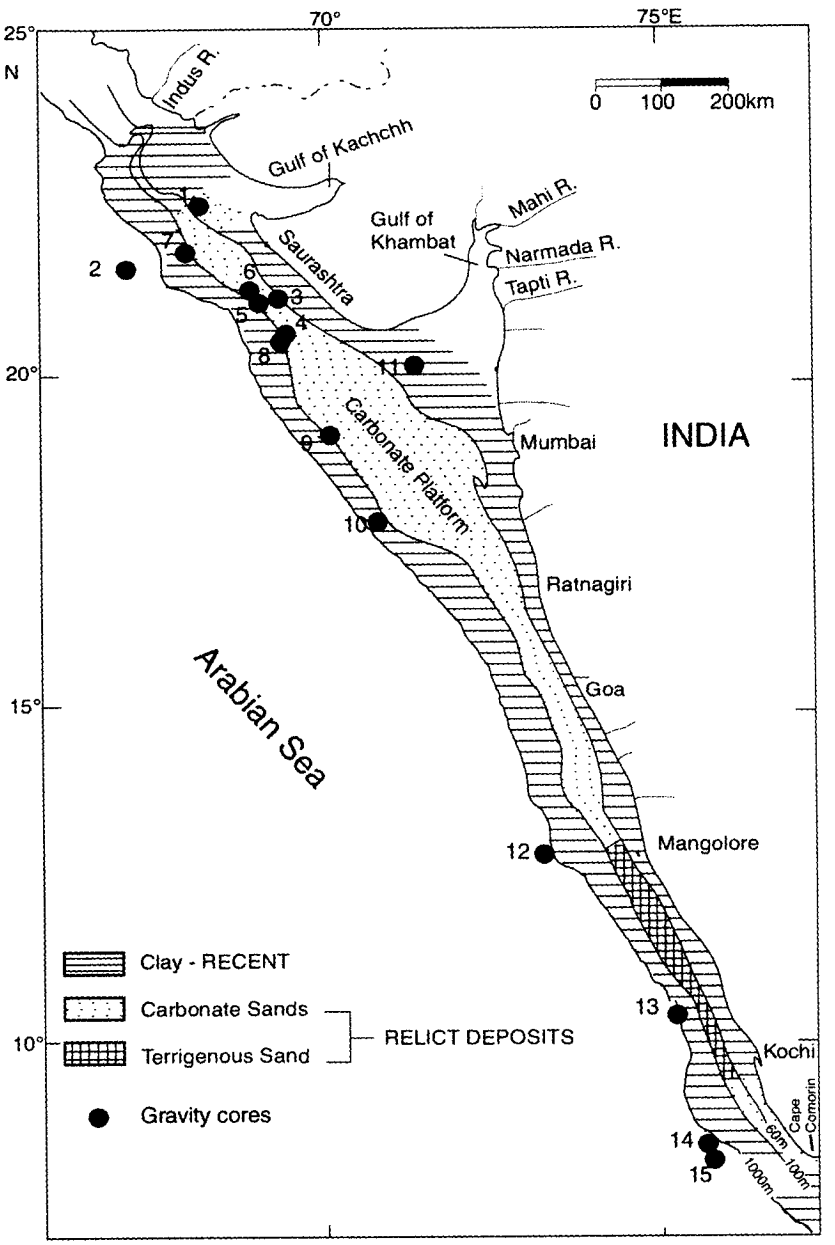

Fig. 3.1. Location of gravity cores on the western margin of India. Geology after Rao and Wagle (1997)

proportion of the hematite and goethite. The S-ratio % is independent of concentration, but HIRM varies with the concentration of high coercivity minerals (Thompson and Oldfield, 1986; Robinson, 1986). Unlike χ_{lf}, remnant properties such as S-ratio%, χ_{ARM} and SIRM are unaffected by variations in the paramagnetic components or carbonate content of the bulk sediment (Rolph et al., 2004).

3.4. Results

The sediments from fifteen gravity cores collected along the western margin of India at depths between 31 m and 1940 m (Fig. 3.1) were investigated for different rock-magnetic properties. Methodology for obtaining these properties is given in Chapter 2. The results obtained were analyzed in relation to the other sedimentological (grain size, acid-insoluble residue, OC, carbonate content) parameters. Oxygen isotope data of the planktonic foraminifers was also given wherever available.

In general, the cores recovered are of three types. Type 1 cores exhibit two distinct sedimentary units: lime mud dominated sediments in the lower section (unit 2) and terrigenous dominated sediments in the upper section (unit 1). Type 2 cores exhibit abundant lime mud or calcareous sand dominated (80-95% carbonate) sediments throughout the core. Type 3 cores contain predominantly terrigenous sediments. For convenience of description, sediment properties are outlined from three different areas.

3.4.1. Off Indus – Gulf of Kachchh (2 cores)

The core off the Gulf of Kachchh (GC-1) was recovered from the shelf at 56 m depth, while the one off Indus (GC-2) was at 1900 m depth (Fig. 3.1). The sediments of GC-1 represent Type 1 core with two sedimentary units. The lower unit 2 section of the core shows carbonate content increases while the acid-insoluble residue (AIR) content decreases from the base to the top of

the unit (Fig. 3.2A, Table 3.1). The median grain size of the mud fraction (<63 μm) ranges between 10 and 12 μm. Sand content is extremely low (<5%) and comprises mica flakes, quartz and pyritized grains. Illite and chlorite are the dominant clay minerals in <2 μm fraction. Magnetic susceptibility values are largely <5 SI units, except at the base of this unit. Unit 1 of the core is characterized by increased sand content, mostly of biogenic origin. Green clay infillings and molds of planktonic and benthic foraminifers largely constitute the coarse fraction. Carbonate content was high at the middle of this unit and then decreases towards the core top (Fig. 3.2A). Although clay minerals are dominated by illite and chlorite, the smectite content increases towards the core top (See Chapter 6, Fig. 6.3). MS values progressively increase from the base of unit 1 to the surface and reach a value of 25 SI units at the core top.

The core GC-2 represents Type 3 variety, dominated by terrigenous material (Fig. 3.2B, Table 3.2). Down- core variations show that the CaCO3 content varies from 28% to 50% and the AIR content from 50% to 72%. MS values are uniformly low (~25–30 SI units) until 18 ka, after which MS increases progressively to about 45 SI units at the core top (Fig. 3.2B). The LGM-Holocene amplitude in δ18O value is 1.98‰ (LGM -0.18‰; Holocene -2.16‰). The down-core variations exhibit a broad hump of high AIR content at about the LGM (54 to 200 cm) coinciding with low values of MS and S-ratio%, high HIRM values, low OC and CaCO3 contents and decreasing δ18O values. At about 16 ka the increase in magnetic parameters begins while AIR is decreasing and CaCO3 increasing (Fig. 3.2B). Thereafter in the Early Holocene sediments the progressive increase in magnetic concentration (MS, χARM and SIRM) and grain size (χARM/χlf and SIRM/χlf) parameters corresponds well with the increased OC content. The δ18O values further decrease during this period and also in late Holocene sediments. Magnetic mineral parameter, S-ratio%, shows a sharp increase and HIRM decreases after 16 ka and remains consistent during Early and Late Holocene sediments. The χfd values vary between 5% and 15% until 18 ka and ~7% for the Holocene sediments. Illite and chlorite are the major clay minerals in

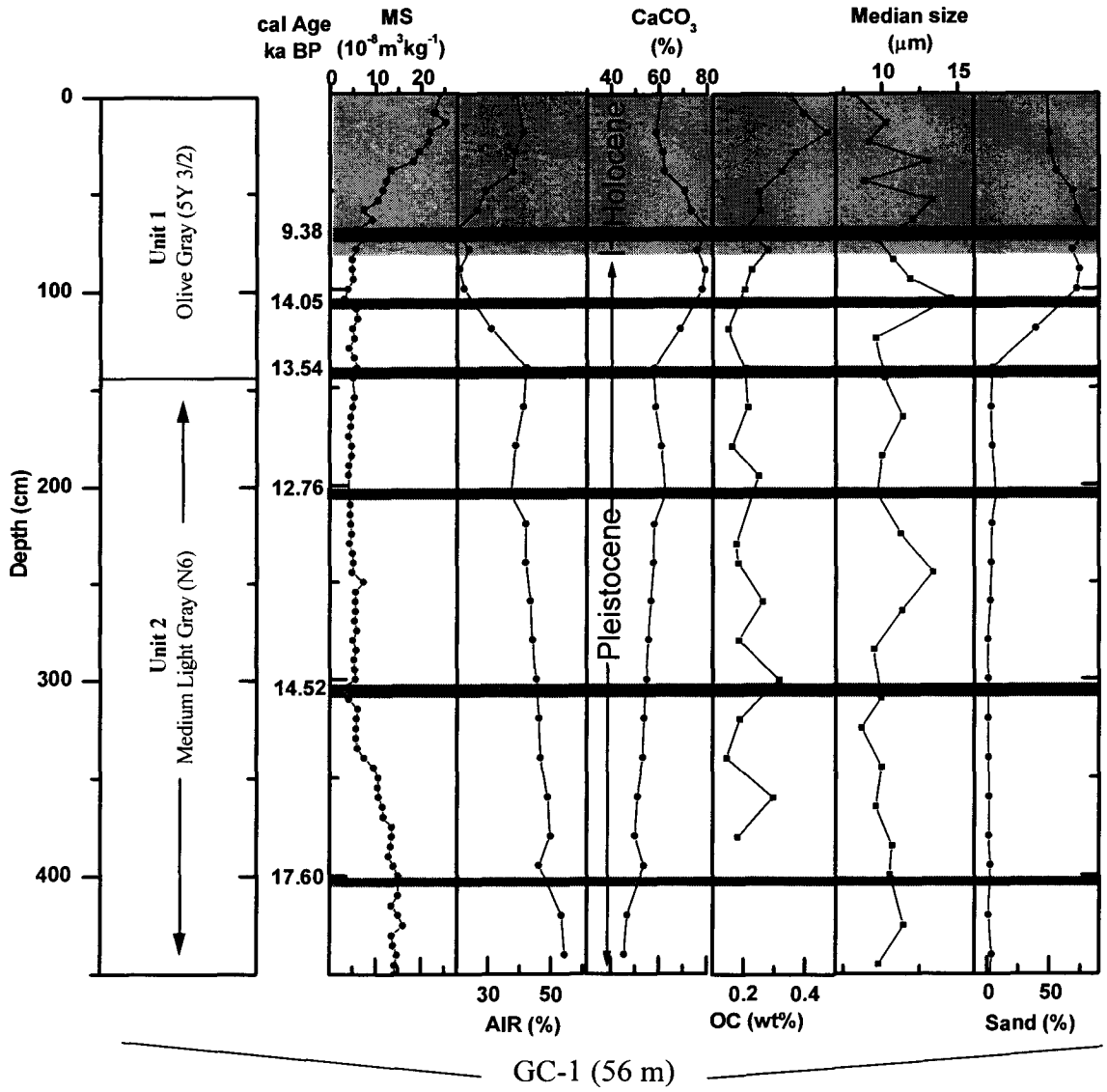

Fig. 3.2A. Down-core variations of Magnetic susceptibility (MS) , acid insoluble residue (AIR), $CaCO_3$, organic carbon (OC), median size of the terrigenous mud and sand content of the sediments in **GC-1**.

glacial sediments and smectite content increases towards core top at the expense of illite and chlorite (unpublished data). Palygorskite reflections are more distinct in the interglacial sediments than that of glacial sediments (Fig. 3.2C)

3.4.2. Saurashtra - Ratnagiri (9 cores)

The cores in this region were recovered at depths between 31 m and 500 m. Of the 9 cores, four cores are characteristic of Type 1 (GC-3-6), four cores are of Type 2 (GC-7-10) and one core (GC-11) is Type 3 sediment. Type 1 cores exhibit a thick (400-500 cm) lime mud-dominated section (unit 2) overlain by a thin (<100 cm to 150 cm) terrigenous sediment-dominated section (unit 1) (Fig. 3.3A-B). In general, the carbonate content of the unit 2 sediments of the different cores (GC-3, GC-4, GC-5, GC-6) ranges from 70% to 95% and AIR ranges from 5% to 30% (Tables 3.3, 3.4, 3.5 and 3.6). Median grain size increases from 10 μm at the base to 15 μm at the top of unit 2. Sand content varies from 5% to 30% and is composed of quartz, mica flakes, glass spicules and diatoms. MS values are uniformly low (<5 SI units) in this unit and do not vary despite increased sand content at certain intervals (see GC-4, GC-6 - Fig. 3.3A, Tables 3.4 and 3.6). Illite and chlorite are the dominant clay minerals in the <2 μm fraction. In the unit 1 sediments of the different cores the decrease in carbonate content is compensated by an increase in the terrigenous fraction (GC-4, GC-6 – Fig. 3.3A). The sand content of unit 1 varies in each core, either increasing from the base of the unit to the core top (GC-3-4) or decreasing (GC-5-6). Intervals of high sand content are composed of authigenic green clay infillings and molds of planktonic and benthic foraminifers. The median grain size of the mud fraction varies between 5 μm and 30 μm. Despite increase in OC, AIR and median grain size from the base to the top of unit 1 (see GC-6 - Fig. 3.3A, Table 3.6) there is not much change in MS values (also see GC-3 - Fig. 3.3A, Table 3.3), except near the core top wherein MS changes up to a value of 100/200 SI units. Progressive increase of MS in unit 1 sometimes corresponds to

increase in sand content (see GC-3-Fig. 3.3A) or median grain size in certain other cores (see GC-4-Fig. 3.3A).

Detailed mineral magnetic properties of GC-5 (Fig. 3.3B, Table 3.5) show an in-phase relationship with AIR in unit 1 sediments. Progressive increase in MS corresponds to the increase in AIR content and OC. Magnetic concentration parameters (MS, SIRM and χ_{ARM}) start increasing from the base of unit 1. The χ_{fd} values range up to 5% throughout the core with minor variations at the lower part of unit 1 sediments. Down-core distribution of SIRM/χ_{lf} and χ_{ARM}/χ_{lf} ratios are coherent with each other with marginally higher ratios in unit 1. Similarly, HIRM values in unit 1 show a general increase from the values displayed in unit 2, but HIRM also shows significant variation within unit 1 (Fig. 3.3B). Within unit 2, the S-ratio remains close to 90% and falling to ~75% in the lower few cm of unit 1 before increasing abruptly in the Holocene. Above this point, S-ratio values are maintained close to 95% for the remainder of the unit 1. The 30 cm zone of lower S-ratio values at the lower part of unit 1 is accompanied by an increased sand content, a decrease in ferrimagnetic grain-size (an increase in ratios with ARM as the numerator - χ_{ARM}/χ_{lf}, χ_{ARM}/SIRM) and the beginning of the increasing trend in OC and AIR% (Fig. 3.3B).

Type 2 cores (GC-7, GC-8, GC-9, GC-10; Figs. 3.4A-B) contain 80%-95% carbonate either in the form of lime mud or calcareous sand. Median grain size of the mud fraction ranges between 10 and 15 μm in the lower section and progressively decreases towards the core top. The MS values (Figs. 3.4A-B) are either negative or slightly positive (GC-7, GC-8, GC-9 - Figs. 3.4A-B, Tables 3.7, 3.8 and 3.9) or range up to a maximum of 4 SI units in different cores (GC-10 -Fig. 3.4B, Table 3.10). The very low or negative MS values correspond to very high carbonate (>85%) content of the cores. The radiocarbon age of the lime sediments varies from 14.5 ka to 10 ka in different cores (Chapter 2, Table 2.2).

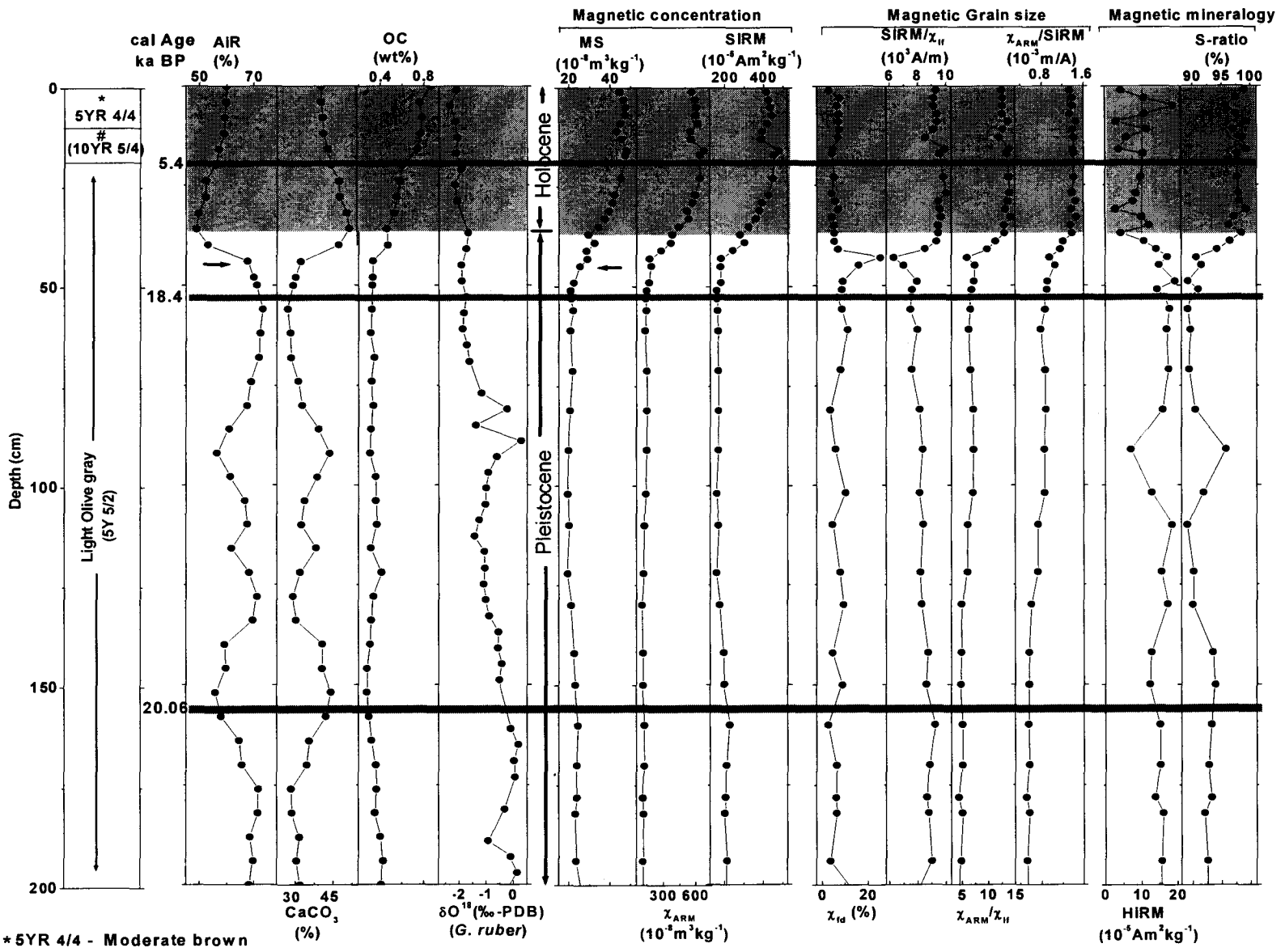

Fig. 3.2B. Down-core variations of sedimentological parameters, $\delta^{18}O$ of the *Globigerinoides ruber* and rock magnetic properties in **GC-2**. Arrows in the figure show changing sedimentary conditions after 16 ka.

The Type 3 core (GC-11, Table 3.11) contains predominantly terrigenous sediments (Fig. 3.5). The AIR content varies from 90% to 95% and smectite is the predominant mineral throughout the core (Unpublished data). MS values are the highest of all the cores studied and range between 250 and 500 SI units.

3.4.3. Off Mangalore - Cape Comorin (4 cores)

The cores in this region are of Type 3 variety and are dominated by terrigenous sediments. The core collected at 1940 m depth off Mangalore (GC-12) was investigated for OC, CaCO3, δ18O and rock magnetic properties (Fig. 3.6, Table 3.12). The OC concentrations are higher during the LGM (22.3 ka – 17.3 ka) and late Holocene, and lower during the early Holocene. Carbonate variations in the core (15-30%) follow the overall trend of OC, except in the late Holocene sediments (upper 20 cm of the core) wherein it shows an inverse relationship with OC (Fig. 3.6). The δ18O values are relatively high at about the LGM (-0.1‰) and started decreasing from 13 ka and lighter values (av. -2.7‰ – Holocene) occur during the early and late Holocene. The glacial and interglacial amplitude in δ18O value is 2.6‰. The MS record of this core is unique as it shows a gradual increase from near the bottom of the core (Fig. 3.6). The MS values are low (<20 SI units) at LGM (22.3 ka – 17.3 ka), gradually increases to 50 SI units at ~12 ka and remains steady to 8.5 ka, after which it progressively increases to a maximum of 90 SI units at ~7.5 ka. MS rapidly decreases to 40 SI units at the core top. In the late Holocene (upper 20 cm) the MS values shows an initial decrease followed by an increase towards core top coinciding with continuous increase in OC and AIR%. The increase of OC during the LGM (22.3 ka – 17.3 ka) coincides with slight increase in magnetic concentration parameters and decrease of AIR content. The down-core variations of MS, SIRM and χARM show broad agreement. The χfd% values are uniformly low, except in the upper 20 cm and below 22 ka BP, wherein relatively high χfd% coincides with low MS values (Fig. 3.6). Variations in the SIRM/χlf and χARM/χlf are parallel with maximum ratios occurring during the late Holocene sediments. Uniformly

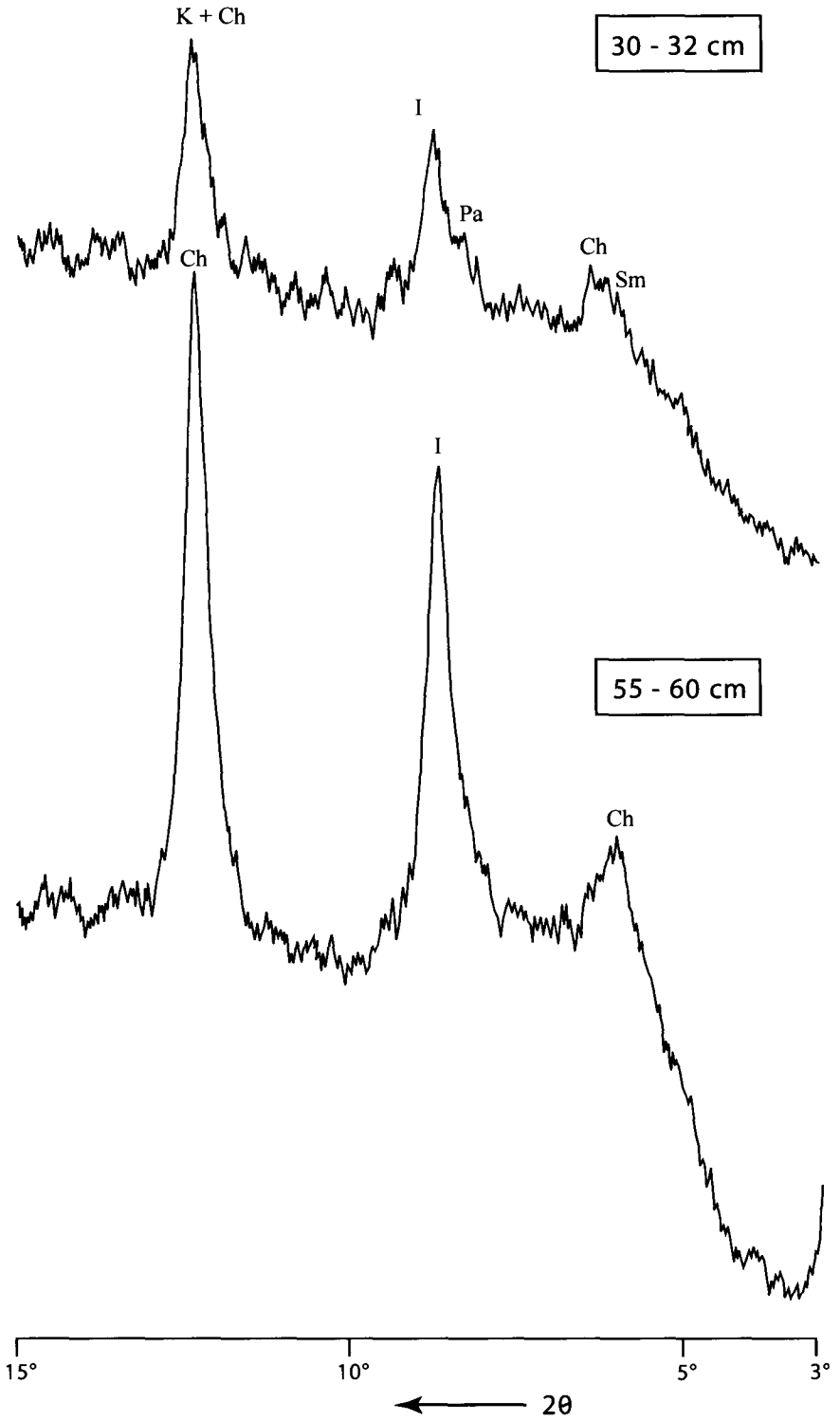

Fig. 3.2C. X-ray diffractograms of the <2 μm clay at LGM (55-60 cm) and Holocene (30-32 cm) intervals of the core **GC-2**; Sm-smectite, Pa-palygorskite, I-illite, K-kaolinite and Ch-chlorite.

low HIRM and high S-ratio% are characteristic throughout the core (Fig. 3.6). Overall the up core increase of magnetic concentration parameters coincides with the decreasing trend of $\delta^{18}O$ values (Fig. 3.6).

A sediment core at 280 m depth off Kochi (GC-13) was earlier investigated for $CaCO_3$, OC, texture and $\delta^{18}O$ values of planktic / benthic foraminifers (Thamban et al., 2001). The results show a strong correlation between $CaCO_3$ and OC, which were relatively high during early deglaciation (18-14 ka) and late Holocene (after 5 ka) and low during early Holocene (between 13.7 and 5 ka) (Fig. 3.7, Table 3.13). On the other hand, the clay content of the core was inversely proportional to the $CaCO_3$ content and was at a maximum (up to 77%) between 13 and 5 ka and relatively low (36-45%) during early deglaciation and late Holocene. The down-core variations of MS and clay content correlate with each other (Fig. 3.7). MS values are relatively low during the LGM and early deglaciation and start increasing from 14 ka BP. A broad hump of 40 SI units occurs between 13 and ~5 ka and then MS decreases to about 10-15 SI units during the late Holocene and at the core top (Fig. 3.7). The glacial-interglacial amplitude in $\delta^{18}O$ ($\Delta\delta^{18}O$) is 2‰. Despite there is a decrease of $\delta^{18}O$ values during the early Holocene, the values of MS and AIR do not change much and are consistently high (Fig. 3.7). The upward decrease of $\delta^{18}O$ values during the late Holocene coincide with the decrease of clay, AIR content and decrease of magnetic concentration parameters (MS, χ_{ARM}, SIRM) but with an increase in magnetic grain size parameters (SIRM / χ_{lf} and χ_{ARM} / χ_{lf}) and S-ratio%. S-ratios are 90-95% in early Holocene and late Pleistocene sediments and sharply decrease to 78% after 5 ka. Thereafter the S-ratio gradually increases to 90% at the surface.

MS values in the sediment cores off Cape Comorin (see GC-14, GC-15; Fig. 3.8, Tables 3.14 and 3.15), collected at about 1400 m depth are <10 SI units (GC-14) and remain more or less uniform for the larger part of late Pleistocene and Holocene sediments. The carbonate content in GC-15 is high (50-60%) during the late Pleistocene and gradually decreases to 40% during

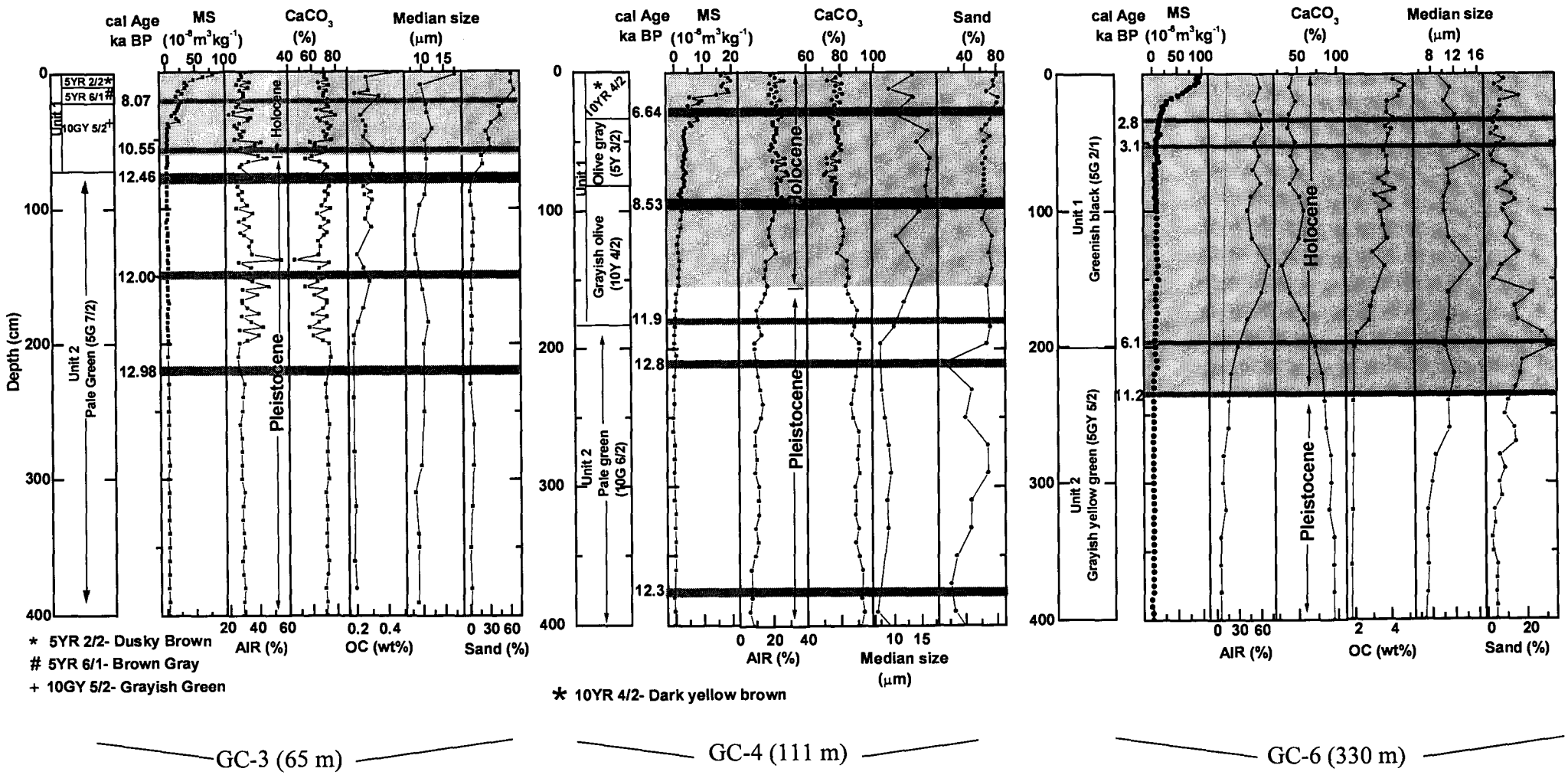

Fig. 3.3A. Down-core variations of magnetic susceptibility (MS) and different sedimentological parameters in **GC-3, GC-4 and GC-6.**

the Holocene and present. MS values in GC-15 vary from 3 to 8 SI units in the upper section and 2-5 SI units in the lower section (Fig. 3.8).

3.4.4. Variations in χ_{fd}%

The χ_{fd}% is a proxy for ultra-fine magnetic particles (Dearing et al., 1996) and indicates the presence of viscous grains at the superparamagnetic (SP) / stable single domain (SSD) boundary (0.03 μm). Low χ_{fd}% values are characteristic in many of the samples studied (Figs. 3.2B, 3.3B. 3.6 and 3.7). High concentrations of paramagnetic and diamagnetic components would lead to low χ_{fd}%. However, the χ_{fd}% values at certain intervals in different cores studied (see Figs. 3.2B, 3.3B, 3.6 and 3.7), range up to 25% and are more than the normally expected limit of ~15% (Dearing et al., 1996). It has been suggested that only the samples with a very narrow grain-size distribution and weakly interacting samples show higher χ_{fd} (30-50%) values (Worm and Jackson, 1999; Muxworthy, 2001). The interval with the highest values of χ_{fd}% correspond to the lowest MS values (see the sediments below 230 cm in GC-12 – Fig. 3.6; upper section of the core GC-13 - Fig. 3.7), not supporting the suggestion of increased superparamagnetic input. Moreover, one would expect the high χ_{fd}% values correlate well with the increased S-ratio%, i.e. magnetic softness, unless the high χ_{fd}% values correspond to an influx of material rich only in superparamagnetic and high-coercivity magnetic minerals. But the high χ_{fd}% values do not correlate with high S-ratio% (Fig. 3.3B and Fig. 3.7). Thus it is likely that the high χ_{fd}% values are erroneous and perhaps occurred when MS values of the sediments are close to the limit of resolution of the instrument, where background fluctuations are of the same order of magnitude as the MS value.

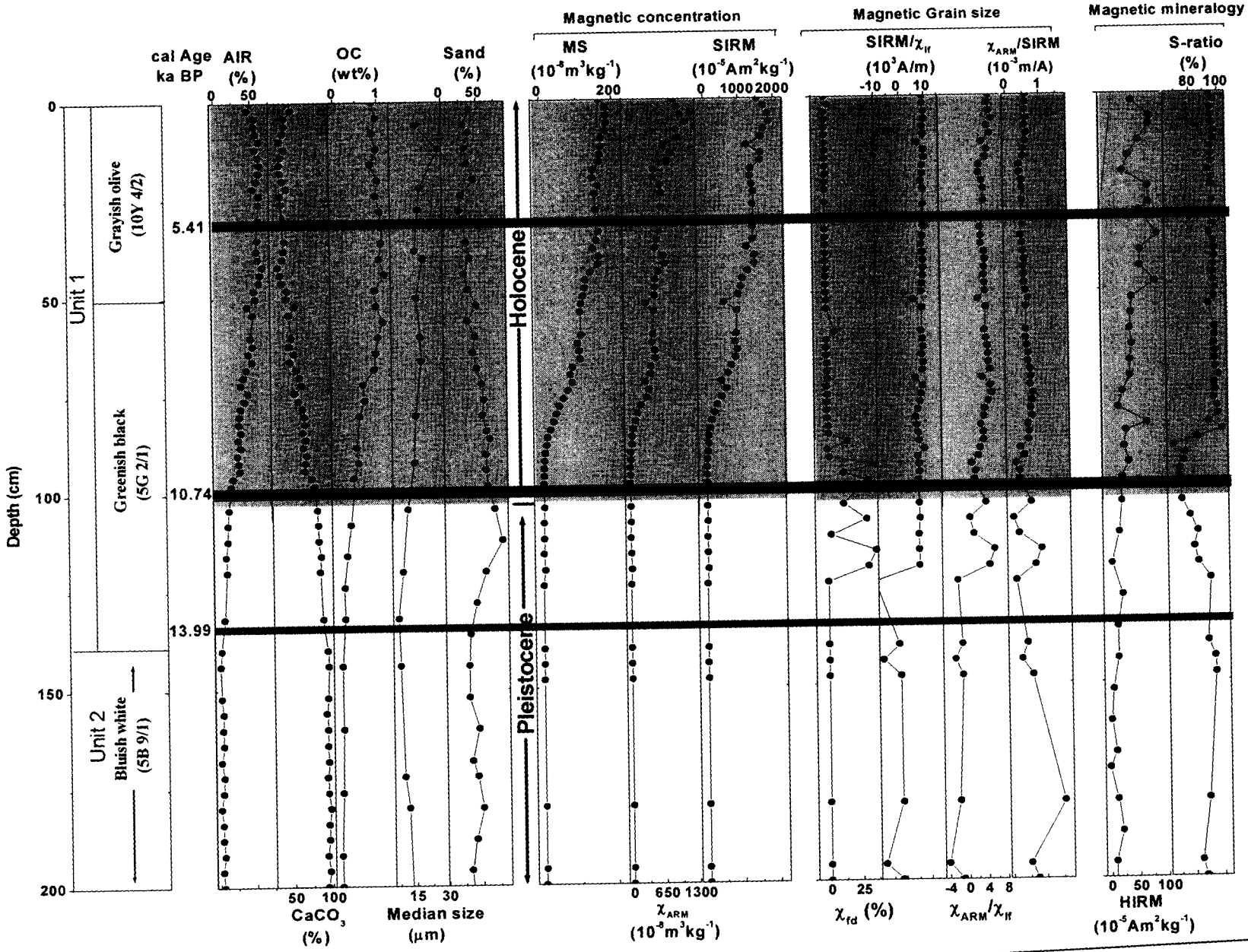

GC-5 (121 m)

-f different sedimentological parameters and rock magnetic properties in **GC-5.**

3.5. Discussion

3.5.1. Provenance of the surficial sediments

Earlier workers reported provenance of the sediments along the western margin of India based on the distribution of clay minerals of the 156 surficial sediments at water depths between 17 and 2000 m (Nair et al., 1982a; Rao and Rao, 1995) and Sr-Nd isotopes of the surface and sub-surface intervals of the sediment cores (Kessarkar et al., 2003) investigated in this study. The results indicate the existence of three mineralogical provinces derived from three different sources, namely, the illite and chlorite-rich assemblage from the Indus, smectite with minor kaolinite, illite and chlorite assemblage from the Deccan Trap basalts and smectite-kaolinite with minor illite, chlorite and gibbsite assemblage from the Gneissic province. The Sr-Nd isotopes provided distinct signatures of these mineral provinces and the influence of physical and chemical weathering on these isotopes.

The MS values in surficial sediments of the continental margins and deep-sea are controlled by several factors: (a) MS largely depends on the supply of land-derived material to the depositional site, which in turn controlled by the composition of source rocks. (b) Authigenic magnetite was reported in the sediments both in the aerobic and in the zone of nitrate reduction (Karlin and Levi, 1983; Peterson and von Dobeneck, 1986; Stolz et al., 1986; Canfield and Berner, 1987; Robert and Chamley, 1987; Yamazaki and Ioka, 1997). Moreover, a high abundance of living magnetotactic bacteria were reported in the upper most sediment of the continental margins of southwest Africa. Therefore, biogenic magnetite, though a minor component of the sediment, contributes towards the total MS signal. (c) Reductive diagenesis in organic-rich near surface sediments also modifies the MS signal by the dissolution of fine-grained magnetite and formation of iron sulfides such as greigite (Lepland and Stevens, 1996; Schmidt et al., 1999). (d) The matrix minerals (dia- or paramagnetic components) in the sediments also contribute

to the bulk susceptibilities. The formation of biogenic magnetite and the process of reductive diagenesis were largely confined to the subsurface sediments in the magnetic profiles studied here, and their influence on the bulk susceptibility of the surficial sediments appears minimal. We found that the changes in MS cannot be explained by varying carbonate content (see below) but are dominated by the provenance of the terrigenous component. As the Type 3 cores and unit 1 sediments of Type 1 cores of all the three regions are dominated by terrigenous material, the MS signatures of the surficial sediments (core tops) should allow us to identify the sediment provinces.

Higher MS values occur in the shallow water cores off Saurashtra – Ratnagiri (GC-3-11; Figs. 3.3-3.5) than in the cores off Indus - Kachchh (GC-1-2; Figs. 3.2A-B) and Mangalore - Cape Comorin (GC-12-15; Figs. 3.6-3.8). Water depth does not have a clear role, with MS values higher for a deeper water core (GC-2) than for a shallow water core (GC-1) from the same region. While in other cases MS values are similar (100 SI units) for cores recovered at different depths (see GC-3 & GC-6 – Fig. 3.3A). Although the core top sediments of the slope cores off Indus-Kachchh (GC-2) and Saurashtra-Ratnagiri (GC-5) contain similar OC values (<1%), their MS values are much different (Figs. 3.2B, 3.3B). The near surface sediments of these cores contain moderate carbonate content and MS signal cannot be explained by varying carbonate content. Authigenic processes are confined to sub-surface depths in the cores. These imply that MS variations in surficial sediments exhibit regional variations in accordance with their mineralogical provinces and the changes in MS may largely reflect the source rock composition and strength of the transporting medium. The cores of the Indus - Kachchh largely contain quartz, illite and chlorite-rich sediments derived from the physical weathering of the Precambrian gneissic rocks and transported through the Indus. MS values are low for the gneissic rocks. Moreover, the diamagnetic and/or paramagnetic characters of the matrix clay-sized minerals (quartz, illite and chlorite) usually have low or negative MS values. The cores off Saurashtra – Ratnagiri on the other hand, contain smectite-dominated

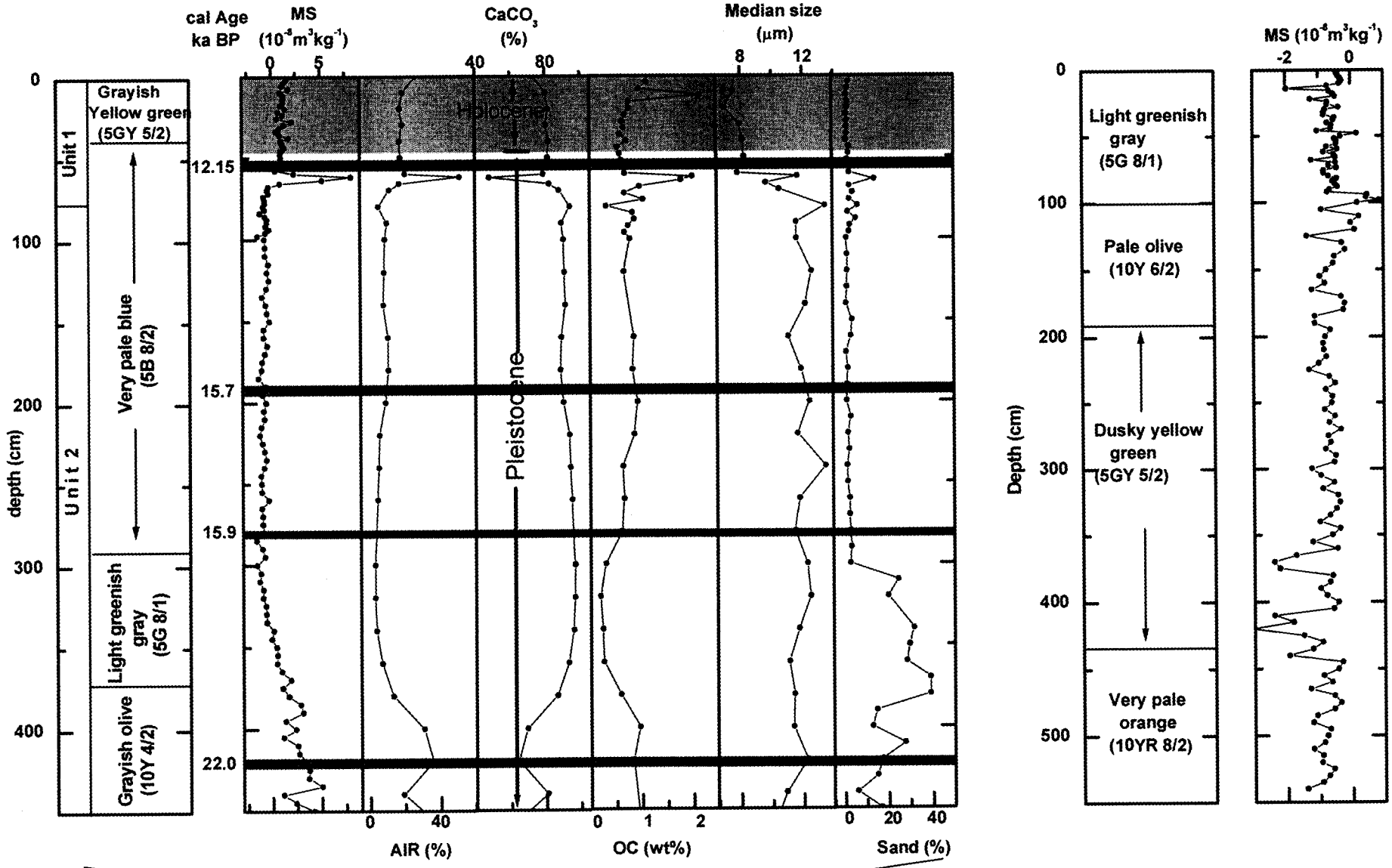

MS and different sedimentological parameters in **GC-7 and GC-8**

sediments derived from the Deccan Trap basalts, which supplies a significant amount of magnetic material. Basalts contain 2-6% iron oxide grains and are enriched with titano-magnetite (Thompson and Oldfield, 1986).

Low MS values in the cores off Mangalore - Cape Comorin may be due to the predominance of kaolinite and smectite derived from chemical weathering of the Gneissic and schistose rocks, which contain poorly magnetizable material. Despite similar source rocks (largely Precambrian gneisses and schists), MS values in the sediments off the Indus are higher than MS values off Mangalore – Cape Comorin. This may be because of two reasons. (a) As the sediments off the Indus are derived from the physical / mechanical weathering of the parent rock, they retain the higher primary magnetic mineral concentrations. Conversely, the hinterland (gneissic) rocks between Mangalore and Cape Comorin have been extensively lateritized and subjected to intense chemical weathering. As a consequence, most of the primary iron has been leached out, producing secondary magnetic minerals, and leaving the parent rocks with low MS values (Thompson and Oldfield, 1986). (b) The cores off Mangalore-Cape Comorin contain higher organic carbon in near surface sediments. Firstly, the OC is diamagnetic and the effect of varying OC content, although little, may have diluted the MS values. Secondly, reductive diagenesis is likely, at least, in some cores close to the denitrification zone (GC-12 – Fig. 3.6) that may have resulted in dissolution of magnetite and therefore decreased MS values.

3.5.2. Down-core variations of magnetic parameters and Climatic inference

i. Controlling Factors for MS variations

Magnetic susceptibility (MS) variations in the sediments are controlled by magnetic mineral concentration, grain size and carbonate content. Detrital magnetite is usually predominant in the sediments. However, the presence of authigenic iron-rich green clay (verdine / glaucony) minerals and biogenic

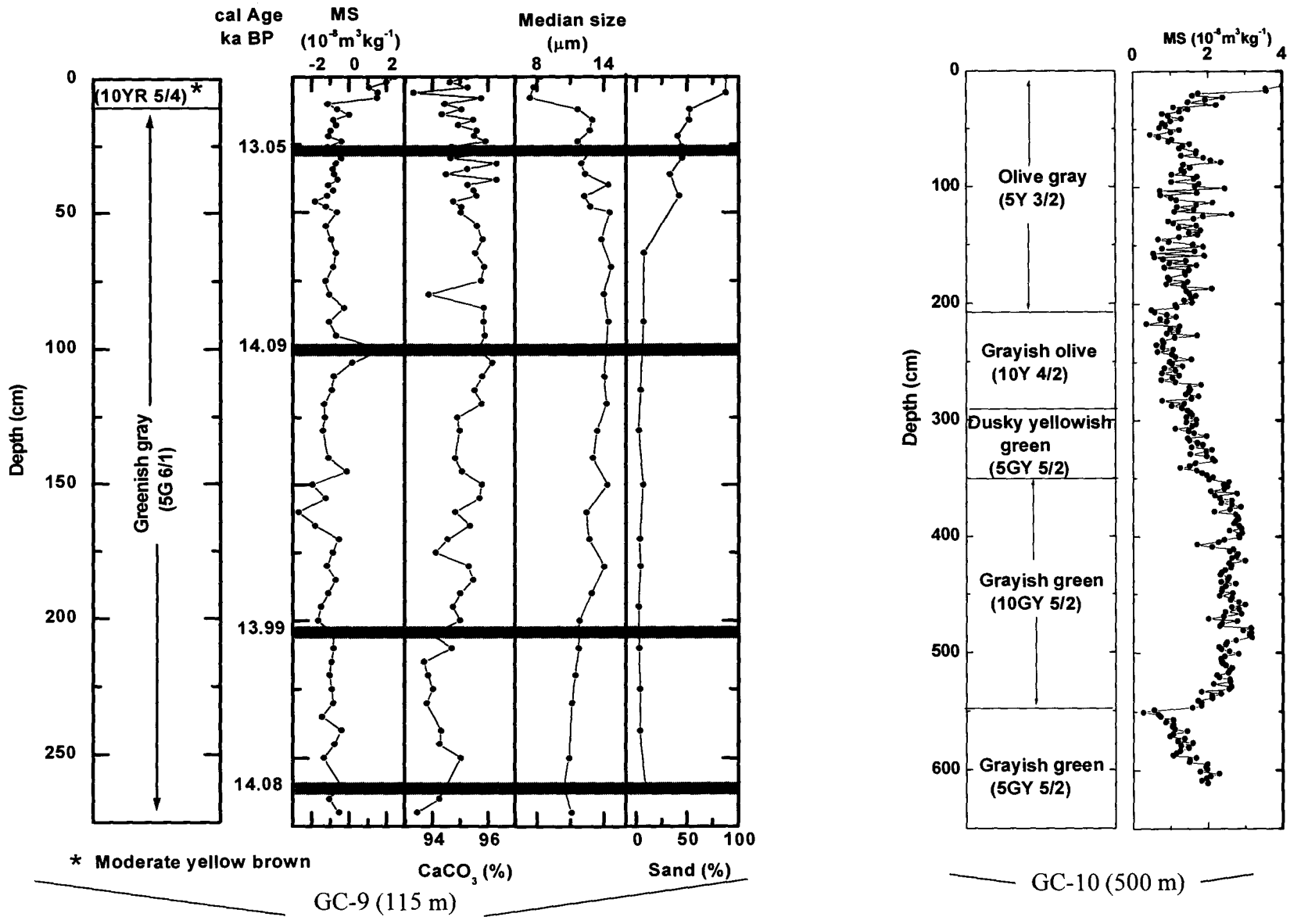

Fig. 3.4B. Down-core variations of magnetic susceptibility (MS) and different sedimentological parameters in **GC-9 and GC-10**

magnetites locally enhance the magnetic signal. The process of reductive diagenesis in organic-rich sediments reduces the MS signal.

a. Authigenic green clays: Iron-rich green clays, usually forming in shallow water depths, occur within the substrates of faecal pellets or skeletal chambers of planktic and benthic foraminifers and are associated with coarse-grained sediments (Odin, 1988). MS concentrations increase with increasing sand content (GC-3 - Fig. 3.3A; GC-9 - Fig. 3.4B), which comprises green clay molds and infillings of foraminifers. This indicates that the MS is partially controlled by authigenic green clay in the shelf/shelf break sediments.

b. Authigenic magnetite: Biogenic magnetite of bacterial / fungal origin, as a source for magnetic minerals, has been reported in the pelagic environments (Yamazaki and Ioka, 1997). It is fine-grained (<1 μm) and is not easily magnetized in a very small-induced magnetic field (Ellwood et al., 2000) produced by the MS meter. However, the magnetic concentration parameters (MS, χ_{ARM}, SIRM) in GC-2 start to increase while AIR is decreasing at about 16 ka (see arrow in Fig. 3.2B). Moreover, the trend of these magnetic parameters shows closer correspondence with the trend in organic carbon. This implies that the magnetic mineral perhaps be dominated by authigenic bacterial magnetite formed in response to increasing OC and the associated impact of environmental conditions, at least in this transition zone. Karlin and Levi (1983) reported the formation of authigenic magnetite of biogenic origin as an integral part of organic matter decomposition and its occurrence was reported both in the aerobic as well as in the zone between nitrate and iron reduction. Kirschvink and Chang (1984) suggested that bacterially precipitated magnetite might be a major source of stable magnetic remanence in some marine sediments. Petermann and Bleil (1993) reported magneto-tactic bacteria between depths of 1 and 4 cm in the sediments and their maximum concentrations occur in the anaerobic zone compared to only small numbers in the aerobic zone. Moskowitz et al. (1993) suggested that the biogenic magnetite and greigite are important source of fine-grained magnetic material that can contribute significantly to stable natural remnant

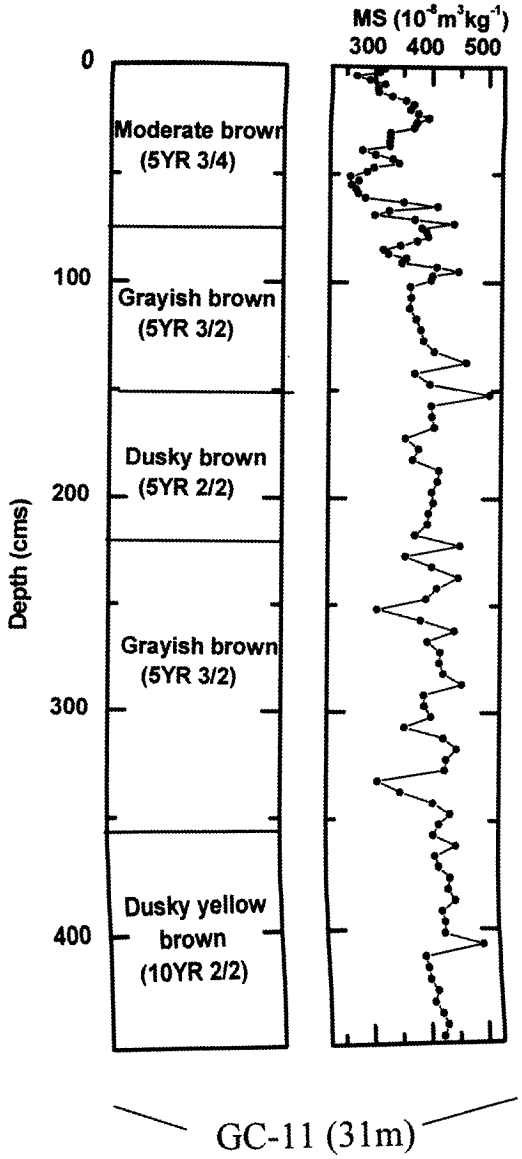

Fig. **3.5.** Down-core variations of magnetic susceptibility (MS) in **GC-11.**

magnetization in recent and ancient sediments. Magnetites are expected to dissolve during subsequent diagenesis. The low OC content (<1%) at these depth intervals may have prevented subsequent dissolution of the magnetite.

c. Carbonate content: MS values are usually influenced by the net carbonate content, which changes either through productivity variations or through dilution of terrigenous / siliceous flux. MS values are 25 SI units for 60% carbonate in GC-1 (Fig. 3.2A) and are 100 and 200 SI units for 70% and 45% carbonate in GC-3 and GC-5, respectively (see Figs. 3.3A-B). Similarly, MS values differ for nearly similar carbonate contents in cores GC-12 – GC-15 (see Figs. 3.6-3.8). These imply that the changes in MS in these cores cannot be explained by varying carbonate content and are dominated by changes in the provenance/grain size of the terrigenous component, together with authigenic processes. Negative or slightly positive MS values in Type 2 cores (Figs. 3.4A and 3.4B) and in unit 2 sediments of the Type 1 cores (Figs. 3.2A, 3.3A) are due to very high amount (90-95% carbonate) of biogenic material (lime mud or carbonate sand). It is well known that the diamagnetic minerals, such as calcite, produce negative MS. Moreover, Ellwood and Ledbetter (1977) showed that a 50% variation in carbonate content could bring only 2-3 units variation in MS. It appears that the MS of paramagnetic minerals is much greater than that of diamagnetic minerals and therefore a small amount of paramagnetic mineral can more significantly influence the MS than the more abundant diamagnetic minerals. As a consequence, the diamagnetic contribution of the varying carbonate content cannot explain the changes in the MS signal. If the carbonate variations are caused by dilution, especially by a terrigenous flux, then the corresponding variations in the MS profile are expected.

d. Grain size: MS values in Type 1 and Type 3 cores largely correspond to increases in the terrigenous silt size, which ranges between 10 and 15 μm. However, the MS increase in certain cores (see GC-1) corresponds with a decrease in median grain size of the silt (Fig. 3.2A) and in others (GC-5; Fig. 3.3B) with an increase in median size of the silt. Increased MS at certain

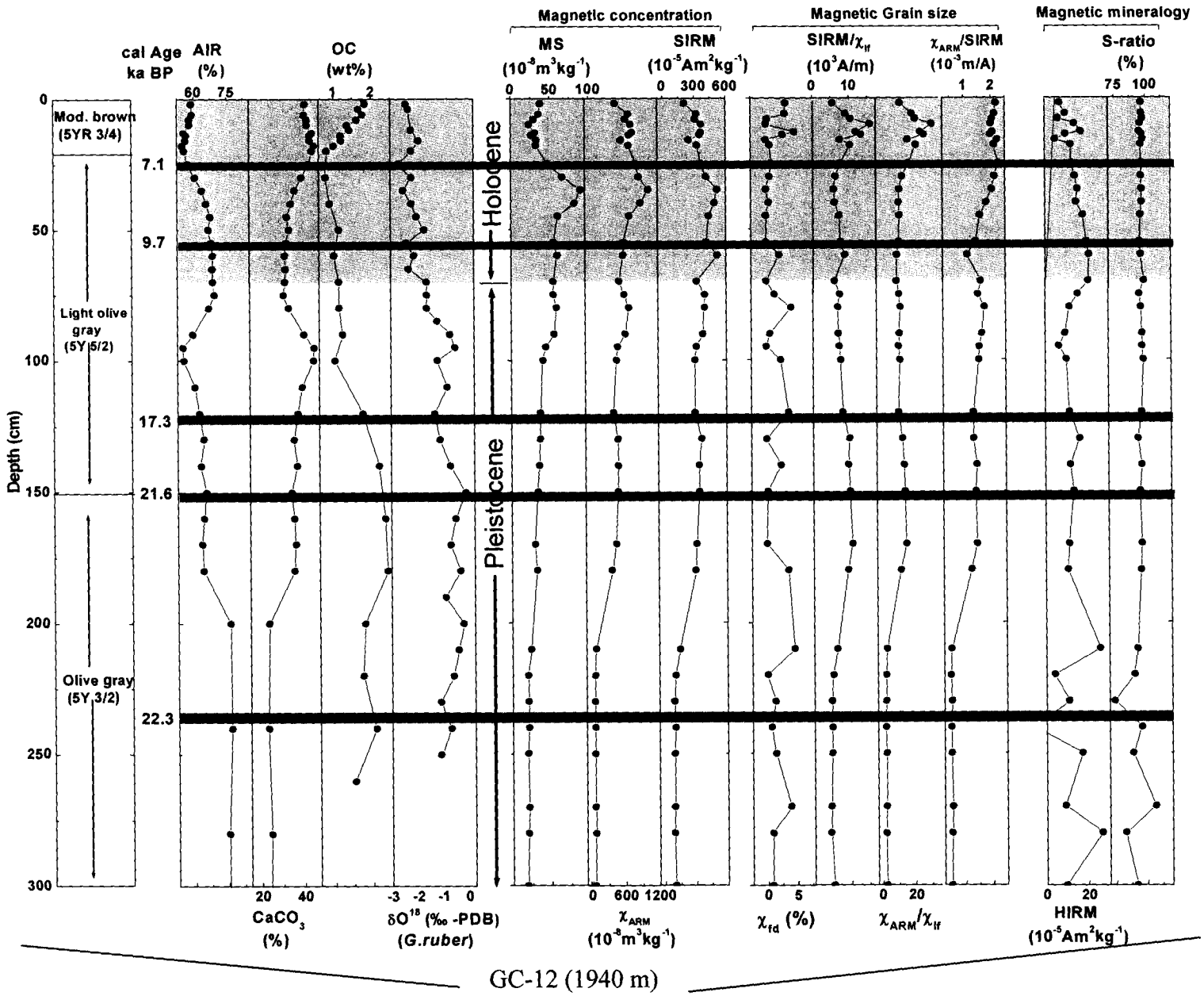

Fig. 3.6. Down-core variations of different sedimentological parameters, $\delta^{18}O$ of the *Globigerinoides ruber* and rock magnetic properties in **GC12.**

intervals in GC-3 (Fig. 3.3A) and GC-9 (Fig. 3.4B) corresponds to the increased sand content, which includes green grains (molds and infillings of iron-rich green clay).

e. Reductive diagenesis: The late Holocene sediments (between 5 and 2 ka) of the core GC-13 show decreased S-ratio%, magnetic concentration / grain size (χ_{ARM}/χ_{lf} and χ_{ARM}/SIRM) parameters and AIR contents that corresponding to the increased carbonate and OC contents (Fig. 3.7). Minimum values of interparametric ratios indicate an increase in ferromagnetic grain size. This may be due to the oxidative decomposition of organic matter, in which magnetite and other iron oxides become progressively reduced due to the processes of reductive diagenesis. Coincidence of increased OC and median grain size of the sediment with no marginal change in MS in GC-6 (Fig. 3.3A) may also be due to dissolution of authigenic magnetite due to reductive diagenesis. In reducing environments even well crystallized ferrimagnetic oxides become unstable and get dissolved and/or transform into iron sulphides. Bloemendal et al. (1993) suggested that reductive diagenesis is a significant determinant of sediment magnetic properties in high productive areas and has the effect of preferentially removing the fine-grained ferrimagnetic fraction. Several workers have shown that reductive diagenesis may greatly modify magnetic mineral inventories in deeper strata by dissolution of primary iron oxides and authigenic formation of magnetic iron sulfides (Schmidt et al., 1999; Brachfeld and Banerjee, 2000).

In GC-5, the reduction in S-ratio% results in a negative hump at the lower part of unit 1 sediments, between 13 and 9 ka (Fig. 3.3B). The S-ratio% starts decreasing with gradual increase in AIR and increase in χ_{ARM}/χ_{lf} and χ_{ARM}/SIRM ratios. Increase of χ_{ARM}/χ_{lf} in this part of the core indicates a much larger amount of finer grain sizes. OC content though increasing is still quite low (<0.5%) in this interval. The decreased S-ratios therefore are less likely due to diagenesis, but may be due to the increased proportions of high coercivity magnetic minerals transported from the shelf. The continental shelf was exposed to sub-aerial conditions during low-sea level stands of the Last

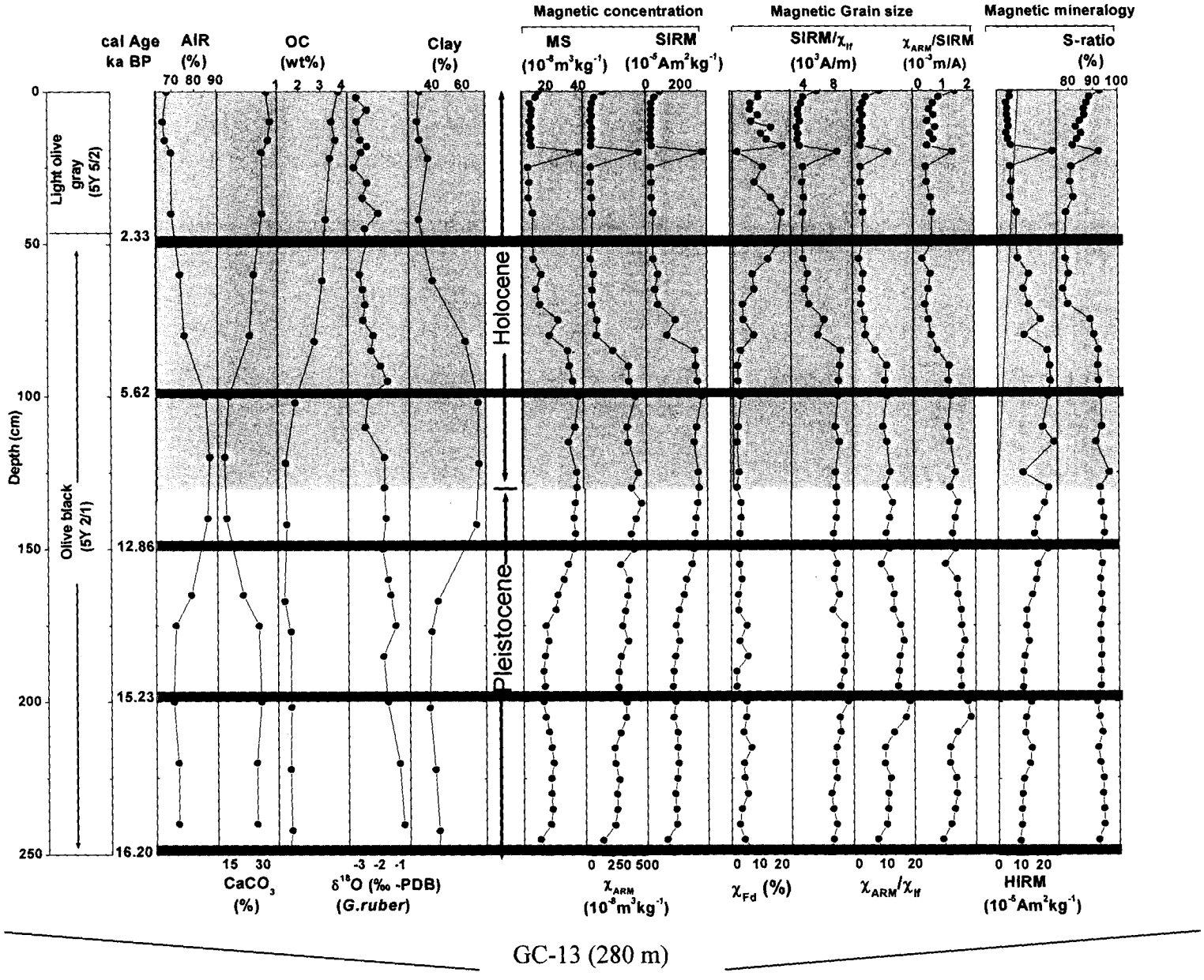

Fig. 3.7. Down-core variations of different sedimentological parameters, $\delta^{18}O$ of the *Globigerinoides ruber*. and rock [illegible] properties in **GC-13.**

Glacial Maxima. As a consequence the iron-rich clay minerals (green grains) and magnetites associated with the outer shelf sediments were oxidized and subsequently transported to the site, resulting in decreased S-ratio% (Fig. 3.3B).

ii. Climate inferences - Northwestern margin of India

Although the amplitudes of MS, χARM and SIRM variations are uniformly low in the late Pleistocene sediments in GC-2 (until 16 ka, see arrows in Fig. 3.2B), the AIR content shows significant down-core variations. In the interval containing the LGM 54-200 cm), increased AIR values correspond with decreased S-ratio% and increased HIRM values (Fig. 3.2B) indicating the presence of high proportions of high coercivity minerals such as hematite or goethite. These minerals are primarily regarded as products of continental weathering and diagnostic of eolian or fluvial influxes (Schmidt et al., 1999). Despite significant decrease in S-ratio%, the overall magnetic concentration parameters have not changed and magnetic grain size parameters showed a small increase (Fig. 3.2B). It could be that the magnetic minerals may have adhered to larger non-magnetic grains or clumped one to the other and transported together. Previous studies have indicated that lower S-ratios are an excellent proxy indicator of aeolian sedimentation in the marine environment (Robinson, 1986; Bloemendal et al., 1988), with hematite and goethite commonly present as staining on aeolian particles (Peck et al., 1994; Karbassi and Shankar, 1994). Palygorskite is a characteristic eolian mineral of Arabian provenance (Kolla et al., 1981a) and dispersal of this mineral is caused by the northwesterly winds that transport large quantities of eolian dust to the Arabian Sea. Relatively small or indistinct reflections of palygorskite in the sediments of the LGM (Fig. 3.2C) imply that the dust flux from Arabia did not reach the site at this time, perhaps due to a weaker SW monsoon. Since the hump of increased AIR and decreased S-ratio% further correspond to the gradual decrease of δ18O values, it is likely that the hematite/goethite flux adhered to flaky illite and chlorite minerals and was transported through fluvial supply. Alternatively, hematite/goethite-rich particles originating in the arid and semi-arid regions of the Indus River drainage basin could have undergone

aeolian transport to the core site. From the magnitude of the glacial/interglacial change in $\delta^{18}O$ value (1.98‰), fluvial supply may not have been the major factor. For example, of the 1.98‰, 1.2‰ accounts for the ice volume effect (Labeyrie et al., 1987) and ~0.5‰ for the regional sea surface temperature changes (Rostek et al., 1997). The remaining value (0.28‰), which can be attributed to local precipitation or river discharge, is insufficient to represent a major fluvial flux (compare the glacial/interglacial amplitude of this core with that of the cores from the SW margin of India). Therefore, the data suggest that hematite and goethite were supplied by dry winds coming from Pakistan and the Indus drainage basin during the LGM, producing the low S-ratio% seen in the lower 1.5 m of core GC-2. A cold and dry climate with weak SW monsoon activity during the LGM is supported by pollen and lake level studies from the northwest India (Singh et al., 1974; Swain et al., 1983; Wasson et al., 1984). Singh et al. (1990) further reported that a hyper-arid climate continued from the LGM to 13,000 yr. BP, due to low precipitation of the summer monsoon.

The changing sedimentary conditions in glacial and interglacial sediments of the core are distinct before and after 16 ka BP (see arrows in Fig. 3.2B). The gradual increase in magnetic concentration / grain size parameters with high S-ratio%, accompanied by increased OC and AIR contents corresponding to the gradual decrease in $\delta^{18}O$ values both during the early and late Holocene sediments (Fig. 3.2B). This indicates increased terrigenous supply due to intensified SW monsoon conditions. Distinct palygorskite peaks in these sediments (Fig. 3.2C) also support increased eolian flux from the Arabian Peninsula brought by the southwesterly winds. Prins et al. (2000) reported that the terrigenous sedimentation in the Indus Fan area was dominated by eolian dust of Arabian origin after 9 ka BP. However, von Rad et al. (1999) reported decreased eolian flux from glacial to interglacial times in the continental margin sediments off Pakistan.

In GC-5, the coincidence of consistently low χlf, χARM and SIRM values with high carbonate flux in sediments older than 13.99 ka suggests minimal

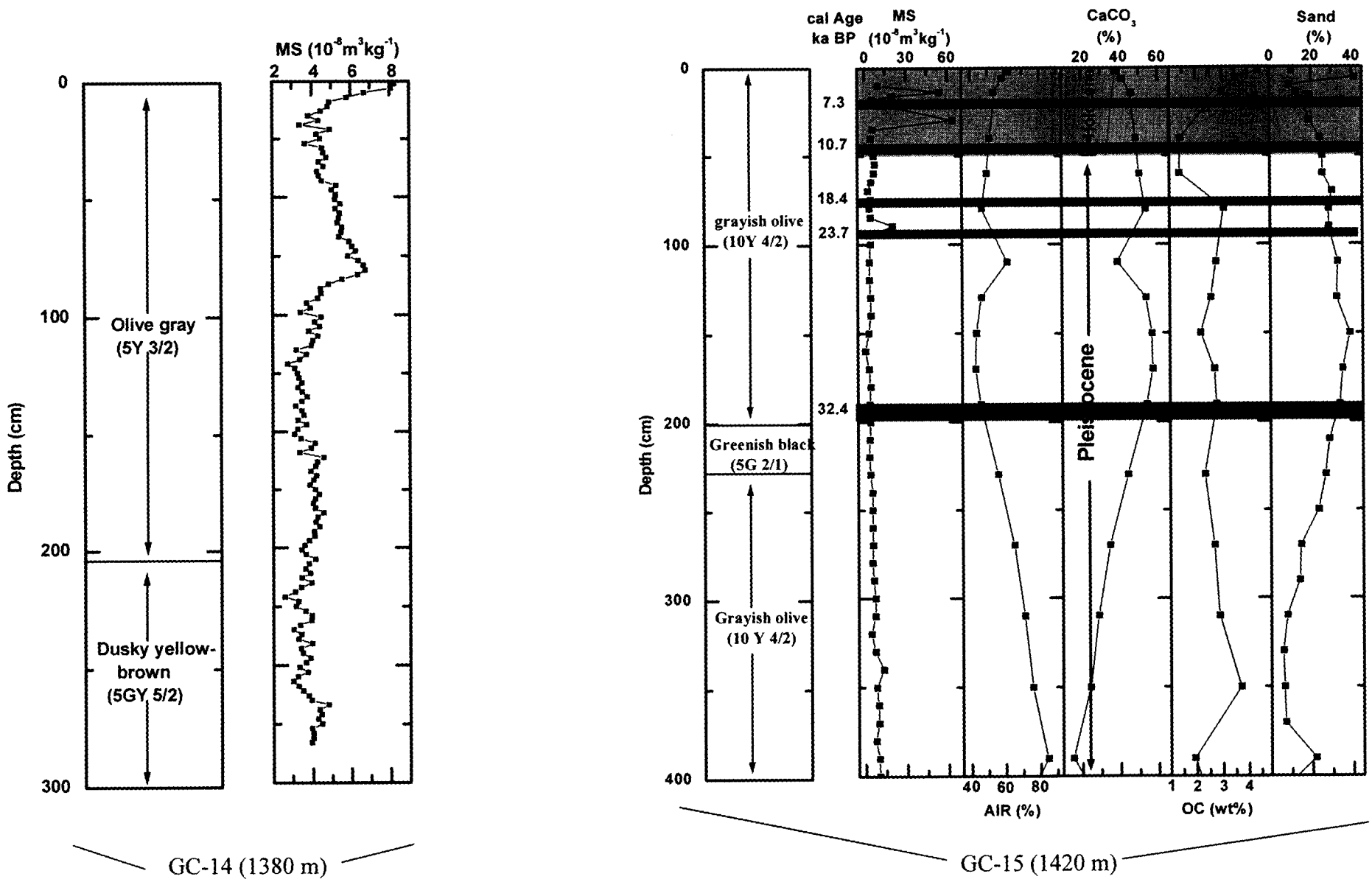

Fig. 3.8. Down -core variations of MS in core **GC-14 and GC-15.**

terrigenous supply that may have allowed the formation of aragonite muds. This core was located at the shelf edge at 121 m depth. The Glacio-eustatic sea level at ~14 ka was at –110 m (Fairbanks, 1989), and the shallow sea level conditions at the core site at that time probably facilitated the production of lime muds. Rao et al. (2005) carried out detailed studies (mineralogy, Sr content, SEM and oxygen isotopes) on the lime (aragonite) muds of these cores and suggested that they largely comprise a mixture of carbonate detritus derived from the disintegration of *Halimeda* bioherms from the shelf and the carbonate platform (see Fig. 3.1) and inorganically formed aragonite muds at insitu depths. The age of the aragonite muds in different cores (ranges between 17.6 ka and 10 ka – see Figs. 3.2-3.4; Chapter 2, Table 2.2) indicates that a carbonate depositional environment was prevalent throughout this time interval. Negative or slightly positive MS values for the lime mud-dominated sediments (unit 2) (see Figs. 3.2–3.4) indicate abundant diamagnetic carbonate influences the MS.

The correspondence of increased AIR with decreased S-ratio and low OC content between 13 ka BP and 9 ka BP (Fig. 3.3B) suggests the presence of increased proportions of high coercivity magnetic minerals transported from the shelf (discussed above). The synchronous and gradual increase in magnetic concentration parameters, AIR content, grain size of the mud fraction and OC of the sediments from the beginning of the Holocene (after 11 ka BP) imply that the site (GC-5) started to receive a gradually increasing terrigenous supply, probably due to intensified monsoonal conditions after the Younger Dryas (11.8-10.8 ka BP - Fairbanks, 1989). The variations in these parameters show an inverse relationship with carbonate content (Fig. 3.3B). Uniformly low values of χ_{fd}%, SIRM/χ_{lf} and χ_{ARM}/χ_{lf} indicate the presence of multidomain grains. There is no much change in magnetic grain size parameters after 11 ka BP, except that χ_{ARM}/χ_{lf} and χ_{ARM}/SIRM show marginal increase in the late Holocene sediments (near to the core top). This implies minor authigenic bacterial magnetite formation within this interval, but that the bulk of the Holocene magnetic material is of detrital origin.

iii. Climate inferences - Southwestern margin of India

The LGM sediments in a core off Mangalore (GC-12) and Kochi (GC-13) exhibit some coherence in magnetic properties. For example, the marginal increase in MS in GC-12 corresponds to relatively reduced AIR values and increased OC and carbonate contents (Fig. 3.6). While in GC-13 relatively low MS values correspond to reduced AIR and increased carbonate and slightly enriched OC content (Fig. 3.7). The $\delta^{18}O$ values are relatively high in both the cores (see Figs. 3.6-3.7). Increase in OC and carbonate is related to the increase in primary productivity. As the SW monsoon was weak during the LGM, as evidenced by several other cores, the increased productivity was attributed to stronger and colder NE monsoon winds leading to the intensification of winter convective mixing. Deep mixing of surface waters, caused by a stronger NE monsoon, induces an injection of nutrients into the euphotic layer leading to enhanced primary production (Fontugne and Duplessy, 1986; Rostek et al., 1997; den Dulk et al., 1998; von Rad et al., 1999; Thamban et al., 2001; Agnihotri et al., 2003; Ivanova et al., 2003). Since nutrients were injected from deeper water layers to the surface layers there was not much change in terrigenous supply from the hinterland and therefore no major MS variations at the LGM (Figs. 3.6-3.7).

On the other hand, increased magnetic concentration / grain size parameters and AIR content in the early Holocene sediments correspond to decreased carbonate and OC and a gradual decrease in $\delta^{18}O$ values in both the cores (Figs. 3.6 – 3.7). This may be related to the intensification of the SW monsoon, reported by several workers (Van Campo, 1986; Overpeck et al., 1996; von Rad et al., 1999; Sirocko et al., 2000; Thamban et al., 2001; Agnihotri et al., 2003). Continuation of high MS values, clay and AIR contents until 5 ka and distinct changes of these parameters after 5 ka (Fig. 3.7), suggest that the intense monsoon conditions extended up to 5 ka BP. Intense SW monsoon conditions produce increased precipitation on land, which results in a large fresh water flux (indicated by reduced $\delta^{18}O$ values-see Figs. 3.6-3.7) and terrigenous supply, which in turn causes increased MS. At the same time, upwelling-induced surface productivity is suppressed or

weakened, resulting in low OC and carbonate content (Figs. 3.6-3.7). Overpeck et al. (1996) have suggested that following deglaciation, monsoons were intensified at two abrupt events, one between 13 and 12.5 ka and the other between 10 and 9.5 ka, with the latter extending to about 5.5 ka. The increased MS values in the early Holocene can therefore be explained by an increased supply of terrestrial material to the seabed. The early Holocene (at interval between 9.7 and 7.1 ka) sediments of GC-12 show an increase followed by decrease in magnetic concentration parameters (Fig. 3.6). This interval is also associated with increase in χ_{ARM}/SIRM and carbonate, and decrease in OC, AIR% and $\delta^{18}O$ with no change in SIRM/χ_{lf}, χ_{ARM}/χ_{lf} and S-ratio% (Fig. 3.6). Since organic carbon is falling, direct authigenic magnetite formation driven by OC decomposition may not be the case for increased MS values. Authigenic green grains occur in the coarse fraction of this interval. Authigenic Fe-rich clays formed within the planktonic foraminifers can explain such MS values. These green clay infilled skeletals were reported on the outer shelf and upper slope (Thamban and Rao, 2000) and may have been transported to the core site during the Holocene sea level transgression.

The mineral magnetic properties in the late Holocene sediments, however, are different in both the cores (Figs. 3.6 and 3.7). MS values in GC-12 initially decrease and then increase towards the core top despite continuous increase in OC and AIR content. The decrease in MS is accompanied by increase in χ_{fd}%, SIRM/χ_{lf} and χ_{ARM}/χ_{lf} (Fig. 3.6). Since reductive diagenesis first removes fine magnetic grains, this process should be registered in χ_{ARM} data, which is very sensitive to changes in the single domain content. χ_{ARM} and SIRM do not decrease noticeably (Fig. 3.6). However, there is a small decrease in the ratio of χ_{ARM} /SIRM, which suggest a small increase in the average grain size of remanence carrying ferrimagnets. Thus the reductive diagenesis has been very limited in this core removing only the very finest ferrimagnets. On the other hand, the late Holocene (75 to 25 cm interval) sediments of the core 13 exhibit consistently reduced magnetic concentration / grain size / mineralogy parameters

accompanied by a gradual reduction in AIR / clay contents and $\delta^{18}O$ values and by increased OC and carbonate contents (Fig. 3.7). It implies that these organic-rich sediments are influenced by reductive diagenesis. Alternatively, since sea level reached its present position at ~ 6 ka, it is likely that much of the terrigenous supply during the late Holocene was deposited on the shallow shelf, and little fine-grained magnetite reached the continental slope, resulting in low MS values.

3.6. Summary and conclusions

- The magnetic susceptibility of the sediments is largely controlled by the detrital magnetite content. Regional variations in magnetic susceptibility are in accord with the mineralogical provinces.

- The highest MS values correspond to the sediments derived from the Deccan Traps, followed by the sediments from the Indus and least in the sediments off southern India.

- Intense chemical weathering in the Precambrian rocks of southern India results in leaching of iron from the source rocks and thereby reducing the MS value of the associated sediments.

- Authigenic green grains (Fe-rich clays) and biogenic magnetite at certain intervals in the cores enhance the total MS signal.

- Reductive diagenesis in organic-rich near surface sediments reduces the MS signal due to the dissolution of fine-grained magnetite.

- The MS contribution from the paramagnetic minerals (ilmenite, garnet, chlorite, smectite, glauconite, olivine, amphiboles, pyroxene) is much greater than that of dia-magnetic minerals (quartz, feldspar, calcite). The MS variations caused by varying carbonate content are minor.

- The glacial sediments in a core off the Indus exhibit low S-ratio% corresponding to high acid-insoluble residue. This implies the presence of high coercivity minerals like hematite and goethite and probable aeolian contribution from Pakistan and Indus drainage basin.

- The glacial sediments of the SW margin of India are characterised by low MS / high S-ratio% associated with low AIR and high OC and carbonate content, implying low terrigenous supply from the hinterland.

- The early Holocene sediments of both the NW and SW margin of India contain high MS / S-ratio% associated with high AIR and decreased $\delta^{18}O$ values. This implies enhanced supply of terrigenous material through fresh water, perhaps due to the intensified monsoonal activity at about this time.

- During the late Holocene, fine-grained magnetite on the continental slope is minor, may be due to stabilized sea levels and deposition of more terrigenous sediment on the shallow shelf.

- The late Holocene organic-rich sediments of the SW margin of India were subjected to reductive diagenesis and rock-magnetic properties were modified. Therefore, a caution needs to be exercised in interpreting the regional climatic signal through sediment magnetic properties.

Table 3.1. Down-core distribution of magnetic susceptibility (MS), acid insoluble residue (AIR), $CaCO_3$, organic carbon (OC), median grain size of terrigenous mud (Median) and sand content in GC-1

Depth (cm)	MS (SI unit)	AIR (%)	$CaCO_3$ (%)	OC (wt %)	Median (μm)	Sand (%)
0	24.09	38.79	61.21	0.35	8.19	48.99
10	22.93	--	--	0.40	--	--
15	25.34	--	--	--	10.29	--
20	21.89	41.20	58.80	0.47	--	50.62
25	21.67	--	--	--	9.20	--
30	19.68	38.29	61.71	0.37	--	51.46
35	18.22	--	--	--	13.10	--
40	13.38	37.77	62.23	0.32	--	56.30
45	12.43	--	--	--	8.91	--
50	11.68	29.17	70.83	0.25	--	69.19
55	10.61	--	--	--	13.37	--
60	7.47	26.50	73.50	0.26	--	72.79
65	9.27	--	--	--	12.09	--
70	6.03	19.47	80.53	0.21	--	80.86
75	7.18	--	--	--	9.79	--
80	5.81	23.87	76.13	0.28	--	69.28
85	4.83	--	--	--	10.77	--
90	4.83	20.83	79.17	0.23	--	74.54
95	5.13	--	--	--	11.90	--
100	4.00	22.12	77.88	0.20	--	72.23
105	3.23	--	--	--	14.57	--
110	5.74	--	--	--	--	--
115	6.13	--	--	--	--	--
120	5.04	31.02	68.98	0.15	--	39.76
125	5.45	--	--	--	9.66	--
130	4.23	--	--	--	--	--
135	5.49	--	--	--	--	--
140	5.84	42.12	57.88	0.20	--	4.91
145	5.14	--	--	--	10.22	--
155	5.33	--	--	--	--	--
160	5.01	41.23	58.77	0.21	--	3.84
165	4.63	--	--	--	11.41	--
170	4.61	--	--	--	--	--
175	4.13	--	--	--	--	--
180	4.77	38.81	61.19	0.16	--	4.95
185	4.78	--	--	--	10.08	--
190	4.26	--	--	--	--	--

Continued....

Continuation of Table 3.1

Depth (cm)	MS (SI unit)	AIR (%)	$CaCO_3$ (%)	OC (wt %)	Median (μm)	Sand (%)
195	4.08	--	--	0.25	--	--
205	4.04	37.18	62.82	--	9.74	7.60
210	4.44	--	--	--	--	--
215	4.44	--	--	--	--	--
220	4.63	42.00	58.00	0.18	--	4.56
250	7.38	--	--	--	--	--
255	5.68	--	--	--	--	--
260	5.58	43.34	56.66	0.26	--	3.07
265	5.68	--	--	--	11.34	--
270	5.43	--	--	--	--	--
275	6.01	--	--	--	--	--
280	5.14	44.19	55.81	0.19	--	1.28
285	5.93	--	--	--	9.53	--
290	5.38	--	--	--	--	--
300	5.52	45.18	54.82	0.31	--	1.51
310	4.12	--	--	--	9.98	--
320	5.91	46.27	53.73	0.19	--	1.31
325	5.76	--	--	--	8.70	--
330	5.73	--	--	--	--	--
340	7.64	46.73	53.27	0.15	--	1.65
345	9.70	--	--	--	10.04	--
355	10.52	--	--	--	--	--
360	10.72	48.83	51.17	0.30	--	1.54
365	11.49	--	--	--	9.62	--
370	11.75	--	--	--	--	--
375	13.55	--	--	--	--	--
380	13.60	49.86	50.14	0.18	--	1.61
385	13.39	--	--	--	10.70	--
390	12.98	--	--	--	--	--
395	13.96	46.16	53.84	--	--	2.70
400	15.00	--	--	--	10.56	--
410	14.87	--	--	--	--	--
415	13.50	--	--	--	--	--
420	14.95	53.29	46.71	--	--	1.26
425	15.98	--	--	--	11.46	--
430	13.60	--	--	--	--	--
440	14.78	54.38	45.62	--	--	4.12
445	14.24	--	--	--	9.80	
450	14.07	--	--	--	--	

Note: MS (SI unit) – $10^{-8}m^3kg^{-1}$

Table 3.2. Distribution of acid insoluble residue (AIR), $CaCO_3$, organic carbon (OC), δO^{18} and rock magnetic parameters in GC-2

Depth (cm)	AIR (%)	$CaCO_3$ (%)	OC (%)	Depth (cm)	δO^{18}	MS (SI unit)	χ_{ARM}	SIRM	χfd (%)	SIRM/χ_{lf}	χ_{ARM}/X_{lf}	χ_{ARM}/ SIRM	HIRM	S- ratio (%)
0	59.92	40.08	0.88	1	-2.09	44.74	560.57	416.22	2.94	9.30	12.53	1.35	4.40	98.94
4	59.84	40.16	0.77	3	--	46.72	592.69	426.73	7.64	9.13	12.69	1.39	10.83	97.46
8	59.23	40.77	0.79	5	-2.34	47.57	603.17	435.04	6.57	9.15	12.68	1.39	18.83	95.67
12	59.04	40.96	0.77	7	--	47.20	597.01	443.73	7.31	9.40	12.65	1.35	10.97	97.53
16	57.22	42.78	0.74	9	-2.16	44.93	616.55	421.29	7.14	9.38	13.72	1.46	3.07	99.27
20	55.92	44.08	0.60	11	--	43.21	548.95	393.46	7.44	9.10	12.70	1.40	11.53	97.07
24	52.55	47.45	0.58	13	-2.07	45.55	551.68	389.33	6.90	8.55	12.11	1.42	5.81	98.51
28	52.39	47.61	0.55	16	--	48.14	669.83	478.08	4.55	9.93	13.91	1.40	3.77	99.21
32	49.65	50.35	0.53	17	-2.12	47.30	634.38	450.76	4.14	9.53	13.41	1.41	10.53	97.66
36	48.82	51.18	0.46	23	-1.92	45.68	638.17	450.51	5.37	9.86	13.97	1.42	10.07	97.76
40	52.96	47.04	0.47	27	--	42.16	591.60	424.53	4.10	10.07	14.03	1.39	8.63	97.97
44	67.78	32.22	0.33	29	-2.07	41.35	566.64	392.11	5.43	9.48	13.70	1.45	7.72	98.03
48	69.91	30.09	0.33	31	--	39.44	520.82	377.88	6.98	9.58	13.21	1.38	2.91	99.23
50	71.11	28.89	0.33	33	--	37.49	531.68	361.23	4.16	9.64	14.18	1.47	10.18	97.18
56	73.11	26.89	0.32	35	--	34.17	439.35	322.64	4.97	9.44	12.86	1.36	12.19	96.22
62	72.16	27.84	0.31	37	-1.68	29.36	381.90	277.63	5.13	9.46	13.01	1.38	4.32	98.44
68	71.80	28.20	0.34	39	--	32.34	364.39	301.62	5.19	9.33	11.27	1.21	10.78	96.43
74	68.86	31.14	0.32	41	-1.75	28.36	276.59	241.12	6.95	8.50	9.75	1.15	14.07	94.17
80	67.36	32.64	0.33	43	--	29.04	172.37	181.90	25.48	6.26	5.94	0.95	17.13	90.58
86	60.68	39.32	0.32	45	-1.93	25.54	190.32	179.26	15.96	7.02	7.45	1.06	15.09	91.58
92	56.45	43.55	0.31	49	-1.90	22.62	165.19	180.18	8.99	7.96	7.30	0.92	19.45	89.21
98	61.41	38.59	0.36	53	-1.75	21.01	135.04	157.86	6.52	7.51	6.43	0.86	16.29	89.68
104	66.39	33.61	0.36	56	-1.84	21.90	143.09	163.83	8.66	7.48	6.53	0.87	17.89	89.08
110	67.63	32.37	0.37	61	-1.89	20.66	129.75	164.16	11.11	7.95	6.28	0.79	17.09	89.59

Continued...

Continuation of Table 3.2

Depth (cm)	AIR (%)	$CaCO_3$ (%)	OC (%)	Depth (cm)	δO^{18}	MS (SI unit)	χ_{ARM}	SIRM	χfd (%)	SIRM/χ_{lf}	χ_{ARM}/χ_{lf}	χ_{ARM}/ SIRM	HIRM	S- ratio (%)
116	61.82	38.18	0.32	71	-1.62	21.98	145.59	166.45	7.92	7.57	6.62	0.87	17.67	89.39
122	68.14	31.86	0.41	81	-0.23	20.45	146.13	166.19	3.37	8.13	7.15	0.88	15.84	90.47
128	71.07	28.93	0.34	91	0.29	19.89	143.72	166.66	5.86	8.38	7.22	0.86	7.10	95.74
134	69.71	30.29	0.32	102	-1.01	19.41	136.22	157.67	10.06	8.12	7.02	0.86	12.91	91.82
140	59.29	40.71	0.31	110	-1.26	20.25	125.19	170.15	4.50	8.40	6.18	0.74	18.57	89.08
146	59.59	40.41	0.28	122	-1.06	19.39	116.40	159.10	7.81	8.20	6.00	0.73	15.66	90.16
152	55.83	44.17	0.28	130	-1.02	21.22	106.39	175.44	9.32	8.27	5.01	0.61	17.43	90.06
158	58.03	41.97	0.30	142	-0.58	22.35	110.88	195.20	4.50	8.73	4.96	0.57	12.76	93.46
164	64.46	35.54	0.32	150	-0.52	23.02	110.76	198.04	8.79	8.60	4.81	0.56	12.24	93.82
170	65.56	34.44	0.36	160	-0.09	24.46	125.63	226.26	2.44	9.25	5.14	0.56	15.20	93.28
176	71.58	28.42	0.37	170	0.03	23.81	120.75	210.04	6.29	8.82	5.07	0.57	15.31	92.71
182	71.43	28.57	0.35	178	--	24.04	107.95	207.97	6.34	8.65	4.49	0.52	13.86	93.33
188	68.56	31.44	0.40	182	-0.32	23.15	118.55	203.01	6.41	8.77	5.12	0.58	16.08	92.08
194	69.64	30.36	0.42	194	-0.10	23.51	113.30	212.18	3.69	9.03	4.82	0.53	15.68	92.61
200	68.21	31.79	0.41	202	-0.23	26.32	117.31	208.68	14.41	7.93	4.46	0.56	15.47	92.59

Note: MS ($10^{-8}m^3kg^{-1}$); χ_{ARM} (m^3kg^{-1}); SIRM ($10^{-5}Am^2kg^{-1}$); SIRM/χ_{lf} ($10^3A/m$); χ_{ARM}/SIRM ($10^{-3}m/A$); HIRM ($10^{-5}Am^2kg^{-1}$)

Table 3.3. Down-core distribution of magnetic susceptibility (MS), acid insoluble residue (AIR), $CaCO_3$, organic carbon (OC), median grain size of terrigenous mud (Median) and sand content in GC-3

Depth (cm)	MS (SI unit)	AIR (%)	$CaCO_3$ (%)	OC (wt %)	Median (μm)	Sand (%)
0	89.82	35.63	64.37	0.47	--	--
2	80.62	28.51	71.49	--	17.634	63.27
4	64.6	29.16	70.84	0.27	--	--
6	48.24	27.27	72.73	--	--	--
8	33.74	34.18	65.82	--	--	62.39
10	36.98	25.6	74.4	--	9.67	--
12	33.63	33.2	66.8	--	--	--
14	22.09	27.7	72.3	0.28	--	67.43
16	28.58	29.87	70.13	0.20	--	--
18	18.67	30.16	69.84	0.35	--	--
22	27.6	22.21	77.79	--	--	--
24	24.34	27.06	72.94	--	10.965	--
26	22.64	25.47	74.53	--	--	45.36
28	20.81	36.03	63.97	--	--	--
30	17.04	23.59	76.41	--	11.168	--
32	11.67	20.28	79.72	0.24	--	47.27
34	19.18	34.96	65.04	--	--	--
36	23.21	32.93	67.07	0.25	--	--
38	4.89	27.19	72.81	--	--	33.64
40	6.56	23.82	76.18	0.27	--	--
42	3.17	25.88	74.12	--	12.263	--
44	3.65	30.08	69.92	0.27	--	25.33
46	2.89	27.37	72.63	--	--	--
48	2.98	28.74	71.26	0.25	--	--
50	3.24	23.82	76.18	--	10.595	29.77
52	2.25	41.42	58.58	--	--	--
54	3.16	37.6	62.4	--	--	--
56	2.83	28.3	71.7	0.31	--	32.04
58	2.29	24.53	75.47	0.28	--	--
62	3.94	39.87	60.13	--	--	18.92
64	3.27	45.48	54.52	--	11.004	--
66	4.35	33.43	66.57	--	--	--
68	3.19	28.61	71.39	0.30	--	20.02
70	2.38	27.19	72.81	0.31	--	--
74	1.81	--	--	--	--	--

Continued...

Continuation of Table 3.3

Depth (cm)	MS (SI unit)	AIR (%)	$CaCO_3$ (%)	OC (wt %)	Median (μm)	Sand (%)
78	2.77	35.21	64.79	0.29	--	2.85
80	0.9	25.23	74.77	0.30	--	--
84	2.09	25.87	74.13	0.25	--	--
88	2.61	29.17	70.83	0.30	--	1.71
90	2.94	26.45	73.55	0.26	10.63	--
94	2.31	28.89	71.11	0.30	--	--
98	2.44	32.16	67.84	--	9.382	3.23
100	2.28	24.79	75.21	0.28	--	--
104	3.18	35.73	64.27	--	--	--
108	2.6	30.16	69.84	0.26	--	6.14
110	0.45	26.51	73.49	--	--	--
114	1.6	33.3	66.7	0.30	--	--
118	4.43	27.63	72.37	--	--	4.73
120	3.59	30.16	69.84	--	8.113	--
124	2.71	35.11	64.89	--	--	--
128	3.7	33.33	66.67	--	--	5.38
130	4.38	--	--	--	--	--
134	3.72	35.11	64.89	0.21	8.368	--
138	2.94	54.88	45.12	--	--	4.58
140	3.69	26.25	73.75	--	--	--
144	3.43	34.6	65.4	0.25	--	--
148	3.25	33.8	66.2	--	--	--
150	3.78	27.1	72.9	--	--	2.21
154	2.92	35.61	64.39	0.29	--	--
158	3.37	46.58	53.42	--	--	--
160	3.38	28.79	71.21	--	9.945	3.18
164	2.99	38.65	61.35	--	--	--
168	3.45	28.4	71.6	--	--	--
170	4.82	28.45	71.55	--	--	1.58
174	3.27	31.75	68.25	0.24	--	--
178	2.80	39.87	60.13	--	--	--
180	3.17	28.19	71.81	--	--	2.6
184	2.76	34.59	65.41	0.21	11.279	--
188	3.02	42.53	57.47	--	--	--
190	3.24	26.7	73.3	--	--	3.67
194	3.09	39.76	60.24	0.18	--	--

Continued...

Continuation of Table 3.3

Depth (cm)	MS (SI unit)	AIR (%)	$CaCO_3$ (%)	OC (wt %)	Median (μm)	Sand (%)
198	3.17	31.65	68.35	--	--	--
200	3.95	26.56	73.44	--	10.211	1.97
210	2.66	25.34	74.66	--	--	--
220	3.42	26.62	73.38	--	--	--
230	3.90	29.66	70.34	--	--	0.6
240	3.70	28.68	71.32	--	--	--
250	3.65	28.43	71.57	--	10.257	--
260	3.71	26.63	73.37	--	--	5.88
270	3.18	27.75	72.25	--	--	--
280	3.87	28.03	71.97	--	--	--
290	4.61	27.88	72.12	--	9.554	5.07
300	2.95	27.47	72.53	--	--	--
310	3.66	29.68	70.32	--	8.161	--
320	3.86	28.53	71.47	--	--	2.82
330	3.50	28.08	71.92	--	--	--
340	4.11	28.79	71.21	--	8.893	--
350	3.89	29.2	70.8	--	8.886	0.29
360	3.28	27.69	72.31	--	--	--
370	3.85	28.32	71.68	--	--	--
380	3.00	29.78	70.22	--	--	1.83
390	3.59	28.94	71.06	--	8.825	--
400	3.64	28.7	71.3	--	--	1.51

Note: MS (SI unit) – $10^{-8}m^3kg^{-1}$

Table 3.4. Down-core distribution of magnetic susceptibility (MS), acid insoluble residue (AIR), $CaCO_3$, median grain size of terrigenous mud (Median) and Sand content in GC-4

Depth (cm)	MS (SI unit)	AIR (%)	$CaCO_3$ (%)	Median (μm)	Sand (%)
0	20.18	23.99	76.01	--	80.65
2	16.60	19.30	80.70	13.56	
4	19.20	22.17	77.83	--	
6	20.00	27.14	72.86	--	76.28
8	17.44	18.68	81.32	--	
10	16.89	22.26	77.74	--	76.86
12	18.78	19.80	80.20	9.28	
14	19.25	22.86	77.14	--	67.59
16	14.95	18.44	81.56	--	
18	5.43	21.56	78.44	13.61	82.12
20	9.77	24.53	75.47	--	
22	8.64	19.99	80.01	--	80.47
24	4.95	22.84	77.16	--	
30	11.45	19.40	80.60	10.02	75.40
32	8.14	25.64	74.36	--	
34	8.34	23.79	76.21	--	71.98
36	5.47	20.56	79.44	--	
38	6.16	20.68	79.32	--	67.02
40	4.11	22.80	77.20	--	
42	3.50	22.59	77.41	16.27	61.36
44	3.62	22.64	77.36	--	
46	3.19	20.97	79.03	--	71.75
48	3.41	20.77	79.23	--	
50	3.65	21.76	78.24	14.28	63.99
52	3.64	19.42	80.58	--	
54	4.16	20.44	79.56	--	66.49
56	4.41	19.05	80.95	--	
58	3.77	22.45	77.55	--	62.79
60	3.50	23.66	76.34	--	
62	3.88	27.59	72.41	16.70	66.00
64	3.15	20.35	79.65	--	
66	3.27	27.54	72.46	--	62.23
68	2.84	22.57	77.43	--	
70	3.34	22.53	77.47	16.28	64.73
72	4.14	28.16	71.84	--	
74	3.36	29.40	70.60	--	64.25
76	2.80	23.00	77.00	--	

Continued...

Continuation of Table 3.4

Depth (cm)	MS (SI unit)	AIR (%)	$CaCO_3$ (%)	Median (μm)	Sand (%)
78	3.55	24.92	75.08	--	64.21
80	3.30	22.33	77.67	--	
82	3.48	22.98	77.02	15.89	63.67
84	2.50	22.84	77.16	--	
86	2.59	22.93	77.07	--	65.58
88	1.73	22.99	77.01	--	
90	2.44	25.44	74.56	16.15	61.61
92	3.89	23.11	76.89	--	
94	3.35	23.75	76.25	--	63.97
100	2.41	21.14	78.86	14.69	66.11
106	1.99	19.85	80.15	--	61.44
112	2.17	17.84	82.16	--	
118	1.41	18.05	81.95	10.55	73.78
124	0.93	19.37	80.63	--	
130	1.13	21.96	78.04	12.54	69.59
136	1.53	15.97	84.03	--	
142	1.47	16.00	84.00	14.37	73.37
148	1.32	15.09	84.91	--	
154	1.42	16.83	83.17	--	67.28
160	0.39	15.46	84.54	--	
166	0.29	13.29	86.71	11.78	
172	0.09	10.24	89.76	--	
178	0.14	--	--	--	
184	0.00	11.77	88.23	9.98	71.33
190	-0.26	13.27	86.73	--	
196	-0.42	9.01	90.99	7.55	66.43
200	-0.63	9.12	90.88	--	
205	0.53	--	--	--	11.91
220	-0.30	11.10	88.90	--	
230	-0.61	12.35	87.65	7.73	47.32
240	-0.31	14.01	85.99	--	
250	-0.80	12.89	87.11	8.32	39.36
260	-0.81	9.65	90.35	--	
270	-0.25	9.50	90.50	8.98	67.55
280	-0.27	10.08	89.92	--	
290	-0.57	9.21	90.79	9.43	67.91
300	-0.21	11.55	88.45	--	

Continued...

Continuation of Table 3.4

Depth (cm)	MS (SI unit)	AIR (%)	$CaCO_3$ (%)	Median (μm)	Sand (%)
310	-0.36	11.46	88.54	8.68	46.79
320	-0.17	11.53	88.47	--	
330	-0.19	9.58	90.42	8.94	46.33
350	-0.08	9.29	90.71	--	28.38
360	-0.15	7.13	92.87	--	20.67
380	-0.46	7.54	92.46	--	
390	-0.27	6.05	93.95	6.98	26.61
400	-0.50	8.33	91.67	--	
410	-0.25	9.66	90.34	11.53	49.95

Note: MS (SI unit) – $10^{-8}m^3kg^{-1}$

Table 3.5. Distribution of acid insoluble residue (AIR), $CaCO_3$, organic carbon (OC), and rock magnetic parameters in GC-5

Depth (cm)	AIR (%)	$CaCO_3$ (%)	OC (%)	Median (μm)	Sand (%)	MS (SI unit)	χ_{ARM}	SIRM	χfd (%)	SIRM/χ_{lf}	χ_{ARM}/X_{lf}	χ_{ARM}/ SIRM	HIRM	S- ratio (%)
2	46.11	53.89		--	40.78	183.95	991.96	1721.13	2.67	9.36	5.39	0.58	48.12	97.20
4	55.62	44.38	0.96	--	--	185.03	1051.69	1838.46	0.00	9.94	5.68	0.57	80.25	95.63
6	55.34	44.66		17.47	31.52	185.71	1148.12	1871.81	0.00	10.08	6.18	0.61	78.16	95.82
8	57.40	42.60	0.88	--	39.08	182.47	970.26	1709.39	0.21	9.37	5.32	0.57	59.81	96.50
10	61.58	38.42		--	--	171.66	996.01	1643.68	0.00	9.58	5.80	0.61	41.95	97.45
12	56.09	43.91	0.97	27.85	32.80	170.24	709.85	1227.21	0.13	7.21	4.17	0.58	32.05	97.39
14	60.51	39.49		--	--	166.44	869.79	1631.52	0.30	9.80	5.23	0.53	75.41	95.38
16	62.22	37.78	0.84	--	36.03	163.38	800.31	1602.27	0.14	9.81	4.90	0.50	76.42	95.23
18	61.27	38.73		--	--	147.22	518.75	1338.76	0.33	9.09	3.52	0.39	60.33	95.49
20	58.25	41.75	0.99	--	45.42	146.24	507.39	1328.01	0.32	9.08	3.47	0.38	90.26	93.20
22	52.97	47.03		19.30	--	160.76	645.60	1368.75	0.12	8.51	4.02	0.47	61.20	95.53
24	61.28	38.72	0.95	--	28.18	151.60	659.97	1414.96	0.09	9.33	4.35	0.47	60.64	95.71
26	60.57	39.43	1.04	--	24.22	155.63	573.81	1382.01	0.00	8.88	3.69	0.42	85.94	93.78
38	57.35	42.65	1.07	16.74	33.88	145.62	539.90	1211.28	0.15	8.32	3.71	0.45	45.59	96.24
40	59.11	40.89	1.01	20.43	39.26	160.98	698.34	1430.54	0.00	8.89	4.34	0.49	43.52	96.96
42	65.01	34.99		--	--	158.98	720.50	1422.94	0.00	8.95	4.53	0.51	41.27	97.10
44	61.84	38.16	1.14	--	30.25	137.32	597.06	1235.53	0.31	9.00	4.35	0.48	45.18	96.34
46	60.28	39.72		--	--	122.91	529.82	1083.21	0.19	8.81	4.31	0.49	41.51	96.17
48	53.42	46.58	0.91	--	35.96	121.70	531.52	1033.67	0.00	8.49	4.37	0.51	40.64	96.07
50	55.01	44.99		17.19	--	116.53	518.17	952.25	0.00	8.17	4.45	0.54	27.64	97.10
52	43.91	56.09	0.94	--	47.71	110.32	334.39	540.69	0.32	4.90	3.03	0.62	19.88	96.32
54	51.08	48.92	1.08	--	34.60	106.88	494.70	906.00	0.29	8.48	4.63	0.55	69.81	92.29
60	48.07	51.93	0.97	18.94	45.00	111.02	476.94	881.68	6.42	7.94	4.30	0.54	33.34	96.22

Continued...

Continuation of Table 3.5

Depth (cm)	AIR (%)	$CaCO_3$ (%)	OC (%)	Median (μm)	Sand (%)	MS (SI unit)	χ_{ARM}	SIRM	χfd (%)	SIRM/χ_{lf}	χ_{ARM}/χ_{lf}	χ_{ARM}/ SIRM	HIRM	S- ratio (%)
62	50.82	49.18	--	--	--	100.22	454.21	849.58	0.60	8.48	4.53	0.53	29.38	96.54
64	45.01	54.99	0.92	--	41.94	104.92	510.28	916.29	0.06	8.73	4.86	0.56	37.21	95.94
66	50.25	49.75	--	19.36	--	107.41	529.98	862.62	0.26	8.03	4.93	0.61	25.71	97.02
68	41.98	58.02	0.88	--	47.50	86.00	432.79	746.51	0.62	8.68	5.03	0.58	24.46	96.72
70	37.87	62.13	--	--	--	79.00	428.06	643.81	0.81	8.15	5.42	0.66	19.41	96.98
72	34.72	65.28	0.62	--	53.80	84.53	310.55	461.25	0.92	5.46	3.67	0.67	5.90	98.72
74	44.35	55.65	--	--	--	72.24	393.32	601.57	0.00	8.33	5.44	0.65	24.39	95.95
76	39.59	60.41	0.66	--	57.23	59.93	340.70	462.70	0.71	7.72	5.69	0.74	14.79	96.80
78	33.92	66.08	--	--	--	47.80	235.63	337.97	0.00	7.07	4.93	0.70	15.50	95.41
80	31.94	68.06	0.54	16.49	54.77	40.49	168.08	255.06	0.00	6.30	4.15	0.66	5.78	97.74
82	31.42	68.58	--	--	--	31.62	125.97	176.58	0.60	5.58	3.98	0.71	2.87	98.37
84	34.42	65.58	--	--	60.76	23.23	76.16	133.88	1.10	5.76	3.28	0.57	10.79	91.94
86	30.16	69.84	--	--	65.19	13.68	53.20	87.38	1.27	6.39	3.89	0.61	-0.98	101.12
88	33.76	66.24	0.47	--	--	11.90	45.87	78.21	15.94	6.57	3.86	0.59	12.44	84.10
90	29.04	70.96	--	--	59.84	7.12	22.21	62.75	0.00	8.82	3.12	0.35	20.77	66.90
92	30.95	69.05	0.51	15.76	--	5.81	15.95	35.76	1.64	6.15	2.75	0.45	8.95	74.98
94	31.94	68.06	--	--	59.36	4.66	6.14	30.90	38.00	6.63	1.32	0.20	7.96	74.24
96	22.66	77.34	0.39	--	--	4.20	8.97	28.50	12.82	6.78	2.13	0.31	8.13	71.45
98	19.61	80.39	0.40	--	61.97	3.54	6.62	21.58	31.62	6.09	1.87	0.31	6.30	70.83
104	16.65	83.35	--	12.29	71.13	2.51	10.34	16.32	12.62	6.50	4.12	0.63	4.46	72.65
108	14.95	85.05	0.33	--	--	2.31	1.69	15.46	30.23	6.69	0.73	0.11	3.37	78.18
112	14.33	85.67	--	--	81.69	2.96	4.79	18.33	2.21	6.19	1.62	0.26	3.07	83.27

Continued...

Continuation of Table 3.5

Depth (cm)	AIR (%)	$CaCO_3$ (%)	OC (%)	Median (μm)	Sand (%)	MS (SI unit)	χ_{ARM}	SIRM	χfd (%)	SIRM/χ_{lf}	χ_{ARM}/χ_{lf}	χ_{ARM}/SIRM	HIRM	S- ratio (%)
116	11.97	88.03	0.24	--		1.33	7.79	8.36	37.74	6.30	5.87	0.93	1.60	80.84
120	13.09	86.91	0.16	9.95	57.84	4.06	19.27	25.57	31.93	6.30	4.75	0.75	4.14	83.82
124	--	--	--	--	--	-0.27	0.51	3.09	0.00	-11.46	-1.88	0.16	0.25	91.93
132	9.47	90.53	0.18	7.59	44.11	--	--	--	--	--	--	--	--	--
140	4.46	95.54	--	--	--	-0.76	0.74	1.54	0.00	-2.02	-0.97	0.48	0.16	89.83
144	2.92	97.08	0.10	8.47	32.85	-0.49	1.24	4.05	0.00	-8.30	-2.55	0.31	0.22	94.65
148	--	--	--	--	--	-1.40	1.33	2.12	0.00	-1.52	-0.95	0.62	0.10	95.08
152	3.98	96.02	--	--	32.45	--	--	--	--	--	--	--	--	--
156	6.19	93.81		--	--	--	--	--	--	--	--	--	--	--
160	5.00	95.00	0.11	--	45.44	--	--	--	--	--	--	--	--	--
164	5.94	94.06	--	--	--	--	--	--	--	--	--	--	--	--
168	3.52	96.48	--	--	35.90	--	--	--	--	--	--	--	--	--
172	5.93	94.07	--	9.87	43.42	--	--	--	--	--	--	--	--	--
176	4.97	95.03	0.09	--	--	--	--	--	--	--	--	--	--	--
180	2.31	97.69	--	12.02	51.24	-1.17	2.11	1.35	0.00	-1.16	-1.81	1.56	0.14	89.83
184	4.12	95.88	--	--	--	--	--	--	--	--	--	--	--	--
188	4.52	95.48	--	--	41.36	--	--	--	--	--	--	--	--	--
192	6.38	93.62	--	--	--	--	--	--	--	--	--	--	--	--
196	3.74	96.26	0.06	--	33.59	-0.33	1.34	2.60	0.00	-7.96	-4.11	0.52	0.40	84.64
200	5.71	94.29	0.06	--	--	-0.94	1.07	1.44	0.00	-1.53	-1.13	0.74	0.18	87.27

Note: MS ($10^{-8}m^3kg^{-1}$); χ_{ARM} (m^3kg^{-1}); SIRM ($10^{-5}Am^2kg^{-1}$); SIRM/χ_{lf} ($10^3A/m$); χ_{ARM}/SIRM ($10^{-3}m/A$); HIRM ($10^{-5}Am^2kg^{-1}$)

Table 3.6. Down-core distribution of magnetic susceptibility (MS), acid insoluble residue (AIR), $CaCO_3$, organic carbon (OC), median grain size of terrigenous mud (Median) and Sand content in GC-6

Depth (cm)	MS (SI unit)	AIR (%)	$CaCO_3$ (%)	OC (wt%)	Median (μm)	Sand (%)
0	90.88	54.77	45.23	4.24	9.12	4.92
2	95.97	--	--	--	--	--
4	90.42	--	--	4.22	--	9.19
6	94.03	--	--	--	--	--
8	86.60	--	--	4.83	--	4.73
10	76.16	60.07	39.93	--	11.24	--
12	69.36	--	--	4.57	--	7.81
14	61.95	--	--	--	--	--
16	52.02	--	--	4.47	--	16.80
18	39.38	--	--	--	--	--
20	28.71	52.73	47.27	3.86	10.19	7.15
22	27.91	--	--	--	--	--
24	21.20	--	--	--	--	7.34
26	22.74	--	--	--	--	--
28	19.20	--	--	3.85	--	6.36
30	16.75	60.27	39.73	--	12.18	--
32	16.54	--	--	4.21	--	4.53
34	14.21	--	--	--	--	--
36	13.22	--	--	--	--	3.94
38	12.71	--	--	3.77	--	--
40	11.70	62.33	37.67	4.09	12.77	5.47
42	9.68	--	--	--	--	--
44	15.61	--	--	3.92	--	2.75
46	10.55	--	--	--	--	--
48	7.34	--	--	--	--	8.97
50	7.67	52.85	47.15	--	12.82	--
52	7.98	--	--	--	--	5.31
54	6.84	--	--	--	--	--
56	7.99	--	--	3.67	--	--
58	6.55	--	--	--	--	--
60	10.74	58.73	41.27	3.84	16.15	2.72
62	9.47	--	--	--	--	--
64	12.70	--	--	--	--	3.47
66	5.41	--	--	--	--	--
68	5.08	--	--	--	--	9.75
70	6.50	50.07	49.93	--	10.87	--
72	5.95	--	--	3.84	--	10.23

Continued...

Continuation of Table 3.6

Depth (cm)	MS (SI unit)	AIR (%)	$CaCO_3$ (%)	OC (wt%)	Median (μm)	Sand (%)
74	7.04	--	--	--	--	--
76	3.45	--	--	3.36	--	12.74
78	6.44	--	--	--	--	--
80	7.16	60.09	39.91	3.70	11.03	10.05
82	5.55	--	--	--	--	--
84	7.19	--	--	4.26	--	5.70
86	7.15	--	--	--	--	--
88	6.36	--	--	3.17	--	12.67
90	4.82	47.40	52.60	--	10.16	--
92	7.49	--	--	3.68	--	14.56
94	7.75	--	--	--	--	--
96	6.65	--	--	3.98	--	9.41
98	6.23	--	--	--	--	--
100	7.88	42.45	57.55	3.45	10.17	8.31
105	7.73	--	--	--	--	--
110	8.11	--	--	3.60	--	12.33
115	7.67	--	--	--	--	--
120	7.32	48.73	51.27	3.83	11.05	10.09
125	7.80	--	--	--	--	--
130	7.00	--	--	3.02	--	16.23
135	8.24	--	--	--	--	--
140	9.58	70.69	29.31	3.66	14.78	7.42
145	7.82	--	--	--	--	--
150	11.42	--	--	--	--	3.76
155	6.79	--	--	--	--	--
160	5.90	60.77	39.23	3.08	10.92	23.12
165	5.07	--	--	--	--	--
170	5.90	--	--	2.87	--	14.22
175	8.95	--	--	--	--	--
180	6.07	41.90	58.10	2.82	10.88	15.86
185	5.51	--	--	--	--	--
190	4.44	--	--	2.14	--	28.01
195	3.25	--	--	--	--	--
200	3.83	28.48	71.52	1.98	10.30	32.36
205	4.92	--	--	--	--	--
210	7.18	--	--	--	--	17.76
215	7.42	--	--	--	--	--

Continued...

Continuation of Table 3.6

Depth (cm)	MS (SI unit)	AIR (%)	$CaCO_3$ (%)	OC (wt%)	Median (μm)	Sand (%)
220	1.55	19.77	80.23	--	11.84	16.84
225	0.88	--	--	--	--	--
230	0.92	--	--	--	--	14.17
235	1.06	--	--	--	--	--
240	0.90	16.56	83.44	1.92	10.78	10.50
245	1.39	--	--	--	--	--
250	0.70	--	--	--	--	8.59
255	0.90	--	--	--	--	--
260	0.90	15.51	84.49	--	10.88	13.44
265	0.77	--	--	--	--	--
270	0.00	--	--	--	--	14.43
275	0.73	--	--	--	--	--
280	0.24	9.50	90.50	1.90	8.58	6.22
285	0.23	--	--	--	--	--
290	-0.59	--	--	--	--	8.63
295	1.08	--	--	--	--	--
300	0.54	8.48	91.52	--	7.96	5.94
305	0.46	--	--	--	--	--
310	0.51	--	--	--	--	7.10
315	0.11	--	--	--	--	--
320	1.32	11.65	88.35	1.85	7.14	3.32
325	0.47	--	--	--	--	--
330	0.53	--	--	--	--	3.25
335	0.80	--	--	--	--	--
340	-0.22	5.03	94.97	--	7.18	2.37
345	0.32	--	--	--	--	--
350	0.17	--	--	--	--	2.51
355	0.14	--	--	--	--	--
360	0.51	5.35	94.65	1.80	7.29	4.60
365	0.24	--	--	--	--	--
370	-0.14	--	--	--	--	4.63
375	0.00	--	--	--	--	--
380	0.00	5.79	94.21	--	7.10	4.24
385	-2.78	--	--	--	--	--
390	-3.20	--	--	--	--	4.47
395	-0.60	--	--	--	--	--
400	-0.64	5.14	94.86	1.82	6.78	4.45

Note: MS (SI unit) – $10^{-8}m^3kg^{-1}$

Table 3.7. Down-core distribution of magnetic susceptibility (MS), acid insoluble residue (AIR), $CaCO_3$, organic carbon (OC), median grain size of terrigenous mud (Median) and Sand content in GC-7

Depth (cm)	MS (SI unit)	AIR (%)	$CaCO_3$ (%)	OC (wt%)	Median (μm)	Sand (%)
0	2.65	26.65	73.35	1.14	7.70	3.27
2	1.59	--	--	--	--	--
4	1.34	--	--	1.11	--	2.48
6	1.16	--	--	--	--	--
8	1.80	--	--	0.97	--	1.96
10	0.97	19.45	80.55	--	7.52	--
12	1.28	--	--	2.15	--	1.32
14	1.29	--	--	--	--	--
16	1.23	--	--	0.77	--	1.94
18	0.98	--	--	--	--	--
20	1.45	17.89	82.11	0.77	7.02	1.79
22	0.77	--	--	--	--	--
24	1.19	--	--	0.69	--	1.27
26	0.64	--	--	--	--	--
28	2.10	--	--	0.64	--	1.67
30	1.34	19.22	80.78	--	7.97	--
32	0.88	--	--	0.67	--	1.50
34	0.53	--	--	--	--	--
36	0.86	--	--	0.60	--	1.67
38	1.83	--	--	-	--	--
40	1.04	17.75	82.25	0.72	8.18	1.37
42	1.15	--	--	--	--	--
44	1.36	--	--	0.55	--	2.62
46	1.03	--	--	--	--	--
48	0.94	--	--	0.59	--	2.38
50	0.99	18.16	81.84	--	8.26	--
52	1.00	--	--	0.62	--	1.87
54	0.50	--	--	--	--	--
56	1.17	--	--	0.71	--	1.57
58	0.41	--	--	--	--	--
60	2.31	20.70	79.30	0.69	7.84	2.78
62	8.19	51.78	48.22	2.01	11.67	--
64	5.21	--	--	1.79	--	14.13
66	0.88	17.36	82.64	--	9.65	--
70	-0.42	11.68	88.32	--	10.51	--
72	-0.27	--	--	0.68	--	4.25
76	-0.69	--	--	1.05	--	2.82
78	-0.64	--	--	--	--	--

Continued...

Continuation of Table 3.7

Depth (cm)	MS (SI unit)	AIR (%)	$CaCO_3$ (%)	OC (wt%)	Median (μm)	Sand (%)
80	-0.83	5.64	94.36	0.33	13.47	6.50
82	-0.70	--	--	--	--	--
84	-1.17	--	--	0.84	--	2.04
86	-0.67	--	--	--	--	--
88	-0.45	--	--	0.87	--	5.70
90	-0.50	10.37	89.63	--	11.60	--
92	-0.56	--	--	0.75	--	2.94
94	-0.25	--	--	--	--	--
96	-0.61	--	--	0.68	--	2.54
98	-1.43	--	--	--	--	--
100	-0.74	9.26	90.74	0.79	11.61	1.26
105	-0.65	--	--	--	--	--
110	-0.64	--	--	--	--	1.70
115	-0.33	--	--	--	--	--
120	-0.48	8.78	91.22	0.67	12.59	1.63
125	-0.28	--	--	--	--	--
130	-0.51	--	--	--	--	1.55
135	-0.99	--	--	--	--	--
140	-0.61	8.22	91.78	--	12.17	1.24
145	-0.47	--	--	--	--	--
150	-0.25	--	--	--	--	3.82
155	-0.81	--	--	--	--	--
160	-0.81	10.69	89.31	0.85	11.06	3.25
165	-0.46	--	--	--	--	--
170	-0.71	--	--	--	--	1.24
175	-1.00	--	--	--	--	--
180	-1.02	11.00	89.00	0.83	11.88	1.86
185	-1.37	--	--	--	--	--
190	-0.57	--	--	--	--	1.60
195	-0.92	--	--	--	--	--
200	-0.58	9.40	90.60	0.93	12.42	1.41
205	-0.80	--	--	--	--	--
210	-0.72	--	--	--	--	3.09
215	-1.08	--	--	--	--	--
220	-1.22	6.03	93.97	0.86	11.67	1.82
225	-0.95	--	--	--	--	--
230	-0.72	--	--	--	--	2.44
235	-0.54	--	--	--	--	--
240	-0.77	5.57	94.43	0.65	13.46	1.53
250	-1.06	--	--	--	--	1.66

Continued...

Continuation of Table 3.7

Depth (cm)	MS (SI unit)	AIR (%)	$CaCO_3$ (%)	OC (wt%)	Median (μm)	Sand (%)
255	-1.03	--	--	--	--	--
260	-0.32	4.73	95.27	0.67	11.78	2.62
265	-1.03	--	--	--	--	--
270	-0.95	--	--	--	--	2.53
275	-0.95	--	--	--	--	--
280	-0.83	4.13	95.87	0.62	11.47	2.94
285	-1.60	--	--	--	--	--
290	-0.96	--	--	--	--	3.41
295	-0.74	--	--	--	--	--
300	-1.54	3.14	96.86	0.30	12.27	2.87
305	-1.15	--	--	--	--	--
310	-1.28	--	--	--	--	24.58
315	-0.91	--	--	--	--	--
320	-0.95	3.27	96.73	0.19	12.47	19.97
325	-0.65	--	--	--	--	--
330	-0.60	--	--	--	--	--
335	-0.58	--	--	--	--	--
340	0.14	3.97	96.03	0.24	11.74	31.57
345	-0.08	--	--	--	--	--
350	0.42	--	--	--	--	29.47
355	0.47	--	--	--	--	--
360	0.45	7.02	92.98	0.26	11.08	28.30
365	0.95	--	--	--	--	--
370	1.85	--	--	--	--	38.95
375	1.06	--	--	--	--	--
380	1.67	13.27	86.73	0.59	11.40	38.92
385	2.85	--	--	--	--	--
390	3.12	--	--	--	--	14.65
395	1.31	--	--	--	--	--
400	2.37	30.61	69.39	0.96	11.35	12.69
405	1.11	--	--	--	--	--
410	2.55	--	--	--	--	27.45
420	3.47	35.94	64.06	0.83	12.26	17.23
425	3.72	--	--	--	--	--
430	3.70	--	--	--	--	14.86
435	5.06	--	--	--	--	--
440	1.14	19.13	80.87	--	10.88	5.86
445	2.38	--	--	--	--	--
450	4.23	--	--	--	--	16.58

Note: MS (SI unit) – $10^{-8}m^3kg^{-1}$

Table 3.8. Down-core distribution of magnetic susceptibility (MS) in GC-8

Depth (cm)	MS (SI unit)	Depth (cm)	MS (SI unit)	Depth (cm)	MS (SI unit)	Depth (cm)	MS (SI unit)
0	-0.35	68	-1.20	190	-1.11	365	-1.72
2	-0.43	70	-0.45	195	-0.64	370	-2.38
4	-0.39	72	-0.67	200	-0.80	375	-2.22
6	-0.32	74	-0.42	205	-0.86	380	-0.59
8	-0.27	76	-0.83	210	-0.84	385	-0.68
10	-0.34	78	-0.82	215	-0.77	390	-0.97
12	-0.71	80	-0.68	220	-1.00	395	-0.78
14	-1.96	82	-0.42	225	-1.30	400	-0.43
16	-0.65	84	-0.55	230	-0.68	405	-0.57
18	-0.54	86	-0.47	235	-0.50	410	-2.38
20	-0.47	88	-0.40	240	-0.79	415	-1.80
22	-1.22	90	-0.64	245	-0.58	420	-3.06
24	-0.70	92	-0.72	250	-0.61	425	-1.49
26	-0.71	94	0.50	255	-0.82	430	-0.91
28	-0.37	96	0.48	260	-0.51	435	-1.21
30	-0.78	98	0.88	265	-0.68	440	-1.94
32	-0.81	100	0.20	270	-0.33	445	-0.31
34	-0.82	105	-0.90	275	-0.71	450	-0.44
36	-0.49	110	0.25	280	-0.64	455	-0.88
38	-0.52	115	0.00	285	-0.80	460	-0.63
40	-0.71	120	0.12	290	-0.49	465	-1.29
42	-0.58	125	-1.35	295	-0.54	470	-0.56
44	-0.60	130	-0.28	300	-1.22	475	-0.36
46	-1.02	135	-0.18	305	-0.94	480	-0.56
48	0.19	140	-0.51	310	-0.55	485	-1.09
50	-0.31	145	-0.55	315	-0.89	490	-1.21
52	-0.49	150	-0.77	320	-0.42	495	-0.69
54	-0.43	155	-0.96	325	-0.36	500	-0.78
56	-0.44	160	-0.80	330	-0.48	505	-0.87
58	-0.73	165	-1.20	335	-0.67	510	-1.20
60	-0.40	170	-0.30	340	-0.98	515	-0.92
62	-0.82	175	-0.20	345	-0.37	520	-0.94
64	-0.51	180	-0.23	350	-0.61	525	-0.58
66	-0.46	185	-1.11	355	-1.20	530	-0.73
				360	-0.45	540	-1.39

Note: MS (SI unit) – $10^{-8}m^3kg^{-1}$

Table 3.9. Down-core distribution of magnetic susceptibility (MS), acid insoluble residue (AIR), $CaCO_3$, median grain size of terrigenous mud (Median) and sand content in GC-9

Depth (cm)	MS (SI unit)	AIR (%)	$CaCO_3$ (%)	Median (μm)	Sand (%)
0	2.41	4.76	95.24	8.31	87.68
2	1.98	5.37	94.63	--	--
4	1.07	4.73	95.27	7.74	--
6	1.54	6.66	93.34	--	87.52
8	1.48	4.25	95.75	7.37	--
10	-1.14	5.56	94.44	--	--
12	-0.61	4.96	95.04	11.68	52.41
14	0.00	5.66	94.34	--	--
16	-0.85	4.54	95.46	12.94	51.51
18	-0.70	5.08	94.92	--	--
20	-0.98	4.40	95.60	12.77	--
22	-1.11	4.51	95.49	--	40.44
24	-0.40	4.09	95.91	11.65	--
26	-1.14	5.30	94.70	--	44.52
28	-0.53	4.09	95.91	12.62	--
30	-0.43	5.36	94.64	--	45.00
32	-0.69	3.69	96.31	11.99	--
34	-0.87	4.75	95.25	--	--
36	-0.79	5.51	94.49	12.33	32.96
38	-0.63	3.70	96.30	--	--
40	-1.12	4.75	95.25	14.40	--
42	-0.83	4.52	95.48	--	--
44	-1.18	4.42	95.58	12.25	41.75
46	-1.81	5.25	94.75	--	--
48	-1.25	4.96	95.04	12.76	--
50	-0.65	4.98	95.02	14.51	--
55	-1.25	4.39	95.61	--	--
60	-0.96	4.20	95.80	13.76	--
65	-0.68	4.45	95.55	--	7.44
70	-0.83	4.13	95.87	14.62	--
75	-1.24	4.26	95.74	--	--
80	-1.07	6.13	93.87	14.01	--
85	-0.26	4.16	95.84	--	--
90	-1.08	4.17	95.83	14.42	7.15
95	-0.72	4.12	95.88	--	--
100	1.76	4.36	95.64	14.19	--
105	0.16	3.84	96.16	--	--
110	-0.82	4.22	95.78	14.04	--
115	-0.91	4.49	95.51	--	4.36

Continued...

Continuation of Table 3.9

Depth (cm)	MS (SI unit)	AIR (%)	$CaCO_3$ (%)	Median (□m)	Sand (%)
120	-1.31	4.24	95.76	14.23	--
125	-1.31	5.11	94.89	--	--
130	-1.40	5.01	94.99	13.39	2.86
140	-1.11	5.19	94.81	13.01	--
145	-0.13	4.94	95.06	--	--
150	-1.95	4.21	95.79	14.32	6.98
155	-1.26	4.31	95.69	--	--
160	-2.69	5.18	94.82	12.43	--
165	-1.79	4.65	95.35	--	--
170	-0.55	5.47	94.53	12.68	3.44
175	-0.87	5.90	94.10	--	--
180	-1.17	4.70	95.30	14.03	4.58
185	-0.71	4.54	95.46	--	--
190	-1.11	5.00	95.00	12.94	--
195	-1.50	5.26	94.74	--	2.69
200	-1.65	5.02	94.98	11.79	--
205	-0.86	6.06	93.94	--	--
210	-0.82	5.30	94.70	11.77	3.07
215	-0.95	6.30	93.70	--	--
220	-1.04	6.16	93.84	11.42	--
225	-0.92	5.98	94.02	--	4.27
230	-0.83	6.20	93.80	11.17	--
235	-1.43	--	--	--	--
240	-0.43	5.68	94.32	--	4.13
245	-0.76	5.73	94.27	--	--
250	-1.35	4.98	95.02	10.88	--
260	-0.42	5.50	94.50	10.41	9.28
265	-1.05	5.75	94.25	--	--
270	-0.54	6.54	93.46	11.12	--

Note: MS (SI unit) – $10^{-8}m^3kg^{-1}$

Table 3.10. Down-core distribution of magnetic susceptibility (MS) in GC-10.

Depth (cm)	MS (SI unit)	Depth (cm)	MS (SI unit)	Depth (cm)	MS (SI unit)	Depth (cm)	MS (SI unit)
13	4.01	91	1.71	167	1.70	245	1.14
15	3.56	93	1.63	169	0.84	247	1.56
17	3.58	95	1.03	171	1.50	249	0.98
19	1.75	97	1.77	173	1.39	251	1.05
21	1.60	99	1.67	175	1.40	253	1.33
23	2.40	101	2.46	177	0.93	255	0.85
25	1.93	103	0.73	179	0.98	257	1.14
27	1.47	105	1.71	181	1.46	259	0.77
29	2.23	107	0.74	183	0.89	261	1.23
31	1.09	109	1.02	185	1.36	263	1.05
33	1.48	111	1.16	187	2.11	265	0.75
35	1.24	113	2.14	189	1.42	267	1.13
37	0.78	115	1.70	191	1.51	269	1.83
39	0.94	117	1.19	193	1.68	271	1.51
41	1.29	119	1.63	195	1.56	273	1.53
43	1.00	121	1.11	197	1.37	275	1.49
45	0.79	123	2.65	199	1.58	277	1.41
47	0.88	125	1.87	201	1.14	279	1.75
49	0.71	127	1.62	203	1.17	281	1.56
51	1.24	129	0.94	205	0.50	283	0.77
53	1.02	131	1.09	207	0.58	285	1.37
55	0.46	133	1.70	209	0.91	287	1.04
57	0.69	135	1.23	211	1.15	289	1.30
59	1.04	137	1.81	213	0.73	291	1.46
61	0.96	139	1.50	215	0.91	293	1.53
63	1.52	141	1.73	217	0.35	295	1.58
65	1.34	143	1.23	219	1.26	297	1.43
67	1.25	145	0.67	221	1.00	299	1.69
69	1.70	147	0.97	223	1.21	301	1.43
71	1.69	149	1.61	225	0.91	303	1.69
73	1.29	151	1.89	227	1.72	305	1.58
75	1.88	153	0.78	229	1.11	307	1.13
77	2.08	155	1.66	231	0.78	309	1.49
79	2.36	157	0.54	233	0.82	311	1.63
81	1.35	159	1.91	235	0.62	313	1.97
83	1.54	160	0.57	237	0.80	315	1.46
85	1.31	162	0.80	239	1.07	317	1.51
87	1.38	163	1.41	241	0.65	319	1.71
89	1.04	165	0.98	243	1.04	321	1.86

Continued...

Continuation of Table 3.10

Depth (cm)	MS (SI unit)
323	1.57
325	2.12
327	1.94
329	1.54
331	1.96
333	2.13
335	2.19
337	1.67
339	1.52
341	1.27
343	1.70
345	1.85
347	1.97
349	2.14
351	2.03
353	2.56
355	2.43
357	2.52
359	2.44
361	2.08
363	2.78
365	2.19
367	2.32
369	2.64
371	2.36
373	2.64
375	2.89
377	2.58
379	2.17
381	2.74
383	2.79
385	2.81
387	2.74
389	2.69

Depth (cm)	MS (SI unit)
391	2.84
393	2.90
395	2.57
397	2.91
399	2.83
401	2.84
403	2.43
405	2.29
407	1.70
409	2.11
411	2.68
413	2.59
415	2.80
417	2.77
419	2.64
421	2.98
423	2.56
425	2.63
427	2.62
429	2.46
431	2.37
433	2.33
435	2.56
437	2.52
439	2.35
443	2.48
445	2.38
447	2.37
449	2.66
451	2.31
453	2.64
455	2.60
457	2.81
459	2.99

Depth (cm)	MS (SI unit)
461	2.62
463	2.82
465	2.46
467	2.88
469	2.42
471	2.00
473	2.78
475	2.37
477	2.32
479	3.15
481	2.94
483	3.16
485	3.11
487	3.17
489	2.74
491	2.50
493	2.47
495	2.29
497	2.35
499	2.58
501	2.81
503	2.44
505	2.34
507	2.36
509	2.39
511	2.48
515	2.57
517	2.54
521	2.30
523	2.57
525	2.59
527	2.14
529	2.61
531	2.55
533	1.83

Depth (cm)	MS (SI unit)
535	2.35
537	2.10
539	2.10
541	1.73
543	1.82
545	1.82
547	1.58
549	0.55
551	0.26
553	0.67
555	0.73
557	1.06
559	0.87
561	1.08
563	1.05
565	1.11
567	1.44
569	1.06
571	0.98
573	1.37
577	1.58
581	1.47
583	1.26
585	1.15
589	1.68
591	1.51
593	1.50
595	1.98
599	1.98
601	1.79
603	2.30
605	2.07
607	1.96
609	1.82
611	1.99

Note: MS (SI unit) – $10^{-8}m^3kg^{-1}$

Table 3.11. Down-core distribution of magnetic susceptibility (MS) in GC-11.

Depth (cm)	MS (SI unit)
1	316.31
3	307.46
5	267.36
7	289.89
9	316.65
11	304.46
13	305.48
15	329.00
17	353.39
19	367.11
21	362.07
23	375.20
25	394.87
27	373.82
29	370.22
31	329.10
33	329.21
35	328.56
37	328.57
39	280.95
41	304.01
43	333.43
45	344.82
47	301.31
49	289.04
51	260.48
53	275.24
55	262.45
57	270.47
59	273.90
61	286.87
63	353.70
65	412.99
67	327.91
69	302.51
71	373.16
73	441.96
75	385.71
77	393.82
79	395.90

Depth (cm)	MS (SI unit)
81	377.40
83	348.20
85	318.79
87	327.41
89	357.84
91	351.04
93	411.56
95	449.74
97	404.15
99	402.01
102	365.08
107	367.24
112	364.29
117	376.30
122	384.74
127	389.46
132	407.76
137	464.52
142	374.51
147	401.11
152	504.95
157	403.52
162	404.76
167	409.15
172	359.28
177	381.81
182	372.18
187	417.04
192	415.15
197	405.37
202	408.41
207	399.82
212	398.23
217	376.34
222	454.97
227	359.72
232	405.85
237	452.40
242	415.76
247	396.60

Depth (cm)	MS (SI unit)
252	311.43
257	387.06
262	446.42
267	399.14
272	422.00
277	420.19
282	427.02
287	460.10
292	393.99
297	394.90
302	405.93
307	360.05
312	427.96
317	451.55
322	433.72
327	430.45
332	313.78
337	353.42
342	411.13
347	440.77
352	421.27
357	411.85
362	451.35
367	415.47
372	421.91
377	442.06
382	438.41
387	450.49
392	427.01
397	431.96
407	496.46
412	395.00
417	400.34
422	401.37
427	414.24
432	407.92
437	420.88
442	428.83
447	421.40
453	434.66

Note: MS (SI unit) – $10^{-8}m^3kg^{-1}$

Table 3.12. Distribution of acid insoluble residue (AIR), $CaCO_3$, organic carbon (OC), δO^{18} and rock magnetic parameters in GC-12

Depth (cm)	AIR (%)	$CaCO_3$ (%)	OC (wt %)	δO^{18}	MS (SI unit)	χ_{ARM}	SIRM	χfd (%)	SIRM/χ_{lf}	χ_{ARM}/χ_{lf}	χ_{ARM}/SIRM	HIRM	S-ratio (%)
2	58.91	41.09	1.83	-2.40	37.79	449.67	207.04	3.38	5.48	11.90	2.17	7.27	96.49
6	59.34	40.66	1.67	-2.30	35.77	679.42	320.86	3.23	8.97	18.99	2.12	9.78	96.95
8	58.07	41.93	1.61	--	29.55	631.11	308.05	0.30	10.42	21.35	2.05	6.50	97.89
10	58.12	41.88	1.36	--	23.43	725.67	364.43	0.00	15.55	30.97	1.99	14.24	96.09
13	55.60	44.40	1.42	-2.20	30.90	751.83	364.26	4.81	11.79	24.33	2.06	17.50	95.19
14	56.70	43.30	1.19	--	26.60	694.41	352.41	2.90	13.25	26.10	1.97	10.06	97.15
16	56.54	43.46	1.20	-1.90	33.17	553.84	248.25	0.00	7.48	16.69	2.23	5.06	97.96
18	54.79	45.21	1.00	--	32.28	690.17	328.49	0.68	10.18	21.38	2.10	12.55	96.18
20	55.71	44.29	0.81	-2.20	--	--	--	--	--	--	--	--	--
25	57.15	42.85	--	-2.70	47.52	813.22	363.68	0.93	7.65	17.11	2.24	12.71	96.51
30	60.64	39.36	0.78	-2.20	65.77	869.46	411.22	0.63	6.25	13.22	2.11	14.43	96.49
35	63.75	36.25	--	-2.50	89.25	1035.95	516.21	0.00	5.78	11.61	2.01	15.70	96.96
40	65.61	34.39	0.90	-2.20	81.67	892.78	490.38	0.50	6.00	10.93	1.82	15.04	96.93
45	67.48	32.52	--	-2.00	60.37	695.64	437.46	0.00	7.25	11.52	1.59	18.28	95.82
50	66.63	33.37	1.13	-1.70	--	--	--	--	--	--	--	--	--
55	67.85	32.15	--	-2.40	54.35	596.55	416.36	0.00	7.66	10.98	1.43	19.92	95.21
60	68.61	31.39	1.00	-2.10	59.31	579.62	518.38	2.21	8.74	9.77	1.12	21.10	95.93
65	68.35	31.65	--	-2.30	53.85	510.98	320.18	0.00	5.95	9.49	1.60	4.81	98.50
70	68.49	31.51	1.13	-1.60	54.10	601.26	396.96	1.39	7.34	11.11	1.51	20.63	94.80
75	69.29	30.71	--	-1.60	57.93	678.07	392.10	4.15	6.77	11.71	1.73	15.50	96.05
80	66.74	33.26	1.14	-1.60	54.96	625.12	378.10	0.61	6.88	11.37	1.65	11.67	96.91
90	59.52	40.48	1.23	-0.70	44.20	480.36	312.72	0.00	7.08	10.87	1.54	9.58	96.94

Continued...

Continuation of Table 3.12

Depth (cm)	AIR (%)	$CaCO_3$ (%)	OC (wt %)	δO^{18}	MS (SI unit)	χ_{ARM}	SIRM	χfd (%)	SIRM/χ_{lf}	χ_{ARM}/χ_{lf}	χ_{ARM}/SIRM	HIRM	S-ratio (%)
95	54.99	45.01	--	-0.50	40.17	464.04	302.70	2.43	7.54	11.55	1.53	6.61	97.82
100	55.35	44.65	1.02	-1.20	37.41	401.99	301.41	3.72	8.06	10.75	1.33	10.01	96.68
110	60.42	39.58	--	-0.80	36.95	481.32	362.64	0.00	9.82	13.03	1.33	23.42	93.54
120	62.45	37.55	1.76	-1.30	35.33	486.60	338.30	2.44	9.58	13.77	1.44	11.56	96.58
130	64.44	35.56	--	-1.10	33.55	480.77	337.60	0.25	10.06	14.33	1.42	16.42	95.14
140	62.98	37.02	2.19	-0.70	29.69	449.76	312.15	0.00	10.51	15.15	1.44	11.93	96.18
150	65.54	34.46	--	-0.10	32.09	375.57	300.75	3.62	9.37	11.70	1.25	13.55	95.50
160	64.39	35.61	2.35	-0.50	--	--	--	--	--	--	--	--	--
170	63.60	36.40	--	-0.70	23.74	78.00	150.71	4.63	6.35	3.29	0.52	11.18	92.58
180	64.32	35.68	2.40	-0.30	19.95	49.44	103.67	0.00	5.20	2.48	0.48	10.56	89.81
190	--	--	--	--	20.20	49.37	94.99	1.36	4.70	2.44	0.52	85.43	10.07
200	76.18	23.82	1.80	-0.20	20.64	48.51	99.57	0.70	4.82	2.35	0.49	25.83	74.06
210	--	--	--	--	19.57	46.94	92.48	1.43	4.73	2.40	0.51	4.00	95.68
220	--	--	--	--	21.06	50.12	94.94	16.57	4.51	2.38	0.53	10.86	88.57
230	--	--	--	--	20.03	46.54	88.91	3.88	4.44	2.32	0.52	-5.66	106.36
240	76.76	23.24	2.09	-0.70	18.91	50.71	99.55	0.88	5.26	2.68	0.51	17.13	82.79
250	--	--	--	--	19.68	50.22	108.09	6.79	5.49	2.55	0.46	8.94	91.73
260	--	--	--	--	19.51	48.13	119.69	0.83	6.13	2.47	0.40	26.60	77.78
270	--	--	--	--	21.67	59.37	142.05	12.86	6.56	2.74	0.42	9.52	93.30
280	75.51	24.49	1.53	--	22.21	68.70	154.87	15.33	6.97	3.09	0.44	8.56	94.48
290	--	--	--	--	22.25	69.12	160.54	5.53	7.22	3.11	0.43	9.83	93.88
300	--	--	--	--	20.24	60.38	140.30	0.00	6.93	2.98	0.43	8.10	94.23

Continued...

Continuation of Table 3.12

Depth (cm)	AIR (%)	$CaCO_3$ (%)	OC (wt %)	δO^{18}	MS (SI unit)	χ_{ARM}	SIRM	χfd (%)	SIRM/χ_{lf}	χ_{ARM}/χ_{lf}	χ_{ARM}/SIRM	HIRM	S-ratio (%)
310	--	--	--	--	18.17	53.97	120.13	0.00	6.61	2.97	0.45	11.48	90.44
320	--	--	--	--	20.56	52.32	114.86	6.76	5.59	2.54	0.46	10.73	90.66
330	--	--	--	--	18.85	49.23	99.22	14.94	5.26	2.61	0.50	11.29	88.62
340	--	--	--	--	14.54	28.60	66.50	3.92	4.57	1.97	0.43	8.74	86.86
350	--	--	--	--	12.46	27.54	49.81	1.26	4.00	2.21	0.55	8.16	83.62
360	76.09	23.91	--	--	--	--	--	--	--	--	--	--	--
370	--	--	--	--	8.35	17.43	30.00	2.53	3.59	2.09	0.58	5.99	80.02
380	77.01	22.99	--	--	10.05	15.38	27.11	0.00	2.70	1.53	0.57	4.66	82.81
400	--	--	--	--	12.13	21.46	49.38	1.95	4.07	1.77	0.43	8.88	82.01
410	--	--	--	--	10.18	12.77	26.45	0.00	2.60	1.25	0.48	4.30	83.75
430	--	--	--	--	11.89	18.47	27.07	8.39	2.28	1.55	0.68	3.35	87.62
440	80.76	19.24	--	--	8.88	16.40	25.66	0.00	2.89	1.85	0.64	4.65	81.88
450	--	--	--	--	10.47	20.37	37.00	0.00	3.53	1.95	0.55	8.10	78.10
470	--	--	--	--	12.86	24.72	46.86	0.00	3.64	1.92	0.53	9.88	78.92
480	--	--	--	--	14.22	33.63	66.54	0.00	4.68	2.36	0.51	12.43	81.31

Note: MS ($10^{-8}m^3kg^{-1}$); χ_{ARM} (m^3kg^{-1}); SIRM ($10^{-5}Am^2kg^{-1}$); SIRM/χ_{lf} ($10^3A/m$); χ_{ARM}/SIRM ($10^{-3}m/A$); HIRM ($10^{-5}Am^2kg^{-1}$)

Table 3.13. Distribution of acid insoluble residue (AIR), $CaCO_3$, δO^{18}, rock magnetic parameters, organic carbon (OC) and clay content in GC-13

Depth (cm)	AIR (%)	$CaCO_3$ (%)	δO^{18}	MS (SI unit)	χ_{ARM}	SIRM	χfd (%)	SIRM/ χ_{lf}	χ_{ARM}/χ_{lf}	χ_{ARM}/ SIRM	HIRM	S-ratio (%)	Depth (cm)	OC (wt%)	Clay (%)
0	67.80	32.20	--	14.88	118.88	81.46	10.55	5.47	7.99	1.46	5.89	92.77	0	3.82	32.20
2	--	--	-3.04	13.36	39.93	49.96	10.30	3.74	2.99	0.80	5.79	88.41	10	3.51	30.60
4	--	--	--	9.77	19.58	33.77	6.83	3.46	2.00	0.58	4.26	87.38	16	3.68	32.00
6	--	--	-2.53	11.05	13.72	33.78	6.80	3.06	1.24	0.41	4.62	86.31	22	3.44	37.80
8	--	--	--	10.56	19.42	32.90	10.27	3.12	1.84	0.59	4.46	86.45	42	3.22	31.50
10	65.90	34.10	-3.02	9.78	10.81	32.60	7.33	3.33	1.10	0.33	4.98	84.71	62	3.06	40.60
12	--	--	--	10.69	20.04	30.69	16.13	2.87	1.87	0.65	5.25	82.89	82	2.68	61.90
14	--	--	--	9.42	12.86	29.39	11.54	3.12	1.36	0.44	4.37	85.14	102	1.80	70.10
16	66.80	33.20	-2.86	10.20	17.87	30.36	14.19	2.98	1.75	0.59	5.03	83.45	122	1.35	70.80
18	--	--	-2.54	10.68	11.89	34.68	21.21	3.25	1.11	0.34	6.35	81.69	142	1.40	69.00
20	69.70	30.30	-2.81	39.57	439.61	324.16	0.95	8.19	11.11	1.36	24.92	92.31	167	1.31	43.50
25	--	--	-3.18	8.50	8.46	31.24	12.35	3.68	1.00	0.27	5.94	80.97	177	1.58	39.10
30	--	--	-2.54	9.24	10.14	32.91	8.65	3.56	1.10	0.31	6.43	80.46	202	1.60	38.30
35	--	--	-2.76	8.76	15.22	32.81	15.93	3.75	1.74	0.46	5.98	81.78	222	1.56	41.80
40	69.70	30.30	-1.98	11.31	21.89	41.35	20.65	3.65	1.94	0.53	8.78	78.77	242	1.62	44.20
50	--	--	-2.61	11.22	19.80	39.45	18.82	3.52	1.76	0.50	8.52	78.40	262	1.43	44.70
55	--	--	--	11.63	4.65	42.87	14.50	3.69	0.40	0.11	9.22	78.49	282	1.42	35.80
60	73.50	26.50	-2.91	16.34	31.53	69.51	7.62	4.25	1.93	0.45	14.06	79.77	302	1.37	39.20
65	--	--	-2.76	13.42	19.03	51.75	8.35	3.86	1.42	0.37	11.59	77.61	322	1.68	44.60
70	--	--	-2.64	15.44	15.85	68.76	2.99	4.45	1.03	0.23	14.10	79.49	333	1.48	43.00
75	--	--	-2.74	26.49	61.14	169.33	3.50	6.39	2.31	0.36	19.27	88.62			

Continued...

Continuation of Table 3.13

Depth (cm)	AIR (%)	$CaCO_3$ (%)	δO^{18}	MS (SI unit)	χ_{ARM}	SIRM	χfd (%)	SIRM/χ_{lf}	χ_{ARM}/χ_{lf}	χ_{ARM}/SIRM	HIRM	S-ratio (%)
80	75.40	24.60	-2.24	21.34	56.51	119.83	8.06	5.62	2.65	0.47	12.04	89.96
85	--	--	-2.35	32.52	204.27	279.58	2.12	8.60	6.28	0.73	22.52	91.95
90	--	--	-1.88	33.56	343.13	282.78	0.74	8.43	10.22	1.21	23.52	91.68
95	--	--	-1.55	35.66	345.20	295.23	1.06	8.28	9.68	1.17	23.74	91.96
100	84.80	15.20	-2.49	39.20	405.02	319.79	2.46	8.16	10.33	1.27	22.56	92.94
110	--	--	-2.64	36.81	328.68	288.00	0.94	7.82	8.93	1.14	20.11	93.02
115	--	--	--	33.02	338.36	275.71	0.53	8.35	10.25	1.23	25.31	90.82
125	--	--	--	37.94	429.45	297.60	1.31	7.84	11.32	1.44	11.40	96.17
130	--	--	-1.71	38.10	366.73	301.55	0.26	7.91	9.63	1.22	22.70	92.47
135	--	--	--	37.02	458.35	295.54	2.24	7.98	12.38	1.55	20.83	92.95
140	85.80	14.20	-1.64	36.01	405.64	283.50	2.19	7.87	11.26	1.43	17.37	93.87
145	--	--	--	37.10	368.56	278.78	1.70	7.51	9.93	1.32	16.33	94.14
150	--	--	-1.81	35.75	389.76	270.33	1.07	7.56	10.90	1.44	22.21	91.78
155	--	--	--	32.72	268.70	260.75	1.32	7.97	8.21	1.03	17.88	93.14
160	--	--	-1.54	30.00	345.38	228.23	2.39	7.61	11.51	1.51	17.30	92.42
165	78.30	21.70	-1.41	26.08	332.63	215.66	0.94	8.27	12.75	1.54	15.44	92.84
170	--	--	--	24.90	309.58	185.20	0.78	7.44	12.43	1.67	12.71	93.14
175	71.40	28.60	-1.16	18.74	283.50	168.47	4.59	8.99	15.13	1.68	12.66	92.48
180	--	--	--	20.54	334.24	185.14	1.56	9.01	16.27	1.81	13.77	92.56
185	--	--	-1.78	18.20	270.01	164.62	5.14	9.04	14.83	1.64	11.80	92.83
190	--	--	--	17.29	248.56	152.42	0.00	8.82	14.38	1.63	11.26	92.61

Continued...

Continuation of Table 3.13

Depth (cm)	AIR (%)	$CaCO_3$ (%)	δO^{18}	MS (SI unit)	χ_{ARM}	SIRM	χfd (%)	SIRM/χ_{lf}	χ_{ARM}/χ_{lf}	χ_{ARM}/SIRM	HIRM	S-ratio (%)
195	--	--	--	17.95	250.93	150.49	0.00	8.38	13.98	1.67	11.19	92.57
200	70.40	29.60	-1.56	17.38	317.30	163.19	4.40	9.39	18.26	1.94	14.64	91.03
205	--	--	--	18.63	316.01	153.87	4.33	8.26	16.97	2.05	12.43	91.92
210	--	--	--	20.69	262.04	174.54	2.89	8.44	12.67	1.50	12.00	93.12
215	--	--	--	22.01	208.04	173.40	6.63	7.88	9.45	1.20	14.81	91.46
220	72.40	27.60	-0.99	23.31	217.84	180.39	3.23	7.74	9.35	1.21	14.09	92.19
225	--	--	--	21.99	251.05	173.01	3.42	7.87	11.41	1.45	11.32	93.45
230	--	--	--	21.95	232.70	158.51	4.76	7.22	10.60	1.47	10.81	93.18
235	--	--	--	22.50	233.22	167.08	2.26	7.43	10.37	1.40	10.42	93.76
240	72.40	27.60	-0.76	21.59	214.27	169.50	1.20	7.85	9.92	1.26	10.39	93.87
245	--	--	--	15.26	102.53	114.15	3.30	7.48	6.72	0.90	9.62	91.57
250	--	--	--	20.08	173.65	143.46	9.47	7.14	8.65	1.21	10.57	92.63
260	73.40	26.60	-0.91	23.13	221.92	167.52	5.41	7.24	9.60	1.32	8.88	94.70
265	--	--	--	22.61	207.32	154.78	2.03	6.84	9.17	1.34	3.92	97.47
270	--	--	--	21.84	195.97	157.87	3.95	7.23	8.97	1.24	9.08	94.25
280	70.40	29.60	-1.01	22.68	145.53	156.71	4.14	6.91	6.42	0.93	8.22	94.76
285	--	--	--	22.77	157.28	150.76	3.99	6.62	6.91	1.04	6.77	95.51
290	--	--	--	24.91	168.65	172.66	5.88	6.93	6.77	0.98	6.65	96.15
300	76.40	23.60	-1.41	28.45	234.95	191.54	1.96	6.73	8.26	1.23	7.79	95.93
310	--	--	--	28.76	221.80	183.26	2.45	6.37	7.71	1.21	5.08	97.23
315	--	--	--	29.15	220.08	198.07	3.42	6.79	7.55	1.11	7.82	96.05
320	79.30	20.70	-1.03	28.03	192.43	195.51	1.47	6.97	6.86	0.98	5.79	97.04
330	78.30	21.70	--	30.66	182.84	192.16	7.66	6.27	5.96	0.95	9.46	95.08

Note: MS ($10^{-8}m^3kg^{-1}$); χ_{ARM} (m^3kg^{-1}); SIRM ($10^{-5}Am^2kg^{-1}$); SIRM/χ_{lf} ($10^3A/m$); χ_{ARM}/SIRM ($10^{-3}m/A$); HIRM ($10^{-5}Am^2kg^{-1}$)

Table 3.14. Down-core distribution of magnetic susceptibility (MS) in GC-14.

Depth (cm)	MS (SI unit)	Depth (cm)	MS (SI unit)	Depth (cm)	MS (SI unit)	Depth (cm)	MS (SI unit)
1	8.24	71	6.07	141	3.49	211	3.89
3	8.08	73	6.25	143	3.59	213	3.45
5	6.69	75	5.85	145	3.30	215	3.94
7	5.80	77	6.37	147	3.71	217	3.43
9	4.91	79	6.66	149	3.26	219	3.12
11	4.84	81	6.73	151	3.11	221	2.60
13	4.48	83	6.35	153	3.44	223	3.28
15	3.85	85	5.55	155	4.15	225	3.16
17	4.34	87	4.86	157	3.95	227	3.65
19	3.39	89	4.46	159	3.38	229	3.97
21	4.94	91	4.47	161	4.61	231	3.95
23	4.26	93	4.31	163	4.26	233	3.37
25	4.44	95	3.74	165	4.17	235	3.04
27	3.68	97	3.93	167	3.93	237	3.43
29	4.53	99	3.41	169	4.23	239	3.30
31	4.60	101	4.47	171	4.07	243	3.41
33	4.75	103	4.14	173	3.89	245	3.50
35	4.37	105	4.38	175	4.15	247	3.89
37	4.60	107	3.84	177	4.34	249	3.67
39	4.29	109	4.30	179	4.15	251	3.34
41	4.37	111	4.05	181	4.05	255	3.25
43	4.52	113	3.96	183	4.16	257	3.01
45	5.26	115	3.20	185	4.59	259	3.29
47	5.03	117	3.72	187	4.28	261	3.52
49	5.23	119	3.37	189	4.17	263	3.80
51	5.19	121	2.77	191	4.36	265	3.94
53	5.46	123	3.13	193	4.09	267	4.82
55	5.22	125	3.25	195	4.11	269	4.34
57	5.42	127	3.34	197	3.83	271	4.45
59	5.38	129	3.48	199	3.61	273	4.28
61	5.33	131	3.29	201	3.46	275	4.47
63	5.55	133	3.51	203	3.67	277	3.96
65	5.52	135	3.75	205	4.15	279	4.03
67	5.41	137	3.48	207	3.81	281	4.04
69	5.91	139	3.17	209	3.66	283	3.95

Note: MS (SI unit) – $10^{-8}m^3kg^{-1}$

Table 3.15. Down-core distribution of magnetic susceptibility (MS), acid Insoluble residue (AIR), $CaCO_3$, organic carbon (OC), and sand content in GC-15

Depth (cm)	MS (SI unit)	Depth (cm)	AIR (%)	$CaCO_3$ (%)	OC (wt%)	SAND (%)
10	9.77	2	62.18	37.82	4.39	10.61
14	54.61	6	58.40	41.60	3.56	41.36
16	20.19	10	--	--	--	9.35
18	5.57	14	53.69	46.31	3.02	12.99
20	6.57	16	--	--	--	19.52
30	63.68	18	--	--	--	14.40
35	6.05	20	53.77	46.23	2.53	16.57
40	4.87	30	--	--	--	19.15
45	7.84	40	51.19	48.81	1.42	24.42
50	6.58	50	--	--	--	25.38
55	7.39	60	49.60	50.40	1.39	25.50
60	6.80	70	--	--	--	30.09
65	4.74	80	46.52	53.48	3.08	28.48
70	2.38	90	--	--	--	28.46
75	4.32	110	61.18	38.82	2.78	32.79
80	3.47	130	46.27	53.73	2.58	32.23
85	4.26	150	43.19	56.81	2.18	38.65
90	20.35	170	42.69	57.31	2.71	35.20
95	4.26	190	45.77	54.23	2.79	33.77
100	4.30	210	--	--	--	28.49
110	3.41	230	55.69	44.31	2.34	26.70
120	3.56	250	--	--	--	23.24
130	4.42	270	65.18	34.82	2.69	14.78
140	4.50	290	--	--	--	14.04
150	3.01	310	71.26	28.74	2.87	7.85
160	0.49	330	--	--	--	5.91
170	3.18	350	75.76	24.24	3.70	6.38
180	4.32	370	--	--	--	7.06
190	3.43	390	84.51	15.49	1.93	21.73
200	4.03	410	74.26	25.74	2.41	--
210	3.40	--	--	--	--	--
220	3.16	--	--	--	--	--
230	4.14	--	--	--	--	--
240	5.38	--	--	--	--	--
250	5.36	--	--	--	--	--
260	5.39	--	--	--	--	--
270	5.76	--	--	--	--	--
280	5.11	--	--	--	--	--

Continued...

Continuation of Table 3.15

Depth (cm)	MS (SI unit)	Depth (cm)	AIR (%)	$CaCO_3$ (%)	OC (wt%)	SAND (%)
290	6.15	--	--	--	--	--
300	7.17	--	--	--	--	--
310	7.30	--	--	--	--	--
320	4.27	--	--	--	--	--
330	7.20	--	--	--	--	--
350	7.93	--	--	--	--	--
360	9.31	--	--	--	--	--
370	9.62	--	--	--	--	--
380	7.41	--	--	--	--	--
390	9.90	--	--	--	--	--
400	10.05	--	--	--	--	--

Note: MS (SI unit) – $10^{-8}m^3kg^{-1}$

Chapter 4

Chapter 4

LIME MUDS AND THEIR GENESIS OFF NORTHWESTERN INDIA DURING THE LATE QUATERNARY

4.1. Introduction

Lime muds are produced by several mechanisms: mechanical disintegration of biogenic skeletal components, disaggregation of calcareous green algae, inorganic precipitation, bioerosion, erosion of tidal-flat deposits, and bio-geochemical processes (Bathurst, 1971). Although lime muds are abundant in the geological past (Matthews, 1966), the depositional conditions of modern carbonates are not conducive for the formation of lime muds. The modern settings for lime muds formation are largely confined to carbonate platforms (Bahamas, Florida, Belize) or shallow-water ramps (Persian Gulf) (Ginsburg, 1956; Lowenstam and Epstein, 1957; Cloud, 1962; Wells and Illing, 1964; DeGroot, 1965; Matthews, 1966; Stockman et al., 1967; Mitterer, 1972; Neuman and Land, 1975; Steinen et al., 1988; Boardman and Carney, 1991; Robbins and Blackwelder, 1992; Milliman et al., 1993; Dix, 2001). Lime muds constitute about 30-50% of the Holocene sediments in the *Halimeda* bioherms from the Great Barrier Reef (Marshall and Davies, 1988). Modern calcareous tube-pelagic muds and pelagic muds were reported at depths between 110 and 210 m and >210 m, respectively on the tropical, northwestern Australia (James et al., 2004). Lime muds have not been found in some recent carbonates of the isolated carbonate platforms of Central America (Gischler and Lomando, 1999). Spiculitic and bryozoan carbonate silts constitute about 20-50% of the modern sediments at depths >80 m of the sub-tropical southwest Australian margin, including the Great Australian Bight (James et al., 1999; 2001).

The formation of lime mud in modern carbonate settings has remained controversial. Despite many attempts it has rarely been possible to relate lime muds unambiguously to a unique source. Inorganic formation is favoured by Cloud (1962), Wells and Illing (1964), De Groot (1965), Milliman et al. (1993) and Dix (2001), whereas disintegration of codiacean algae and other skeletal materials by Lowenstam and Epstein (1957), Matthews (1966), Stockman et al. (1967) and Neuman and Land (1975). Lime mud origin has been linked to dense carbonate mud suspensions (whitings) formed from biogeochemical processes (Broecker and Takahashi, 1966; Morse et al., 1984; Morse and Mackenzie, 1990; Robbins and Blackwelder, 1992). Shinn et al. (1985 and 1989) have also reported that the whitings have resulted from the resuspension of deposited lime mud because of stirring by fish/ocean currents/storms. Lime mud formation through micritization, diminution (Reid et al., 1992) and syndepositional recrystallization of sediment grains (Miliolid and *Halimeda*) (Macintyre and Reid, 1995; Reid and Macintyre, 1998) in shallow tropical seas has also been reported. The muds on the Australian margins are largely biofragmental fine fraction (James et al., 1999, 2001, 2004).

Therefore the purpose of this chapter is to investigate the origin of lime muds of deep-water, open-ocean shelf off northwest India at depths between 56m and 121 m using five gravity cores. A variety of methods (grain size, scanning electron microscope (SEM), Sr content, stable isotopes and associated minerals) were employed to understand the sources of muds and influences of late Quaternary climatic and sea level changes on their deposition.

4.2. Geologic Setting

A drowned carbonate platform is the largest topographic feature on the northwestern margin of India (Fig. 4.1). This platform was isolated and separated from the coast by a huge clastic depocenter – the Dahanu depression - in which pro-delta sediments were deposited since the Eocene (Basu et al., 1980). At present the depression was filled up and forms the

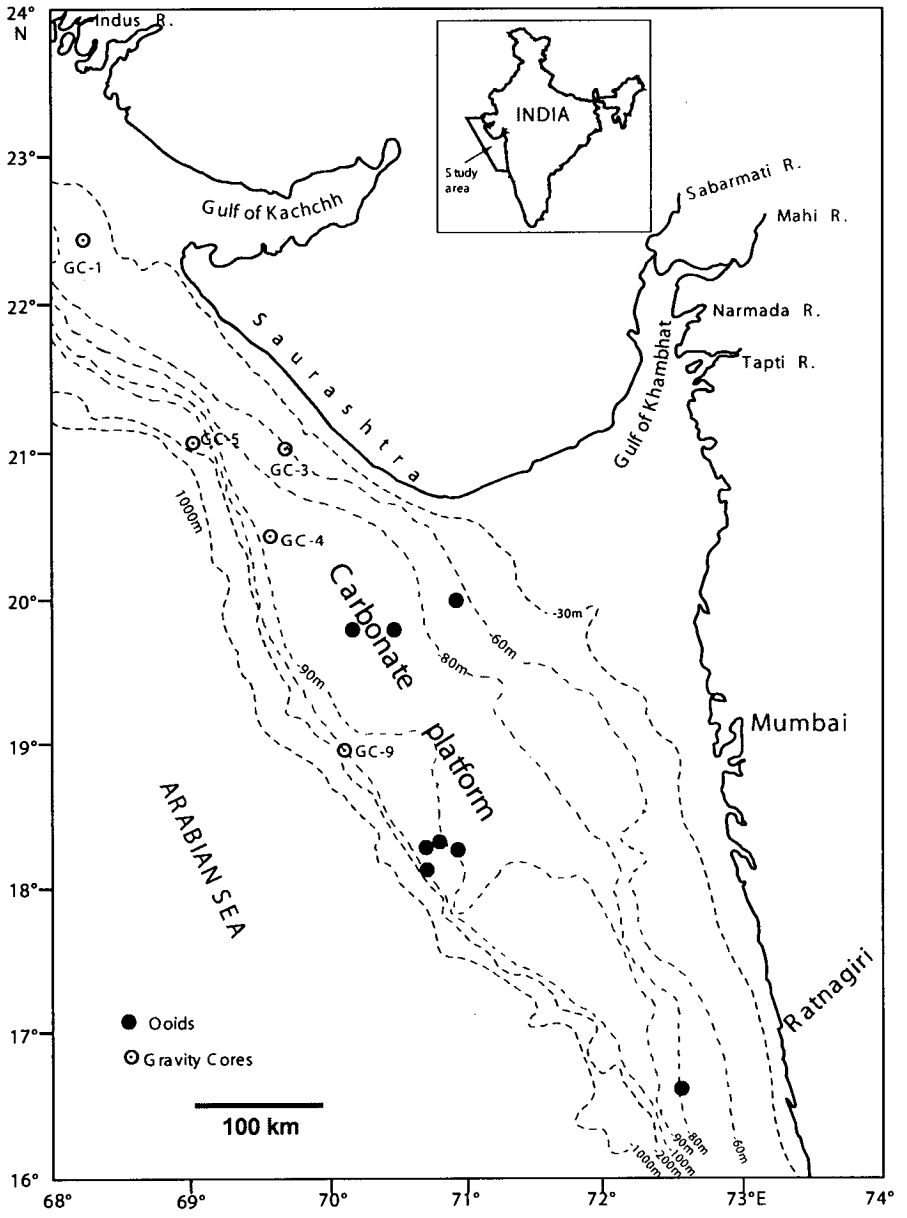

Fig. 4.1. Location of the gravity cores and ooids used for lime mud investigation

inner shelf, consisting of modern silici-clastic sediments. The eastern margin of the platform is now connected to the inner shelf and the platform thus forms an outer shelf with water depths ranging between 60 and 110 m. It consists of relic sandy carbonate sediments. As the western slopes of the platform are steep, the term 'carbonate ramp' does not apply. Therefore the term drowned platform or outer shelf seems to be ideal. The width of the continental shelf (including platform) is greatest (~345 km) off Mumbai, decreasingly to 70 km off Saurashtra. The shelf break occurs at about 80-120 m off Saurashtra and at about 90 m offshore of Mumbai (Rao and Wagle, 1997). Major sources of terrigenous sediments to this part of the shelf are from the Indus, located about 100 km from the north of the Gulf of Kachchh and the Narmada and Tapti Rivers, which debouch enormous volumes of sediments into the Gulf of Khambat (Fig. 4.1) and, a few minor rivers draining the Saurashtra coast.

4.3. Previous Studies on the Carbonate Platform

The relic deposits on the platform consist of abundant aragonite faecal pellets, ooids, *Halimeda* grains and a few bivalves, benthic and planktic foraminifers (Rao et al., 1994). It also contains indurated aragonite muds, *Halimeda*- and pelletal limestones, coralline algal nodules, a few coral fragments, oyster shells and dolomite encrustations (Nair, 1971; Nair et al., 1979; Rao et al., 1994, 2003a and b). The measured radiocarbon ages, determined by the Accelerator Mass Spectrometer on the platform, are 17,500 yr BP for the dolomite crusts obtained from 64 m and 17,950 yr BP and 21,000 yr BP for aragonite ooids obtained from 72 m and 88 m, respectively (Rao et al., 2003b). These suggest that the platform may not have been exposed sub-aerially during the Last Glacial Maximum (LGM). Other radiocarbon ages on the platform range between 12,940 yr BP (14.3 ka) and 7,250 yr BP (7.6 ka) (Fig. 4.2) and do not correspond with that of the glacio-eustatic sea level changes (Rao et al., 2003a). Vaz et al. (1993) reported lime muds between 150 and 500 m off the Gulf of Kachchh at depths and suggested that these lime muds are detrital and transported from shallow depths.

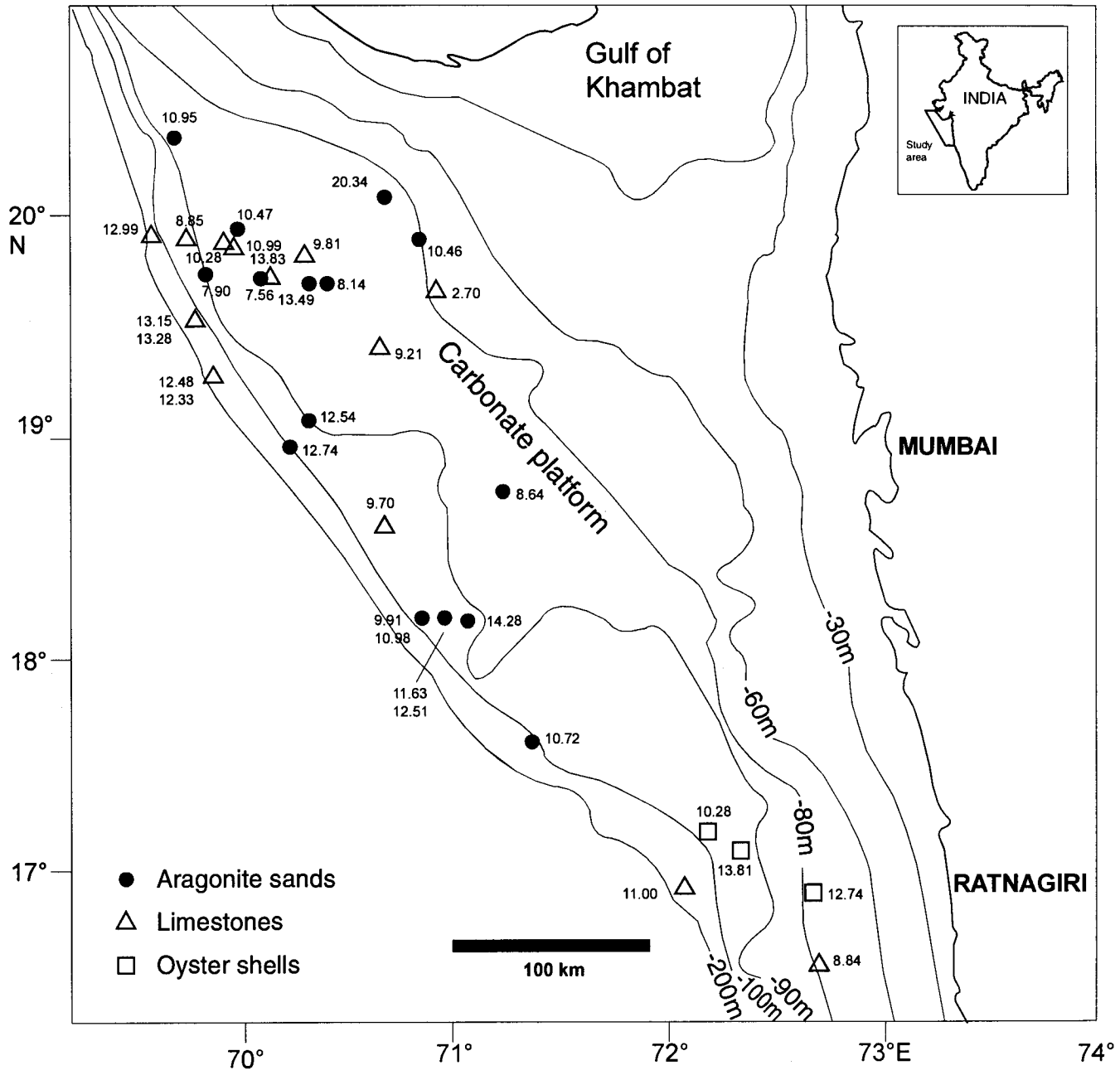

Fig. 4.2. Calibrated radiocarbon ages (ka) of relic sediments on the carbonate platform

4.4. Results

The sediments in the gravity cores exhibited two distinct sedimentary units, a lower unit 2 and an upper unit 1. Unit 2 was thicker and consisted abundant lime muds. Unit 1 was thinner and consisted of a mixture of terrigenous and carbonate sediments, or predominantly terrigenous sediments. The carbonate content of the lime muds was the lowest (60%) in GC-1 (see Fig. 4.3; Table 4.1) that increased to 75% in GC-3 (Fig. 4.4; Table 4.2), to 90% - 95% in GC-4, GC-5 and GC-9 (Figs. 4.5-4.7; Tables 4.3-4.5). The lime muds in shallow cores therefore contained less carbonate than in cores closer to the shelf break and near the carbonate platform.

4.4.1. Gravity cores from the continental shelf (GC-1 and GC-3)

i. Transition

The transition between the two sedimentary units in GC-1 and GC-3 cores occurred at about 140 cm and 78 cm, respectively.

ii. Grain size

In GC-1, the median and peak grain sizes of the lime muds (unit 2) were ~ 5 μm and 10 μm, respectively at the bottom, but increased gradually to 10 μm and 20 μm upwards toward the boundary between the two units (Fig. 4.3, Table 4.1). In GC-3 (Fig. 4.4, Table 4.2), the median (<10 μm) and peak grain sizes (7-15 μm) of the lime muds were smaller than that in GC-1.

iii. Coarse fraction

Sand content was distinctly small (<5%) in unit 2 of these cores. In GC-1 it comprised mica, quartz, pyrite, rounded bioclasts / pellets, *Uvigerina sp.* and ostracods at different intervals. The sand content between 140 and 80 cm was high (up to 75%; see Fig. 4.3) and comprised 3-4 cm sized aragonite crusts, green grains, green clay infillings of planktic / benthic foraminifers and their aggregates. In GC-3, unit 2 comprised subrounded to rounded bioclasts,

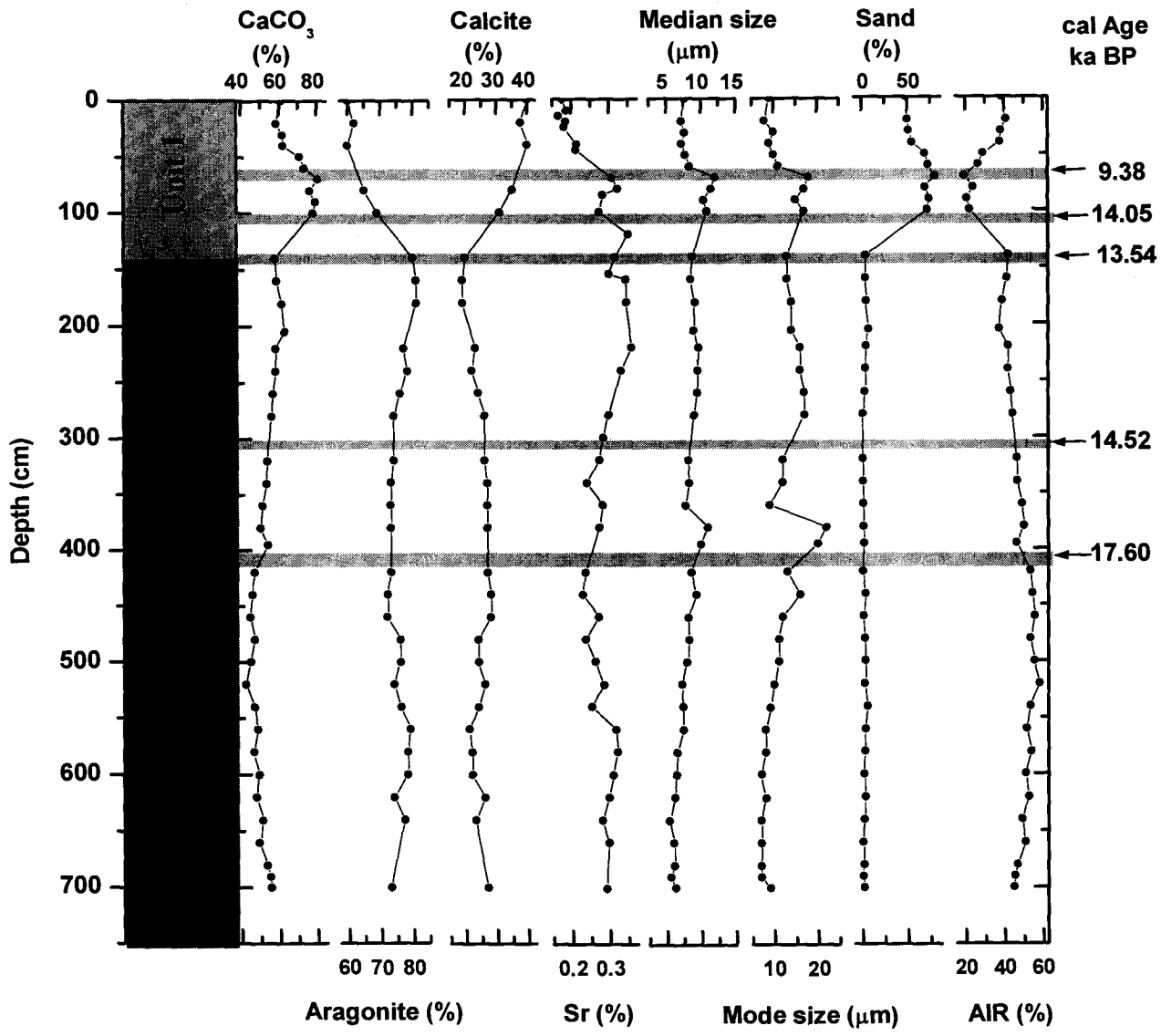

Fig. 4.3. Down-core variation of carbonate ($CaCO_3$), aragonite, calcite, strontium content (Sr), median and mode grain size of the bulk sediment (<63 μm fraction), sand and acid insoluble residue (AIR) content in **GC-1**.

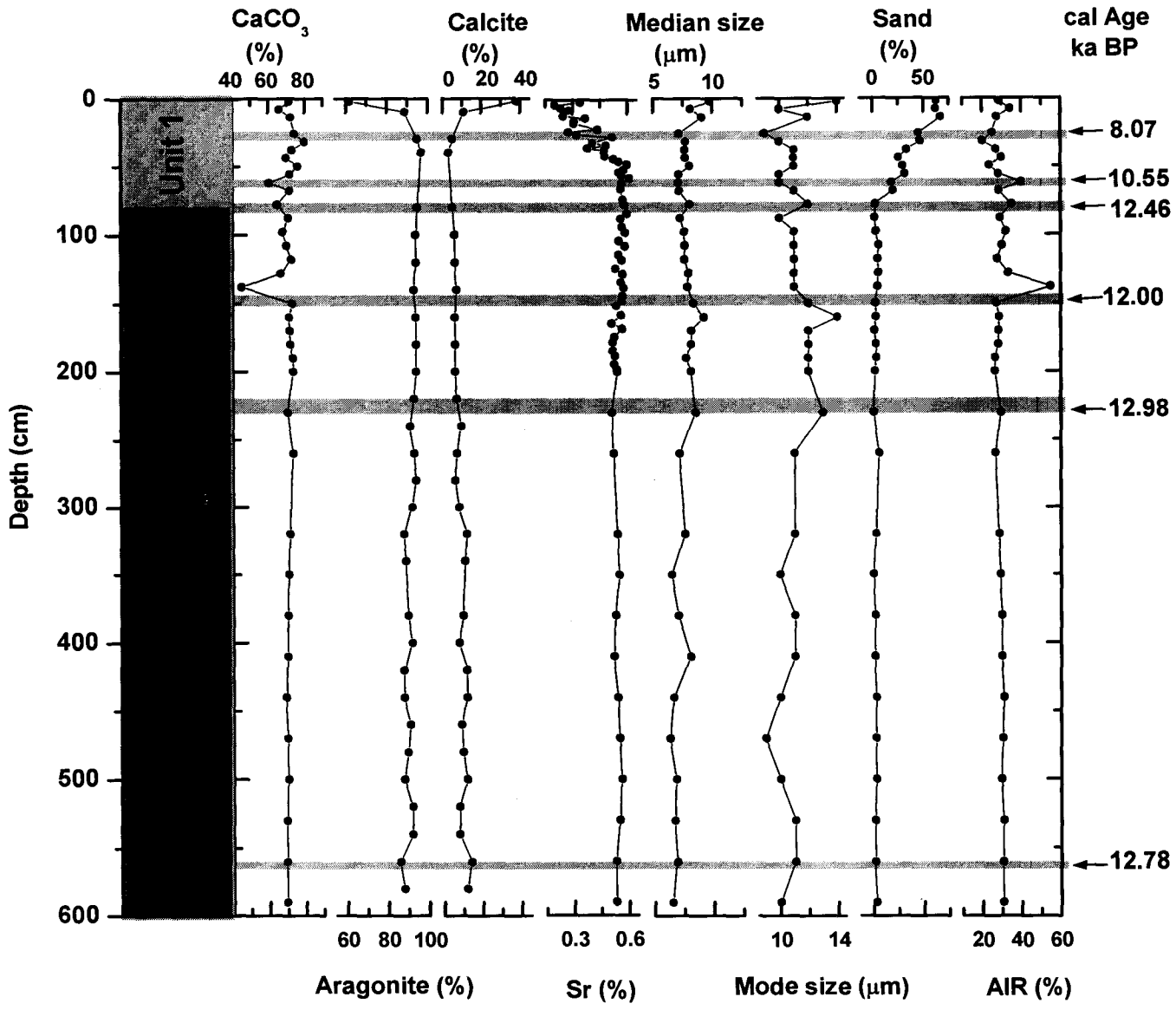

Fig. 4.4. Down-core variation of carbonate ($CaCO_3$), aragonite, calcite, strontium content (Sr), median and mode grain size of the bulk sediment (<63 μm fraction), sand and acid insoluble residue (AIR) content in **GC-3.**

pelletal material, ostracods, transparent bivalves and a few skeletal debris at different intervals.

iv. Mineralogy and Petrology

Lime muds predominated in unit 2 of these cores and that contained 50-60% carbonate in GC-1 and ~75% in GC-3. Aragonite, quartz, calcite, feldspar and chlorite were found in varying proportions in both the cores (Fig. 4.8A-B). The weight percentage of aragonite in carbonates varied from 73 to 80% in GC-1 but was >90% in GC-3. Illite and chlorite with minor smectite were dominant clay minerals in unit 2 of both the cores. The unit 1 sediments in GC-1 also contained illite, chlorite with increased proportion of smectite, while that of GC-3 was found to be smectite-rich but illite and chlorite-poor. Aragonite needles were abundant in < 4 μm fraction of the sediment (Fig. 4.10a) whereas detrital particles were with a few adhering aragonite crystallites in the 4-16 μm fraction (Fig. 4.10b) of the unit 2 sediments. Blunt edges were characteristic of the needles (Fig. 4.10a-b).

v. Geochemistry

The Sr content in GC-1 was low (0.16%) at the top of the core and gradually increased to 0.21% at 80 cm. Higher Sr values (avg. 0.29%) occurred between 81 and 140 cm of unit 1 and also in unit 2 (avg. 0.29%) sediments (Fig. 4.3, Table 4.1). The Sr content of GC-3 (Fig. 4.4, Table 4.2) was higher than that in GC-1. It was 0.34% at the core top and increased gradually to 0.55% towards the boundary between units 1 and 2, but remained uniform at the same level (avg. 0.55%) in unit 2 sediments. Low Sr values well coincided with low weight percentage of aragonite (Fig. 4.9A). When weight percentage of aragonite was higher (85 and 95%) Sr values ranged between 0.20% and 0.65%.

The $\delta^{18}O$ values of the lime muds were always negative and ranged between -0.1‰ and -0.5‰ (avg. -0.25‰) and -0.3‰ and -0.5‰ (avg. -0.45‰) in GC-1 and GC-3, respectively (Table 4.6). Similarly, the $\delta^{13}C$ values ranged between 2.6‰ and 2.9‰ (avg. 2.7‰) and, 2.4‰ and 3.0‰ (avg.

2.9‰) in GC-1 and GC-3, respectively (Table 4.6). The isotope values of the lime muds in GC-1 and GC-3 formed a separate group and with no specific relationship with the increased weight percentage of aragonite (Fig. 4.9B-C).

vi. Radiocarbon ages

The age of lime muds of GC-1 between 400 cm and 140 cm of the core (from the core top) ranged between 17.6 ka and 12.8 ka. Aragonite encrustations at 105 cm belonged to 14.1 ka while sediments at 70 cm to 9.4 ka (see chapter 2, Table 2.2). Older and coarse-grained sediments overlie the younger and fine-grained sediments at the transition depth between unit 2 and unit 1 (Fig. 4.3). The transition seems to have occurred after 12.8 ka (Fig. 4.3). The age of the lime muds (unit 2) in GC-3 ranged between 13.0 ka and 12.0 ka. The sediments with lower age were sandwiched between those with relatively higher ages and the transition from unit 2 to unit 1 seems to have occurred after 12 ka (Fig. 4.4).

4.4.2. Gravity cores from the shelf break (GC-4, GC-5, GC-9)

i. Transition

The transition between unit 1 and 2 occurred at 184 cm in GC-4, 136 cm in GC-5 and 60 cm in GC-9 (Figs. 4.5-4.7). Lime muds were abundant in unit 2 of all these cores.

ii. Grain size

The median and mode grain sizes of the lime muds in GC-5 varied from 18 to 22 μm and 30 μm, respectively at the core bottom but both decreased gradually to 10 μm at the transition boundary (Fig. 4.6, Table 4.4). In GC-4 and GC-9, the median and peak grain sizes of the lime muds were 10 and 15 μm, and 12 and 20 μm, respectively (Figs. 4.5 and 4.7, Tables 4.3 and 4.5).

iii. Coarse fraction

Sand content of unit 2 sediments in GC-4 and GC-5 was relatively high (25 to 50% - Figs. 4.5-4.6) than in GC-9 (<25%, Fig. 4.7). The sand comprised largely spherical to ovoid particles and pelletal material (see SEM photos in Fig. 4.12), which were aragonitic in composition. Transparent bivalves, planktic foraminifers, ostracods and fragmented skeletal particles were <1% at certain intervals.

iv. Mineralogy and Petrology

The lime muds in GC-5 and GC-9 contained more carbonate (>95%) than that of GC-4 (90%). Aragonite and (low-Mg) calcite were the carbonate minerals (Fig. 4.8C-D). The abundance of aragonite was >95 wt % in all these cores. Some lime mud intervals in unit 2 of GC-5 were devoid of terrigenous minerals, while others were mixtures of carbonate (aragonite, calcite) and terrigenous minerals (quartz and feldspar) (Fig. 4.8C). The unit 1 sediments of GC-4 and GC-5 were more terrigenous in nature, which increased with a corresponding decrease in carbonate content (Figs. 4.5-4.6). Illite and chlorite were dominant clay minerals in the unit 2 sediments of all the cores and also in unit 1 sediments of GC-9. Smectite followed by illite and chlorite occurred in abundance in unit 1 sediments of GC-4 and GC-5.

Lime muds exhibited a few clots of aragonite needles in the < 4 μm fraction (Fig. 4.11a). However, in all other size fractions of the silt, lime muds exhibited a unique characteristic of clusters or aggregates morphologically similar to spheroid or ovoid-type particles (Fig. 4.11b, d, f, h). The particles were well-developed in higher silt-size fractions. Repeated investigations on the untreated and hydrogen peroxide-treated lime muds of different size fractions under SEM confirmed the presence of spheroids and ovoid-type particles and not artefacts in the laboratory. On higher magnification, the spheroid or ovoid-type particles consisted of wrapped aragonite needles (Fig. 4.11 b, d, f, h). Upon further magnification, the needles exhibited rounded ends or blunt edges (Fig. 4.11c). Some free needles were rod-shaped (Fig. 4.11e). Jointed partly radiating needles (Fig. 4.11g and 11i) and needles

wrapped in a smooth envelope of aragonite as if the needles are emanating from a quiver (see between arrows in Fig. 4.11g) were also seen. In some cases coccoliths were associated with the aragonite needles (Fig. 4.11a). Lime muds in the size fractions 63 -125 μm and >125 μm (Fig. 4.12a-b) also contained similar spherical and ovoid particles, formed by aggregation of aragonite needles (Fig. 4.12c-d). In some cases larger spheres were composed of aggregates of smaller spheres (Fig. 4.12b). In fact, abundance of these particles increased the coarse fraction content in unit 2 sediments of GC-4 and GC-5 (Figs. 4.5-4.6). Heavily fragmented prismatic or smaller rods of aragonite needles were also seen at some places (Fig. 4.12e). Fig. 4.12f shows disintegration of aragonite needles from the skeletal materials.

v. Geochemistry

The Sr contents at the core tops of GC-4 and GC-5 were 0.3% and 0.1%, respectively (Fig. 4.5; Fig. 4.6), increased gradually towards transition zone between units 1 and 2 and remained high in the latter unit (average 0.66% in GC-5, 0.58% in GC-4). The average Sr contents in the unit 1 (0.76%) and unit 2 (0.77%) sediments of GC-9 (Fig. 4.7) were higher than that of GC-4 and GC-5. The Sr values of lime muds in these cores were lower than in aragonite ooids (0.85% to 0.94%) from the adjacent carbonate platform (see Fig. 4.9A) and ooids of the Persian Gulf and the Bahamas (0.96% to 0.99% - Milliman, 1974). The plot of Sr content of the lime muds and ooids from the platform against their aragonite content showed that, despite aragonite content was >95% in both ooids and lime muds, the Sr values of ooids were highest and fall at one extreme end and, the values of lime muds of GC-4 were lowest and fall at the other extreme end (Fig. 4.9A). The lime muds of GC-5 plot between ooids and lime muds of GC-4 (Fig. 4.9A). All points of GC-5 to GC-9 plot one upon the other and therefore cannot be seen in Fig. 4.9A.

The $\delta^{18}O$ values (avg. 0.67‰) of lime muds in these cores were more positive than that of shelf cores and ranged between 0.0‰ and 1.4‰. The $\delta^{13}C$ values (avg. 3.97‰) were between 3.8‰ and 4.4‰ (Table 4.6). The

plots of aragonite content vs. isotope values ($\delta^{18}O$ and $\delta^{13}C$) of lime muds in different cores and ooids of the carbonate platform (Fig. 4.9B and C) exhibited similar isotopic values for the same aragonite content. The oxygen and carbon isotope values of lime muds of GC-5 were within the range found for ooids, but those in lime muds of GC-4 were lower than the ooid range (Fig. 4.9B-C). Fig. 4.9D indicates that the isotope values of lime muds of all cores fall on a regression line, with ooids and lime muds of GC-5 at one end and lime muds of GC-1 and GC-3 and some values of the *Halimeda* and *Penicillus* at the other extreme end. The isotope values for lime muds of GC-4 were between the two. It is interesting to note that the isotope values of lime muds in all the cores were within the range of values of sedimentary aragonite needles (see Fig. 4.9D) of organic origin, reported by Lowenstam and Epstein (1957).

vi. Radiocarbon ages

The radiocarbon ages (Chapter 2, Table 2.2) of the lime muds in GC-5 represent a longer time scale (16.1 ka and 14.0 ka) than in GC-4 (12.8 and 11.9 ka) and GC-9 (14.1 ka and 13.0 ka) (see Figs. 4.5-4.7). The close interval radiocarbon dating in GC-5 indicates a condensed section of sediments at the transitional depths and, the transition from unit 2 and unit 1 seems to have occurred much before 10.7 ka (Fig. 4.6). In GC-4 the transition occurred after 11.9 ka. The thickness of the sediments in unit 1 of GC-9 was small.

4.5. Discussion

4.5.1. Origin of lime muds

The aragonite content of the lime muds varied from 73-80 wt % in GC-1 and >90% in GC-3 and >95% in other cores (GC-4, GC-5 and GC-9). The lime muds therefore, are referred to here as aragonite muds or aragonite-dominated lime muds.

i. Cores at the shelf

The origin of lime muds is discussed based on their size, mineralogy, Sr content and stable isotopes.

a. Grain size: Stockman et al. (1967) and Stieglitz (1972) suggested that the aragonite needle muds formed by inorganic processes or disintegration of codiacean algae are smaller in size (<15 μm) but those derived from the biological and mechanical disintegration of resistant skeletal materials exhibit recognizable skeletal silts in the size range 15-62 μm. There are no recognizable skeletal silts in lime muds from the shelf cores to suggest that the muds were disintegrated from resistant skeletals. As the median size of the muds is smaller (Figs. 4.3-4.4) they may be either inorganically precipitated or disintegrated from aragonite algae.

b. Sr content: The Sr values of the muds (0.29% in GC-1, 0.55% in GC-3), however, do not support inorganic origin of aragonite, because the values are much lower than that in the experimentally precipitated aragonite (range, 1.08% - 1.25%), inorganic aragonite muds from the Bahamas (0.72% to 1.06%) or in coastal lagoons of the Abu Dhabi (0.94%) (see Bathurst, 1971). The Sr values in GC-1 are closer to that of the lime muds of Florida, derived from the mechanical disintegration of mollusks (<0.4%), while those in GC-3 are higher (0.55%) than that in mollusks and lower than that in high-Sr (0.63 to 0.85%) skeletals, such as codiacean algae and corals. However, no clue was found in the silt / coarse fraction to suggest that Sr was derived from mollusks and/or codiacean algae. Since the decrease in Sr well coincides with that in weight percentage of aragonite (Fig. 4.9A), one may argue that low Sr content lime muds might have been due to the dilution of other carbonate mineral phases and terrigenous sediments (Fig. 4.8A-B), or Sr loss during recrystallization of metastable minerals in diagenesis. Since the samples with high aragonite content (90%) contain only 0.6% Sr (see Fig. 4.4) inorganic origin for the lime muds, or Sr loss during diagenesis may not be the causes here. Aragonite needles most likely have been derived from the codiacean algae. Abundant terrigenous clays (45-55%) and minerals (mica, illite, chlorite,

quartz and feldspar – Fig. 4.8A) are indicative of Indus origin (see Rao and Rao, 1995), and the association with lime muds suggest that the muds are reworked and subsequently admixed with the Indus sediments. The lime muds in this core are bio-detrital.

c. Stable isotopes: Depleted and distinctly different stable isotopes of these lime muds compared to that in the cores at the shelf break (Table 4.6; Fig. 4.9B and 9C) suggest different origin for the shelf muds. The $^{18}O/^{16}O$ ratios of the muds follow that of the overlying water and decrease with rising water temperature (Bathurst, 1971). If muds are derived from skeletal materials, the isotope ratios should have varied with the taxonomy of the organisms. Muds disintegrated from codiacean algae are expected to show depleted oxygen and enriched carbon isotope ratios. As the present isotopic values are significantly depleted, lime muds may have formed either in water masses of different characteristics rather than in open shelf, or altered after their formation.

Core GC-1 was retrived off the Gulf of Kachchh (Fig. 4.1). The maximum water depth in the Gulf is 40 m where tides of 5-6 m high occur at present. The Gulf sediments consist of relic dolomite crusts and fossil corals, and their depth of occurrence and age do not correspond with that on the Glacio-eustatic sea level (Rao et al., 2003a). Lime muds at present do not form either in the Gulf or in the tidal flats north of the Gulf of Kachchh. It is likely that the waters in the Gulf may have been conducive for the growth of aragonite-producing plants at ~15 ka. Subsequently, these muds were reworked, admixed with Indus-derived clastic sediments and redeposited on the shelf and at the core site. Lime muds of younger ages underneath the older muds and aragonite encrustations support the argument that these muds were reworked. The core GC-3 is located closer to the carbonate platform. Higher Sr values (0.25% to 0.6%) for higher aragonite content (85-95% - Fig. 4.9A) probably suggest that the aragonite muds are mixture derived from the shelf and carbonate platform.

ii. Cores at the Shelf break/Upper slope

The lime muds in GC-4, GC-5 and GC-9 are dominantly aragonitic (>95%) with characteristic needles. Needles of aragonite have been interpreted as either inorganic in origin or derived from the disintegration of aragonite-producing skeletal components. Acid-insoluble residue associated with the muds was <5% to 10% in different cores (Figs. 4.5-4.7).

a. Grain size: The aragonite needle muds of inorganic origin or disintegrated from codiacean algae are smaller in size (<15 μm) and those derived from the resistant skeletals are larger in size (15-62 μm) (Stockman et al., 1967; Stieglitz, 1972). Although the median sizes of the lime muds are high (10 - 22 μm - Figs. 4.5-4.7), there are no recognizable skeletals or fossils either in the silt or coarse fraction to indicate the mud originated from resistant skeletals. The larger grain size of the muds is due to the aggregation of individual needles into spheroids and ovoid-type particles in various size fractions (Fig. 4.11). Therefore, particle size alone is insufficient to track the origin for the muds. Coarse fraction components consisting of aragonite needle bound spheroids (Fig. 4.12a) and small spheroids aggregating into larger spheroids (Fig. 4.12b) along with the repeated observations on the untreated and H_2O_2-treated muds confirmed the presence of spheroid and ovoid-type particles.

b. Morphology of the needles: Inorganically formed aragonite needles are usually pointed, and those from aragonite alga are prismatic with blunt edges (Loreau, 1982; Macintyre and Reid, 1992). The aragonite blades with blunt terminations and prismatic ends (Fig. 4.11c), rods showing rounded ends (Fig. 4.11g), jointed needles (Fig. 4.11g & i) and rods emanating from the envelope of mineralized aragonite (Fig. 4.11g) are typical characteristics to suggest that they were formed from the disintegration of the soft tissues of algae (see Loreau, 1982; Macintyre and Reid, 1992). However, only a few skeletal materials show disintegration into aragonite needles (Fig. 4.12f). Smaller pointed needles at one end in <4 μm fraction (Fig. 4.11a) may suggest contribution from inorganic origin but were broken down subsequently during

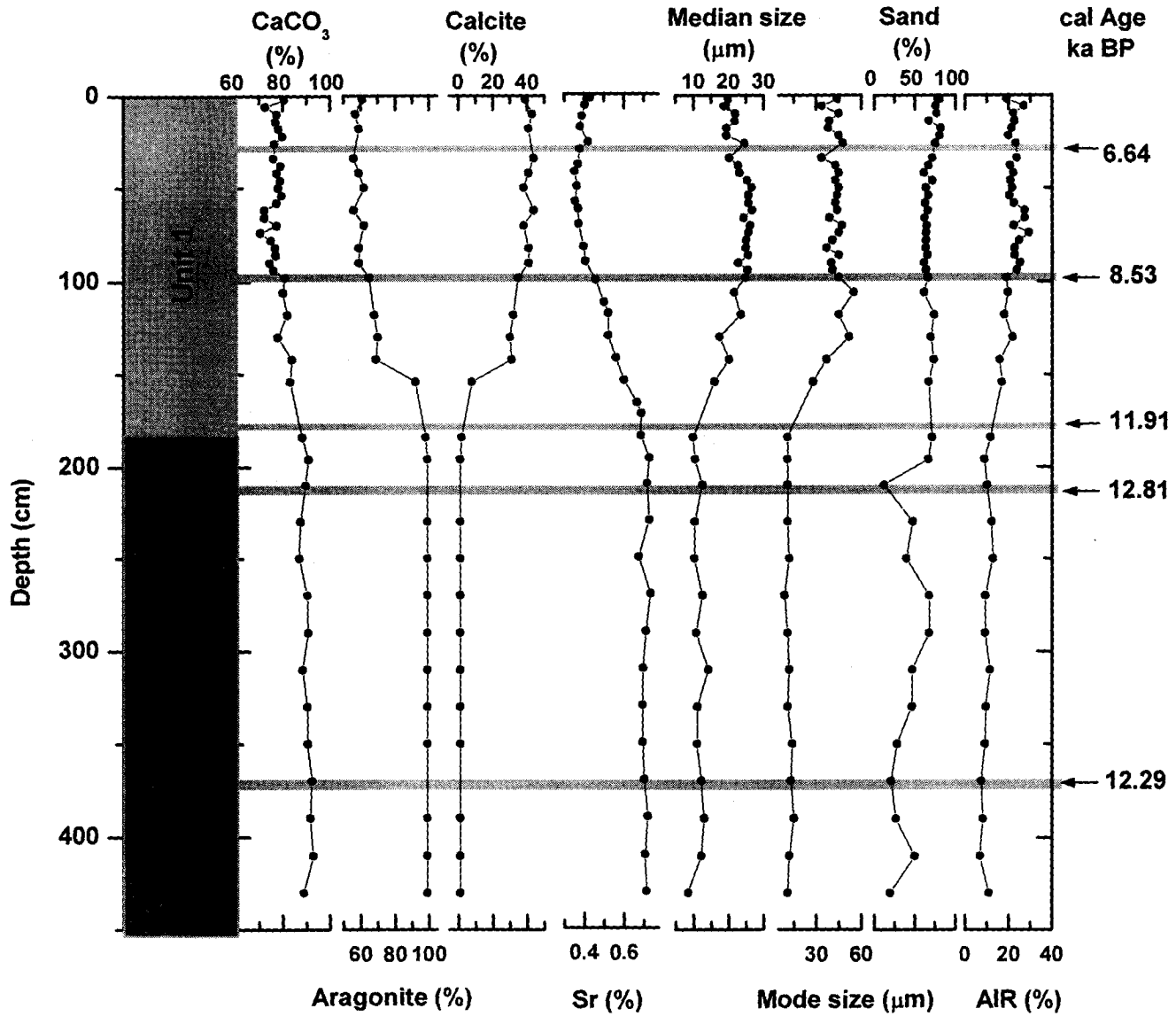

Fig. 4.5. Down-core variation of carbonate ($CaCO_3$), aragonite, calcite, strontium content (Sr), median and mode grain size of the bulk sediment (<63 μm fraction), sand and acid insoluble residue (AIR) content in **GC-4.**

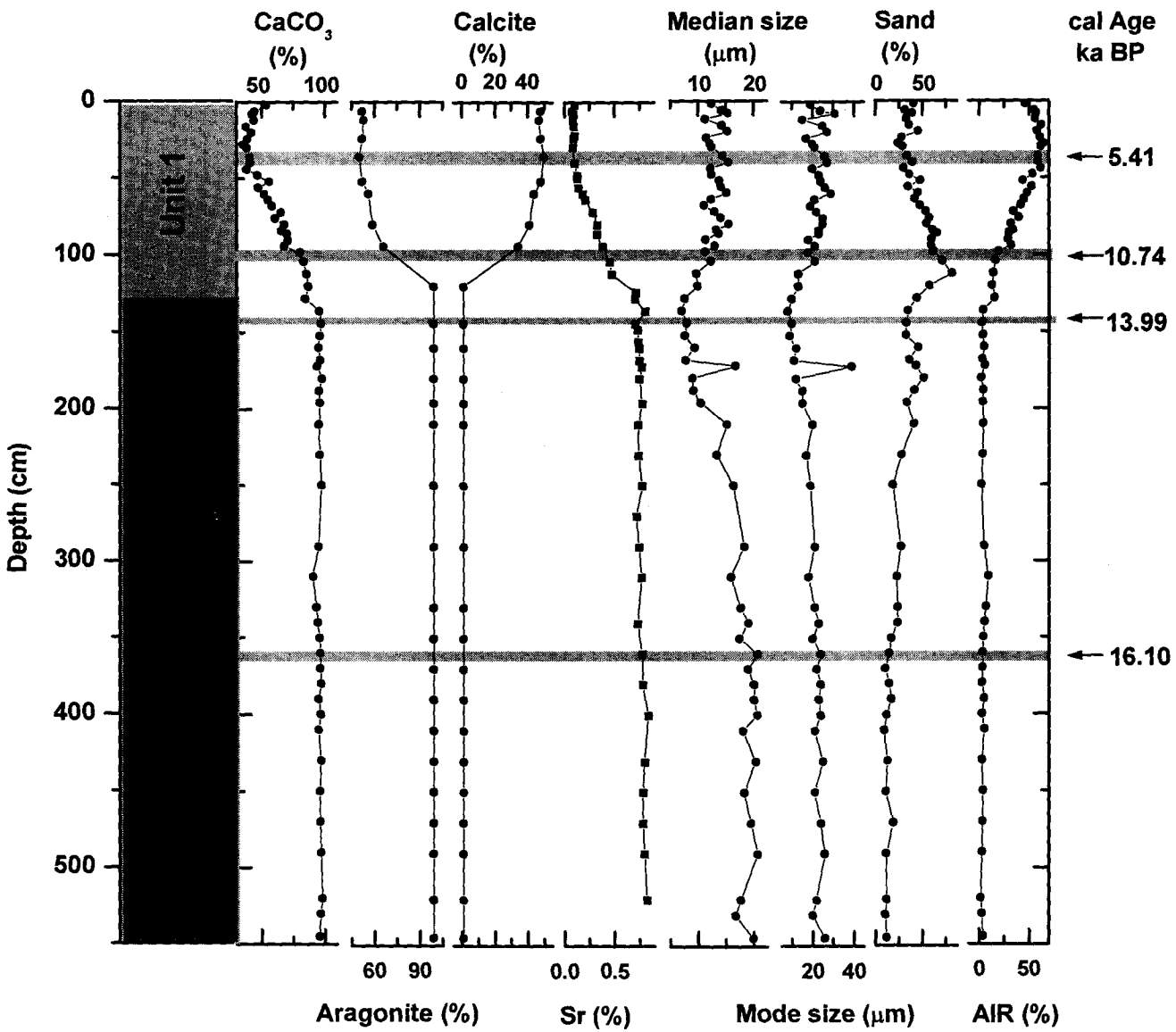

Fig. 4.6. Down-core variation of carbonate ($CaCO_3$), aragonite, calcite, strontium content (Sr), median and mode grain size of the bulk sediment (<63 μm fraction), sand and acid insoluble residue (AIR) content in **GC-5**.

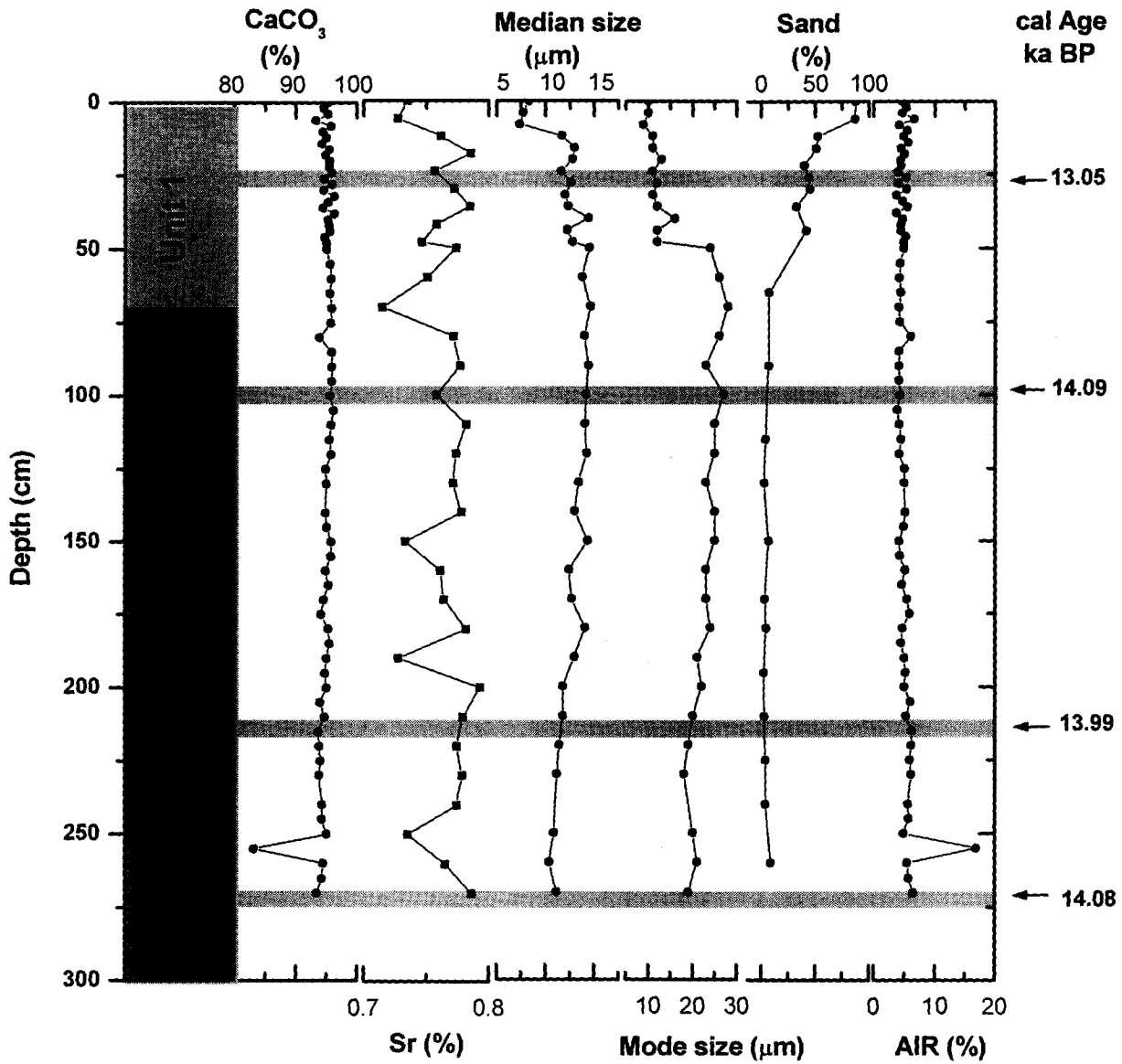

Fig. 4.7. Down-core variation of carbonate ($CaCO_3$), strontium content (Sr), median and mode grain size of the bulk sediment (<63 μm fraction), sand and acid insoluble residue (AIR) content in **GC-9.**

transportation. Occurrence of free needles (Fig. 4.11e) is characteristic of inorganic origin. The petrology therefore indicates that the aragonite needles decomposed from codiacean algae are admixed with that of needles precipitated by inorganic processes.

c. Sr content: The Sr content of the inorganically precipitated aragonite needles (>0.85-1%) is higher than that derived from disintegration of high-Sr (<0.85%) skeletal materials (Milliman et al., 1993). The Sr values of the lime muds (0.58% to 0.77% - Figs. 4.5-4.7) would be compatible with a large proportion of aragonite needles derived from post-mortem disaggregation of the high-Sr (0.63 to 0.85%) skeletals, such as corals and other codiacean algae. A few coral fragments are known to occur on the carbonate platform (Rao et al., 2003a). Since the mechanical production of silt and clay-sized sediment from the corals is generally small (<2% - Milliman, 1974), larger contribution of aragonite needles may be from codiacean algae. This argument is well supported by the reported occurrence of *Halimeda* bioherms on the carbonate platform (Rao et al., 1994). The platform contains no lime muds but well rounded, smaller (< 2 mm) size *Halimeda* grains (Rao et al., 1994) than the actual size (5 mm) of *Halimeda* plates, implying that the original *Halimeda* plates were decomposed and the muds thus produced were transported to the shelf break. Heavily fragmented prismatic aragonite needles (Fig. 4.12e) support high-energy conditions and disintegration from aragonite secreting skeletals. Most of the coarse fraction components do not provide clue to the origin of aragonite needles. It may be because the whole skeletal component was disintegrated into aragonite needles, as has been shown in the case of *Penicillus* (Stockman et al., 1967). The Sr values of lime muds thus simply point to an organic origin.

d. Alteration of original minerals: Stockman et al. (1967) and Neuman and Land (1975) suggested that codiacean alga contributes abundant aragonite muds to sediments. Recent work has shown that needles constitute only 25-40% of many of these algae and that most of the aragonite is in the form of cryptocrystalline equant nannograins or minimicrite (Macintyre and Reid,

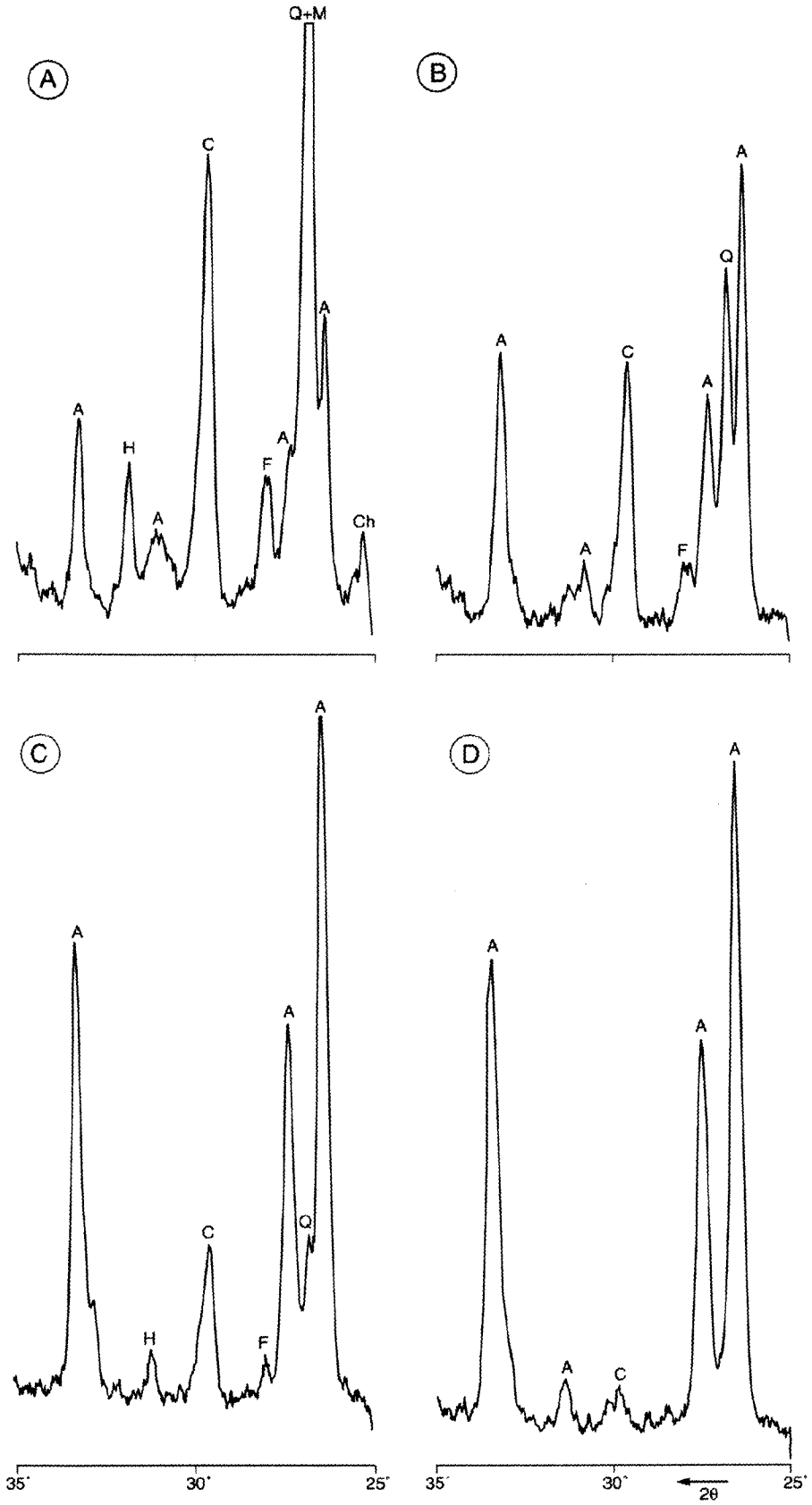

Fig. 4.8. Representative X-ray diffractograms of the lime muds in cores GC-1 (A), GC-
GC-5 (C) and GC-4 (D). Ch-chlorite, A-aragonite, C-calcite, Q-quartz, M-mica,
F-feldspar, H-halite.

1995). Reid and Macintyre (1998) further reported alteration in all types of skeletal grains regardless of their original mineralogy and accompanied by mineralogical changes from Mg-calcite to aragonite or from aragonite to Mg-calcite. A close association between cryptocrystaline grains and lime muds was found not only in northern Belize lagoon but also in the Bahamas and Persian Gulf, suggesting that the crypto-crystalline grains are the fundamental source of lime muds. The lime muds studied here, on the other hand, contained abundant aragonite with traces of (low-magnesium) calcite (Fig. 4.8C-D). There were no cryptocrystalline nannograins or minimicrites observed under SEM. This suggests that the alteration of aragonite to Mg-calcite is insignificant at the time of lime mud formation. As pointed out in the morphology section there were a few free needles to suggest inorganic origin. The other morphological features of the needles and Sr content of the lime muds studied here suggest that the muds are predominantly organic with some mixture from inorganic origin.

e. Stable isotopes: The stable isotope values of aragonite muds are within the range for ooids and sedimentary aragonite needles, but much higher than that for Halimeda and Penicillus (Fig. 4.9D). Needles form from Penicillus and Rhiphocephalus but not Halimeda. If aragonite needles released from the decomposition of plants such as Penicillus and Rhiphocephalus, one would expect high negative to low negative δ18O values (Milliman, 1974). Despite the fact that the sedimentary aragonite needles are of organic origin (Lowenstam and Epstein, 1957), their values are slightly higher than that of Penicillus and Rhiphocephalus (see Fig. 4.9D). This implies that equilibrium precipitation (in isotopic composition) of needle muds occurs in algal muds undergoing decomposition. If ooids are considered as inorganic in origin, the δ18O values in ooids are in equilibrium with the ambient environment and δ13C values range between +4‰ and +5‰ (Deuser and Degens, 1967). Recent studies, however, noted biogenic influence in the formation of ooids (Folk and Lynch, 2001). There are evidence that the cortical layers in the ooids collected off northwestern India are formed by encrustation of thin microbial laminations suggesting biogenic influence (Rao et al. in preparation). Placement of the

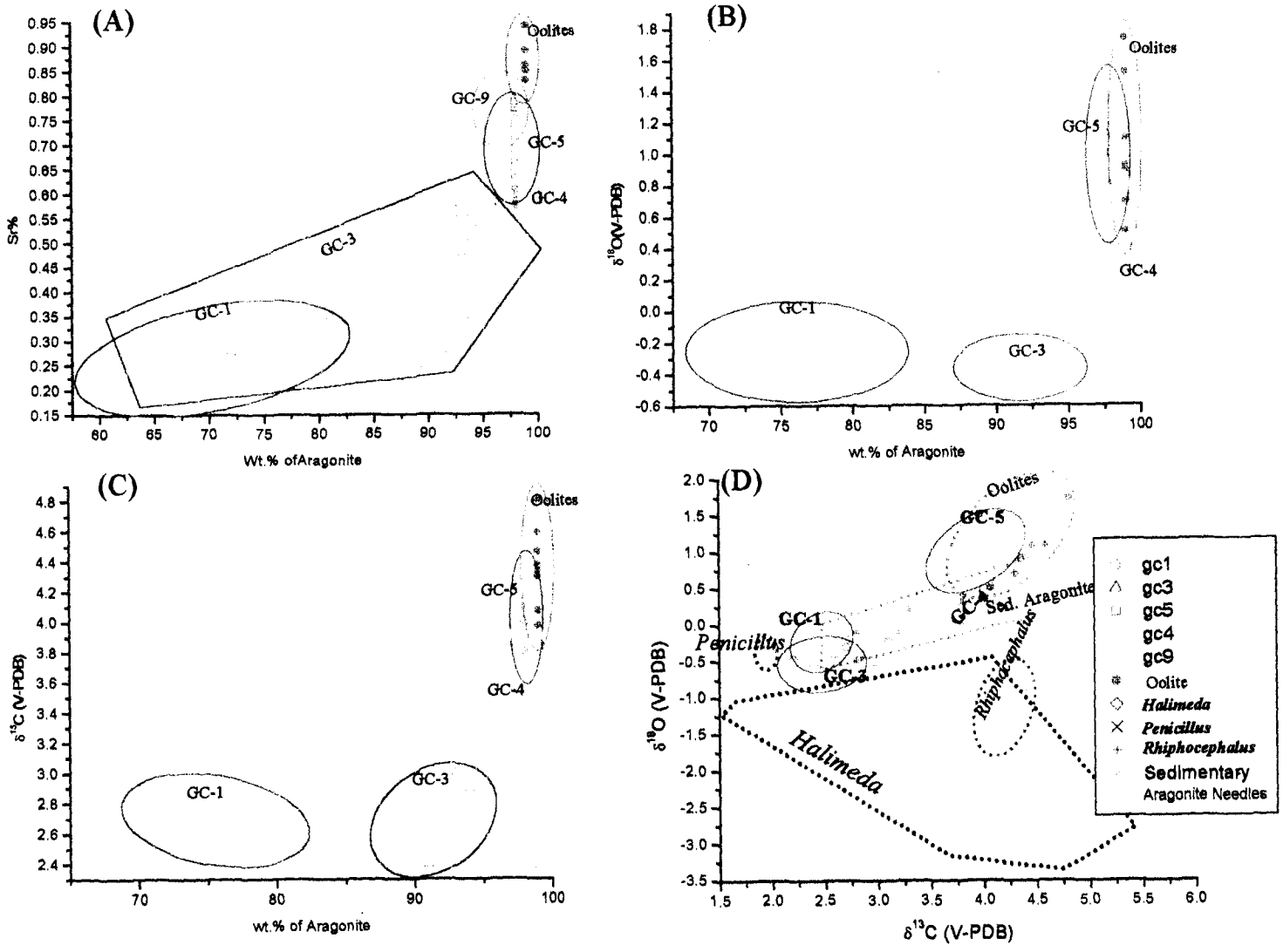

Fig. 4.9. Scatter plots of the aragonite muds. Weight percentage of aragonite versus Sr (A), $\delta^{18}O$ (B), $\delta^{13}C$ (C). (D) A plot between $1\delta^{13}C$ and $\delta^{18}O$. Stable isotope values of *Halimeda, Penicillus, Riphocephalus* and sedimentary aragonite needles are from Lowenstam and Epstein (1957).

isotopic values of aragonite muds in GC-4 and GC-5 on the regression line and between ooids and sedimentary aragonite needles (Fig. 4.9D) imply biogenic influence on aragonite formation and resetting of the original isotopic signal of aragonite needles, after separating from aragonite algae. Stable isotope signal may therefore support organic origin.

The processes involved in the aggregation of individual aragonite needles into spheroid and ovoid-type particles (Fig. 4.11) are not known. The lime muds of relatively older age occurred above that of younger age. This implies that the lime muds were transported to the shelf break. Aragonite needles are largely disintegrated from aragonite containing algae. Organic matter is usually high in the sediments associated with algae. Micro-algal (cyanobacterial) laminae transformed into dolomite crusts by microbial processes were indeed reported on the carbonate platform (Rao et al., 2003b). The available organic matter probably facilitated cementation of individual needles into aggregates during early diagenesis and/or transportation at the sea floor. Alternately, spheroid and ovoid-type particles may be of faecal origin. Relating faecal pellets to their organisms is not easy as different animals may produce rather similar pellets. Moreover, it is not known what organisms contribute micron to several micron size particles. Millimeter-sized aragonite faecal pellets derived from crustaceans have been reported abundantly on the adjacent carbonate platform (Rao et al., 1994).

4.5.2. Controls on the sedimentation of lime muds

There is a mismatch in the age of lime muds in unit 2 of both cores (17.6 ka to 12.76 ka in GC-1 and 12.98 ka to 12.0 ka in GC-3; Figs. 4.3 and 4.4) and depths at which the cores recovered, when compared with the Glacio-eustatic sea level position at that time. For example, the Glacio-eustatic sea level was at ~-110 m at 17.6 cal ka and at ~-70 m at 13 cal ka (Fairbanks, 1989; Liu and Milliman, 2002). Therefore, one would expect only deposition of terrigenous sediments at the core sites because of the sub-aerial position of the continental shelves at that time. The presence of marine

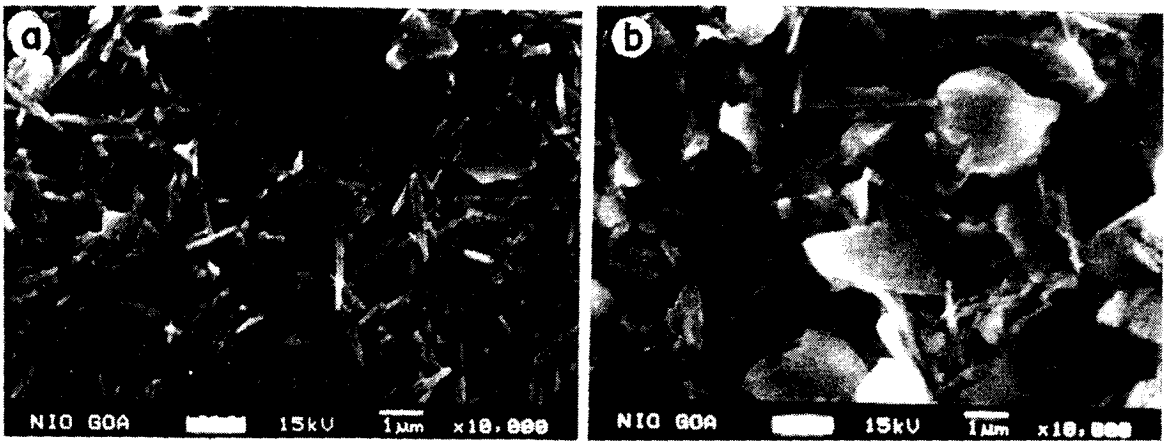

Fig. 4.10. Scanning Electron Micrographs of lime muds in GC-1: (a) showing aragonite needles in < 4 µm associated with detrital particles and (b) a few needle muds adhered to lithogenic particles.in 4-16 µm fractions.

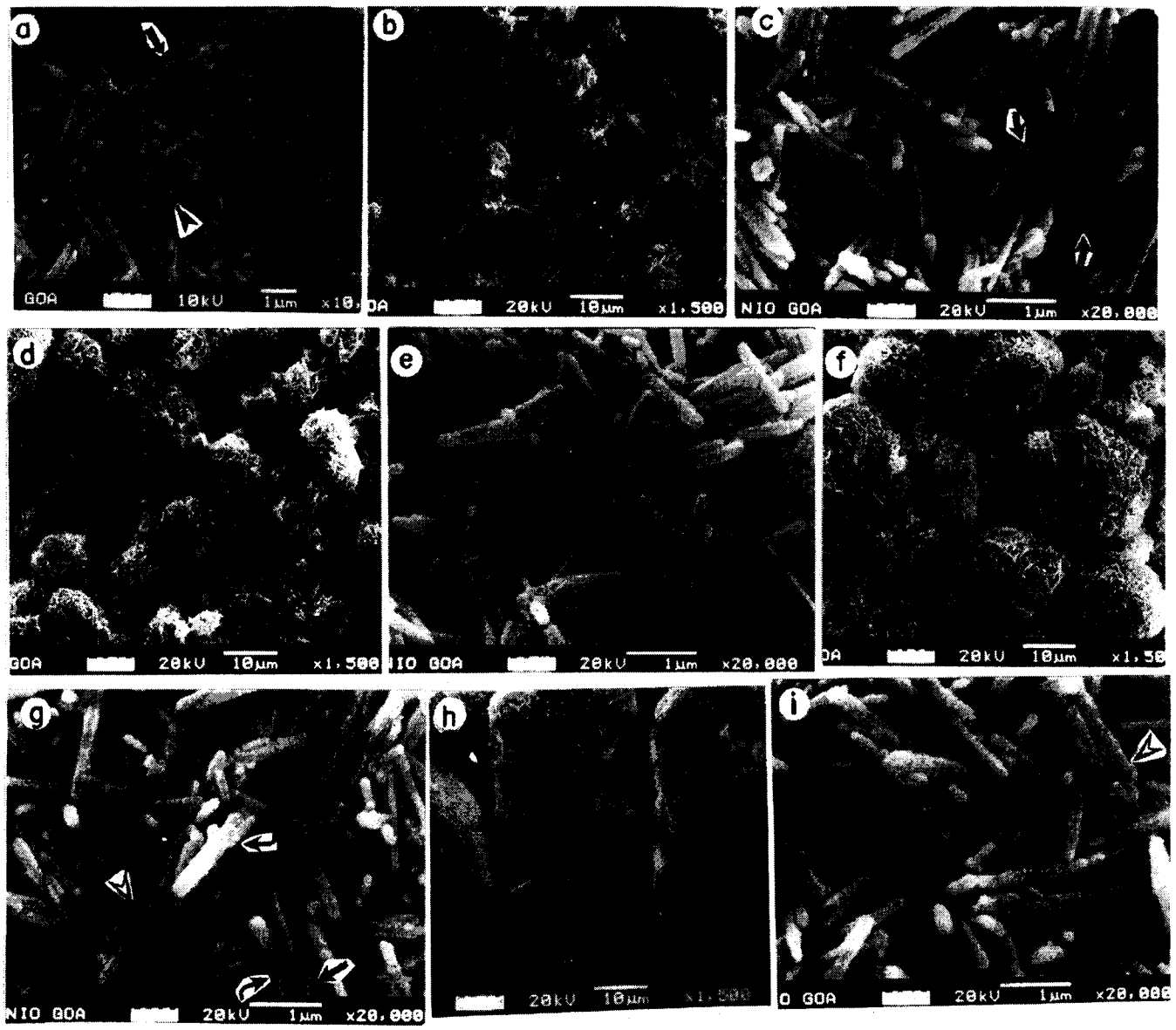

Fig. 4.11. Scanning Electron Microscope (SEM) photographs. Different magnifications of the lime muds in the size fractions <4 µm (a), 4-8 µm (b-c), 8-16 µm (d-e), 16-32 µm (f-g) and 32 to 63 µm (h-1) from GC-4 and GC-5 cores. Arrows in 'a' showing 'pointed aragonite needles', in 'c' showing blunting at the edges, in 'g' jointed needles and needles emanating from quiver (between arrows) and in 'i' jointed needles

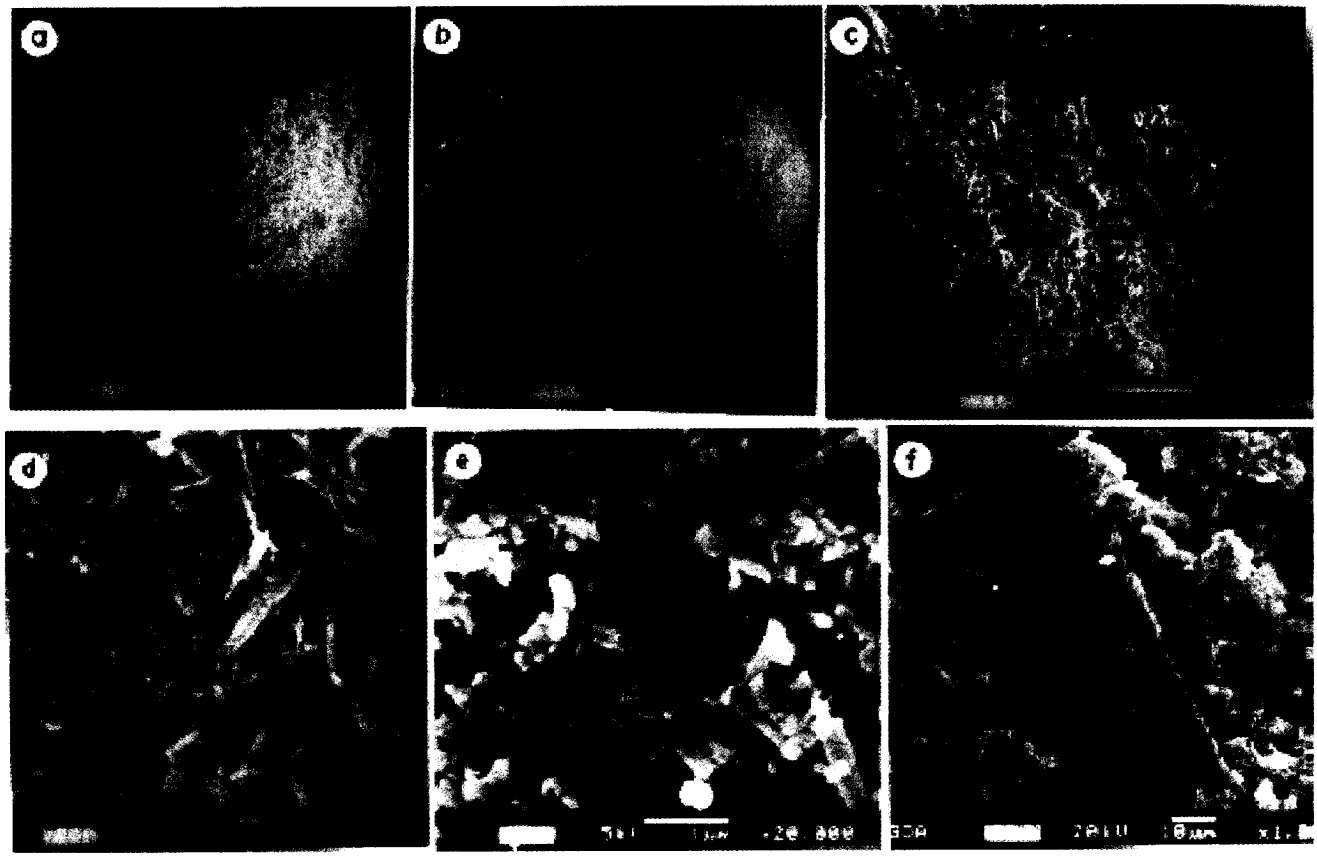

Fig. 4.12. Scanning Electron Microscope (SEM) photographs of lime muds in the size fractions: (a) >63 -125 µm, (b) >125-250 µm, (c) enlargement of 'b' at the edges, (d) further enlargement of 'c' showing pointed and blunt aragonite needle edges, (e) heavily broken fragments of prismatic aragonite needles and (f) aragonite needles disintegrating from a skeletal.

(lime mud) sediments dated 17.6 ka and 13 ka at water depths 56 m and 65 m implies that the sediment in the unit 2 of the cores was reworked to the present core site. Since GC-1 is located off the Gulf of Kachchh (Fig. 4.1), the lime muds were likely to have formed initially in the Gulf and subsequently reworked to the shelf region. This implies the existence of shallow marine / lagoonal conditions in the Gulf during LGM that could have favoured the lime mud formation. Rao et al. (2003b) reported fossil corals and dolomite encrustations dated at 14.3 ka at 35 m water depth in the Gulf of Kachchh and suggested that the age and depth of the limestones do not correspond well with that of the glacio-eustatic sea level curve (Fairbanks, 1989) for the late Quaternary and early inundation of the Gulf. Iyengar and Radhakrishna (2005) reported that the greater part of the Saurashtra formed an island of explosive volcanic activity and the Gulfs of Khambat and Kachchh were linked and maintained marine connection from early Cretaceous to late Pleistocene and early Holocene (5000 years ago).

Among the other three cores (GC-4, GC-5 and GC-9; Figs. 4.5-4.7) the ages of lime muds recovered in GC-4 are in the range younger (13 ka - 12 ka) than that of GC-5 (16.1 ka - 14 ka) and GC-9 (14 ka - 13 ka). The sediment intervals sandwiching of younger age sediments between two older layers in all the cores (see chapter 2, Table 2.2) strongly suggests reworking. The core GC-5 is located at 121 m off Saurashtra, whereas GC-4 (111 m) and GC-9 (115 m) are collected off the platform, which was at shallow depths but not exposed sub-aerially during the LGM (Rao et al., 2003a). Despite not knowing the exact positions of sea level at LGM the following may be valid. The rise of sea level in the first phase of deglaciation (from 22 ka to 14 ka BP) was only 20 m (Fairbanks, 1989). Relatively shallow water conditions, slow sea level rise and low detrital flux most probably favoured lime mud deposition at GC-5. Absence of lime muds younger than 14 ka in GC-5 (Fig. 4.6) may be due to the global event, melt water pulse (MWP)1A that started at ~13.8 ka during which the sea level rise was rapid (24 m in <1000 yrs - Fairbanks, 1989). This may have caused a hiatus in sedimentation at ~14 ka at the shelf break and lime muds were transported farther from the shelf edge. Thinner unit 1

sediments, trace contents of acid-insoluble residue and 13 ka aged sediments close to the core top in GC-9 (Fig. 4.7) indicate least sedimentation and possible hardground conditions at the sampling site after 13 ka.

Lime muds deposition continued in cores GC-3 and GC-4 until 11.9 ka. The transition from unit 2 (lime muds) to unit 1 (increase in terrigenous content) sediments occurred after 12 ka (Fig. 4.4; Fig. 4.5). This change in depositional environment may be due to the combined influence of changes in climatic conditions, the Younger Dryas event (13 – 11.7 ka) and melt water pulse (MWP)1B. The SW monsoon was reactivated, after the LGM, at ~13 ka with its maxima intensity at ~ 10 ka (van Campo, 1986; Thamban et al., 2001). Since the decrease of carbonate in the core coincides with the increase of terrigenous content in unit 1 sediments, the increased terrigenous supply from the hinterland indeed may have reached the platform and inhibited carbonate sedimentation. The slow sea level rise due to the Younger Dryas favoured reworking of lime muds in these cores. Carbonate sedimentation ceased after the Younger Dryas event. In fact, the later half of the Younger Dryas event coincides with the beginning of the melt water pulse (MWP) 1B during which the sea level rise was rapid (28 m in <1000 years; Fairbanks, 1989). The rapid sea level rise, increased terrigenous detritus because of climatic change may have influenced carbonate sedimentation. Therefore the change in sea level and climatic conditions at ~12 ka probably ceased lime mud sedimentation on this platform.

4.6. Summary and conclusions

- Gravity cores studied here contain abundant lime muds in the lower section and terrigenous-dominated sediments in the upper section.

- Lime muds are largely aragonitic in composition and are admixed with 30% to 50% terrigenous sediments on the shelf and <5% terrigenous material at the shelf break / slope.

- The grain size of the lime muds varies from 5 to 27 μm. The larger grain size in the shelf break/slope cores was due to aggregation of lime muds into ovoid and/or spheroidal grains.

- The Sr values of the lime muds in the shelf cores (0.18-0.61%) are much less than that of the shelf break/slope cores (0.10-0.83%).

- The Sr values of the slope cores are less than that of the inorganically formed aragonite needles from other regions and oolites.

- Depleted stable isotope ratios of the lime muds of the continental shelf indicate that the muds were formed either in water masses of different characteristic or altered after their formation.

- The lime muds at the shelf may have formed initially from the aragonite-producing plants and subsequently reworked and admixed with terrigenous sediments. .

- The age of the lime muds on the shelf ranges ~17-12 BP, implying submergence of the Gulf of Kachchh during early deglaciation and neo-tectonic activity in the Gulf region.

- The Sr values, stable isotopes and morphology of the aragonite needles at the shelf break/slope indicate that the lime muds were of organic origin and largely decomposed from codiacean algae.

- The organic matter associated with the muds may have facilitated cementation of individual needles into aggregates during early diagenesis and/or transportation at the sea floor.

- The age of the lime muds in the shelf break/slope varies from ~16-12 ka BP in shelf break / slope cores.

- Younger radiocarbon ages of lime muds between older ones in the slope cores indicate that the lime muds were reworked from the shelf or carbonate platform.

- The lime muds ceased to deposit after 14 ka in deeper water cores may be due to the global event (rapid rise in sea level)- associated with Melt Water Pulse (MWP)1A at 14 ka BP.

- The lime muds-dominated sediments gradually grade into terrigenous-dominated sediments after 12 ka BP. This change in depositional environment may be due to the combined influence of changes in regional climatic conditions, the Younger Dryas event and MWP1B.

Table 4.1. Down-core distribution of CaCO3, aragonite, calcite, median and mode grain size of bulk sediment (<63 μm), sand, acid insoluble residue (AIR) and strontium (Sr) content in GC-1

Depth (cm(	$CaCO_3$ (%)	Aragonite (%)	Calcite (%)	Median (μm)	Mode (μm)	Sand (%)	AIR (%)	Depth (cm)	Sr (%)
0	61.21	60	40	7.74	9	48.99	38.79	0	0.18
20	58.80	62	38	7.27	8	50.62	41.20	10	0.19
30	61.71	--	--	7.66	10	51.46	38.29	15	0.17
40	62.23	60	40	7.33	9	56.30	37.77	20	0.19
50	70.82	--	--	7.77	10	69.19	29.18	25	0.18
60	73.50	--	--	8.41	11	72.79	26.50	40	0.21
70	80.53	--	--	12.08	18	80.86	19.47	45	0.21
80	76.13	65	35	11.43	17	69.28	23.87	70	0.31
90	79.17	--	--	10.46	15	74.54	20.83	80	0.32
100	77.88	69	31	10.88	17	72.23	22.12	85	0.28
140	57.88	80	20	8.80	13	4.91	42.12	100	0.27
160	58.76	81	19	8.45	13	3.84	41.24	120	0.35
180	61.19	81	19	9.12	14	4.95	38.81	140	0.32
205	62.82	--	--	8.93	14	7.60	37.18	155	0.30
220	57.99	77	23	9.63	16	4.56	42.01	160	0.34
240	57.97	78	22	9.56	16	4.07	42.03	180	0.35
260	56.66	76	24	9.44	17	3.07	43.34	220	0.36
280	55.81	74	26	9.01	17	1.28	44.19	240	0.33
320	53.72	74	26	8.15	12	1.31	46.28	280	0.30
340	53.27	73	27	8.28	12	1.65	46.73	300	0.28
360	51.16	73	27	7.77	9	1.54	48.84	320	0.27
380	50.13	73	27	10.96	22	1.61	49.87	340	0.24
395	53.84	--	--	9.95	20	2.70	46.16	360	0.28
420	46.71	73	27	8.55	13	1.26	53.29	380	0.27
440	45.62	72	28	9.30	16	4.12	54.38	420	0.24
460	44.24	72	28	8.14	12	2.10	55.76	440	0.23
480	46.95	76	24	8.14	11	2.76	53.05	460	0.27
500	44.77	76	24	7.89	11	3.21	55.23	480	0.24
520	42.08	74	26	7.21	10	3.05	57.92	500	0.26
540	46.71	76	24	7.37	9	6.36	53.29	520	0.28
560	48.56	79	21	7.44	8	3.24	51.44	540	0.25
580	46.27	78	22	6.53	8	2.79	53.73	560	0.32
600	49.27	78	22	6.44	7	2.04	50.73	580	0.32
620	47.60	74	26	6.18	8	3.46	52.40	600	0.31
640	50.89	77	23	5.38	7	2.24	49.11	620	0.30
660	49.20	--	--	5.97	7	1.14	50.80	640	0.28
680	53.30	--	--	6.12	7	2.38	46.70	660	0.30
690	54.89	--	--	5.57	7	1.12	45.11	700	0.29
700	55.36	73	27	6.21	9	2.13	44.64	--	--

Table 4.2. Down-core distribution of $CaCO_3$, median and mode grain size of bulk sediment (<63 μm), sand, acid insoluble residue (AIR), aragonite, calcite and strontium (Sr) content in GC-3

Depth (cm)	$CaCO_3$ (%)	Median (μm)	Mode (μm)	Sand (%)	AIR (%)	Depth (cm)	Arago-nite %	Calci-te %	Depth (cm)	Sr (%)	Depth (cm)	Sr (%)
2	71.49	9.79	14	63.27	28.51	2	62	38	2	0.34	124	0.53
8	65.82	8.14	10	62.39	34.18	10	89	11	4	0.20	128	0.57
14	72.30	9.14	12	67.43	27.70	30	95	5	6	0.23	134	0.56
26	74.53	7.19	9	45.36	25.47	40	97	3	8	0.28	138	0.58
32	79.72	7.72	10	47.27	20.28	80	95	5	12	0.25	144	0.57
38	72.81	7.67	11	33.64	27.19	100	94	6	14	0.37	148	0.56
44	69.92	7.74	11	25.33	30.08	120	94	6	16	0.31	151	0.54
50	76.18	8.08	11	29.77	23.82	140	93	7	18	0.31	158	0.56
56	71.70	7.14	10	32.04	28.30	160	94	6	22	0.44	164	0.51
62	60.13	7.14	10	18.92	39.87	180	94	6	24	0.28	168	0.57
68	71.39	7.19	11	20.02	28.61	200	94	6	26	0.32	174	0.52
78	64.79	8.06	12	2.85	35.21	220	93	7	28	0.52	178	0.51
88	70.83	7.28	10	1.71	29.17	240	91	9	32	0.41	184	0.52
98	67.84	7.61	11	3.23	32.16	260	93	7	34	0.48	188	0.53
108	69.84	7.65	11	6.14	30.16	280	94	6	36	0.38	194	0.52
118	72.37	7.61	11	4.73	27.63	300	92	8	38	0.47	198	0.54
128	66.67	7.99	11	5.38	33.33	320	88	12	42	0.48	200	0.54
138	45.12	7.87	11	4.58	54.88	340	89	11	44	0.52	230	0.51
150	72.90	8.37	12	2.21	27.10	380	90	10	46	0.55	260	0.52
160	71.21	9.24	14	3.18	28.79	400	92	8	48	0.60	320	0.55
170	71.55	8.17	12	1.58	28.45	420	88	12	52	0.58	350	0.55
180	71.81	8.14	12	2.60	28.19	440	88	12	54	0.55	380	0.53
190	73.30	7.76	12	3.67	26.70	460	91	9	56	0.56	410	0.52
200	73.44	8.14	12	1.97	26.56	480	90	10	58	0.61	440	0.54
230	70.34	8.54	13	0.60	29.66	500	88	12	62	0.57	470	0.55
260	73.37	7.15	11	5.88	26.63	520	92	8	66	0.56	500	0.56
320	71.47	7.62	11	2.83	28.53	540	92	8	74	0.57	530	0.55
350	70.80	6.50	10	0.30	29.20	560	86	14	78	0.58	560	0.53
380	70.22	7.05	11	1.83	29.78	580	88	12	84	0.60	590	0.53
410	70.08	8.07	11	1.52	29.92				88	0.56		
440	69.11	6.63	10	2.68	30.89				94	0.57		
470	69.79	6.32	9	2.12	30.21				98	0.59		
500	70.42	6.83	10	2.81	29.58				104	0.55		
530	69.43	6.69	11	1.48	30.57				108	0.58		
560	69.49	6.92	11	1.45	30.51				114	0.55		
590	69.50	6.48	10	2.59	30.50				118	0.57		
									Cont..			

Table 4.3. Down-core distribution of $CaCO_3$, aragonite, calcite, strontium (Sr) content, median and mode grain size of bulk sediment (<63 μm), sand and acid insoluble residue (AIR) in GC-4

Depth (cm)	$CaCO_3$ (%)	Arago-nite (%)	Calci-te (%)	Sr (%)	Median (μm)	Mode (μm)	Sand (%)	AIR (%)
2	80.70	61	39	0.43	19.93	44	80.65	19.30
6	72.86	--	--	0.40	18.77	34	76.28	27.14
10	77.74	57	43	0.39	21.96	45	76.86	22.26
14	77.14	--	--	--	21.84	39	67.59	22.86
18	78.44	59	41	0.38	19.51	38	82.12	21.56
22	80.01	--	--	--	19.46	45	80.47	19.99
26	76.59	--	--	0.42	24.62	48	75.40	23.41
34	76.21	56	44	0.38	20.35	34	71.98	23.79
38	79.32	--	--	0.37	22.85	43	67.02	20.68
42	77.61	59	41	0.35	23.23	45	61.36	22.39
46	79.03	--	--	--	25.29	43	71.75	20.97
50	78.24	62	38	0.36	26.63	45	63.99	21.76
54	79.56	--	--	--	25.65	44	66.49	20.44
58	77.55	--	--	0.36	25.74	43	62.79	22.45
62	72.41	56	44	0.37	26.81	44	66.00	27.59
66	72.46	--	--	--	24.33	39	62.23	27.54
70	77.47	62	38	0.37	26.22	47	64.73	22.53
74	70.60	--	--	--	25.64	45	64.25	29.40
78	75.08	--	--	--	25.10	41	64.21	24.92
82	77.02	59	41	0.40	24.93	37	63.67	22.98
86	77.07	--	--	0.41	25.52	45	65.58	22.93
90	74.56	59	41	--	22.86	40	61.61	25.44
94	76.25	--	--	--	25.41	41	63.97	23.75
98	80.98	65	35	0.46	24.84	45	66.11	19.02
106	80.15	--	--	--	21.68	55	61.44	19.85
118	81.95	68	32	0.52	23.54	45	73.78	18.05
130	78.04	70	30	0.52	17.42	52	69.59	21.96
142	84.00	69	31	0.56	20.25	37	73.37	16.00
154	83.17	92	8	0.60	16.06	28	67.28	16.83
184	88.23	98	2	--	9.91	11	71.33	11.77
196	90.99	99	1	0.73	10.51	11	66.43	9.01
210	89.79	--	--	0.72	12.54	11	11.91	10.21
230	87.65	99	1	0.73	10.42	11	47.32	12.35
250	87.11	99	1	0.68	10.21	12	39.36	12.89
270	90.50	99	1	0.73	12.56	9	67.55	9.50
290	90.79	99	1	0.71	10.72	11	67.91	9.21
310	88.54	99	1	0.70	14.16	12	46.79	11.46

Continued...

Continuation of Table 4.3

Depth (cm)	$CaCO_3$ (%)	Arago-nite (%)	Calci-te (%)	Sr (%)	Median (μm)	Mode (μm)	Sand (%)	AIR (%)
330	90.42	99	1	0.69	11.05	11	46.33	9.58
350	90.71	99	1	0.69	10.94	14	28.38	9.29
370	92.46	--	--	0.70	12.13	13	20.67	7.54
390	91.67	99	1	0.72	13.07	15	26.61	8.33
410	93.06	99	1	0.71	12.17	12	49.95	6.94
430	89.06	99	1	0.71	8.42	11	20.04	10.94

Table 4.4. Down-core distribution of $CaCO_3$, aragonite, calcite, strontium (Sr) content, median and mode grain size of bulk sediment (<63 μm), sand and acid insoluble residue (AIR) in GC-5

Depth (cm)	$CaCO_3$ (%)	Arago-nite (%)	Calci-te (%)	Sr (%)	Median (μm)	Mode (μm)	Sand (%)	AIR (%)
2	53.89		--	0.10	12.45	19	40.78	46.11
6	44.66	52	48	0.08	14.29	24	31.52	55.34
8	42.60	--	--	0.09	15.38	31	39.08	57.40
12	43.91	53	47	0.08	11.31	15	32.80	56.09
16	37.78	--	--	0.09	14.32	25	36.03	62.22
20	41.75	--	--	0.10	15.33	27	45.42	58.25
24	38.72	52	48	0.09	11.54	17	28.18	61.28
28	35.54	--	--	--	12.15	20	24.22	64.46
30	37.99	--	--	0.08	12.46	21	28.66	62.01
36	40.55	50	50	--	14.46	26	33.88	59.45
40	40.89	--	--	0.10	15.52	27	39.26	59.11
44	38.16	--	--	--	12.35	20	30.25	61.84
48	46.58	--	--	0.13	12.45	23	35.96	53.42
52	56.09	52	48	0.13	13.84	24	47.71	43.91
56	47.41	--	--	0.14	14.20	26	34.60	52.59
60	51.93	56	44	0.18	15.15	29	45.00	48.07
64	54.99	--	--	0.21	12.38	21	41.94	45.01
68	58.02	--	--	--	11.11	19	47.50	41.98
72	65.28	--	--	0.28	13.00	22	53.80	34.72
76	60.41	--	--	--	14.09	25	57.23	39.59
80	68.06	59	41	0.33	15.53	25	54.77	31.94
84	65.58	--	--	--	13.32	23	60.76	34.42
86	69.84	--	--	0.33	13.74	23	65.19	30.16
90	70.96	--	--	--	11.41	18	59.84	29.04
94	68.06	66	34	0.38	13.02	21	59.36	31.94
98	80.39	--	--	--	11.30	18	61.97	19.61

Continued...

Continuation of Table 4.4

Depth (cm)	$CaCO_3$ (%)	Arago-nite (%)	Calci-te (%)	Sr (%)	Median (μm)	Mode (μm)	Sand (%)	AIR (%)
104	83.35	--	--	0.45	12.30	21	71.13	16.65
112	85.67	--	--	0.47	9.70	13	81.69	14.33
120	86.91	99	1	0.72	9.95	13	57.84	13.09
128	84.47	--	--	0.71	7.66	10	44.11	15.53
136	95.72	--	--	0.81	7.07	8	34.84	4.28
144	97.08	99	1	0.71	8.00	10	32.85	2.92
152	96.02	--	--	0.74	7.66	9	32.45	3.98
160	95.00	99	1	0.75	9.40	12	45.44	5.00
168	96.48	--	--	0.75	7.74	11	35.90	3.52
172	94.07	--	--	0.77	16.78	39	43.42	5.93
180	97.69	99	1	0.75	9.04	12	51.24	2.31
188	95.48	--	--	--	9.15	15	41.36	4.52
196	96.26	99	1	0.78	10.45	15	33.59	3.74
210	95.53	99	1	0.74	15.29	20	41.09	4.47
230	95.94	--	--	0.74	13.38	17	27.76	4.06
250	97.30	99	1	0.78	16.43	19	18.42	2.70
290	95.05	99	1	0.72	18.36	21	26.88	4.95
310	90.58	--	--	0.74	15.94	18	22.39	9.42
330	93.27	99	1	0.77	17.72	21	23.34	6.73
340	94.48	--	--	0.73	19.10	23	23.56	5.52
350	95.62	99	1	0.78	17.51	20	16.80	4.38
360	96.60	--	--	--	20.78	24	14.53	3.40
370	96.36	99	1	--	19.01	22	10.52	3.64
380	97.06	--	--	0.78	20.09	24	14.57	2.94
390	94.93	99	1	--	20.11	23	16.49	5.07
400	96.87	--	--	0.83	20.73	24	11.84	3.13
410	95.03	99	1	--	18.13	21	9.09	4.97
430	97.07	99	1	0.80	20.39	25	12.76	2.93
450	96.22	99	1	0.78	18.32	21	10.78	3.78
470	96.56	99	1	0.78	19.60	24	18.77	3.44
490	97.06	99	1	0.80	20.83	26	11.33	2.94
520	98.02	99	1	0.82	17.71	22	11.77	1.98
530	96.82	--	--	--	16.78	20	10.58	3.18
545	96.25	99	1	--	20.01	26	11.53	3.75

Table 4.5. Down-core distribution of CaCO3, strontium (Sr) content, median and mode grain size of bulk sediment (<63 μm), sand and acid insoluble residue (AIR) in GC-9

Depth (cm)	$CaCO_3$ (%)	Sr (%)	Median (μm)	Mode (μm)	Sand (%)	AIR (%)
0	95.24	0.73	8.31	10	87.68	4.76
2	94.63	--	--	--	--	5.37
4	95.27	--	7.74	10	--	4.73
6	93.34	0.73	--	--	87.52	6.66
8	95.75	--	7.37	9	--	4.25
10	94.44	--	--	--	--	5.56
12	95.04	0.76	11.68	11	52.41	4.96
14	94.34	--	--	--	--	5.66
16	95.46	--	12.94	11	51.51	4.54
18	94.92	0.79	--	--	--	5.08
20	95.60	--	12.77	13	--	4.40
22	95.49	--	--	--	40.44	4.51
24	95.91	0.76	11.65	11	--	4.09
26	94.70	--	--	--	44.52	5.30
28	95.91	--	12.62	12	--	4.09
30	94.64	0.77	--	--	45.00	5.36
32	96.31	--	11.99	11	--	3.69
34	95.25	--	--	--	--	4.75
36	94.49	0.78	12.33	12	32.96	5.51
38	96.30	--	--	--	--	3.70
40	95.25	--	14.40	16	--	4.75
42	95.48	0.76	--	--	--	4.52
44	95.58	--	12.25	12	41.75	4.42
46	94.75	--	--	--	--	5.25
48	95.04	0.75	12.76	12	--	4.96
50	95.02	0.77	14.51	24	--	4.98
55	95.61	--	--	--	--	4.39
60	95.80	0.75	13.76	26	--	4.20
65	95.55	--	--	--	7.44	4.45
70	95.87	0.72	14.62	28	--	4.13
75	95.74	--	--	--	--	4.26
80	93.87	0.77	14.01	26	--	6.13
85	95.84	--	--	--	--	4.16
90	95.83	0.78	14.42	23	7.15	4.17

Continued...

Continuation of Table 4.5

Depth (cm)	$CaCO_3$ (%)	Sr (%)	Median (μm)	Mode (μm)	Sand (%)	AIR (%)
95	95.88	--	--	--	--	4.12
100	95.64	0.76	14.19	27	--	4.36
105	96.16	--	--	--	--	3.84
110	95.78	0.78	14.04	25	--	4.22
115	95.51	--	--	--	4.36	4.49
120	95.76	0.77	14.23	25	--	4.24
125	94.89	--	--	--	--	5.11
130	94.99	0.77	13.39	23	2.86	5.01
140	94.81	0.78	13.01	25	--	5.19
145	95.06	--	--	--	--	4.94
150	95.79	0.73	14.32	25	6.98	4.21
155	95.69	--	--	--	--	4.31
160	94.82	0.76	12.43	23	--	5.18
165	95.35	--	--	--	--	4.65
170	94.53	0.76	12.68	23	3.44	5.47
175	94.10	--	--	--	--	5.90
180	95.30	0.78	14.03	24	4.58	4.70
185	95.46	--	--	--	--	4.54
190	95.00	0.73	12.94	21	--	5.00
195	94.74	--	--	--	2.69	5.26
200	94.98	0.79	11.79	22	--	5.02
205	93.94	--	--	--	--	6.06
210	94.70	0.78	11.77	20	3.07	5.30
215	93.70	--	--	--	--	6.30
220	93.84	0.77	11.42	19	--	6.16
225	94.02	--	--	--	4.27	5.98
230	93.80	0.78	11.17	18	--	6.20
240	94.32	0.77	--	--	4.13	5.68
250	95.02	0.74	10.88	20	--	4.98
260	94.50	0.77	10.41	21	9.28	5.50
265	94.25	--	--	--	--	5.75
270	93.46	0.79	11.12	19	--	6.54

Table 4.6. Distribution of aragonite, stable isotope ratio of carbon ($\delta^{13}C$) and oxygen ($\delta^{18}O$) in GC-1, GC-3, GC-4, GC-5, oolites. *Halimeda, Penicillus, Rhiphocephalus* and sedimentary aragonite needles.

Core Number	Depth interval (cm)	Aragonite (wt %)	$\delta^{13}C$ (V-PDB)	$\delta^{18}O$ (V-PDB)
GC-1	115-120	79	2.6	-0.5
	165-170	81	2.7	-0.2
	245-250	77	2.7	-0.1
	305-310	76	2.7	-0.3
	355-360	70	2.9	-0.1
GC-2	40-41	97	3	-0.5
	140-142	93	2.9	-0.4
	198-200	94	2.8	-0.4
	280-285	94	2.8	-0.4
	340-345	89	2.7	-0.3
	400-405	92	2.8	-0.4
	460-465	91	2.4	-0.5
	520-525	92	2.6	-0.4
GC-5	66-67	55	0.1	-0.9
	164-166	>95	3.8	1
	220-225	>95	4	1
	280-285	>95	4.4	1.4
	340-345	>95	4.3	1.3
	400-405	>95	4.3	1.3
	460-465	>95	4.4	1.3
	520-525	>95	4	0.5
GC-4	72-73	56	1	-0.7
	130-132	69	1.9	-0.2
	200-205	>95	3.8	0.1
	230-235	>95	4.1	1.1
	260-265	>95	3.8	0
	300-305	>95	3.8	0.4
	340-345	>95	4	0.4
	380-385	>95	3.8	0.8
	420-425	>95	3.8	0.8

Continued...

Continuation of table 4.6

	Aragonite (wt %)	$\delta^{13}C$ (V-PDB)	$\delta^{18}O$ (V-PDB)
Oolites from the platform	>95	4.81	1.73
	>95	4.37	0.92
	>95	4.3	0.69
	>95	4.07	0.5
	>95	4.46	1.09
	>95	4.34	0.89
	>95	4.59	1.09
	>95	3.97	1.51
Halimeda#	--	4.2	-0.6
	--	2	-1.3
	--	3.8	-2.7
	--	4.2	-3.1
	--	5.5	-2.8
Penicillus#	--	2.2	-0.4
Rhiphocephalus#	--	4.4	-1.4
	--	4.4	-0.9
Sedimentary aragonite#	--	4.6	0.5
	--	4.9	0.5
	--	4.2	0.2
	--	3.8	0.3
	--	3.2	-0.1
	--	2.8	-0.5
	--	2.8	-0.1
	--	3.1	-0.2
	--	3.3	0.2

#- data from Lowenstam and Epstein (1957)

Chapter 5

Chapter 5

ORGANIC CARBON RECORD IN SEDIMENT CORES FROM THE NORTHWESTERN MARGIN OF INDIA: INFERENCES ON PRODUCTIVITY VARIATIONS DURING THE LATE QUATERNARY

5.1. Introduction

Arabian Sea is an area of highest seasonal productivity in the World Ocean (Qasim, 1977). The high biological productivity in the euphotic zone results in high organic matter production, part of which settles to the bottom and gets buried under the sediments. Since organic carbon (OC) is the basic element of all organisms, it is the most straightforward indicator of palaeo-productivity (Ruhlemann et al., 1999). Two schools of thought, *viz.* 'the production hypothesis' and 'preservation hypothesis' exist for the enrichment of OC in the sediments and are widely debated over the last two decades. These factors highlight the relative importance of one parameter over the other for organic carbon enrichment. Some workers consider that anoxia is the most important deciding factor (Demaison and Moore, 1980; Canfield, 1989; Demaison, 1991; Paropkari et al., 1992, 1993), while others (Muller and Suess, 1979; Pederson and Calvert, 1990; Pederson et al., 1992; Calvert et al., 1995; Thompson et al., 1997; Babu et al., 1999) suggest that productivity in conjunction with factors like sediment character and texture are important for high organic content in the sediments. On the basis of redox sensitive indicator, Mn/Al, Cowie et al. (1999) postulated that oxygen availability is not the sole factor controlling the OC distribution. Besides anoxia and/or productivity, the role of mineral surface area, grain size etc. was also investigated for OC enrichment. Keil and Cowie (1999) investigated the relationship between OC content and mineral surface area (MSA) and found high ratios of OC/MSA for the sediments deposited within the oxygen minimum zone (OMZ) and stated that OC preservation is enhanced

within the locale of the oxygen minimum in the NE Arabian Sea sediments. Schulte et al. (2000) found a weak correlation between total OC and MSA within the OMZ sediments and no co-relation for the sediments outside the OMZ.

Bordovskiy (1965) studied the effect of grain size and OC preservation and observed that the OC content increases as the particle size decreases. Several workers discussed the role of sedimentation rates in preservation of OC. Kolla et al. (1981b) found that the degree of preservation of organic matter along the Indian margin is about 15-80 times higher than that in the region off the Arabian Peninsula and highlighted the importance of sedimentation rate and oxygen minimum conditions for high organic matter in sediments of the Indian margin. Cho et al. (1999) observed that sedimentation rate together with biological productivity and chemistry of water column are responsible for controlling the geographical variation of organic carbon. Suthhof et al. (2000) investigated the role of OC input, sedimentation rate and bottom water oxygenation in the northern Arabian Sea (off Pakistan) and suggested that these factors influence the alteration of sedimentary organic matter. Schulte et al. (2000) observed that the depositional environment of the Indus Fan offers the best condition for enhanced preservation of organic matter and described high OC as a combined effect of OMZ and moderate sedimentation rates.

In this chapter the down-core variations in organic carbon (OC), organic carbon/total nitrogen (C/N) ratio, $CaCO_3$ content, coarse fraction content, planktonic foraminiferal distribution and median grain size of terrigenous mud in the sediments from six gravity cores recovered from the continental shelf and slope off northwest India are presented. The objectives of the present chapter are to determine the (a) sources of organic carbon in the shelf and slope cores, (b) role of productivity / preservation and other controlling factors in enrichment of organic carbon and (c) to better understand the influence of sea level changes,

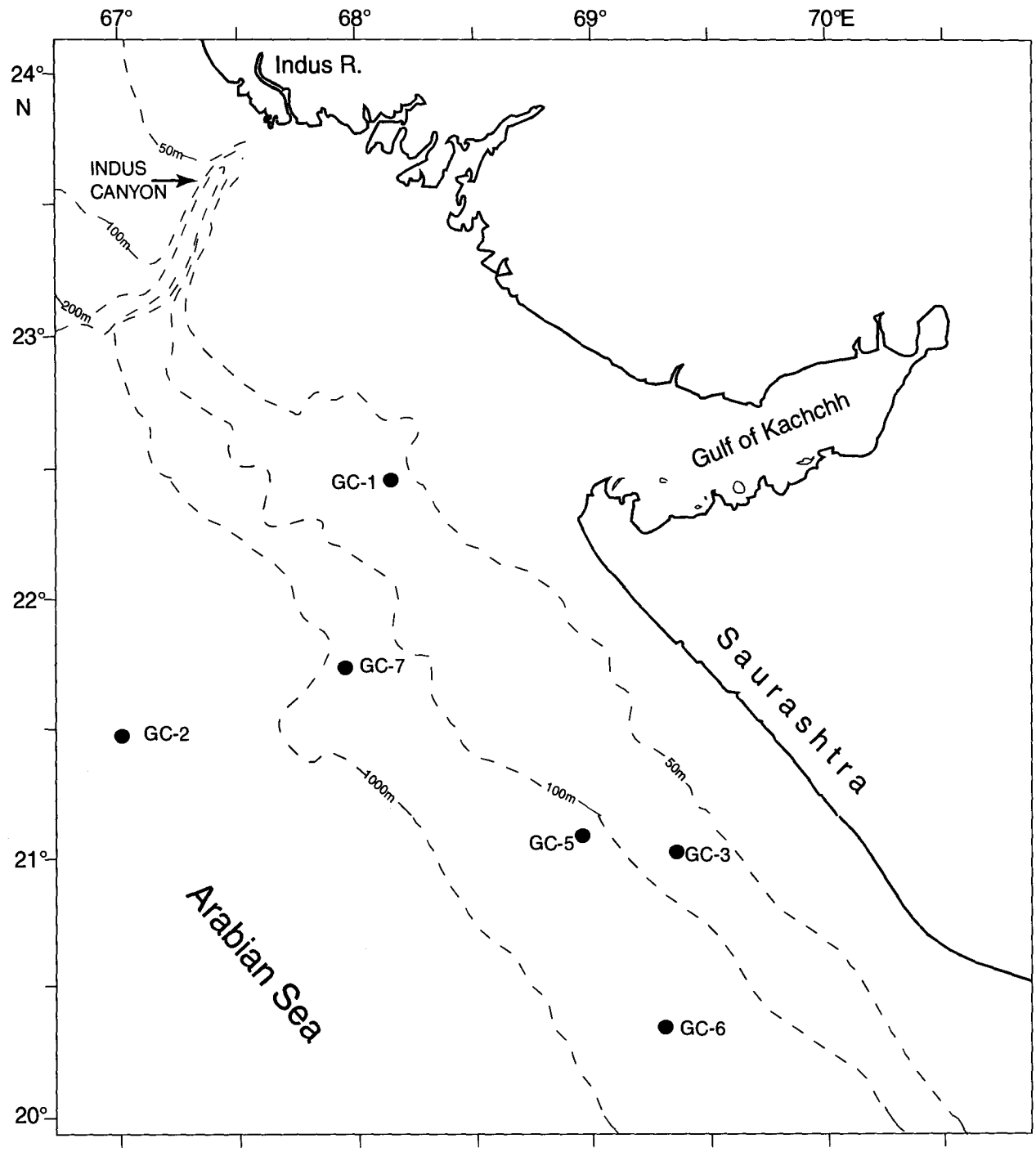

Fig. 5.1. Location of gravity cores used for organic carbon studies

and neo-tectonic activity and environmental conditions recorded in the sediments during the late Quaternary.

5.2. Previous studies

Wiseman and Bennett (1940) were the first to report the distribution of organic matter in the sediments of the Arabian Sea. Subsequently several workers reported the distribution and characteristics of organic matter in the western margin of India (Murty et al., 1969; Kidwai and Nair, 1972; Setty and Rao, 1972; Rajamanickam and Setty, 1973; Paropkari, 1979; Rao and Rao, 1989; Ramamurty and Murty, 1989; Paropkari et al., 1992, 1993; Calvert et al., 1995; Thamban et al., 1997; Nath et al., 1997; Babu et al., 1999; Rao and Veerayya, 2000; Bhushan et al., 2001; Thamban et al., 2001; Agnihotri et al., 2002, 2003; Pattan et al., 2003). Organic carbon studies from the northern Arabian Sea are mostly from the continental shelf and slope off Pakistan (von Rad et al., 1995; Cowie et al., 1999; Keil and Cowie, 1999; von Rad et al., 1999; Schulte et al., 2000; Suthhof et al., 2000) and some are from the deeper depths (Reichart et al., 1997). Rixen et al. (2000a&b) studied the organic carbon flux in the Arabian Sea using data from the sediment trap experiments. Organic carbon distribution maps for the entire Arabian Sea (Kolla et al., 1981b), the northern Arabian Sea (Stewart et al., 1965) and western margin of India (Ramamurty and Murty, 1989; Paropkari et al., 1992; Babu et al., 1999) were prepared. The controlling factors for the enrichment of organic carbon in sediment cores recovered from different physiographic setups on the SW margin of India were also studied (Paropkari et al., 1993; von Rad et al., 1995; Calvert et al., 1995; Babu et al., 1999; Thamban et al., 1997; Cowie et al., 1999; Kiel and Cowie, 1999; Schulte et al., 2000; Prabhu and Shankar, 2005). However, there is no such systematic study for the sediment cores from the NW margin of India.

5.3. Climatic set up

The Arabian Sea is under the influence of two monsoon mechanisms. During the summer monsoon (June – September), strong southwesterly winds blow across the Arabian Sea causing offshore Ekman transport, which enhances the seasonal upwelling and biological productivity (Wyrtki, 1973; Banse, 1987; Shallow, 1984; Bauer et al., 1991; Rixen et al., 2000a). During the winter monsoon (December-February) the northeast monsoon winds invoke onshore Ekman transport, which suppresses the upwelling and biological productivity is generally low, except in some areas off Pakistan. The productivity values are high (>0.75gC/m^2/day) in the area north of the Gulf of Kachchh and south of Cochin as compared to the western coast of India from Gulf of Kachchh to Cochin (<0.75gC/m^2/day; Paropkari et al., 1992). The strong monsoonal winds bring large seasonal changes in hydrography and particle fluxes in the Arabian Sea. It has been shown that the entire Arabian Sea is characterised by a permanent intense oxygen minimum zone (OMZ) between depths of 150 and 1200 m (Wyrtki, 1971).

During the last two decades, efforts have been made to understand the link between the intensity of monsoon and organic carbon fluxes and its preservation in the sediment records. Rixen et al. (2000a) showed that the variation in the strength of findlater jet is the dominant factor determining organic carbon fluxes in the Arabian Sea. Organic carbon fluxes during the Holocene are controlled by the changes in the SW monsoon intensity (Rixen et al., 2000a and b; Naidu and Shankar, 1999). Monsoon proxies have shown that the SW monsoon was weak during the Last Glacial Maximum (LGM) (Sirocko et al., 2000) and intensified after the LGM around 11,000 ^{14}C yrs BP (van Campo, 1986). Some studies, however, have shown high productivity indices during the glacial time and relatively low productivity indices during periods coinciding with intensification of the SW monsoon in the early Holocene (Reichart et al., 1998;

Thamban et al., 2001; Lee et al., 2003). It has been shown that the winter monsoon (NE) was stronger during the LGM (Duplessy, 1982; Sarkar et al., 1990).

5.4. Results

The temporal variations in organic carbon, $CaCO_3$, sand content, planktonic foraminiferal percentage and median size of six sediment cores from the NW margin of India (GC-1, GC-2, GC-3, GC-5, GC-6 and GC-7, shown in Fig. 5.1) are presented here (Tables 5.1-5.6; Figs. 5.2-5.7). Total nitrogen was determined for two sediment cores, GC-5 and GC-7. Organic carbon (C) / Total nitrogen (N) ratios were also presented for these cores (Fig. 5.5 and Fig. 5.7). The cores GC-1 and GC-3 are from the continental shelf at water depths 56 m and 65 m, respectively. The cores GC-5, GC-6 and GC-7 are from the upper continental slope at depths 121 m, 330 m and 420 m, respectively. The core GC-2 is from the lower continental slope at 1900 m depth. Both the shelf and upper slope cores showed two distinct sediment units, the lower unit 2 is dominated by lime muds and upper unit 1 dominated by terrigenous material. Results were presented with reference to unit 2 and unit1 of each core.

5.4.1. Cores from the continental shelf (GC-1, GC-3)

i. Organic Carbon

In GC-1 the unit 2 sediments extend from core bottom to 140 cm and unit 1 from 140 cm to core top. The OC content ranges from 0.1% to 0.5% in GC-1 and 0.2% to 0.4% in GC-3. In GC-1, the OC values are relatively low (0.2%-0.3%) in unit 2 sediments. While in unit 1 sediments, it increases progressively from 0.2% to 0.5% from base (140 cm) to 20 cm and then decreases to 0.3% in the upper 20 cm of the core (Fig. 5.2, Table 5.1). In GC-3, OC shows low amplitude fluctuations (0.2 to 0.3 %) between core bottom and 32 cm of the core.

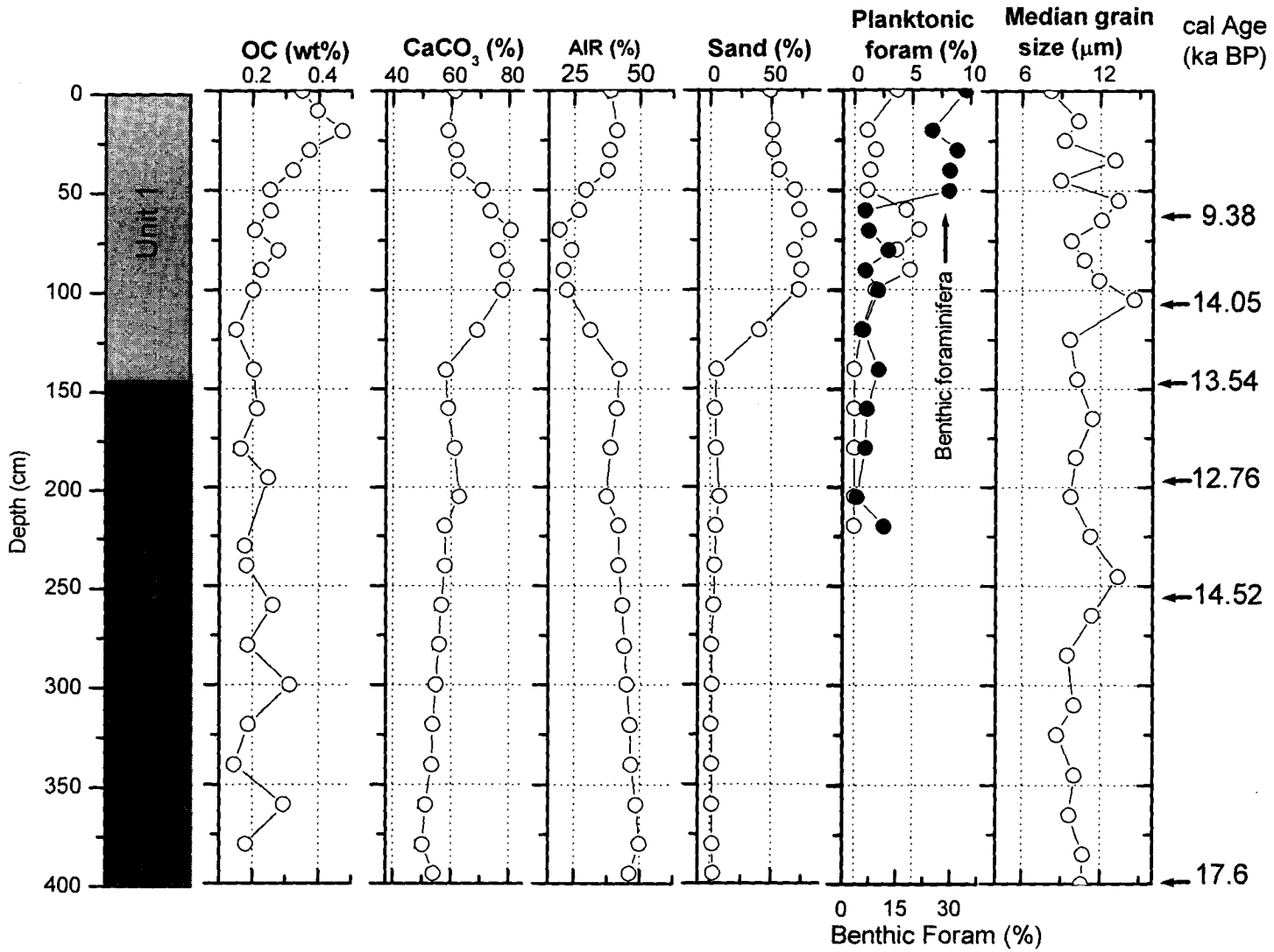

Fig. 5.2. Down-core distribution of organic carbon (OC), carbonate ($CaCO_3$), acid insoluble residue (AIR), sand content, foraminifera (Planktonic and Benthic) content and median grain size of the terrigenous mud in **GC-1.**

It increases to a value of 0.47% in the upper 32 cm of the core (Fig. 5.4, Table 5.3).

ii. $CaCO_3$ content

Variations in carbonate content of GC-1 are larger (50 to 80%) than that of GC-3 (70 to 77%). In GC-1, the carbonate content shows a gradual increase from 50% to 62% in unit 2 sediments (Fig. 5.2, Table 5.1). A hump of high carbonate (with a maximum value of 78% at 100 cm) occurs in the lower unit 1 (between 140 and 50 cm) sediments. Carbonate content then decreases to 60% at the core top (Fig. 5.2). In GC-3, the variations in carbonate content range from 70%-77% between 200 cm and 18 cm and decrease to <70% in the upper 18 cm of the core (Fig. 5.4, Table 5.3).

iii. Acid-insoluble residue (AIR)

The AIR content is relatively high (20-50%) in GC-1 than in GC-3 (23-30%). In GC-1, the AIR content varies from 40 to 50% in unit 2 sediments. A negative hump of low AIR content (a minimum of 22%) occurs in the lower unit1 sediments (140 to 50 cm) and then it increases to 40% towards the core top (Fig. 5.2, Table 5.1). In GC-3, the AIR content does not show systematic variations but varies from 23% to 30% in the lower part (200-18 cm) and 27% to 30% in the upper 18 cm of the core (Fig. 5.4, Table 5.3).

iv. Sand content

In GC-1, the sand content is uniformly low (1-7%) in unit 2 sediments. Within unit 1 it increases sharply to 72% between 140 cm and 70 cm and then reduces to 50% in the upper 70 cm (Fig. 5.2). The >125 μm fraction of the sediment between the core bottom and 60 cm contains higher proportions of shell fragments than benthic foraminifers, planktonic foraminifers, molluscs and carbonate mud aggregates. Pyrite grains are abundant in the interval between core bottom and 240 cm. A major change in coarse fraction occurs in the upper

60 cm of the core, wherein the relative proportions of the benthic foraminifers and mud aggregates increase. The sand between 140 and 70 cm comprises 3-4 cm size aragonite encrustations, green grains and green clay infillings of foraminifers. In GC-3, the sand content is low (2-6%) in unit 2 sediments (200 cm – 78 cm) and increases gradually from 3% to 67% in unit 1 (78 cm to the core top) (Fig. 5.4). The highest sand content (67%) is recorded closer to the core top. It comprises of abundant shell fragments followed by benthic foraminifers, planktonic foraminifers, molluscs and lime mud aggregates. Benthic foraminiferal species dominates over the planktonic foraminifers in the entire core. Lime mud aggregates are abundant in the lower unit.

v. Planktonic foraminifers

The planktonic foraminiferal content co-varies with sand (coarse fraction) and $CaCO_3$ content in GC-1 and sand content in GC-3. The planktonic foraminiferal content is little in unit 2 sediments of GC-1. Within the unit 1 sediments it increases sharply between 140 and 60 cm, with a maximum abundance of 4 to 5% at 90-60 cm of the core and then decreases to 2-4% in the upper 60 cm of the core. In GC-3, the planktonic foraminiferal content is distinctly low in unit 2 and lower unit 1 sediments (upto 50 cm) and increases to 9% in the upper 50 cm of the core.

vi. Median grain size

The median grain size of the terrigenous mud ranges from 9 μm to 15 μm in GC-1 (Fig. 5.2). It is relatively low (<12 μm) in unit 2 and increases to 15 μm at 105 cm of the core. Thereafter it gradually decreases towards the core top. In GC-3, the amplitude of median grain size variation is 4 μm (8-11 μm) between 200 cm and 10 cm of the core and reaches a value of 18 μm at the core top.

In GC-1, low OC coincides with low $CaCO_3$, sand and planktonic foraminiferal content in unit 2 sediments (Fig. 5.2). There is a gradual increase in OC, despite $CaCO_3$ decreases in unit 1. Grain size variations are much lower in

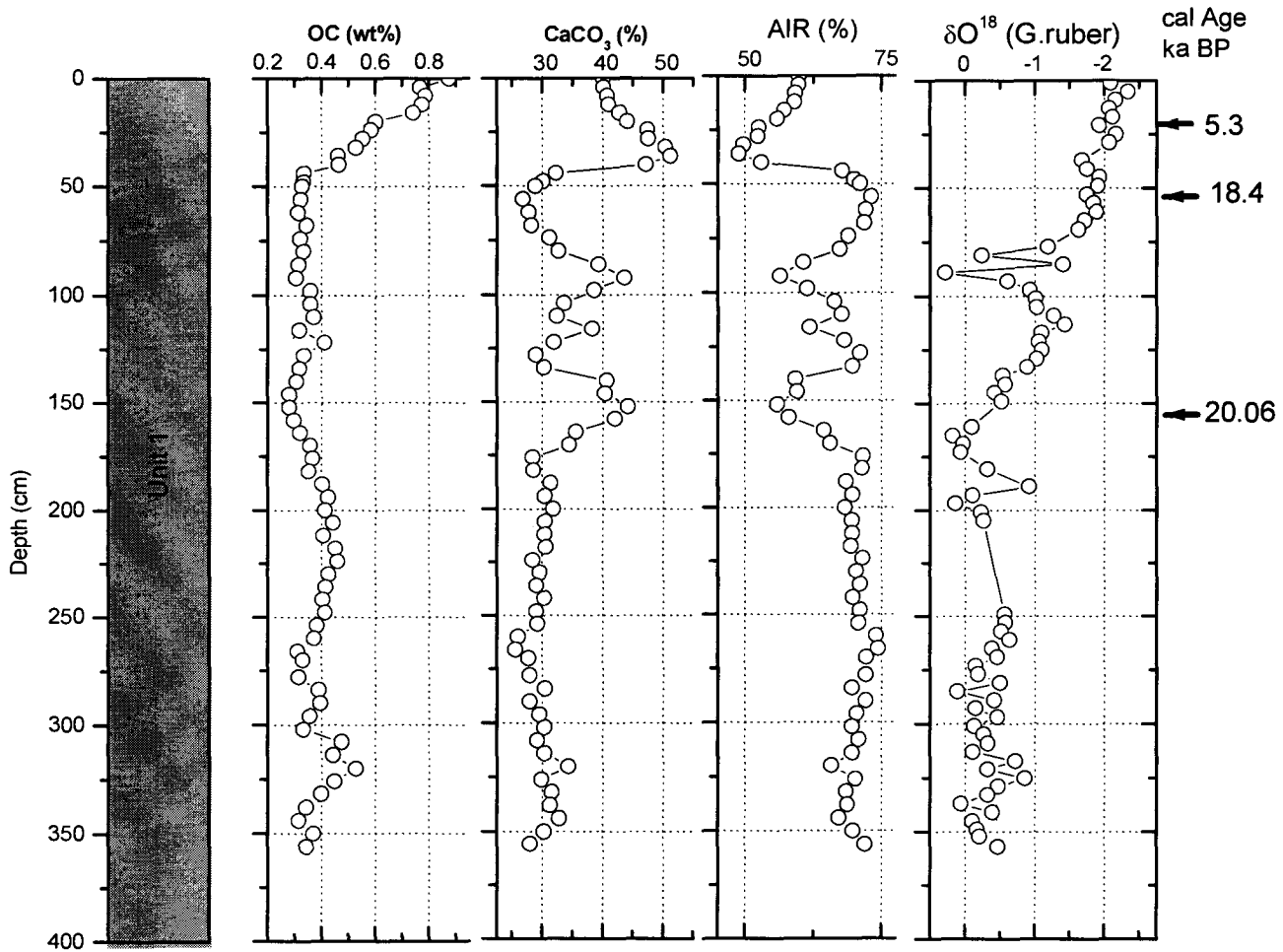

Fig. 5.3. Down-core distribution of organic carbon (OC), carbonate ($CaCO_3$), acid insoluble residue (AIR) and δO^{18} in **GC-2**

the lower part compared to that in the upper part of the cores. No characteristic relation was observed between OC and median grain size of terrigenous material. In unit 1 and 2 of both the cores, $CaCO_3$ shows positive correlation with sand content and planktonic foraminifer percentage in both the units except in the upper 20 cm of GC-3 (Figs. 5.2 and 5.4). In GC-3, the average OC remains at <0.3%, despite there is change in sand and planktonic foraminiferal content (Fig. 5.4). The OC record shows good correlation with the percent of planktonic foraminifers in the sediments near to the core top in GC-3.

5.4.2. Cores from the shelf edge and upper continental slope (GC-5, GC-6 and GC-7)

i. Organic Carbon

The cores show distinct variations in OC content from one unit to the other unit of the same core and from one core to the other. In general, lime mud unit (2) in the lower part of the core contain low OC content relative to the upper terrigenous-mud dominated unit (1). In GC-5, the average OC concentration is 0.1% in the lower unit 2 (core bottom to 144 cm) sediments. It progressively increases to 1% at the transition zone of unit2/1 (interval 144 to 56 cm) and remains at about 1% in the upper unit 1 sediments (Fig. 5.5, Table 5.4). The OC content in GC-6 (Fig. 5.6) is higher (2-5%) than the other shelf (0.2 to 0.4% in GC-1 and GC-3) and slope cores (0.1 to 1% in GC-5, GC-7 and GC-2). It is relatively low (~2%) in unit 2 sediments, progressively increases to 4% in the lower unit 1 sediments and remains at about 4-5% in the upper unit 1 sediments (Fig. 5.6, Table 5.5). In GC-7, the average OC content is ~1% at the core bottom (500-400 cm), gradually decreases to 0.1% at interval between 360 cm and 300 cm. Thereafter the OC content fluctuates between 0.5 and 1% in the upper 300 cm of the core (Fig. 5.7, Table 5.6).

ii. Total Nitrogen and organic carbon/ total nitrogen (C/N) ratio

The total nitrogen content in GC-5 and GC-7 varies from 0.01% to 0.16% and 0.02% to 0.2%, respectively. In GC-5, the total nitrogen content is low (<0.1%) in the interval between 200 cm and 72 cm and relatively high (>0.1%) in the upper 72 cm of the core (Table 5.4). The C/N ratio is largely 8 - 10 between 200 cm and 50 cm and gradually decreases to 6 in the upper 50 cm of the core (see Fig. 5.5). In GC-7, the total nitrogen content is relatively high (>0.1%) at interval of 480 cm - 400 cm and decreases to <0.1% in the interval between 400 cm and 16 cm. It is about >0.1% in the upper 16 cm of the core (Table 5.6). The C/N ratio is <9 in the lower part (core bottom to 325 cm) and fluctuates between 8 and 10 in the larger portion of the remaining core, except at the interval 100-75 cm where it reaches up to 14.

iii. $CaCO_3$ content

Carbonate content in GC-5, GC-6 and GC-7 varies from 35-96%, 30-91% and 60-96%, respectively. In GC-5, the carbonate content is high (96%) in unit 2 sediments and decreases gradually to 40% in unit 1 sediments (Fig. 5.5). In GC-6 the $CaCO_3$ content ranges from 91% to 60% in unit 2 (core bottom to 200 cm), decreases to about 40% at about 140 cm and remained at 40 - 60% in the upper 140 cm of the unit 1 sediments (Fig. 5.6). In GC-7, the carbonate content is low (60 to 80%) between 500 and 400 cm of the unit 2 sediments and then increases and range between 80 and 90% in the remaining unit 2 (400 to 75 cm) and unit 1 sediments (see Fig. 5.7).

iv. Acid-insoluble residue (AIR)

In GC-5, the AIR content is low in unit 2 sediments (~4%) and gradually increases from 4 to 53% from the base to the core top of unit 1 sediments (Fig. 5.5). In GC-6, the AIR content varies from 8-29% in unit 2 (core bottom to 200 cm) and gradually increases from 29 to 61% from base to the core top of unit 1 sediments (Fig. 5.6). In GC-7, the AIR is 20-40% in lower unit 2 sediments (core

bottom to 400 cm) and ~10% in upper unit 2 sediments (350-76 cm) and increases to a value of 20% in unit 1 sediments (Fig. 5.7).

v. Sand content

The sand content in GC-5 varies from 33 to 45% in unit 2 sediments. It gradually increases from 44% to 82% at 116 cm and then decreases to 41% at the core top (Fig. 5.5). The >125μm fraction of the sediment consists of abundant carbonate sands. The relative abundance of foraminifers, molluscs and shell fragments starts increasing from 120 cm to core top. In GC-6, sand content ranges from 7% to 30% in unit 2 sediments (core bottom to 200 cm) and then gradually decreases to 5-10% in unit 1 sediments (Fig. 5.6). The coarse fraction consists of planktonic and benthic foraminifers in the upper 300 cm of the core with greater abundance of planktonic foraminifers. In GC-7, the sand content is relatively high (10-40%) from core bottom to 300 cm interval and low (1-4 %) between 300 cm and core top (Fig. 5.7). The >125μm fraction consists of more or less equal proportion of planktonic and benthic foraminifers and mollusc shells in the lower part (520 cm to 64 cm) and dominantly planktonic foraminifers in the upper 64 cm of the core. Foraminifers and shells dominate in the >125 μm fraction. Lime mud aggregates occur in the finer sand fraction (63-125 μm) between 310 cm and 60 cm interval of the core.

vi. Planktonic Foraminifers

The content of planktonic foraminifers is negligible in unit 2 sediments but increases to 30% in unit 1 sediments of GC-5 (Fig. 5.5). In GC-6, the planktonic foraminiferal content ranges from 30-50% in unit 2 sediments, remain at about 50-70% in the lower part of unit 1 (200-40 cm) and then decreases to 40% in the upper 40 cm sediments (Fig. 5.6, Table 5.5). In GC-7 (Fig. 6.7), the percentage of planktonic foraminifers is relatively high (25-50%) in the lower unit 2 (500-300 cm) and low (10-35%) in the upper unit 2 (275-76 cm) sediments. The content of planktonic foraminifers is highest (>50%) in unit 1 sediments.

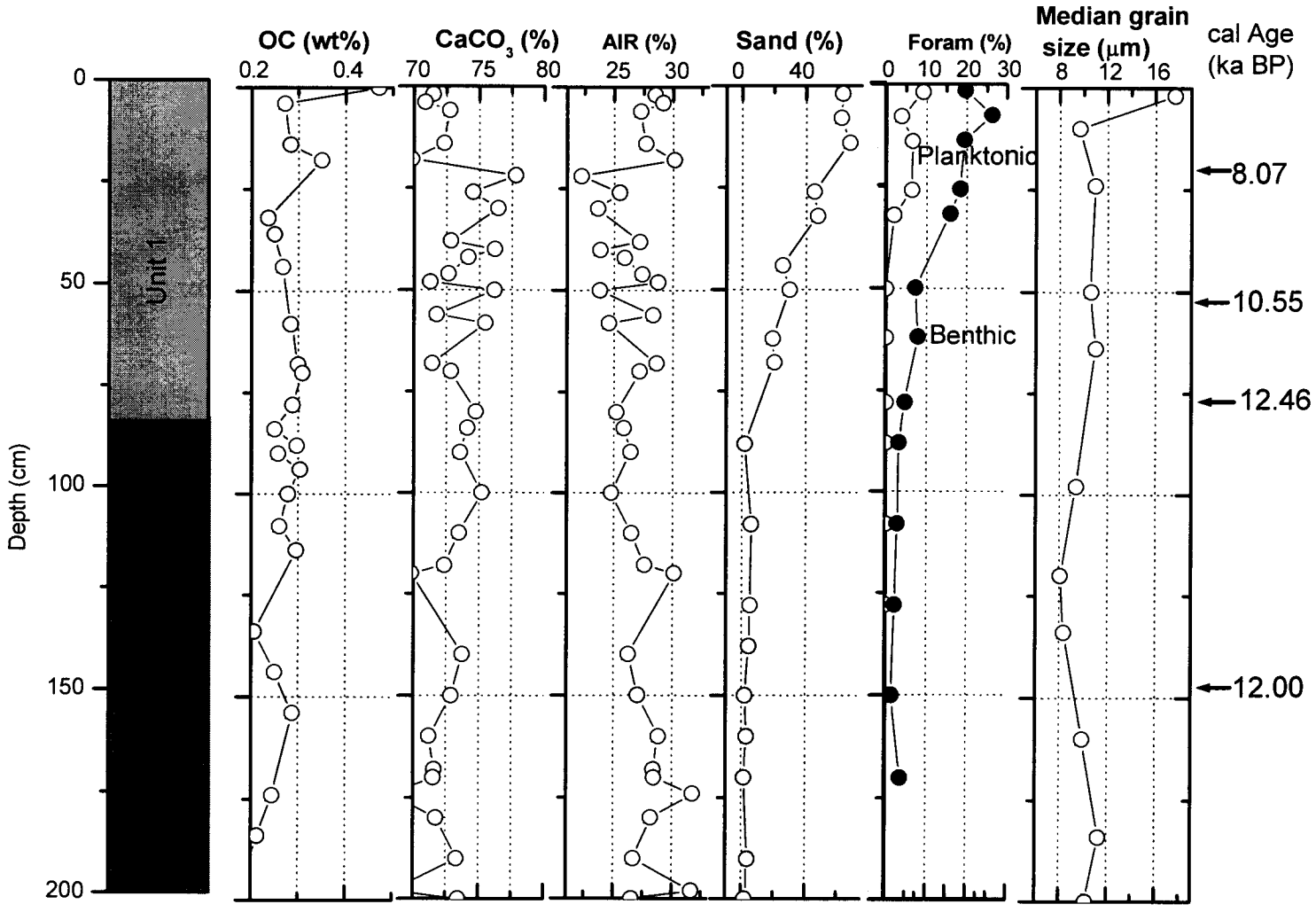

Fig. 5.4. Down-core distribution of organic carbon (OC), carbonate ($CaCO_3$), acid insoluble residue (AIR), sand content, foraminifera (Planktonic and Benthic) content and Median grain size of the terrigenous mud in **GC-3**

vii. Median grain Size

The median grain size of the terrigenous mud ranges from 8-28 μm, 8-13 μm and 7-13 μm in GC-5, GC-6 and GC-7, respectively. In GC-5, the average median size is 10 μm in unit 2 and ~20 μm in unit 1 sediments (Fig. 5.5). In GC-6, the median grain size is <8 μm in unit 2 (below 280 cm) but fluctuates between 10 μm and 13 μm (Fig. 5.6). In GC-7, the average median size is 12 μm in unit 2 (500-62 cm) and sharply decreases to 8 μm in unit 1 sediments of the core (Fig. 5.7).

In GC-5 and GC-6, OC shows negative correlation with $CaCO_3$ (Figs. 5.5 and 5.6). In GC-5, relatively low sand content coincides with low OC in unit 2 sediments. In the upper unit, OC shown negative correlation with sand content (Fig. 5.5). In GC-6, the $CaCO_3$ exhibit negative correlation with OC in the unit 2 sediments. In the lower 50 cm of unit 1 (200-150 cm interval), OC shows negative correlation with $CaCO_3$ and sand content (Fig. 5.6). The OC shows a good correlation with planktonic foraminifers in the interval between 240 cm and 75 cm, that represent mid to late Holocene. In GC-7, the average OC content in unit 2 sediments is slightly higher than that of Unit 1 sediments. OC is negatively correlated with $CaCO_3$ and shows no characteristic relationship with sand percentage in the lower part (400-300 cm) (Fig. 5.7). The percentage of planktonic foraminifers is high (25-50%) in unit 2 and also in the upper unit 1 (>45%) sediments (Fig. 5.7).

5.4.3. Core from the lower continental slope (GC-2)

The OC content fluctuates between 0.3% and 0.5% in the lower part (core bottom to 44 cm) and increases from 0.3% to 0.87% in the upper 44 cm of the core. (Fig. 5.3, Table 5.2). The carbonate content is about 30% in the lower part of the core (356-176 cm) and fluctuated between 26 and 45% in the upper 176

cm of the core. Variation in the amplitude of carbonate is ~20% in the interval 176 to 56 cm. Carbonate content sharply increases to the highest value of 51% at 36 cm interval and decreases to 40% in the upper 36 cm of the core. OC shows positive correlation with $CaCO_3$ in the lower part (core bottom to 176 cm) and in the interval between 50 cm and 36 cm of the core and negative correlation in the other parts of the core. The AIR content is ~70% in the lower (356-176 cm) part of the core and fluctuates from 55% to 74% in the interval between 176 and 56 cm. It decreases sharply from 74% to 48% in the interval 56 to 36 cm and again increases to 59% in the upper 36 cm of the core. The $\delta^{18}O$ values show heavier isotopic composition in the lower part of the core in the interval of 358-160 cm. The $\delta^{18}O$ values become lighter from 175 cm to the core top. The LGM-Holocene amplitude in $\delta^{18}O$ value is 1.98‰ (LGM -0.18‰; Holocene -2.16‰).

5.5. Discussion

5.5.1. Organic carbon in cores from the continental shelf (GC-1, GC-3)

i. Unit 2 sediments

The average OC content is low (<0.5%) in unit 2 sediments of both the cores. The very low OC (av. 0.2% - 0.3%) coincides with low sand (<7%) and negligible planktonic foraminiferal content (Figs. 5.2 & 5.4). In GC-1, the carbonate content is lower (50-60%) and AIR content (40-50%) is higher than in GC-3 (70-75%, 25-30%). The carbonate is largely in the form of lime muds, which contain aragonite (70-80%) and low-magnesium calcite (20-30%) in GC-1 and largely aragonite (90-95%) in GC-3. Since aragonite is of marine origin, aragonite may have initially formed in brackish or carbonate saturated shallow marine conditions. On the basis of the ages of lime muds and Glacio-eustatic sea levels positions, a mismatch between the two was identified and explained the existence of shallow marine / lagoonal conditions in the Gulf during LGM that favoured the lime mud formation. Subsequently the Gulf was subjected to neo-

tectonic activity and lime muds were reworked to the shelf region. The low OC in lime mud sediments may be due to the reworked nature of sediments. Since the lower unit contains 40-50% AIR and negligible amount of sand and foraminifers (Fig. 5.2), it is most likely that the OC was partly reworked and partly transported from land along with the terrigenous sediments.

GC-3 is located off Saurashtra, where the hinterland is marked by flat-topped basaltic ridges and highly varied coastline with a narrow belt of low ridges and cliffs of miliolite limestones (Chamyal et al., 2003). Miliolites are calcite in composition and of Quaternary age (Baskaran et al., 1989). As lime muds are aragonitic, the contribution of lime material from miliolite limestones to the core site (GC-3) may be minimal. Moreover, GC-3 is located close to the carbonate platform, which at present lies at depths between 60 m and 110 m. The lime muds are of 12.5 to 12 ka in age and associated with low OC (0.2 to 0.3%). It is likely that the muds formed within the lagoons of the platform and subsequently transported to the shelf at 65 m depth. Therefore, the OC in the lower unit of the shelf cores is reworked and transported to the core sites along with the carbonate and terrigenous sediments.

The high AIR content (50-60%) may have diluted the OC content in GC-1. The pyrite aggregates in unit 2 of GC-1 indicate reducing conditions. Pyrite forms when H_2S released during the microbial sulphate reduction of organic matter in sub-oxic/anoxic marine environment reacts with reactive iron compounds (Berner, 1984; Canfield, 1989) and its formations is controlled by quantity and reactivity of organic matter and availability of Fe (Schenau et al., 2002). Thus the presence of pyrite also indicates that part of the organic matter may have been consumed and therefore low OC values. The oxic water column at core sites may have decomposed OC rapidly. Thus the OC content in the lower unit of the cores is detrital and its concentration is controlled by dilution of reworked sediments and oxic water column conditions.

ii. Unit 1 sediments

In unit 1 sediments of GC-1, the initial marginal increase in OC during ~13 to 9 ka (140-70 cm) coincides with an increase in $CaCO_3$, sand and planktonic foraminiferal content. Besides, this interval contains abundant green grains and aragonite encrustations of 3-4 cm size at 110 cm. The aragonite encrustations dated 14 cal ka are found in between sediments of younger aged (13.54 and 9.38 cal ka BP) sediments (Fig. 5.2) implying that the sediments in this part of unit 1 are also reworked and marginal increase in OC is most likely due to the organic matter associated with the biogenic material and green grains. Though the relative abundance of planktonic foraminifers is less (<6%) in the upper 140 cm –70 cm of the core, the >125 μm fraction contains relatively increased benthic foraminiferal species (6-12%), which in turn provide evidence of productivity and availability of organic carbon. In the upper 70-20 cm (~9-3 cal ka BP) of the core, the increase in OC from 0.2 to 0.5% coincides with the increase in AIR content (20%-40%), decrease in sand (80%-50%) and increase in the combined abundance of planktic and benthic foraminifers (10%-33%). The decrease (5%-1%) in the planktonic foraminiferal content in this interval coincides with the relative increase (6%-32%) in the benthic foraminifers. Thus the increased OC may have been largely due to the terrigenous sediments with some contribution from the foraminiferal content. The upper 20 cm (~3 ka BP to present) sediments of the core contain decreased OC (0.5-0.3%) despite an increase in the planktic and benthic foraminiferal content (26-38% - Fig. 5.2). Moreover, the decrease in OC coincides with a minor decrease in AIR content (41-38%, Fig. 5.2). Thus in the upper part (70 cm to the core top) of unit 1, the OC variations are largely controlled by AIR content with a little from foraminifers and other benthic species. The median grain size of the mud fraction is <13 μm, indicating considerable amount of finer silt and clay constituting the terrigenous mud; this leads to better preservation of OC in sediments. Mc Cave et al. (1995) suggested that the silt finer than 10 μm behaves in the same way as clay. Calvert et al. (1995) studied

the possible influence of sediment texture over OC preservation in the eastern Arabian Sea sediments and found that the clayey silts / silty clays retain more OC than that of sandy sediments. Calvert and Pederson (1992) postulated that the relatively low OC content in the outer shelf sediments off western India is due to coarser sediments. Within the unit 1 sediments, the sediments between 140 and 70 cm interval showed higher sedimentation rate (16.8 cm ka^{-1}) and lower OC (av. 0.2%) than that of upper 70 cm of the core (7.5 cm $ka^{-1;}$ av. 0.3%) (see Fig. 5.2). But the sediments are coarser in the former than in the latter. This implies that the sources of supply and texture of the sediments play a major role in organic carbon distribution. Although the rates of sedimentation in unit 2 sediment is higher (64 cm ka^{-1}) than that of unit 1 (10.3 cm ka^{-1}), the OC content is lower (0.2-0.3%) in unit 2 than in unit 1 (0.2-0.5%, Fig. 5.2). This implies that the nature of sediments, texture, sources and supply of OC, and oxygen content in the overlying water column play a major role in OC distribution.

The marginal decrease of OC (0.3% to 0.2%) in the interval 76-32 cm in unit 1 sediments of GC-3 (Fig. 5.4) coincides with an increase in $CaCO_3$ (71-78%), sand (2-47%) and planktic and benthic foraminiferal content (5-18%) and decrease in AIR content (29-22%). Further, the increase in OC (0.2 to 0.4%) in the upper 32 cm of the core corresponds with the decrease in $CaCO_3$ (80-70%) and increase in AIR (20-30%), sand (40-60%) and planktonic (2-10%) as well as benthic foraminifers (16-26%). Within the unit 1, OC variations correlate with AIR, which seems to be the dominant controlling factor. The low OC content despite high sand (containing considerable amount of benthic and planktic species) in unit 1 (Fig. 5.4) may be due to reworked nature of sediments, oxic conditions and low sedimentation rates (5.6 cm ka^{-1}). The OC may be terrigenous in origin. The carbonate-rich (>70% $CaCO_3$; dominantly aragonite in composition) sediments dated 12.46 ka BP in unit 1 indicate reworking (since the Glacio-eustatic sea level was at ~ -70 m at 12.5 ka BP and prevalence of exposed conditions at 65 m – the water depth at GC-3 – see chapter 4). As aragonite is the dominant

mineral, the explanation given for unit 2 sediments of the core (i.e. formed in the adjacent lagoonal/shallow water conditions and subsequent reworking) may be valid for carbonate-richness of the unit 1 sediments. The sediments younger than 10.55 ka BP in unit 1 (see Fig. 5.4) show increased AIR content and represent their sedimentation after the core site was submerged by the Glacio-eustatic sea level and existence of shallow marine conditions (the Glacio-eustatic sea level was ~ -60 m during this period). Thus the intermixing of reworking carbonate flux from the platform and terrigenous flux from the land resulted in fluctuation in carbonate and AIR content and OC content in unit 1 sediments.

Thus the OC in unit 1 sediments of the shelf cores (GC-1 and GC-3) was supplied largely from continental source with some contribution from reworking of the carbonate sediments. The sediment texture, sedimentation rate and oxic water column conditions have influenced the overall preservation of OC enrichment.

5.5.2. Organic carbon in cores from the shelf edge and continental slope (GC-5, GC-6 and GC-7)

i. Unit 2 Sediments

As in shelf cores, the organic carbon in unit 2 sediments of upper slope cores (GC-5, GC-6 and GC-7) is associated with lime muds. The core GC-5 was recovered at 121 m water depth and low OC content (av. 0.1%) is associated with >95% $CaCO_3$, <5% AIR, ~40% sand and negligible planktonic foraminiferal content (Fig. 5.5). The high sand content is due to pelletization of carbonate muds (see Chapter 4, Fig. 4.11 and 4.12). Carbonate is largely aragonitic (>95%) in composition. The C/N ratio of organic matter (<10) also attests marine origin. The ages of the lime muds (close to the upper end of unit 2) at intervals 132 cm and 124 cm are 13.99 and 14.5 ka, respectively. Following Fairbanks' sea level curve, the Glacio-eustatic sea level at 14 ka was at -90 m and started rising rapidly at a rate of 21 m per 1000 years and this event has been referred to as

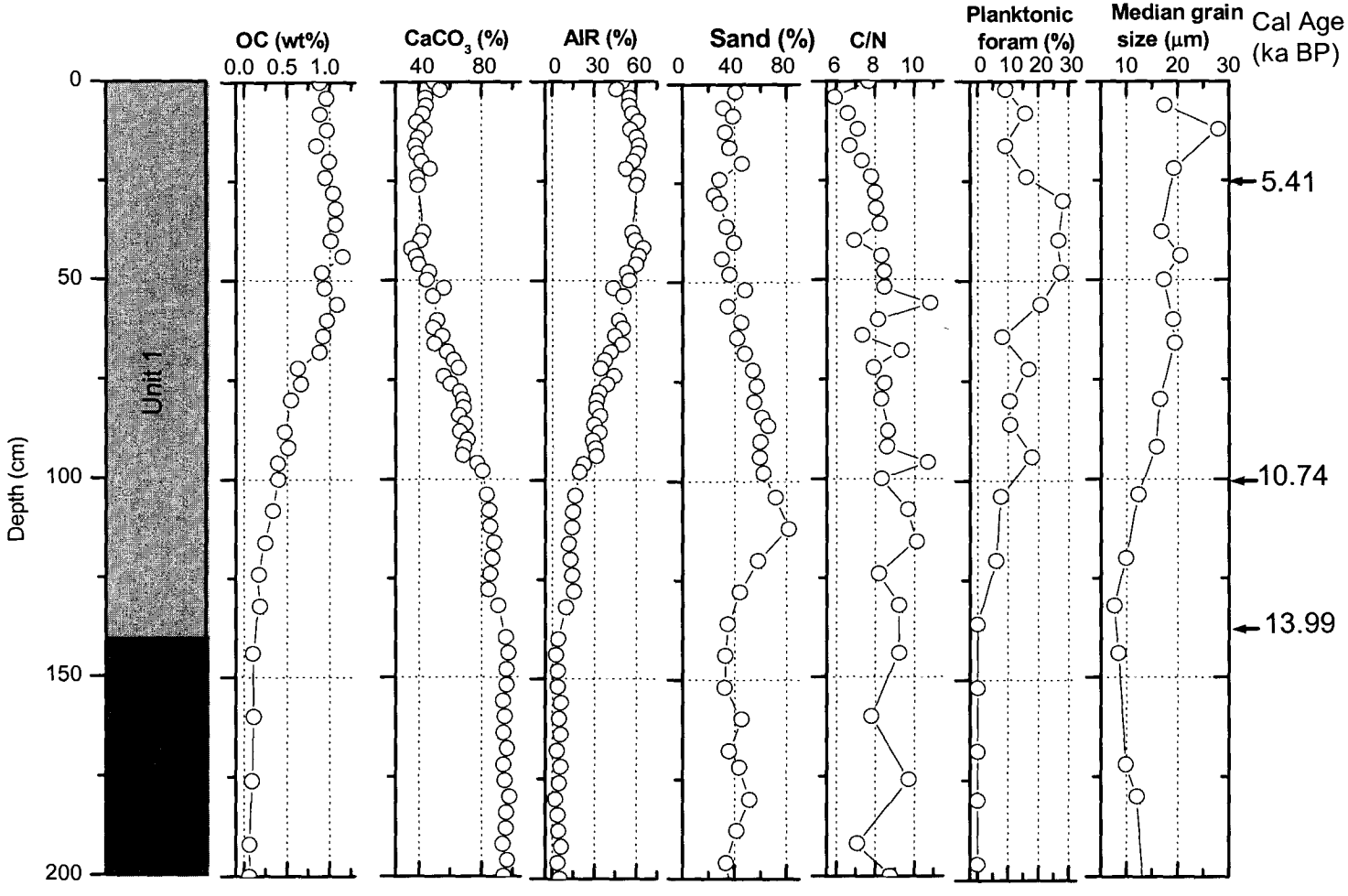

Fig.5.5. Down-core distribution of organic carbon (OC), carbonate ($CaCO_3$), acid insoluble residue (AIR), sand content, C/N ratio, planktonic foraminifera content and median grain size of the terrigenous mud in **GC-5.**

melt water pulse (MWP)-1A. This implies that the water depth at the core site was about 30 m and lime muds at the core site may have formed insitu before the rapid rise of sea level at 14 ka or detrital-derived from the outer shelf or carbonate platform (see Fig. 5.5). Since the younger age lime muds occur below the older aged muds (unpublished data) at least part of the lime mud formation must have been transported to the core site. The unit 2 sediments are older than 14 ka BP and productivity is low during early deglaciation on the western margin of India (von Rad et al., 1995). In other words the low OC content in unit 2 sediments of GC-5 is therefore due to (1) low OC supply from the productivity and little from the lime muds and (2) existence of oxic-depositional conditions.

The core GC-6 was recovered at 330 m (Fig. 5.6). Unit 2 sediments contain ~2% OC, 70-90% $CaCO_3$, 10-30% AIR, <20% sand with 10-50% planktonic foraminifers. The age of the lime muds at 230 cm is 11.26 ka, implying that lime mud deposition was much before 11.26 ka. The Glacio-eustatic sea level at 11.26 ka was at ~ -40 m (after MWP - 1B dated 11.6 -11.4 ka cal BP during which sea level reached from 60 m to 42 m, Liu and Milliman, 2002). This implies that the water depth at the core site during lime mud deposition was at least ~250 m, implying the existence of oxygen minimum conditions (between 150 m and 1200 m) at the core site. Two sources of OC are likely at the core site: (a) OC deposited from the surface water productivity, as evidenced by the abundance of planktonic foraminifers (Fig. 5.6) and (b) OC associated with lime muds that have been transported to the core site.

Differences in environmental conditions at GC-5 and GC-6 are as follows. a) GC-6 received OC supply both from surface water productivity and detrital supply, whereas core GC-5 received largely from bio-detrital supply. (b) Presence of OMZ conditions at GC-6, but oxic conditions at GC-5, (c) Median grain size is finer (8-12 μm) in GC-6, but relatively coarser (18 μm) in GC-5 (d) AIR content is more (10-30%) in GC-6 but less (<5%) in GC-5. Enhanced OC in GC-6 may

therefore be due to increased productivity associated with OMZ conditions. Better preservation under finer grain size may have also been a factor for OC enrichment. In GC-5, largely detrital OC, oxic conditions and winnowing of finer sediments are responsible for low OC content.

Despite GC-7 (420 m) was located within the OMZ (150-1200 m), the OC content of unit 2 sediments is low (0.1 to 1%). Other parameters such as carbonate and AIR content, sand content, C/N ratios are consistently uniform in the upper unit 2 (300 to 70 cm) but vary below (300 cm -480 cm). Increased OC content (0.76-0.96%) between 480 cm and 400 cm coincides with increased sand and planktonic foraminifers implying that marine organic carbon in these sediments. The C/N ratio (av. 8) also indicates marine source of OC. The unit 2 sediments between 280 cm and 180 cm correspond to the early deglacial period (15.88 – 15.7 ka – Fig. 5.7). Two factors may be envisaged for OC content. (a) Despite the core site was within in OMZ both during the Last Glacial Maximum and early deglaciation the OC content is low (0.62 to 0.93%) implying low supply of OC. Low productivity conditions may have prevailed during early deglaciation and continued until 12 ka. Low planktonic foraminiferal content in the upper unit 2 sediment supports this argument. (b) The sediments between 300 cm and 50 cm are lime-mud dominated and deposited between 15.9 ka and about 12 ka. This implies that the sediments were deposited at a rate of about 60 cm per 1000 years. This type of very high sedimentation occurs where mass transportation is prevalent. In this case transportation of lime mud sediment was from the adjacent continental shelf/platform. Therefore the OC associated with lime muds was transported to the core site and preserved due to rapid burial of OC under high rate of sedimentation and oxygen minimum conditions.

ii. Unit 1 Sediments

The thickness and rate of sedimentation in unit 1 sediments vary in each core. For example, the unit 1 sediments are 136 cm in GC-5, 200 cm in GC-6

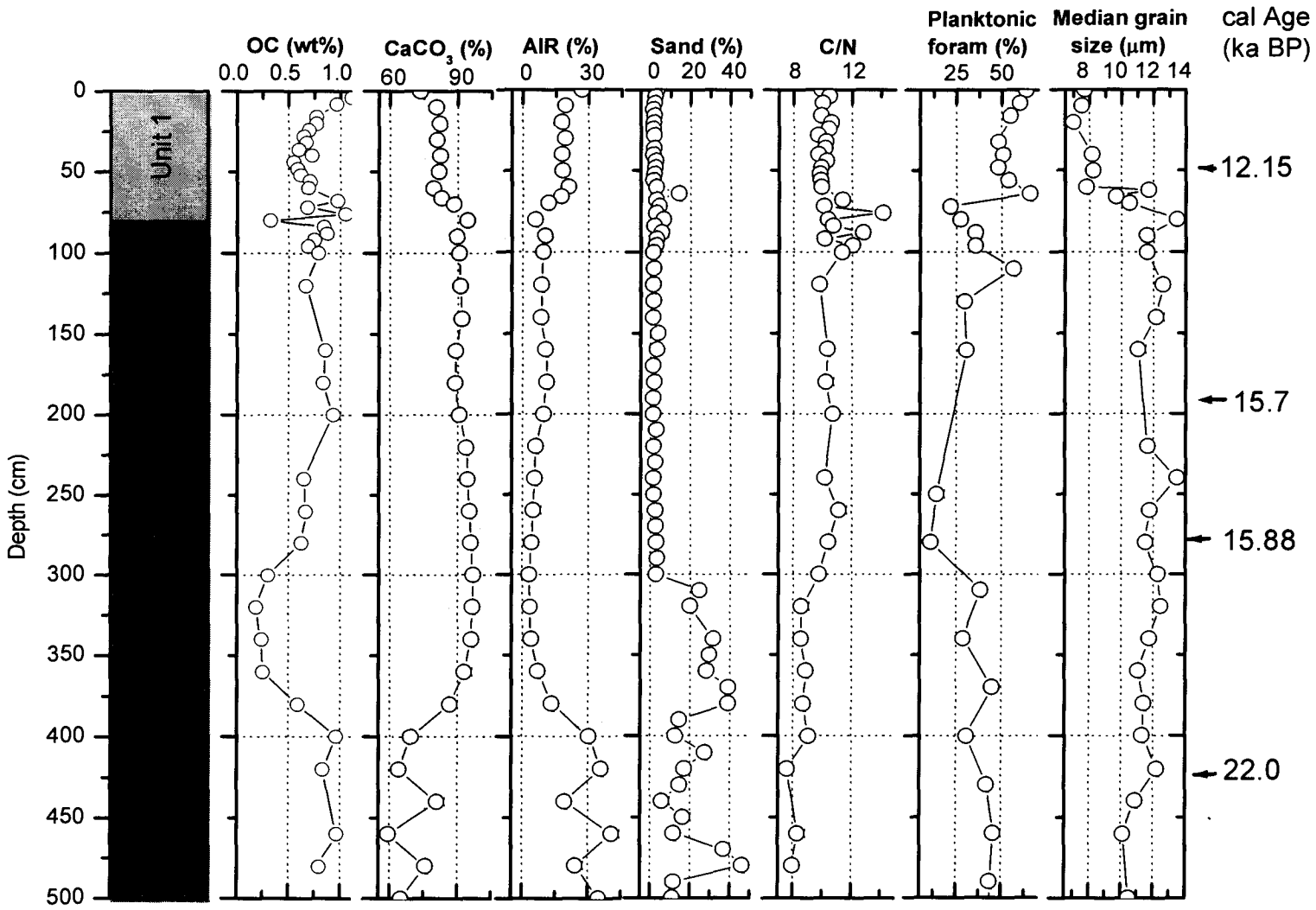

Fig. 5.7. Down-core distribution of organic carbon (OC), carbonate ($CaCO_3$), acid insoluble residue (AIR), sand content, C/N ratio, planktonic foraminifera content and median grain size of the terrigenous mud in **GC-7.**

and 80 cm thick in GC-7 deposited at a rate of 9.31 cm/ka, 17.76 cm/ka and 4.11 cm/ka, respectively. The age of the sediments at the base of unit 1 also varies; it is 14 ka BP in GC-5 (see Fig. 5.5), 11 ka BP in GC-6 and 12 ka BP in GC-7. GC-5 is located at the shelf edge. Although the base of unit 1 is at 14 ka in GC-5, the sediments quickly reach to 10.7 ka BP with in 20 cm and distinct change is visible from that point (see Fig. 5.5). These imply that the change in sedimentary environment from unit 2 to unit 1 occurred at about 12-11 ka BP. The OC increases progressively in the lower part of unit 1 and reach a value of about 1% in GC-5 at about 7 ka BP and 4% in GC-6 at about 6 ka BP (Figs. 5.5 and 5.6). Thereafter it remains steady towards core top in GC-5 but reaches a value of 5% in GC-6. In GC-7, OC decreases from 1% to 0.5% in the lower part and increases (0.5% to 2.15%) in the upper part of unit 1 sediments (Fig. 5.7).

The OC content in the lower unit 1 sediments of GC-5 and GC-6 shows negative correlation with $CaCO_3$ and sand percentage and positive correlation with AIR. However, there is an increase in planktonic foraminiferal content and median grain size of the sediment (Figs. 5.5 and 5.6). Bhushan et al. (2001) explained the inverse relation between OC and $CaCO_3$ as a result of post-depositional effects due to sulphate reduction, which leads to dissolution of carbonate. OC is usually preserved in the sediments with high detrital content deposited at high sedimentation rates. Sheu and Huang (1989) and Paropkari et al. (1991) suggested that the direct covariance between OC and $CaCO_3$ indicates control by primary productivity. As the OC content is low (mostly <0.5%) in the lower part of unit 1 (GC-5), the overall decrease in carbonate content may not be due to post-depositional effects but be due to gradual decrease in lime mud supply from the shelf or carbonate platform.

In GC-5 and GC-6, the gradual increase in OC corresponds to the increase in terrigenous supply and planktonic foraminifers. The increase in foraminiferal content may be due to the result of increased upwelling and

associated primary productivity. The surface water productivity increases either due to increased supply of nutrients through upwelling or terrigenous discharge that in turn enriches the OC content at the core sites. Increased OC content starting at about 11 ka (10.74 ka in GC-5 and 11.26 ka in GC-6) probably marks the increased monsoonal intensification. The clay mineral data from these cores also show signs of monsoon intensification during early Holocene (see chapter 6). The palaeomonsoonal studies and upwelling indices have shown that monsoon intensification occurred between 13 and 6 ka BP on the Indian subcontinent coinciding with northern hemisphere summer insolation maxima (Prell, 1984; van Campo, 1986; Sirocko et al., 1993; Naidu, 1996), with the maximum intensity after ~9-8 ka BP (Thamban et al., 2001).

Although the planktonic foraminiferal record in GC-5 and GC-6 matches well with the monsoonal records, the OC record shows a mismatch wherein low OC values coincide with the period of intensified monsoon. For example, the OC content increases progressively until ~7 ka from <0.5% to 1% in GC-5 and remained high (1%) even in mid- and late Holocene sediments (see Fig. 5.5). Similarly, the OC content progressively increases to 4% until ~6 ka in GC-6 and continued to remain high in mid- and late Holocene sediments and increases to 5% at the core top. These imply that the OC enrichment (mid to late Holocene) is not only controlled by supply of OC from primary productivity, but also controlled by the secondary preservational factors such as sediment texture and sedimentation rate. The mid- to late Holocene sediments contain more terrigenous matter largely in the finer silt size (10-15 μm) range, favouring better preservation of OC. It has been established that OC content increases as particle size decreases (Bordoviskiy, 1965). Calvert et al. (1995) postulated that the distribution of organic carbon on the eastern margin of Arabian Sea could be influenced by purely textural parameters. The relatively low OC in the shelf sediments and high OC content in the slope sediments off western India are due

to coarser sediments in the shelf and finer sediments on the slopes (Calvert and Pederson, 1992).

In unit 1 sediments, the sedimentation rate is highest in GC-6 (17.76 cm ka^{-1}), followed by GC-5 (9.31 cm ka-1) and GC-7 (4.11 cm ka-1). The OC content varies from 2 to 5% in GC-6, 0.5 to 1% in GC-5 and 0.1 to 0.9% in GC-7. This implies that high OC is preserved at high rates of sedimentation. Kolla et al. (1981b) suggested that the high OC values in the sediments of the Indian margin are due to its preservation as a result of anoxia and high sedimentation rates. High sedimentation rate together with OMZ provide rapid burial of organic matter and its preservation. The very high rate of sedimentation will, however, dilute the organic matter (Tissot and Welte, 1978).

Thus in the slope cores, the OC concentration in unit 1 sediments is controlled by surface water productivity, dissolved oxygen content and better preservation under moderate to high sedimentation rate and finer grain size.

5.5.3. Organic Carbon in a sediment core from the lower continental slope (GC-2)

This core is located at 1900 m within the oxygenated water below the oxygen minimum zone (Fig. 5.1). With the limited data set available on this core (GC-2), I would like to state definite conclusions can not be drawn at this stage and interpretation on the data at best should be considered as tentative. As and when I receive more radiocarbon dates (Accelerator Mass Spectrometer dates) and chemistry data (analyses were requested) on this core detailed interpretations will be presented in future publications.

The OC values are <1% (Fig. 5.3). The core contains terrigenous-dominated sediment throughout and thus distinct from the other cores. Between

core bottom and 176 cm of the core, the low OC (<0.4%) coincides with low $CaCO_3$ (av. 30%). Though the OC content remains steady (0.2% to 0.4%) carbonate and AIR content fluctuate at the interval between 176 cm and 50 cm, which corresponds to the Last Glacial Maximum (LGM) (see Fig. 5.3). The sediments were also deposited at a rate of 64.5 cm/ka between 156 cm and 50 cm. Two possibilities exist for low OC and changing carbonate and AIR contents. (a) The weak correlation between OC and $CaCO_3$ and high rates of sedimentation may be due to the reworking of sediments from the upper continental slope. During the lowered sea levels, the River Indus might have also debouched sediments directly on to the continental slope, favouring reworking of sediments. (b) The rock-magnetic properties clearly indicate that there is no increase in magnetic susceptibility but the S-ratio% becomes lower during this time, implying the presence of aeolian-derived material transported along with abundant illite and chlorite (see Chapter 3 for details). This could have also contributed for low OC in the sediments. Prevalence of arid conditions during the LGM was reported by several workers (von Rad et al., 1995; Cowie et al., 1999)

Organic carbon content remains low until 16ka BP. Thereafter it gradually increases but slowly towards the core top. The trend in OC increase coincides with decrease in acid-insoluble residue and increase in carbonate content and rock-magnetic parameters (MS, χ_{ARM}, SIRM) (see chapter 3, Fig. 2B). This has been interpreted due to the changing sedimentary conditions because of the initiation of sea level rise that keeps away the terrigenous flux favouring the formation of authigenic magnetite by magnetotactic bacteria.

The sediments corresponding to early deglaciation are thin in this core. The increase in OC (0.74% - 0.87%) coincides with increase in AIR and $\delta^{18}O$ values in the Holocene sediments. This may be due to the increased fresh water flux that resulted in increased surface productivity and increased OC to the sea floor.

5.5.4. OC record along the western continental margin of India - A comparative study.

The surficial sediments of the western margin of India show high organic carbon (~4%) in the inner shelf, low (<1%) in the outer shelf and >2% on the slope (with values up to 16% at mid slope - Rao and Rao, 1989; Ramamurty and Murty, 1989; Naidu et al., 1992). OC values >1% are seen in the continental margin off India-Pakistan and the highest OC values (5-10%) are seen along the Indian continental margin at depths of 200-1500 m mostly coincinding with OMZ (Kolla et al., 1981b). Suthhof et al. (2000) found high OC values (1.2-2.9%) associated with laminated sediments of OMZ, in bioturbated sediments immediately below the OMZ, and below the regions of high productivity in the western Arabian Sea. Cowie et al. (1999) reported maximum OC values (3-4 %) near the lower boundary of OMZ in the northern Arabian Sea (off Pakistan margin).

On the basis of surface productivity (Qasim, 1977), Babu et al. (1999) divided the western continental margin of India into 3 zones, viz. area A, B and C, as region of high productivity (0.75-1.00 $gCm^{-2}day^{-1}$), moderate to high productivity (>0.50-0.75 $gCm^{-2}day^{-1}$) and low productivity (<0.50 $gCm^{-2}day^{-1}$), respectively. The study area falls in the moderate to high productivity area (Fig 5.8).

i. Surface sediments

An evaluation of the OC data from the core top samples from the 3 areas (area A, B and C) reveals several parameters in conjunction with surface water productivity operate for the enrichment of OC. For example, the highest OC concentration is shown by cores recovered from the topographic high off Goa (AAS 6/2 and AAS 6/3, see Thamban et al., 1997) at depth of 329 m and 355 m,

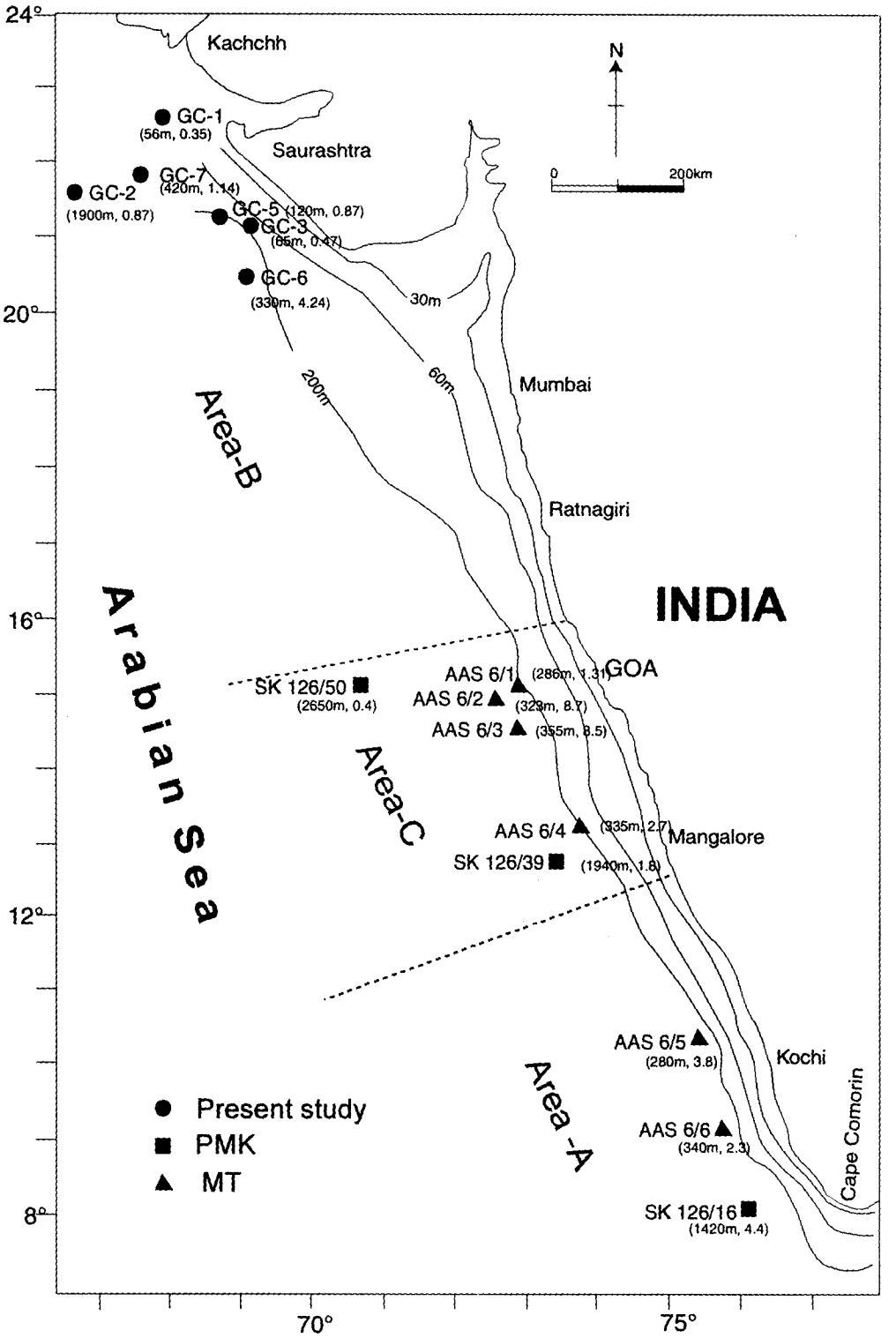

Fig. 5.8. Location of gravity cores along the continental margin of India. (● -cores of present study; ▲ -data from Thamban, 1998;■ -data from Kessarkar, 2003). Water depth and the surface OC values are shown in brackets.

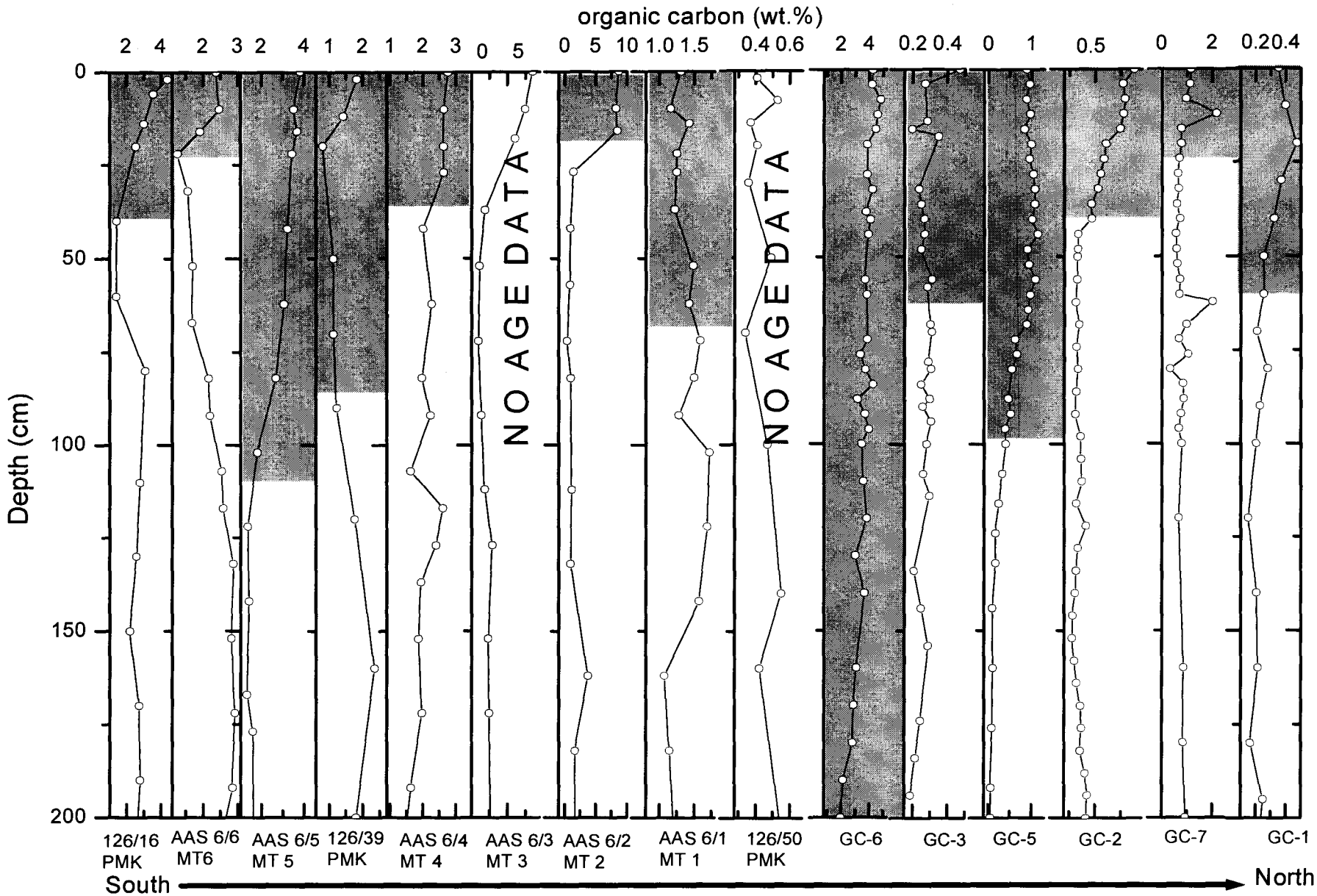

Fig. 5.9. Down-core distribution of organic carbon content in the cores from the continental margin of India. The shaded portion represent Holocene. (Data source:- PMK- Kessarkar, 2003; MT- Thamban, 1998; GC- present study)

respectively. These cores fall in Area C of low productivity (see Fig. 5.8). The high concentration of OC in these cores is attributed to the combined effect of surface water productivity and its better preservation by finer sediments (Thamban et al., 1997). Similarly, a core from the upper slope collected at 330 m in area B of moderate productivity (GC-6) shows higher OC (>4%) concentration compared to the upper slope cores in area A of high productivity (AAS 6/5, AAS 6/6) that contain 2.3-3.8% OC content (Fig. 5.8).

ii. Holocene sediments

The cores from the upper continental slope of the northwestern (GC-5, GC-6, GC-7) and southwestern (AAS 6/1, AAS 6/4 and AAS 6/5) margin of India and cores from the continental terrace (AAS 6/6) and topographic highs (AAS 6/2 and AAS 6/3) exhibit a progressive increase in OC content in the early Holocene and high concentration during mid- and late Holocene (Fig. 5.9). The maximum OC content corresponds to those cores that show higher rate of sedimentation. For example, in area A, AAS 6/5 from the slope at 280 m contains high OC with highest sedimentation rate (~11 cm/ka) (Fig. 5.9). Similarly, in area B, core GC-6 contains 4 - 5% OC and highest rate of sedimentation (17.76 cm/ka) (Fig. 5.9). This implies sedimentation rate plays a major role in OC enrichment.

The lowest OC (<1%) occurs in the cores from water depths of 56 m (GC-1), 65 m (GC-3), 1900 m (GC-2), 2650 m (SK 126/50, Kessarkar, 2003). Though the water depths of these cores are located either above or below the present day OMZ, it cannot be ascertained that oxic condition is the sole factor responsible for low OC content. This is because the cores with high OC concentrations are also found at depths below the OMZ (see core SK 129/39 - Fig. 5.11). It appears that the sediment grain size and reworking also contribute for OC variations.

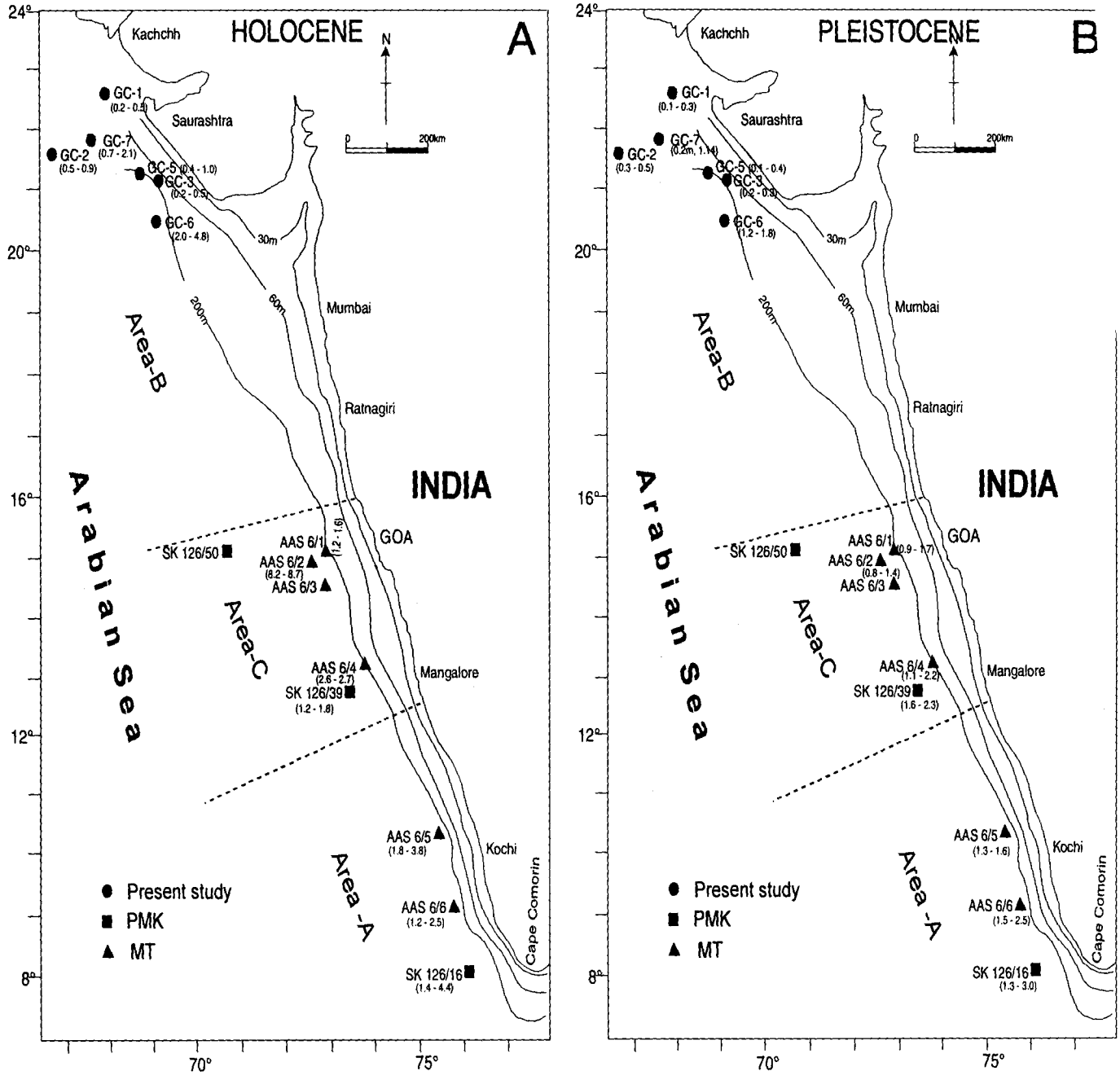

Fig. 5.10. Core locations and organic carbon value ranges (A)Holocene and (B) Pleistocene

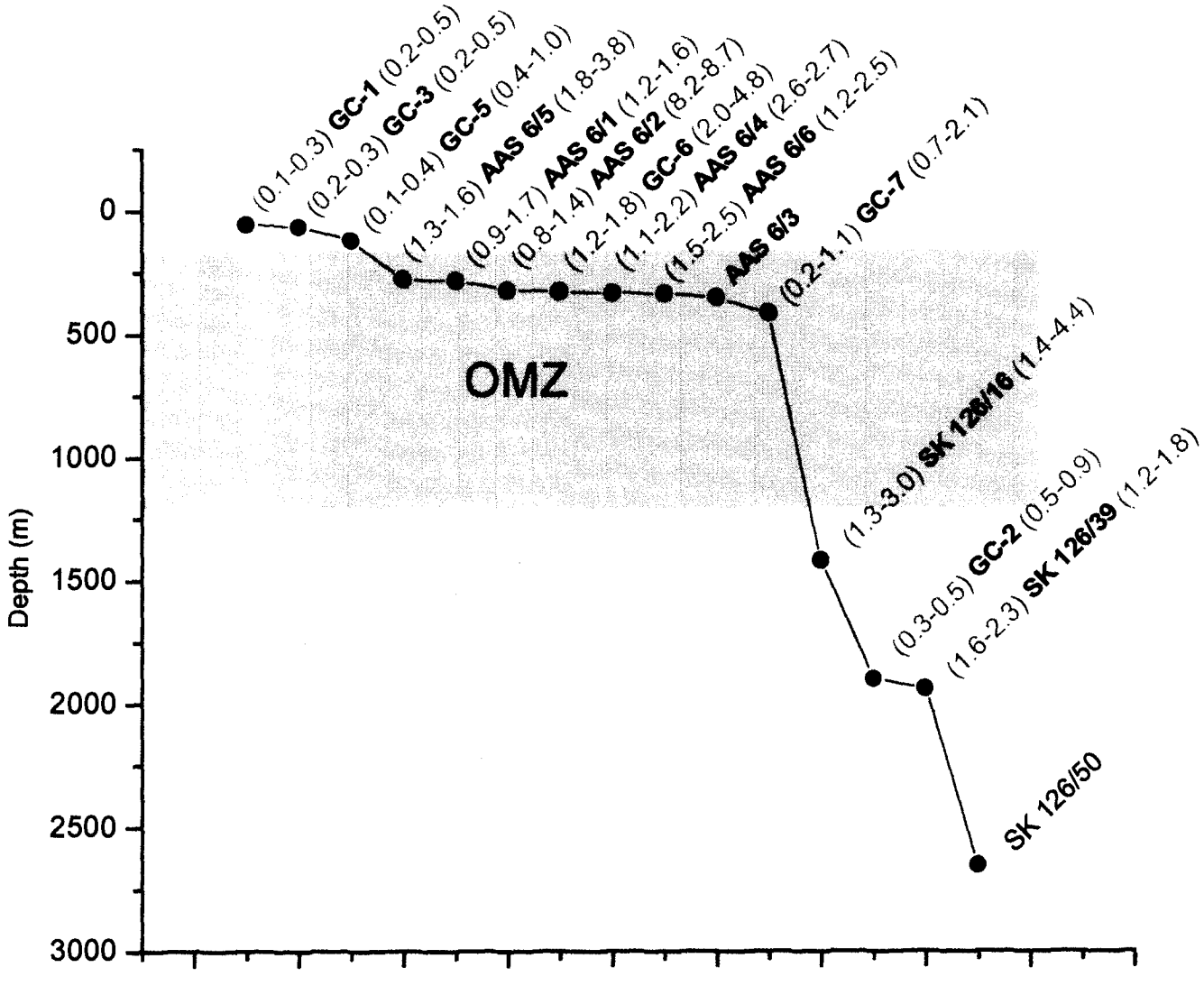

Fig. 5.11. Graph showing the core depths with respect to the present day oxygen minimum zone. Late Pleistocene OC values are shown in red and Holocene values in blue

iii. Late Pleistocene Sediments

Cores from the lower continental slope of southwestern margin of India (SK126/16, SK126/39; Kessarkar, 2003) and from the continental terrace (AAS 6/6; Thamban et al., 1997) show two intervals of OC maxima, one corresponds to LGM and early deglacial times and the other corresponds to mid- and late Holocene (Figs. 5.9 and 5.10) with OC minima corresponding to early Holocene. The high OC in LGM is related to the influence of NE monsoon (Thamban et al., 2001, Kessarkar et al., 2005). This study indicates low OC content in the sediments of the NW margin of India during early deglaciation, which agrees well with the observation from the Pakistan margin. This implies OC along the margin is influenced by localised productivity variations in relation to hydrographic conditions.

It is therefore concluded that the spatial and temporal distribution of OC is controlled by a combination of several factors such as surface water productivity, oxygen concentration at the sea floor, sediment texture, sedimentation rate and physiography of the sea floor.

5.6. Summary and conclusions

- The organic carbon in the sediments of the shelf cores range from 0.18% to 0.47% and largely supplied from continental sources. In the late Pleistocene sediments of these cores OC was mostly reworked and associated with lime muds.

- The sediment texture, sedimentation rate and oxic water column at shallow shelf have influenced the OC content in the sediments.

- The late Pleistocene sediments of the upper slope also contain abundant lime muds.

- Within the continental slope, the cores from the oxygen minimum contain more OC (1.02%-4.83%) than those above (0.06%-1.14%) and below the oxygen minimum (0.28%-0.88%).

- The early deglacial sediments, in general, contain low OC content and agree well with that of the Pakistan margin.

- A distinct change in sedimentary environment occurs at ~12–11 ka BP in the early Holocene sediments.

- OC content increases progressively from 12-11 ka BP to until 7-6 ka BP and remains high in mid and late Holocene sediments. This implies high OC production was after 7-6 ka BP.

- The record of high OC content in the Holocene sediments mismatches with the past monsoon intensity record, which suggests that monsoon intensity was maximum at ~ 9-8 ka BP. This implies that factors other than productivity also play a major role in OC enrichment.

- Intervals of high OC also coincide with high sedimentation rate and finer grain size.

- The abundant aeolian transported material in the glacial sediments of the core off Indus may be responsible for low OC content.

- The glacial sediments of the northwestern margin of India contain low OC than that of the southwestern margin of India. This implies OC variations are controlled by localized hydrographic conditions.

- Comparison of the OC data between NW and SW margin of India suggests that high OC is not always associated with high productivity areas.

- It appears that a combination of several factors influences the special and temporal distribution of organic carbon.

Table 5.1. Down-core distribution of organic carbon (OC), $CaCO_3$, acid insoluble residue (AIR), sand, planktonic foraminifera content and median size of terrigenous mud in GC-1

Depth (cm)	OC (wt. %)	$CaCO_3$ (%)	AIR (%)	Sand (%)	Planktonic foraminifera (%)	Depth (cm)	Median size (μm)
0	0.35	60.63	39.37	48.99	3.68	0	8.19
10	0.40	59.87	40.13	--	--	15	10.29
20	0.47	60.64	39.36	50.62	1.11	25	9.20
30	0.37	62.49	37.51	51.46	1.84	35	13.10
40	0.32	65.25	34.75	56.30	1.32	45	8.91
50	0.25	71.57	28.43	69.19	1.09	55	13.37
60	0.26	76.79	23.21	72.79	4.46	65	12.09
70	0.21	81.14	18.86	80.86	5.56	75	9.79
80	0.28	80.24	19.76	69.28	3.64	85	10.77
90	0.23	80.00	20.00	74.54	4.76	95	11.90
100	0.20	80.80	19.20	72.23	1.82	105	14.57
120	0.15	68.61	31.39	39.76	0.65	125	9.66
140	0.20	57.36	42.64	4.91	0.00	145	10.22
160	0.21	61.05	38.95	3.84	0.00	165	11.41
180	0.16	62.82	37.18	4.95	0.00	185	10.08
195	0.25	64.50	35.50	7.60	0.00	205	9.74
230	0.18	65.12	34.88	4.56	0.00	225	11.30
240	0.18	61.54	38.46	4.07	0.00	245	13.37
260	0.26	59.09	40.91	3.07	0.00	265	11.34
280	0.19	57.65	42.35	1.28	0.00	285	9.53
300	0.31	58.09	41.91	1.51	0.00	310	9.98
320	0.19	57.12	42.88	1.31	0.00	325	8.70
340	0.15	56.98	43.02	1.65	0.00	345	10.04
360	0.30	54.50	45.50	1.54	0.00	365	9.62
380	0.18	51.25	48.75	1.61	0.00	385	10.70

Table 5.2. Down-core distribution of organic carbon (OC), $CaCO_3$ and acid insoluble residue (AIR) in GC-2

Depth (cm)	OC (wt. %)	$CaCO_3$ (%)	AIR (%)
0	0.88	40.08	59.92
4	0.77	40.16	59.84
8	0.79	40.77	59.23
12	0.77	40.96	59.04
16	0.74	42.78	57.22
20	0.60	44.08	55.92
24	0.58	47.45	52.55
28	0.55	47.61	52.39
32	0.53	50.35	49.65
36	0.46	51.18	48.82
40	0.47	47.04	52.96
44	0.33	32.22	67.78
48	0.33	30.09	69.91
50	0.33	28.89	71.11
56	0.32	26.89	73.11
62	0.31	27.84	72.16
68	0.34	28.20	71.80
74	0.32	31.14	68.86
80	0.33	32.64	67.36
86	0.32	39.32	60.68
92	0.31	43.55	56.45
98	0.36	38.59	61.41
104	0.36	33.61	66.39
110	0.37	32.37	67.63
116	0.32	38.18	61.82
122	0.41	31.86	68.14
128	0.34	28.93	71.07
134	0.32	30.29	69.71
140	0.31	40.71	59.29
146	0.28	40.41	59.59
152	0.28	44.17	55.83
158	0.30	41.97	58.03

Depth (cm)	OC (wt. %)	$CaCO_3$ (%)	AIR (%)
164	0.32	35.54	64.46
170	0.36	34.44	65.56
176	0.37	28.42	71.58
182	0.35	28.57	71.43
188	0.40	31.44	68.56
194	0.42	30.36	69.64
200	0.41	31.79	68.21
206	0.44	30.48	69.52
212	0.41	30.36	69.64
218	0.45	30.57	69.43
224	0.46	28.43	71.57
230	0.43	29.59	70.41
236	0.41	28.98	71.02
242	0.40	30.33	69.67
248	0.41	29.00	71.00
254	0.38	29.20	70.80
260	0.37	26.04	73.96
266	0.31	25.62	74.38
270	0.33	27.76	72.24
278	0.31	27.88	72.12
284	0.39	30.45	69.55
290	0.40	27.93	72.07
296	0.36	29.52	70.48
302	0.33	30.35	69.65
308	0.47	29.18	70.82
314	0.44	30.36	69.64
320	0.53	34.28	65.72
326	0.45	29.83	70.17
332	0.40	31.56	68.44
338	0.34	31.28	68.72
344	0.32	32.79	67.21
350	0.37	30.25	69.75
356	0.34	28.01	71.99

Table 5.3. Down-core distribution of organic carbon (OC), $CaCO_3$, acid insoluble residue (AIR), sand, planktonic foraminifera content and median size of terrigenous mud in GC-3

Depth (cm)	OC (wt. %)	$CaCO_3$ (%)	AIR (%)	Sand (%)	planktonic foraminifera (%)	Depth (cm)	Median size (μm)
0	0.47	64.87	35.13	63.27	9.21	2	17.63
4	0.27	76.81	23.19	--	--	10	9.67
8	0.20	77.12	22.88	62.39	3.76	24	10.97
12	0.20	81.90	18.10	--	--	50	10.60
14	0.28	78.38	21.62	67.43	6.50	64	11.00
18	0.35	79.70	20.30	--	--	98	9.38
24	0.19	81.33	18.67	45.36	6.38	120	8.11
32	0.24	82.57	17.43	47.27	2.05	134	8.37
36	0.25	81.49	18.51	--	--	160	9.95
40	0.27	77.72	22.28	--	--	184	11.28
44	0.27	78.96	21.04	25.33	0.00	200	10.21
48	0.25	77.32	22.68	--	--	250	10.26
52	0.20	79.14	20.86	29.77	0.00	290	9.55
58	0.28	79.08	20.92	--	--	310	8.16
64	0.20	78.36	21.64	18.92	--	340	8.89
68	0.30	77.73	22.27	20.02	0.00	350	8.89
70	0.31	76.40	23.60	--	--	390	8.83
78	0.29	77.86	22.14	2.85	--	420	8.28
84	0.25	75.80	24.20	--	0.00	440	8.44
88	0.30	75.22	24.78	1.71	--	460	7.84
90	0.26	75.78	24.22	--	--	480	8.78
94	0.30	75.49	24.51	3.23	0.00	520	8.94
100	0.28	76.78	23.22	--	--	540	7.06
108	0.26	75.42	24.58	6.14	--	580	8.09
114	0.30	75.32	24.68	--	0.00		
124	0.20	76.44	23.56	5.38	--		
134	0.21	74.78	25.22	4.58	0.00		
144	0.25	75.83	24.17	--	--		
154	0.29	73.38	26.62	2.21	0.00		
164	0.20	74.05	25.95	3.18	--		
174	0.24	74.49	25.51	1.58	--		
184	0.21	74.96	25.04	3.67	0.00		
194	0.18	75.08	24.92	1.97	0.00		

Table 5.4. Down-core distribution of organic carbon (OC), total nitrogen (N), C/N ratio, $CaCO_3$, acid insoluble residue (AIR), sand, planktonic foraminifera content and median size of the terrigenous mud in GC-5

Depth (cm)	OC (wt. %)	N (wt.%)	C/N ratio	$CaCO_3$ (%)	AIR (%)	Sand (%)	Planktonic foraminifera (%)	Depth (cm)	Median size (μm)
0	0.88	0.12	7.64	54.54	45.46	40.78	9.25	6	17.47
4	0.96	0.16	5.93	49.32	50.68	31.52	--	12	27.85
8	0.88	0.13	6.56	49.20	50.80	39.08	15.65	22	19.30
12	0.97	0.14	7.10	50.92	49.08	32.80	--	38	16.74
16	0.84	0.13	6.65	51.72	48.28	36.03	8.99	44	20.43
20	0.99	0.14	7.29	54.10	45.90	45.42	--	50	17.19
24	0.95	0.12	7.78	49.08	50.92	28.18	15.94	60	18.94
28	1.04	0.13	7.99	47.74	52.26	24.22	--	66	19.36
32	1.07	0.13	8.02	47.10	52.90	28.66	28.07	80	16.49
36	1.07	0.13	8.24	52.30	47.70	33.88	--	92	15.76
40	1.01	0.15	6.88	49.80	50.20	39.26	26.35	104	12.29
44	1.14	0.14	8.31	46.93	53.07	30.25	--	120	9.95
48	0.91	0.11	8.44	55.52	44.48	35.96	27.34	132	7.59
52	0.94	0.11	8.47	59.69	40.31	47.71	--	144	8.47
56	1.08	0.10	10.81	57.13	42.87	34.60	20.73	172	9.87
60	0.97	0.12	8.12	57.63	42.37	45.00	--	180	12.02
64	0.92	0.13	7.30	61.74	38.26	41.94	8.00	210	13.63
68	0.88	0.10	9.29	62.57	37.43	47.50	--	250	15.87
72	0.62	0.08	7.90	71.22	28.78	53.80	16.67	270	18.09
76	0.66	0.08	8.46	69.85	30.15	57.23	--	290	16.51
80	0.54	0.07	8.30	74.35	25.65	54.77	10.38	300	18.08
88	0.47	0.05	8.64	73.69	26.31	65.19	10.66	330	15.26
92	0.51	0.06	8.59	77.24	22.76	59.84	--	350	17.99
96	0.39	0.04	10.70	82.80	17.20	59.36	17.96	370	16.47
100	0.40	0.05	8.26	85.74	14.26	61.97	--	390	17.80
108	0.33	0.03	9.68	89.36	10.64	71.13	7.59	410	17.71
116	0.24	0.02	10.09	92.95	7.05	81.69	--	430	17.74
124	0.16	0.02	8.17	96.55	3.45	57.84	6.17	450	17.89
132	0.18	0.02	9.19	96.01	3.99	44.11	0.00	470	17.85
144	0.10	0.01	9.21	97.66	2.34	34.84	--	490	17.10
160	0.11	0.01	7.79	97.78	2.22	45.44	0.00	520	17.22
176	0.09	0.01	9.69	97.79	2.21	43.42	0.00	545	17.12
192	0.06	0.01	7.04	98.12	1.88	33.59	0.00		
200	0.06	0.01	8.76	97.85	2.15	41.09	0.00		

Table 5.5. Down-core distribution of organic carbon (OC), $CaCO_3$, acid insoluble residue (AIR), sand, planktonic foraminifera content and median size of terrigenous mud in GC-6

Depth (cm)	OC (wt. %)	$CaCO_3$ (%)	AIR (%)	Sand (%)	Planktonic foraminifera (%)	Depth (cm)	Median size (μm)
0	4.24	52.70	47.30	4.92	44.75	0	9.12
4	4.22	52.18	47.82	9.19	--	10	11.24
8	4.83	50.35	49.65	4.73	40.06	20	10.19
12	4.57	53.23	46.77		--	30	12.18
16	4.47	57.05	42.95	16.80	55.44	40	12.77
20	3.86	56.66	43.34	7.15	--	50	12.82
24	4.07	51.56	48.44		24.64	70	10.87
28	3.85	55.29	44.71	6.36	--	80	11.03
32	4.21	50.34	49.66	4.53	42.26	90	10.16
38	3.77	51.30	48.70	3.94	--	100	10.17
40	4.09	46.52	53.48	5.47	49.61	120	11.05
44	1.92	38.90	61.10	2.75	--	160	10.92
48	3.59	54.65	45.35	8.97	60.84	180	10.88
56	3.67	49.26	50.74	5.31	--	200	10.53
60	3.84	46.97	53.03	2.72	69.57	220	11.84
64	2.27	44.94	55.06	3.47	62.04	240	10.78
72	3.84	55.92	44.08	10.23	--	260	10.88
76	3.36	57.95	42.05	12.74	49.54	280	8.58
80	3.70	54.35	45.65	10.05	--	300	7.96
84	4.26	50.85	49.15	5.70	--	320	7.14
88	3.17	55.26	44.74	12.67	52.26	340	7.18
92	3.68	54.46	45.54	14.56	--	360	7.29
96	3.98	52.85	47.15	9.41	--	380	7.10
100	3.45	58.13	41.87	8.31	57.35	400	6.78
110	3.60	58.42	41.58	12.33	--	420	6.22
120	3.83	53.29	46.71	10.09	55.51	440	6.72
130	3.02	55.80	44.20	16.23	--	460	6.27
140	3.66	47.38	52.62	7.42	56.40	480	6.12
150	1.54	37.96	62.04	3.76	--	500	5.99
160	3.08	62.88	37.12	23.12	67.90	--	--
170	2.87	54.74	45.26	14.22	--	--	--
180	2.82	60.81	39.19	15.86	54.55	--	--
200	1.98	71.09	28.91	32.36	56.25	--	--
220	1.84	80.23	19.77	16.84	40.08	--	--
240	1.80	83.44	16.56	10.50	30.23	--	--
260	1.72	84.49	15.51	13.44	47.59	--	--
280	1.80	90.50	9.50	6.22	12.33	--	--
300	1.20	91.52	8.48	5.94	10.08		

Table 5.6. Down-core distribution of organic carbon (OC), total nitrogen (N), C/N ratio, $CaCO_3$, acid insoluble residue (AIR), sand, planktonic foraminifera content and median size of terrigenous mud in GC-7

Depth (cm)	OC (wt. %)	N (wt.%)	C/N ratio	$CaCO_3$ (%)	AIR (%)	Sand (%)	Planktonic foramini-fera (%)	Depth (cm)	Median size (μm)
0	1.14	0.12	9.92	76.76	23.24	3.27	63.41	0	7.697
4	1.11	0.11	10.45	77.26	22.74	2.48	--	10	7.523
8	0.97	0.10	10.00	79.14	20.86	1.96	60.1	20	7.021
12	2.15	0.20	10.70	82.94	17.06	1.32	--	30	7.968
16	0.77	0.08	9.92	83.54	16.46	1.94	54.87	40	8.178
20	0.77	0.07	10.61	83.63	16.37	1.79	--	50	8.259
24	0.69	0.07	10.44	83.75	16.25	1.27	58.29	60	7.843
28	0.64	0.07	9.68	83.63	16.37	1.67	--	62	11.672
32	0.67	0.07	10.23	83.11	16.89	1.5	48.21	66	9.646
36	0.60	0.06	10.16	83.9	16.1	1.67	--	70	10.506
40	0.72	0.07	9.71	83.14	16.86	1.37	50.82	80	13.469
44	0.55	0.05	10.27	81.89	18.11	2.62	--	90	11.6
48	0.59	0.06	9.91	82.85	17.15	2.38	48	100	11.61
52	0.62	0.06	9.84	83.55	16.45	1.87	--	120	12.593
56	0.71	0.07	9.91	83.61	16.39	1.57	53.9	140	12.173
60	0.69	0.07	9.92	82.47	17.53	2.78	--	160	11.064
62	2.01	0.23	8.91	50.58	49.42		--	180	11.882
64	1.79	0.19	9.60	73.36	26.64	14.13	65.37	220	11.665
68	0.97	0.09	11.35	91.19	8.81	2.82	--	240	13.46
72	0.68	0.07	10.10	93.67	6.33	4.25	21.74	260	11.78
76	1.05	0.07	14.16	91.95	8.05	2.82	--	280	11.472
80	0.33	0.03	10.36	95.81	4.19	6.5	27.27	300	12.269
84	0.84	0.08	10.74	93.17	6.83	2.04	--	320	12.469
88	0.87	0.07	12.78	93.17	6.83	5.7	35.61	340	11.744
92	0.75	0.07	10.14	93.7	6.3	2.94	--	360	11.079
96	0.68	0.06	12.04	94.37	5.63	2.54	35.42	380	11.399
100	0.79	0.07	11.31	93.97	6.03	1.26	56.37	400	11.345
120	0.67	0.07	9.80	93.94	6.06	1.63	29.52	420	12.259
160	0.85	0.08	10.39	92.71	7.29	3.25	30.77	440	10.878
180	0.83	0.08	10.22	92.38	7.62	1.86	21.64	460	10.137
200	0.93	0.09	10.71	92.63	7.37	1.41	--	480	10.457
220	0.86	0.08	10.26	93.15	6.85	1.82	--	500	10.504
240	0.65	0.06	10.18	94.19	5.81	1.53	14.39	520	9.969
260	0.67	0.06	11.13	94.4	5.6	2.62	--	540	11.397
280	0.62	0.06	10.43	94.85	5.15	2.94	11.00	560	11.414
300	0.30	0.03	9.80	95.88	4.12	2.87	--	580	11.07
320	0.19	0.02	8.60	95.95	4.05	19.97	38.64	--	--

Continued...

Continuation of Table 5.6

Depth (cm)	OC (wt. %)	N (wt. %)	C/N ratio	$CaCO_3$ (%)	AIR (%)	Sand (%)	Planktonic foraminifera (%)	Depth (cm)	Median size (μm)
340	0.24	0.03	8.55	94.61	5.39	31.57	28.72	--	--
360	0.26	0.03	8.92	92.71	7.29	28.3	44.92	--	--
380	0.59	0.07	8.70	81.65	18.35	38.92	--	--	--
400	0.96	0.11	9.10	67.42	32.58	12.69	30.69	--	--
420	0.83	0.11	7.63	61.42	38.58	17.23	42.07	--	--
440	1.59	0.15	10.44	78.35	21.65	5.86	--	--	--
460	0.97	0.12	8.33	62.09	37.91	12.02	--	--	--
480	0.79	0.10	7.98	75.77	24.23	46.03	43.88	--	--

Chapter 6

Chapter 6

PROVENANCE OF THE SEDIMENTS OF THE NORTHWESTERN MARGIN OF INDIA DURING THE LATE QUATERNARY

6.1. Introduction

Fine-grained lithogenic material is an important component of the sea floor sediments, especially on the continental margins. These sediments are largely detrital and therefore their primary source is from the physical and chemical weathering and erosion of rocks on the adjacent continents and transported to the sea largely by fluvial or aeolian processes. Weathering of sea floor rocks also contributes minor detrital sediments to the deep sea. Fine-grained sediments usually comprise both clay minerals and amorphous materials. Illite, chlorite, kaolinite and smectite are the major clay mineral groups that commonly occur in the marine sediments. Illite belongs to the mica group and is abundant in major rocks and quite resistant to chemical and physical weathering. High illite points to increased physical weathering (Singer, 1984; Chamley, 1989). Chlorite is a primary mineral formed by metamorphic processes and is abundant in low-grade metamorphic rocks, sedimentary argillites and shales. Chlorite is also a high latitude clay mineral and found in greatest abundance in the polar regions of the world, where chemical weathering is less intense relative to physical/mechanical weathering (Griffin et al., 1968). Kaolinite is a low latitude clay mineral and formed by intense chemical weathering of rocks and reflects the intensity of soil forming processes in the source region. Smectite is also a product of chemical weathering and abundant in volcanic regimes. Montmorillonite is a mineral of smectite group. Several workers used montmorillonite, instead of smectite. palygorskite and sepiolite are magnesium-rich silicate minerals found in clay fraction and are usually transported to the sea by aeolian processes.

The relative amount of clay minerals in the ocean is controlled by the rock type, climate, drainage pattern and topography of the source region and the transport paths from continents to marine environments. The transporting medium can be fluvial or aeolian. Their distribution in the marine environment is further controlled by depositional processes, especially the current circulation pattern and the settling of clay minerals in response to the salinity and energy conditions. The particle size, buoyancy and electrochemical characters of the sediments intervene in the depositional processes. White House and Mc Carter (1958) observed a preferential settling of kaolinite and illite compared to smectite in low salinity water, where clay floccules formation often occurs preferentially by surficial adsorption of cations (Powers, 1959). As a result of this, estuarine conditions favour the deposition of more illite and kaolinite than that of smectite (Chamley, 1989). Montmorillonite exhibits preferential settling in low-energy environment (Stanley and Liyanage, 1986). Gibbs (1972) critically examined the theories related to chemical alteration of clay minerals under marine environment and suggested that there occurs no differentiation by composition of clay minerals with time and further suggested that size sorting of clay minerals is the dominant mechanism for lateral variations in clay mineral distribution. Clay minerals have also been used as palaeoclimate markers. Hallan (1966) was the first to report climatic variations in Quaternary sediments through clay mineralogy and found abundance of smectite and kaolinite during interglacial stages and increased amounts of illite and chlorite during glacial stages (cf. Chamley, 1989).

6.2. Previous studies

Investigations on clay mineral distribution in the World Ocean demonstrate increasing concentration of chlorite towards high latitudes, more illite in the northern ocean than in their southern counter parts, high content of kaolinite in the equatorial oceans and higher levels of montmorillonite in the southern oceans than in the northern regions (Gorbunova, 1966; Griffin et al., 1968; Rateev et al.,

1969; Goldberg and Griffin, 1970). A few workers (Gorbunova, 1966; Rateev et al., 1969) suggested that the clay minerals follow a latitudinal zonation, while others (Biscaye, 1965; Griffin et al., 1968; Goldberg and Griffin, 1970; Kolla et al., 1976; 1981a; 1981b) indicated detrital nature of clay minerals. Within the Indian Ocean, Gorbunova (1966) found high values of chlorite in the Arabian Sea sediments and the zone of maximum chlorite content is same as that of maximum illite content. Maximum kaolinite is found near Madagascar and in a belt extending southwest from Java (Gorbunova, 1966). High montmorillonite is found near the volcanic provinces. In the Arabian Sea high illite is found in the north, reflecting a strong input from the Himalayas and arid regions to the north (Goldberg and Griffin, 1970). High chlorite concentration is also found in the northern Arabian Sea. High montmorillonite concentrations are found parallel to the Indian peninsula with its source in the augite basalts of the Deccan Traps and its concentrations decrease seaward, Kaolinite is found to be low and more or less uniform (Goldberg and Griffin, 1970). Contribution of aeolian input to the marine sediments is important component in the Arabian Sea (Darwin, 1846; Radczewski, 1939; Rex and Goldberg, 1958; Goldberg and Griffin, 1970; Windom, 1975; Kolla et al., 1981a). Aeolian transport is mainly from the Arabian Peninsula and Iran-Makran-Thar region. Aerosol samples from the northern Arabian Sea contain illite, chlorite, kaolinite and montmorillonite in decreasing order of abundance (Chester et al., 1985). Sirocko et al. (1991) and Sirocko and Lange (1991) found illite, smectite, kaolinite, chlorite and palygorskite, in decreasing order of abundance in the dust plumes from Arabia and high chlorite in the dust plumes from Iran and Pakistan. Dolomite is also an important dust component in the northern Arabian Basin. Palygorskite in the northern Arabian Sea is from the Mesozoic rocks of the Arabian Peninsula and indicative of Arabian/Eastern African provenance (Sirocko and Lange, 1991). Aston et al. (1972) reported a source area of dust comprising abundant illite from the Rajastan desert in the Arabian Sea.

Several workers reported clay minerals in the sediments of the western continental margin of India (Stewart et al., 1965; Gorbunova, 1966; Griffin et al., 1968; Rateev et al., 1969; Goldberg and Griffin, 1970; Mattait et al., 1973; Popov and Gershanovich, 1978; Kolla et al., 1981a; Nair et al., 1982a and b; Bhattacharya, 1984; Ramaswamy and Nair, 1989; Rao, 1991; Rao and Rao, 1995). Nair et al. (1982a and b) identified four distinct clay mineral provinces along the inner continental shelf. These are 1) the montmorillonite-kaolinite-illite-chlorite zone off the Gulf of Katchchh, 2) the montmorillonite-rich zone between the Gulf of Cambay and Ratnagiri, 3) the transition zone consisting of montmorillonite and kaolinite between Ratnagiri and Bhatkal and 4) the montmorillonite-poor, gibbsite zone from Bhatkal to Quilon. Illite and chlorite-rich assemblage derived from the Indus is predominant to the north of the Gulf of Kachchh. Montmorillonite-rich assemblage with minor kaolinite, illite and chlorite derived from the Deccan Trap basalts occurs along the inner shelf of Saurashtra and on the continental slope from Saurashtra to Goa. Kaolinite content is more on the shelf and slope between Goa and Cochin and is derived from the gneissic rocks of the peninsular India (Rao and Rao, 1995). Macro-tides operating at the Gulf of Kachchh and Gulf of Khambat influenced alongshore transport of clays. Nair et al., (1982b) and Chauhan (1994) postulated that the tides in the Gulf of Kachchh act as dynamic barriers to the transport of Indus-borne sediments to the south of the Gulf. Studies by Rao (1991) and Rao and Rao (1995) further revealed that the effect of tidal barrier is moderate on the outer shelf and insignificant on the continental slope. A recent study on the Gulf of Khambat, based on IRS-P4 satellite imageries (OCM and LISS-III) of different stages of tide cycle, season and years showed that the sediments are getting dispersed under the influence of strong tidal currents and settled within the Gulf (SAC -ISRO, 2003).

The objectives of the present chapter are to report the clay mineral distribution in the sediments of the gravity cores off northwestern India and apply

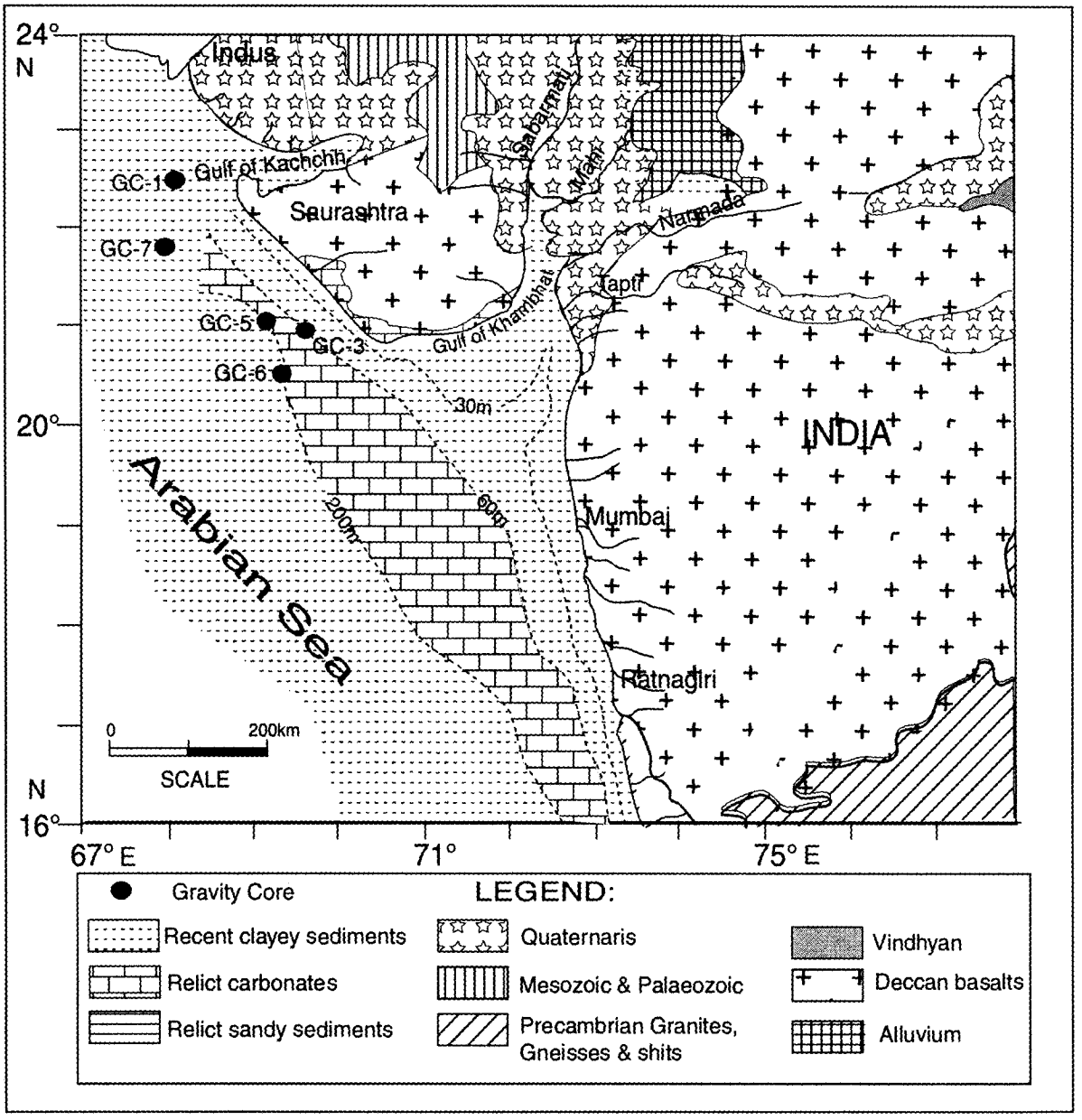

Fig. 6.1a. Location of the cores used for clay mineral investigations. General Geology of the NW margin of India is also shown

these variations to better understand the provenance and palaeoclimatic conditions during the late Quaternary. Clay mineralogy including illite crystallinity and illite chemistry, clay content and median grain size of the terrigenous mud content of the sediments were investigated in five gravity cores and results are presented below.

6.3. Physiographic, geologic and climatic set up

The sediment cores utilised for clay mineralogy are located off the Gulf of Kachchh and Saurashtra. The Gulf of Kachchh is located 100 km away from the mouth of the Indus River, which brings enormous sediments from the Himalayas and alluvial soils of the Pakistan into the Arabian Sea. The third largest peninsular river Narmada and Tapti discharges sediments through the Gulf of Khambat. These rivers drain the mountain regions of central India, including the Vindhyan and Satpura ranges and the Mesozoic and Tertiary formations of northwestern India (Fig. 6.1a). Minor rivers like Sabarmati and Mahi also bring sediments in this part of the margin. The suspended sediment distribution pattern off Indus to Gulf of Khambat is shown in Figs 6.1b. Deserts of Rajastan contribute aeolian dust in the study area (Aston et al., 1972).

The Saurashtra is located astride the Tropic of Cancer and forms an important part of the dry lands of western India and climatic conditions are mainly influenced by the SW monsoon (Chamyal et al., 2003). The hinterland is marked by flat-topped ridges of Deccan Traps and sedimentary sequences ranging in age from Jurassic to Pleistocene. Cliffs of miliolitic limestone (Chamyal et al., 2003) and a thin veneer of Tertiary and Quaternary sediments are found in the coastal Saurashtra (Bhattacharya and Subrahmanyam, 1986- See Fig. 6.1a). The Deccan trap covers an area of 500,000 sq. km. The Deccan plateau falls in the rain-shadow of the Western Ghats and hence receives <60 cm rain (Krishnan, 1982). The drainage system in the Saurashtra follows a radial pattern,

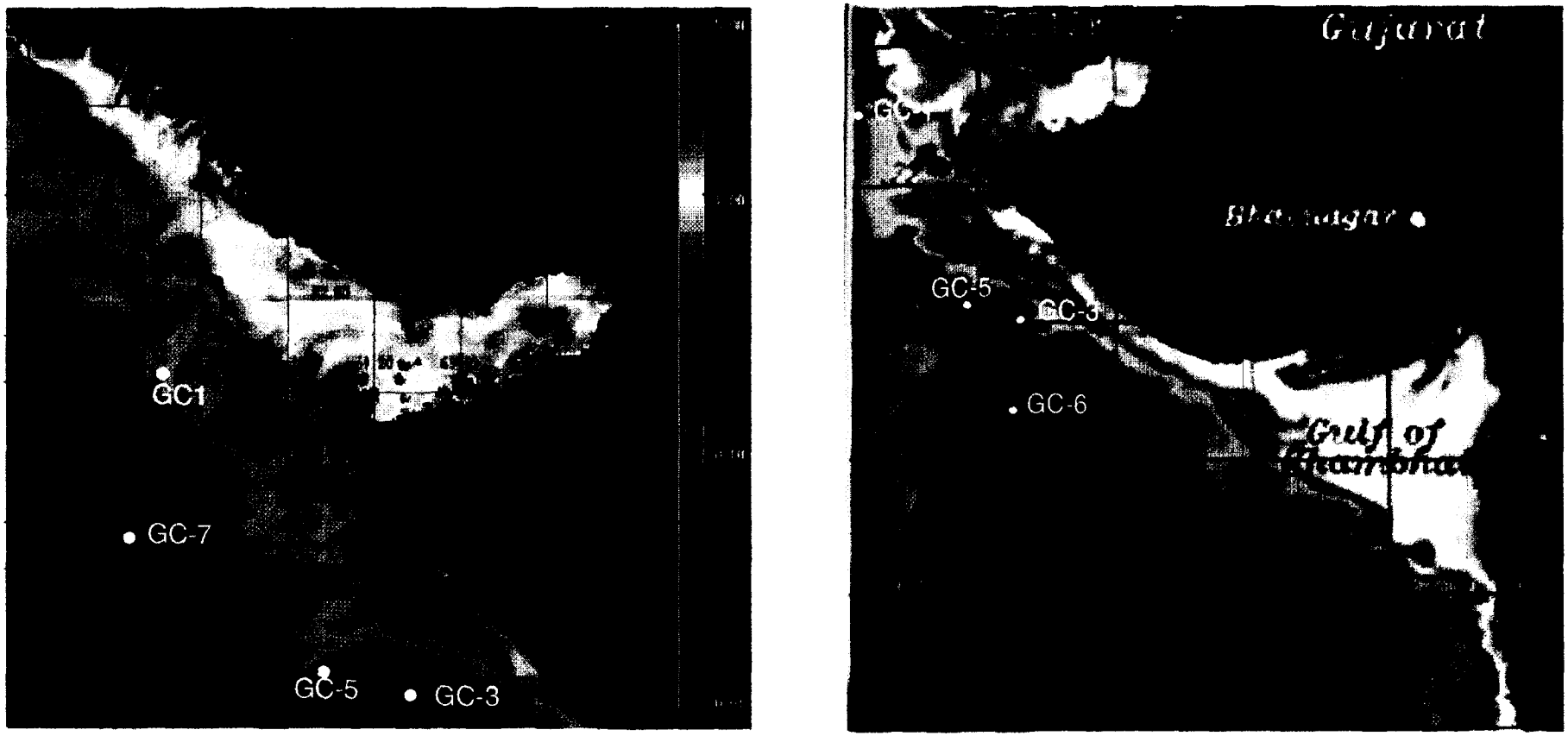

Fig. 6.1b. Suspended sediment concentration and distribution:- (A) from the Indus mouth derived from Sea Wifs data; Date of acquisition- 30/12/2000; sediment concentration in mg/l (after Kunte et al., 2005) and (B) from the Narmada and Tapti date of acquisition-01/02/2000 (after SAC, 2003).

with the rivers flowing in all directions along tectonic slopes from central highland (Chamyal et al., 2003). Tectonic framework of the hinterland, physiographic features and geology of the continental shelf and slope of the study area are given in detail in the Introduction chapter of the thesis (pl. see Chapter 1).

6.4. Results

The sediments from five sediment gravity cores, two from the continental shelf (GC-1 and GC-3) and three from the shelf break and slope (GC-5, GC-6 and GC-7) recovered at depths between 56 m and 420 m, were investigated. The results on clay content (<2 μm fraction), median grain size of the terrigenous mud (<63 μm) and clay mineralogy of the <2 μm fraction of the sediments are presented in this chapter. As in earlier chapters, the results were described with reference to unit 2 and 1 corresponding to lower and upper section of each core, respectively. Unit 2 sediments are largely lime muds. Units are shown in figures. The representative X-ray Diffractograms for the shelf cores (GC-1 and GC-3) and slope cores (GC-5, GC-6 and GC-7) are shown in Fig. 6.2a and 6.2b, respectively.

6.4.1. Sediment Cores from the continental shelf (GC-1 and GC-3)

i. Clay content and median grain size

In GC-1, the clay content varies from 6 to 8% in unit 2 sediments and shows an increasing trend in unit 1 (the upper 140 cm), reaching a maximum of 11% at the core top. Median grain size of the sediments ranges from 8 to 15 μm (Fig. 6.3). It is about 10 μm in unit 2 sediments and higher values (10-15 μm) occur in unit 1 sediments (Fig. 6.3, Table 6.1). Decrease in clay content coincides with increase in grain size in unit 1 sediments (Fig. 6.3). In GC-3, the clay content varies from 5 to 10% (Fig. 6.4, Table 6.2). The maximum clay content (10.4%) is recorded at about 134 cm in unit 2 sediments. The amplitude

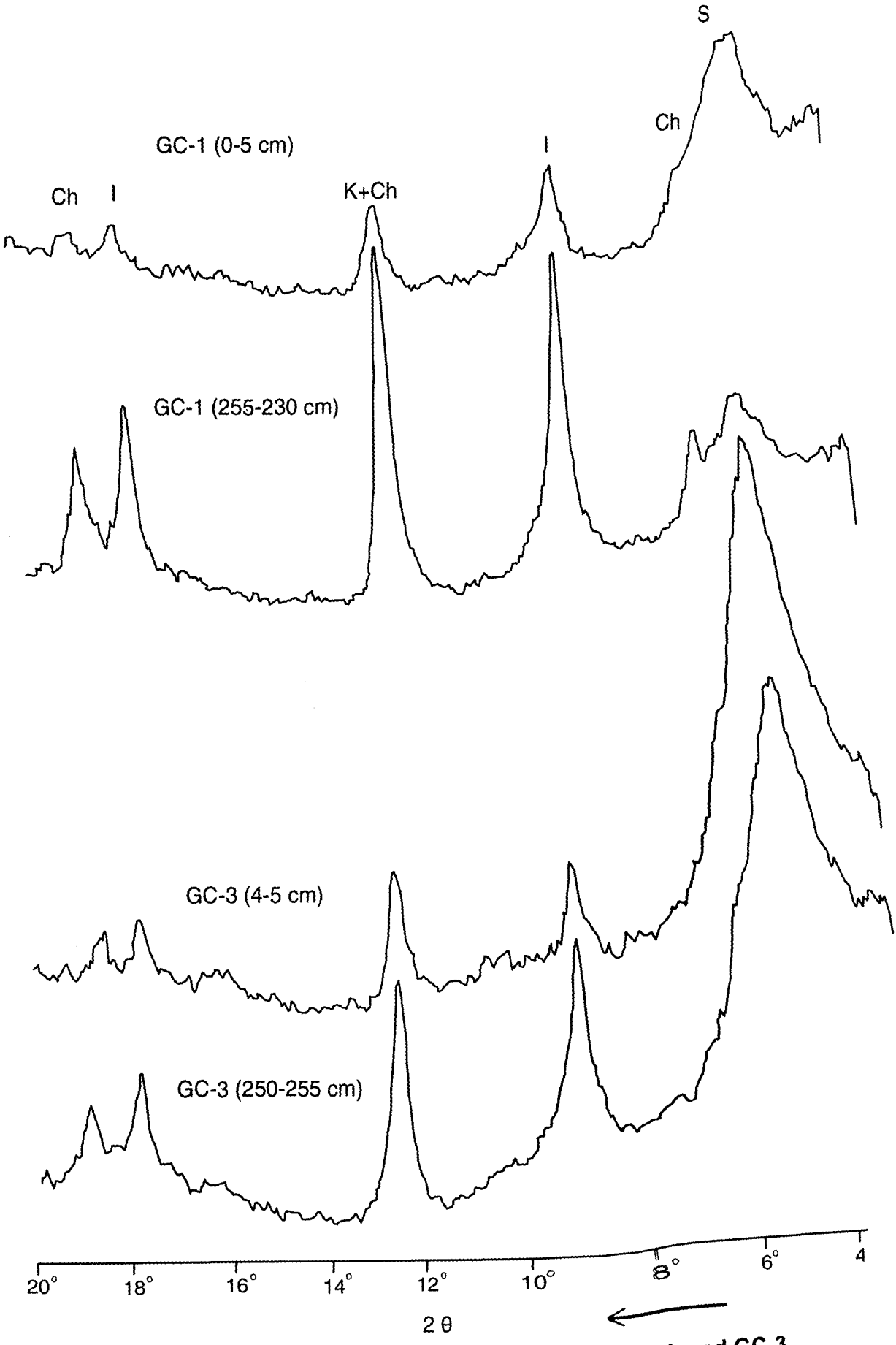

Fig. 6.2a. Representative X-ray diffractograms of **GC-1 and GC-3**

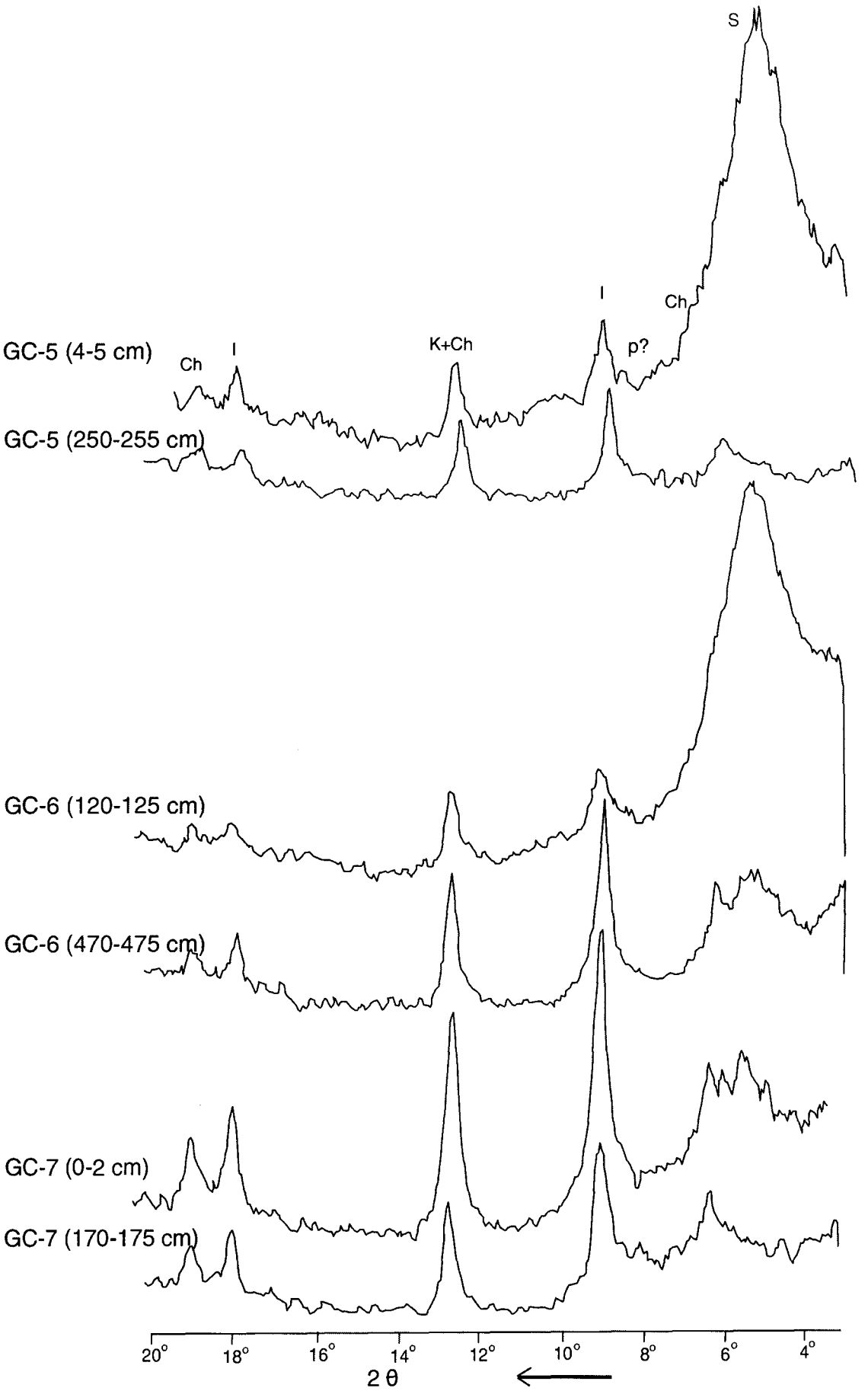

Fig. 6.2b. Representative X-ray diffractograms of **GC-5, GC-6 and GC-7**

of median size variation is 3 μm (8-11 μm) in the sediment interval of 200 to 10 cm. The core top sediments showed median grain size up to 18 μm.

ii. Clay mineralogy

The down-core distribution of major clay minerals and their ratios are shown in Fig. 6.3 and 6.4. Illite (I) is the most dominant mineral followed by smectite (S), chlorite (Ch) and kaolinite (K). GC-1 contains higher illite and lower smectite than in GC-3. Illite and smectite distribution is more or less uniform in unit 2 sediments of both the cores. In unit 1 sediments of GC-1, smectite content suddenly increases with a corresponding decrease of illite at about 14 ka BP. Thereafter smectite content gradually decreases and illite increases towards the core top. While in GC-3 such sharp changes are uncommon in unit 1 sediments, except that smectite content gradually increases and illite decreases from base to the core top of unit 1. Kaolinite variations are within the error limits but chlorite shows a gradual decrease from the base of unit 1 to the core top. The trend in S/I ratio in both the cores follow that of smectite variations. In GC-1 the K/Ch ratio of unit 1 sediments is than that of unit 2. In GC-3 S/I and K/Ch ratios follow that of smectite variations.

Crystallinity of the illite is measured as the half height width (HHW) of the 10Å peak, where the relatively higher width of the peak indicates poor crystallinity and lower width indicates better crystalline illite. In unit 2 sediments of GC-1 the HHW of illite ranges between 4 and 5 (Fig. 6.3, Table 6.1). In unit 1 sediments the width of illite shows an overall increasing trend from 4 to 8. Similarly, the HHW of illite is <6 in unit 2 sediments of GC-3 (Fig. 6.4, Table 6.2). The HHW reaches upto 10 in the lower part and <6 in the upper part of unit 1 (Fig. 6.4). Illite chemistry is expressed by the ratio of illite 5Å /10Å peak area, where the ratio below 0.5 represents Fe, Mg-rich illite and characteristic of physically eroded, unweathered rocks, and ratio above 0.5 represents Al-rich illite that formed by strong hydrolysis (Gingele, 1996). The ratio of illite 5Å /10Å reflection is nearly

constant (at 0.5) for several samples of unit 2 sediments, except at the bottom where it ranges from 0.6 to 0.7 (Fig. 6.3, Table 6.1). This ratio is largely <0.5 in unit 1 sediments (see Fig. 6.3). Similarly in GC-3, the ratio of illite 5Å /10Å reflection is ~0.5, except at the transition sediments of unit 2 and unit 1 (between 12 and 10.5 ka BP) where it is <0.5 (see Fig. 6.4, Table 6.2).

6.4.2. Sediment Cores from the continental slope (GC-5, GC-6 and GC-7)

Gravity cores GC-5, GC-6 and GC-7 were recovered at water depths of 121 m, 330 m and 420 m, respectively (Fig. 6.1a). The down-core variations in sedimentological parameters and clay mineralogy are shown in Figs. 6.5, 6.6 and 6.7.

i. Clay content and median grain size

The down-core distribution of clay content and average median grain size of the mud fraction varies from core to core. The clay content is ~5% in both unit 2 and unit 1 sediments of GC-5, except at the transition zone (180 - 86 cm) of unit2/1, where it increases to a maximum of 11% (Fig. 6.5, Table 6.3). The median grain size is ~18 μm in the lower part of unit 2 (up to 300 cm) and then gradually decreases to <10 μm at the boundary of unit 2/1. It gradually increases from <10 to 20 μm from base to the core top of unit 1 sediments (see Fig. 6.5). In GC-6 the relatively high clay coincides with low median grain size in the lower portion of unit 2 sediments (up to 300 cm). Thereafter the clay content decreases and median grain size increases and both remains steady at the transition of unit2/1 and in unit 1 sediments (Fig. 6.6, Table 6.4). In GC-7 the low clay content (<5%) coincides with relatively high median grain size (10-12 μm) in unit 2 sediments. The clay content gradually increases and remains high (10-12 %) in unit 1 sediment and grain size gradually decreases and remains low in unit 1 sediments (Fig. 6.7, Table 6.5).

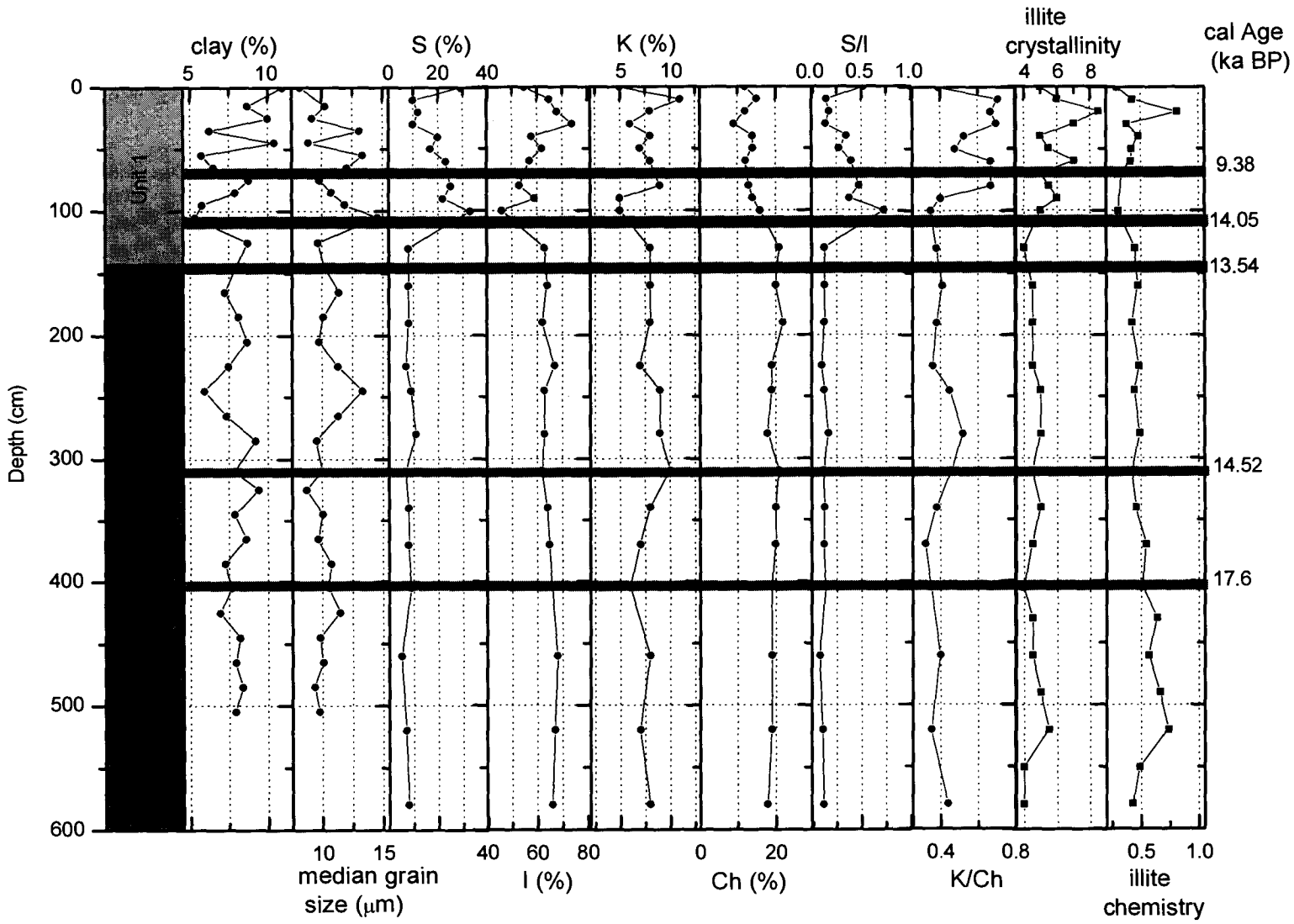

Fig 6.3. Down-core variations in clay content, median grain size, clay minerals, illite crystallinity (HHW) and illite chemistry (5Å/10 Å) in **GC-1.** (S- smectite, I- illite, Ch- chlorite, K- kaolinite)

ii. Clay mineralogy

The representative X-ray diffractograms of unit 2 and unit 1 sediments of each core are shown in Fig. 6.2b. In unit 2 sediments of GC-5, illite (>50%) is the most dominant mineral, followed by smectite, chlorite, and kaolinite. There is a gradual decrease of illite and chlorite in the upper unit 2 and transition zone of unit2/1 sediments (Fig. 6.5, Table 6.3). Smectite content gradually increases from 10% to 60% from base to the core top of unit 1 sediments. Kaolinite co-varies with smectite, whereas illite and chlorite exhibit a gradual decrease from base to core top of unit 1 (Fig. 6.5). S/I and K/C ratios co-vary with smectite and kaolinite contents.

Illite (70%) and chlorite (10-20%) contents in GC-6 (Fig. 6.6) are more than that of GC-5 (Fig. 6.5). They are uniformly high in unit 2 sediments and decrease gradually from transition of unit2/1 to the middle of unit 1 and then again increase towards core top (Table 6.4). On the other hand, smectite and kaolinite co-vary and their distribution is exactly opposite to that of illite and chlorite. Smectite, kaolinite contents and S/I ratios indicate that they increase in unit 1 sediments than that of unit 2 and their abundance is high in the middle of unit 1 coinciding about 4-5 ka BP (see Fig. 6.6). In GC-7, illite and chlorite contents are same as that of GC-6. Despite sharp changes in clay content and median grain size at the transition of unit 2 and unit 1 such sharp change is not visible in clay minerals. However, marginal decrease in illite and increase in smectite occur from unit 2 to unit 1. Distribution of kaolinite and chlorite in this core is not consistent. S/I ratio follows that of smectite (Fig. 6.7, Table 6.5).

The HHW of illite is uniformly low (4-5) in unit 2 sediments of GC-5, except at interval 270-196 cm (reach up to 8). The low values continue in the lower part of unit 1 and then range between 6 and 8 in the upper unit 1 sediments (Fig. 6.5, Table 6.3). The ratio of illite 5Å /10Å reflection is at ~0.5 at the bottom of the core and gradually decreases towards upper portions of unit 2 and unit 1. The ratio

>0.5 was observed only in the mid-portion of unit 1 sediments that corresponds to 6-7 ka BP (Fig. 6.5). In GC-6, the HHW of illite is ~4 in the entire unit 2 sediments and a broad hump of high values (reaching up to 9) were observed in the lower unit 1 sediments and then decreases to 5 towards the core top. The ratio of illite 5Å /10Å reflection is largely <0.5 in both unit 2 and unit 1 sediments and there is no consistency in this ratio (Fig. 6.6, Table 6.4). In GC-7 the HHW of illite is <4 in the lower part (up to 200 cm) of unit 2 and between 4 and 6 in the upper part of unit 2 (200-80 cm) and unit 1 sediments. The ratio of illite 5Å /10Å reflection is largely <0.5 throughout the core (Fig. 6.7, Table 6.5)

6.5. Discussion

6.5.1. Limitations of clay mineralogy

The sediment cores investigated here are carbonate-dominated lime muds in unit 2 and terrigenous mud - dominated sediments in unit 1. Moreover, the sediments are more silty than clayey in both the units. The clay content of the acid-insoluble residue is about 10%. Although sufficient care was taken, minor variations would occur during preparation of the oriented slides, especially when clay content is low. It has been suggested that the clay mineral studies are more reliable when clay content of the sediment is 30% or more.

It is also well known that the interpretation of clay mineral concentration data suffers from the ambiguity of percentage values because change in the relative abundance of an individual clay mineral may signal either an increase in one component or a decrease in one or more other components. In order to overcome this problem the ratios of major clay minerals, S/I and K/Ch, were used along with percentage data, illite crystallinity and illite chemistry. Despite this, I would like to state that the results presented here are at best semi-quantitative and good enough for qualitative variations in clay minerals. In this chapter only major changes in clay mineral distribution are discussed.

6.5.2. Provenance and temporal variations of clay minerals

i. Cores from the continental shelf (GC-1 and GC-3):-

a. Unit 2 sediments

The core GC-1 is located off the Gulf of Kachchh, whereas GC-3 is off Saurashtra and at the eastern edge of the carbonate platform (see Fig. 6.1a). The unit 2 sediments are carbonate-dominated in both the cores. However, the radiocarbon ages of unit 2 sediments of GC-1 range between ~17 ka and 14 ka, while those in GC-3 are about 12 ka. The Glacio-eustatic sea level was at -120 m during the Last Glacial Maxima (22,000 cal yr BP) and -60 m at about 10,000 ^{14}C yr BP. (Fairbanks, 1989). The lime mud ages of 17-14 ka at 56 m water depth in GC-1 imply inundation of Gulf much prior to the expected time by Glacio-eustatic sea level due to neo-tectonic activity in the region and reworking of lime muds to the site (discussed at length in chapter 4 and 5). Therefore, terrigenous sediments associated with lime muds must have also been reworked. The percentage of clay minerals and S/I (av. 0.13) and K/C (av. 0.35) ratios of unit 2 sediments suggests illite and chlorite are the dominant minerals. Mica flakes are also present in the coarse fraction of the sediments. On the basis of the distribution of clay minerals in surficial sediments, earlier workers have demonstrated that illite and chlorite, and mica in coarse fraction are abundant in the Indus-borne sediments and are transported to the Kachchh region (100 km away from the river mouth) by alongshore currents (Goldberg and Griffin, 1970; Hashimi et al., 1978; Kolla et al., 1976, 1981a; Nair et al., 1982a; Rao, 1991; Chauhan, 1994; Rao and Rao, 1995). The Indus brings sediments largely from the Himalayas and also semi-arid alluvial soils of Pakistan and north India. Konta (1985) reported that the major catchment area of the River Indus is the Himalayas and carry significant amounts of illite (45%) and chlorite (30%) and less kaolinite (5%) and no smectite in its suspended load. It is therefore suggested that the illite, chlorite-rich sediments were reworked to the core site (GC-1) from the north of the Gulf of Kachchh during the late Pleistocene. The

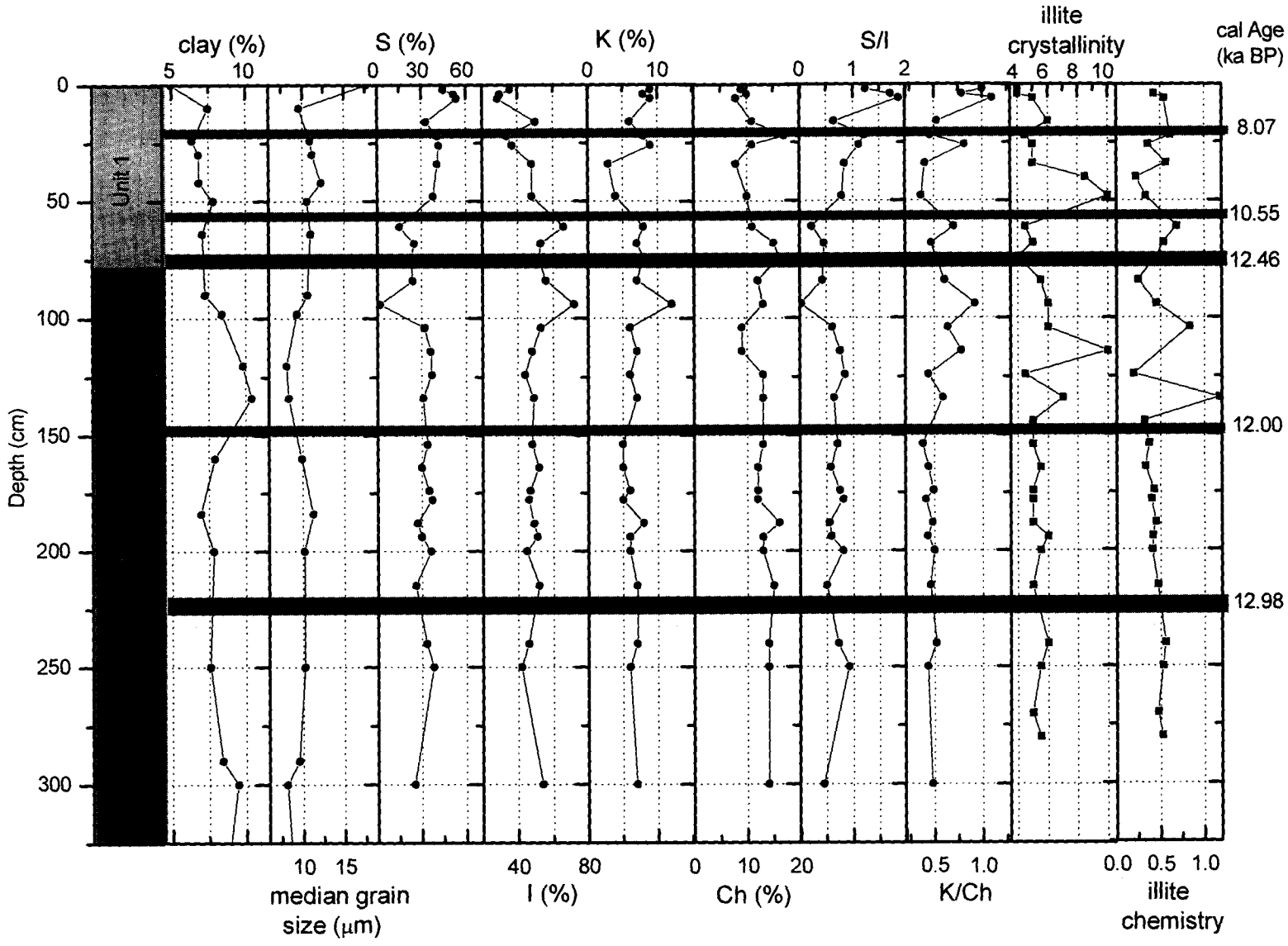

Fig 6.4. Down-core variations in clay content, median grain size, clay minerals, illite crystallinity (HHW) and illite chemistry (5Å/10 Å) in **GC-3**. (S- smectite, I- illite, Ch- chlorite, K- kaolinite)

HHW values of illite (4-5) and majority of unit 2 samples showing nearly constant ratio (0.5) of illite 5Å /10Å reflection (except at the core bottom) indicate better crystalline, Fe, Mg-rich illites suggesting that it is derived from the physical weathering of the Himalayan source. Fe, Mg-rich illite is characteristic of physically eroded, un-weathered rocks and indicates low hydrolysing conditions in the source area (Gingele, 1996).

Although the clay content of unit 2 sediments of GC-1 and GC-3 is same, the proportions of smectite increase (up to 30%) and illite decrease (60-40%) in GC-3. The ages of lime muds for unit 2 of GC-3 sediments are younger than that of GC-1. Since Deccan Traps are the principle rock type off Saurashtra one would expect smectite-dominated sediments. Two possibilities exist for the dominance of illite in these sediments. (a) The Indus transported material carried by long-shore currents may have admixed with hinterland weathering products and got deposited at the core site. As core GC-3 is farther from the Indus as compared to GC-1, the material transported must have reduced with increasing distance. (b) Alternatively, as the Sabarmati, Mahi rivers and tributaries of Narmada drain through the Aravalli mountain ranges, consisting of Precambrian metamorphic and igneous complexes, illite may have been released from these formations, transported along with smectite and deposited at core site. Less crystalline and Al-rich illites are expected from peninsular source. Higher crystalline (HHW is <6) and Fe, Mg-rich illites as indicated by illite chemistry reflect that illites are largely the physical or mechanical weathering products supporting the Himalayan source. Chemistry or Sr-Nd isotopes of clays are to be analysed to confirm the exact source.

b. Unit 1 sediments

In GC-1, the smectite content, S/I and K/Ch ratios increase sharply and illite and illite crystallinity values decrease at about 14 ka BP (see Fig. 6.3). Moreover, coarser sediments consisting of green grains and aragonite

encrustations are associated with this lower part of unit 1 sediments (see Chapter 4 for details). Since the sediments are reworked, the change in sedimentary environment implies flooding of the Gulf due to sudden sea level rise coinciding with melt water pulse (MWP)1A at about 14 ka BP (Fairbanks, 1989). As a consequence the earlier deposited sediments in the Gulf were reworked. The gradual decrease of smectite and increase of illite in the early and mid-Holocene sediments (Fig. 6.3) indicate long-shore sediment transport from the Indus is still active and the barrier effect of tides operating at the Gulf was insignificant during this time. The decrease of illite and increase of smectite in late Holocene sediments indicate that the influence of tides at the Gulf was much more active as a barrier for long shore sediment transport. Illite crystallinity and ratios of 5Å /10Å reflection of illite decrease suggesting the development of hydrolysing conditions in the source area, may be due to intense monsoon conditions in the early Holocene.

Smectite (15-54%), kaolinite (4-9%) contents and S/I ratios (0.23 to 1.87) gradually increase from base to the core top of unit 1 sediments in GC-3, suggesting increasing influence of hinterland flux at the depositional site. The decrease of illite (66-30%) and chlorite (15-8%) towards the core top also suggests decreased flux from the Indus. Rao and Rao (1995) reported the dominance of smectite over illite in the outer shelf sediments off Saurashtra and suggested that the effect of tidal barrier is moderate. The mineral studies on the shelf sediments off Saurashtra have indicated the abundance of chlorite, characteristic of the Indus province in the surface sediments (GSI, 1975). The clay mineral studies, using Differential Thermal Analyses (DTA), have shown the abundance of illite in the outer shelf sediments and montmorillonite limited to the inner shelf (GSI, 1975). Suspended sediment concentration inferred from satellite data on the continental shelf off Saurashtra also shows that, the surface sediment fronts from the Narmada and Tapti rivers are limited to the shallow

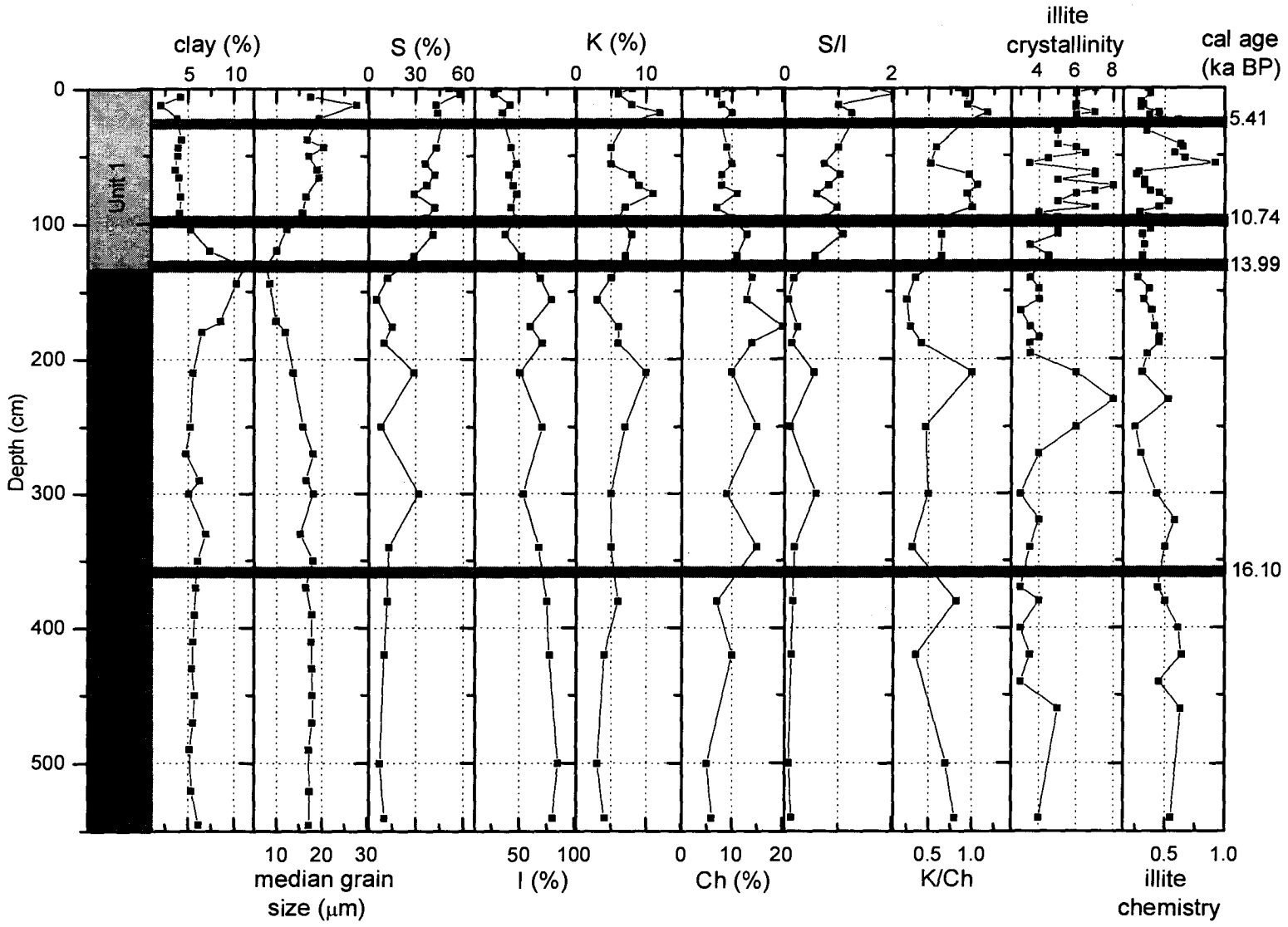

Fig. 6.5. Down-core variations in clay content, median grain size, clay minerals, illite crystallinity (HHW) and illite chemistry (5Å/10 Å) in **GC-5.** (S- smectite, I- illite, Ch- chlorite, K- kaolinite)

depths (SAC, 2003). Thus the core top sediments of GC-3 represent sediment input from both Saurashtra as well as Indus, the former being dominant.

ii. Cores from the shelf edge and continental slope (GC-5, GC-6 and GC-7)

a. Unit 2 sediments

The unit 2 sediments of GC-5, GC-6 and GC-7 are of late Pleistocene age (see Figs. 6.5-6.7) range between 16 and 11 ka BP (see Cal ages shown in Figs. 6.5-6.7). This implies that the sediments were deposited during the lowered sea levels. All these sediments are dominated by illite and chlorite with minor smectite and kaolinite. The source for the illite, chlorite-rich sediments could be the River Indus, largely debouching its sediments directly onto the continental slope during the lowered sea levels. The illite and chlorite contents are highest in GC-7 (70-80%; 10-17%), followed by GC-5 (69-85%; 5-20%) and GC-6 (64-69%; 13-20%). This suggests that higher concentrations are found closer to the Indus and concentrations decrease away from the Indus (see Fig. 6.1a for core locations). The long shore currents may have transported sediments to the core sites. Illite and chlorite-rich sediments on the continental slope and beyond off Saurashtra were reported to be from Indus source (Stewart et al., 1965, Vallier, 1974, Cronan et al., 1974).

b. Unit 1 sediments

GC-5 is located at the shelf edge (121 m depth). The unit 1 sediments exhibit gradual increase in smectite (12-58%) and kaolinite (3-12%) contents and decrease in illite (79-28%) and chlorite (14-7%) contents from base to the core top (see Fig. 6.5). The variations in S/I (0.17-2.06) and K/Ch (0.35-1.17) follow that of smectite and kaolinite. The smectite-rich sediments are characteristic of the black cotton soils of the Deccan Traps, which are abundant on the Saurashtra Peninsula. The change in sedimentary conditions starts at the base of the unit 1 that corresponds to ~14 ka BP (Fig. 6.5). The gradual change in

mineralogy and dominance of smectite over illite towards the core top emphasize three aspects: (a) The sediments deposited are an admixture of two sources, the Indus flux and the hinterland flux from Saurashtra. (b) The intensity of long shore currents transporting sediments from the Indus decreased with time, may be due to the shifting of southerly current onto the shelf with rising sea level during the late Pleistocene and Holocene. (c) The cross shelf transport of the hinterland flux is distinct and increased with time and maximum during the late Holocene. On the basis of the distribution of clay minerals in surficial sediments, Rao (1991) demonstrated cross-shelf transport processes on the continental shelf off Saurashtra.

Unlike that of GC-5, the unit 1 sediments of GC-6 range from ~11 ka BP to present (Fig. 6.6). The unit 1 sediments between 11.2 ka BP and ~4 ka BP also recorded gradual increase in smectite (28-59%) and decrease in illite (64-29%) contents (see Fig. 6.6). Thereafter illite content increases from 29% to 57% and smectite decreases from 59% to 22% towards the core top. S/I ratio follows that of smectite variations. The change in sedimentary conditions within the unit 1 sediments may be due to changing monsoonal intensity. The period of increase in smectite content (11 – 4 ka BP) corresponds to the early to mid Holocene during which the intensity of monsoons was high (van Campo, 1986). As a consequence the sediment flux from the Narmada and Tapti sources increased and cross-shelf processes transported more flux to the continental slope. Intensity of monsoons reduced relatively and sea level conditions become stabilised during the late Holocene. Therefore, sediment flux was largely deposited on the inner shelf and little transported to the continental slope.

Unlike GC-5 and GC-6, the unit 1 sediments in GC-7 are thin and sediments representing 12, 000 years are only 60 cm thick. The sediments are largely calcareous sediment-dominated. Marginal increase in smectite (9 to 15%) and S/I ratio (0.10-0.22) and decrease in illite (76 to 67%) indicate that the

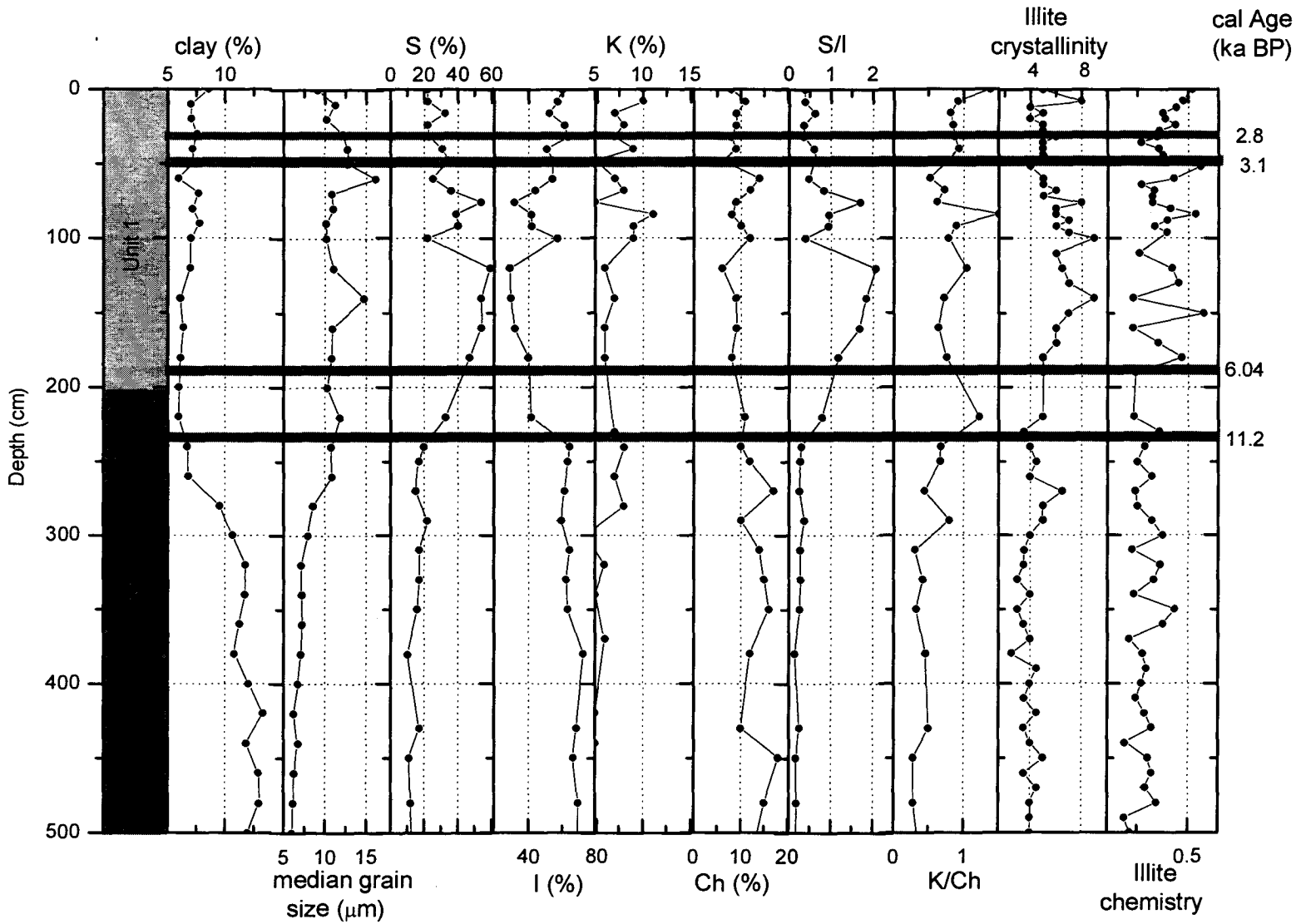

Fig. 6.6. Down-core variations in clay content, median grain size, clay minerals, illite crystallinity (HHW) and illite chemistry (5Å/10 Å) in **GC-6.** (S- smectite, I- illite, Ch- chlorite, K- kaolinite)

sediments are again an admixture of Indus-derived sediment and hinterland flux. Goldberg and Griffin (1970) have provided a detailed map of chlorite distribution in the northern Arabian Sea, showing chlorite content increases westward from the Indus Fan toward the Persian Gulf. Kolla et al. (1981a) reported abundant illite (40-50%) in the sediments of the Indus Fan and the western Arabian Sea. They have also reported ~30% chlorite in the sediments of the northern Arabian Sea and the Gulf of Oman with a general decrease towards Indian coast. Sirocko and Lange (1991) reported 30-50% illite in the Arabian Sea sediments. High illite content points to increased physical weathering activity. Further, the evidence for weathering regime can be obtained from illite crystallinity (Kubler Index), which thought to reflect the chemical weathering intensity of the source area (Singer, 1984; Chamley, 1989).

Earlier studies have also shown little variations in kaolinite content throughout the Arabian Sea and thus suggested kaolinite cannot be used as a palaeoclimatic tracer (Biscaye, 1965, Lange, 1982). Even in this study, kaolinite variations, sometimes, are not consistent with smectite. This may be due to the poor-resolution of chlorite and kaolinite reflections in slow scan X-ray diffractograms that leads to errors in estimation of the two minerals.

6.5.3. Palaeoclimatic records from crystallinity and chemistry of illite

Singer (1984) and Chamley (1989) used illite crystallinity as a tool to infer intensity of chemical weathering in the source area. Stronger chemical weathering leads to an opening of the illite structure resulting in poor crystallinity. Well-crystallized illite indicates less hydrolysing power of the source environment due to more arid climatic conditions and/or intense physical weathering (Lamy et al., 1998). Chamley (1989) suggested that the illite crystallinity can be used to distinguish cold-dry conditions associated with glacial stages from warm-humid, more hydrolysing interglacial conditions. Illite chemistry is based on the ratio of

illite 5Å/10Å peak reflection. The ratio >0.5 indicates Al-rich illites formed during strong hydrolysis (see Gingele, 1996). The sediment cores investigated here show that the better crystalline illites are not always correspond with Fe, Mg-rich illites. For example, a large hump of low-crystalline illites can be seen at about 11 ka in unit 1 sediments of GC-3 (Fig. 6.4). But there is no correspondence in illite chemistry towards Al-rich illites and illites are still Fe, Mg-rich (Fig. 6.4). Similarly, a large hump of low-crystalline illites occurs at about 15 ka in unit 2 sediments of GC-5 (Fig. 6.5). But the illite chemistry at this time still shows Fe, Mg-rich illites. The Holocene sediments of the same core showed progressive shift towards poor-crystalline illites. Illite chemistry for the corresponding period is not consistent, though Al-rich illites occur at places (Fig. 6.5) Poor-crystalline illites correspond to Fe-Mg illites in lower unit 1 sediments of GC-6 (see Fig. 6.6). It therefore appears that in a given climate, the crystallinity of illite responds much faster than illite chemistry. The illite crystallinity variations (Figs. 6.3, 6.4, 6.5, 6.6 and 6.7) recorded in sediment cores investigated here may be assigned to temporal variations in climate and resulting changes in the intensity of chemical/physical weathering in the source areas.

i. Cores from the continental shelf

The illites in unit 2 sediments of GC-1 and GC-3 are of late Pleistocene age (17 ka BP to 12 ka BP) and showed better illite crystallinity values (HHW= 4-6). These illites were derived from the Himalayas transported by the Indus, in GC-1, and/or from the Precambrian gneisses in the Aravallis in GC-3 (see provenance section). The better crystalline illites may be the manifestation of cold and dry conditions. Several workers reported cold and dry conditions prevailed during the glacial periods and dry conditions continued until 12 ka BP (Prell and Hutson, 1979; Prell et al., 1980; Bryson and Swain, 1981; Duplessy, 1982; Thamban et al., 2001). Poorly-crystalline, Al-rich illites increase towards the late Holocene in GC-1 and poor-crystalline illites occur at about 11 ka BP (at 50 cm of the core) in GC-3. The soils in the hinterland may have been subjected

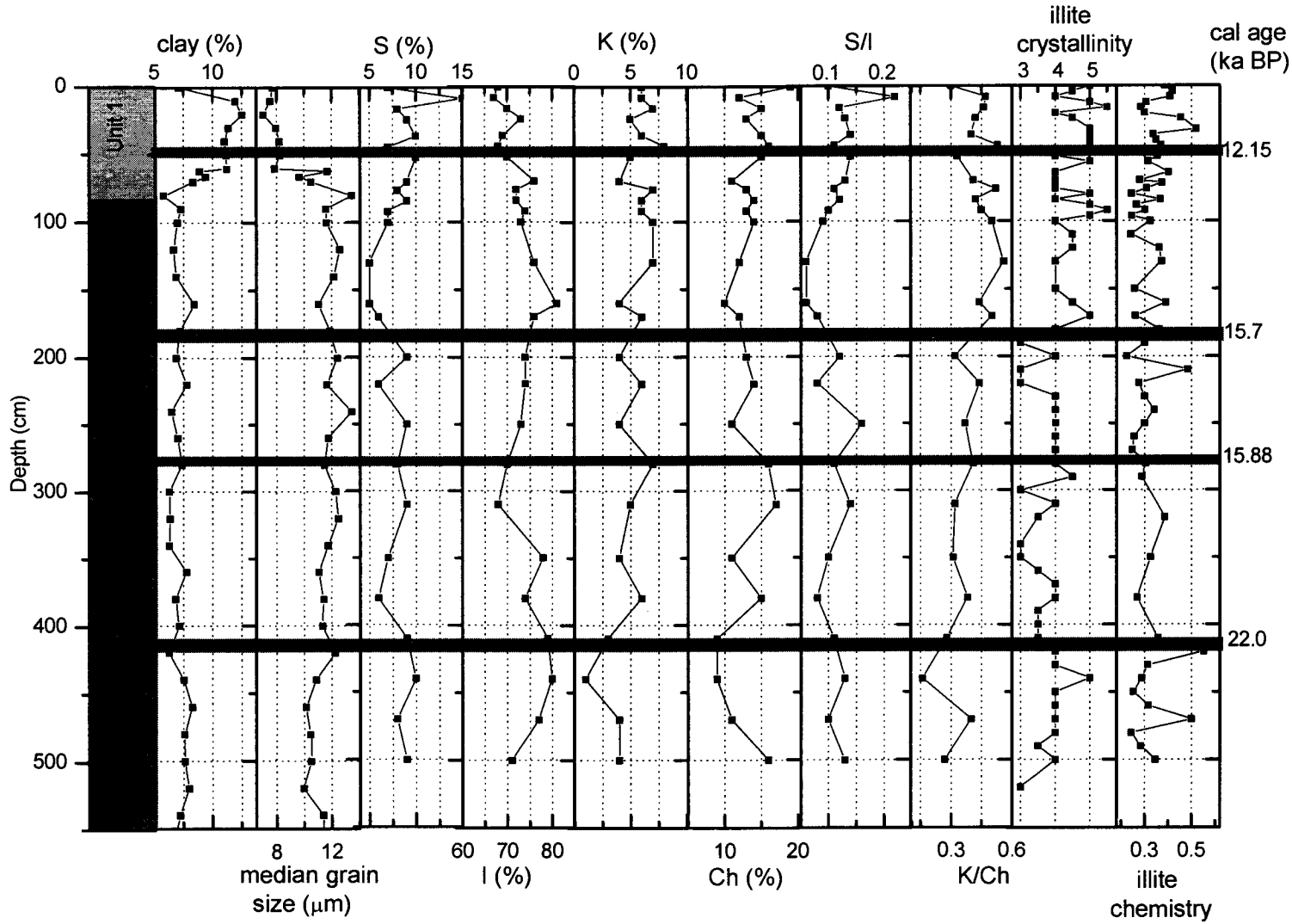

Fig 6.7. Down-core variations in clay content, median grain size, clay minerals, illite crystallinity (HHW) and illite chemistry (5Å/10 Å) in **GC-7**. (S- smectite, I- illite, Ch- chlorite, K- kaolinite)

to more hydrolysing conditions due to intensified monsoons in the early Holocene and resulted in poor-crystalline, Al-rich illites.

ii. Cores from the shelf edge and continental slope.

Relatively high crystalline, Fe, Mg-rich illites are characteristic of most of the late Pleistocene sediments (unit 2) of all the cores from the continental slope. The source for illite was from the Himalayas transported through the Indus. Physical/mechanical weathering of Himalayan sedimentary sections resulted in this type of illite. Although dry conditions prevailed at about 15 ka BP, illites are poor-crystalline in unit 2 sediments of GC-5 (Fig. 6.5). I could not offer any explanation. Since the core is located at the shelf edge, it is presumed reworking of the clays resulted in poor-crystalline illites. A distinct hump of poor-crystalline illites in the early Holocene sediments of the same core (Fig. 6.5) may be due to strong hydrolysing humid conditions resulted from the strengthening of monsoon during this period. Reconstructions of precipitation from lake records in Tibet and northwest India showed that maximum precipitation occurred between 10 and 6 ka (Bryson and swain, 1981; Swain et al., 1983; Gasse et al., 1991; Gasse and Van campo, 1994). The core GC-6 also shows similar poor-crystalline illites until 5 ka BP. Thereafter there is a fall in the crystallinity index values at about 3.1 and 2.8 ka BP (see Fig. 6.6) indicating a weakening of hydrolyzing conditions; this may be due to the reduction in strength of the monsoon. Monsoon proxies and climatic expressions have revealed that the intensity of monsoon started declining since ~5 ka BP (Kutzbach, 1981; Sirocko et al., 1993; Naidu, 1996; Reichart et al., 1997). Naidu (1996) reported the lowest upwelling indices between 3.5 to 1.2 ka BP

6.5.4. Palaeoclimatic signatures from grain size

The down-core distribution of clay content and median grain size of the terrigenous mud indicates significant variations in the mode of sediment input.

The size of the particles deposited depends on several factors, which include the intensity and type of weathering, strength and viscosity of the transporting medium, density of the particle and hydrodynamic conditions operating at the site of deposition.

The median grain size of the terrigenous fraction is largely ~10 μm (lower limit of sortable silt fraction). Silt coarser than 10 μm displays size sorting in response to hydrodynamic processes. The silt finer than 10 μm behaves in the same way as clay (Mc Cave et al., 1995) because of the entry of clay minerals in the compositional spectrum (Weaver, 1989; Mc Cave, 1985). Sediment concentration also regulates suspended sediment transport. As the clay content increases its viscosity increases and the settling velocity of particle settling through the fluid decreases and greater energy is required to keep the particles in suspension if the concentration is more (Anderson and Kurtz, 1985). Theoretical and laboratory flume studies have shown that particles finer than approximately 30 μm are maintained in suspension by very slow moving bottom currents (<4 cm/s). Thus it is generally assumed that deposition of fine silt and clay occurs through some form of physico-chemical or biological aggregation and that size variations in deep sea sediments are due to compositional differences, not due to depositional processes (Oser, 1972; Van Andel, 1973).

Variations in the median grain size of the mud and clay content are minor in the lower section of unit 2 sediments of all the cores investigated, except GC-5 and GC-6. In these slope cores more terrigenous clay content is associated with finer grain size in lower unit 2 sediments (see Fig. 6.5 and 6.6). This may be due to more input of terrigenous flux because of direct deposition of sediments onto the continental slope during the lowered sea levels. The sediments at the transitional zone of unit2/1 and unit 1 showed two distinct variations. (a) Grain size that is inversely proportional to the clay content (see Figs. 6.3 and 6.7). Decrease in clay content may be due to gradual rise in sea level and deposition

of more clay in continental shelf areas. (b) Variations in median grain size seem to follow smectite variations in GC-1, GC-3, GC-5 and GC-6 (Figs. 6.3 - 6.6). Maximum grain size variations are seen in a core at the shelf edge (GC-5). First of all, the gradual increase in grain size corresponds to the early and mid-Holocene (Fig. 6.5), during which the monsoon intensity was high. The strength of monsoon probably played some role in transporting coarser particles to the continental slope. Since grain size increase is continuous until late Holocene (despite reduced monsoons), the explanation offered may not be the sole reason. High-energy gravity currents are often present at the shelf edge. Under these conditions finer particles may have been winnowed to the deeper regions. Co-variations of increased grain size and smectite are often puzzling. It may be because of the smaller grain size of smectite. In fact, it remains in suspension for longer time. Therefore it may have transported farther, flocculated and deposited at the core site. Clay mineral distribution studies in recent sediments have indicated a transport differentiation based on size sorting (Gibbs, 1972). Because of its finer size, the cross shelf transportation of abundant smectite was reported on the continental slope off Saurashtra (Rao, 1991). LANDSAT imageries of the eastern Arabian Sea have shown that the sediment brought during the summer monsoon remain in suspension and start settling down with the onset of winter (Nayak and Sahai, 1985). This longer stay in suspension may have provided conditions for compositional difference based on grain size. However, the decrease in grain size corresponding to increase in smectite in unit 1 sediments of GC-7 (Fig. 6.7) remains unexplained.

6.5.5. Contribution from Aeolian dust

Clay mineralogical studies in the Arabian Sea sediments have shown dust contribution from Africa, Arabia, Pakistan and northern India in the northern and western Arabian Sea (Stewart et al., 1965; Gorbunova, 1966; Gold berg and Griffin, 1970; Kolla et al., 1976, 1981a; Chester et al., 1985; Naidu et al., 1985; Sirocko and Lange, 1991). Attempts were made to identify minerals of aeolian

origin (palygorskite and sepiolite) in the sediment cores by the X-ray diffraction technique on powder samples as well as clay mounts. There are no promising results implying that the Aeolian fraction if present must be <5% of the sediment. However, minor reflections of palygorskite were observed at the Holocene sediment intervals of the core GC-2 collected at 1900 m off Indus (see Chapter 3, Fig. 3.2C). Thus the dust contribution from Africa and Arabia is negligible in the sediment cores investigated. Aston et al. (1972) reported illite transported by eolian processes from the Rajastan desert. Although abundant illites are present off the Gulf of Kachchh direct evidence characteristic of aeolian origin cannot be ascertained in this study. The late Pleistocene sediments (LGM) in GC-2 also show low S-ratio% associated with increased acid-insoluble residue indicating possible aeolian transported illite (see chapter 3), source of which needs to be further investigated.

6.6. Summary and conclusions

- Reworked sediments are present in the late Pleistocene sediments of the shelf core collected off the Gulf of Kachchh. Abundant illite and chlorite in these sediments represent the Indus-derived material.

- The late Pleistocene sediments on the continental shelf off Saurashtra contain an admixture of clay minerals derived from the Indus and hinterland.

- Increased smectite in the early and mid-Holocene sediments of both the shelf cores suggests larger supply of hinterland flux. The influence of tides operating at the Gulf of Kachchh acting as a barrier to the long shore sediment transport can be seen only in the late Holocene sediments.

- Increased clay content in the late Pleistocene sediments of the cores on the continental slope indicates direct supply of terrigenous material on to the continental slope during the lowered sea levels.

- Abundant illite and chlorite in the late Pleistocene sediments of all the continental slope cores suggest their derivation from the Himalayas and transported by the Indus.

- Illite, chlorite-rich sediments in the late Pleistocene change over to smectite and kaolinite-rich sediments in the Holocene. This reflects changing sedimentary environment at the core site from Indus-dominated to hinterland-dominated clays.

- The progressive increase in smectite content during the Holocene in a core off Saurashtra suggests increased cross shelf transport of clays from the hinterland.

- Continuous increase in median grain size despite decrease in clay content in the sediment cores suggests winnowing of fine-grained material is effective in the upper slope sediments, most probably due to gravity currents operating at the shelf edge.

- Intensified monsoon conditions during the early and mid-Holocene are evident from the increased concentrations of smectite in the slope cores.

- Illite crystallinity and illite chemistry measured from the X-ray diffractograms reveal crystallinity of illite responds much faster for the changing weathering conditions than illite chemistry.

- Contribution of aeolian dust to the study area is insignificant, except in a core off Indus. Low S-ratio% and illite dominance at LGM indicate arid conditions. If present it must be <5% of the sediment that cannot be identified by X-ray diffraction studies.

- Sr-Nd isotopes are very much essential to characterize specific sources of illites off Saurashtra.

Table 6.1. Down-core distribution of major clay minerals (S-smectite, I-illite, K- kaolinite, Ch- chlorite), half height width of illite peak (HHW), illite 5Å/10 Å ratio, clay content and median grain size of terrigenous mud in GC-1

Depth (cm)	S (%)	I (%)	K (%)	Ch (%)	S/I	K/Ch	HHW	Illite 5Å/10Å	Depth (cm)	Clay (%)	Median (μm)
0	29	55	5	12	0.53	0.39	5.0	0.30	0	10.95	8.19
10	10	65	11	15	0.15	0.71	6.0	0.43	15	8.71	10.29
20	12	68	8	12	0.18	0.67	8.5	0.82	25	10.00	9.20
30	10	74	6	9	0.14	0.70	7.0	0.38	35	6.24	13.10
40	20	58	8	14	0.35	0.53	5.0	0.48	45	10.42	8.91
50	17	62	7	14	0.28	0.48	5.5	0.42	55	5.74	13.37
60	23	57	8	12	0.40	0.67	7.0	0.41	65	6.51	12.09
80	25	53	9	13	0.48	0.67	5.5	0.39	75	8.76	9.79
90	22	59	5	14	0.38	0.40	6.0	0.38	85	7.89	10.77
100	33	46	5	16	0.73	0.35	5.0	0.31	95	5.79	11.90
130	8	63	8	21	0.13	0.38	4.0	0.45	105	5.32	14.57
160	8	64	8	20	0.13	0.41	4.5	0.47	125	8.70	9.66
190	8	62	8	22	0.13	0.38	4.5	0.42	145	7.95	10.22
225	7	67	7	19	0.10	0.36	4.5	0.48	165	7.25	11.41
245	9	63	9	19	0.13	0.45	5.0	0.44	185	8.11	10.08
280	11	63	9	18	0.17	0.52	5.0	0.49	205	8.67	9.74
310	7	62	10	21	0.12	0.46	4.5	0.42	225	7.46	11.30
340	8	64	8	20	0.13	0.38	5.0	0.46	245	5.93	13.37
370	8	65	7	20	0.12	0.32	4.5	0.54	285	9.19	9.53
405	9	66	6	19	0.14	0.35	4.0	0.51	310	7.85	9.98
460	5	68	8	19	0.08	0.40	4.5	0.57	325	9.40	8.70
520	7	67	7	19	0.11	0.35	5.5	0.74	365	8.59	9.62
580	8	66	8	18	0.12	0.44	4.0	0.43	385	7.24	10.70
									405	7.67	10.56
									425	6.91	11.46
									465	7.92	10.06
									485	8.36	9.34
									505	7.92	9.76

Table 6.2. Down-core distribution of major clay minerals (S-smectite, I-illite, K- kaolinite, Ch- chlorite), half height width of illite peak (HHW), illite 5Å/10Å ratio, clay content and median grain size of terrigenous mud in GC-3

Depth (cm)	S (%)	I (%)	K (%)	Ch (%)	S/I	K/Ch	HHW	Illite 5Å/10Å	Depth (cm)	Clay (%)	Median (μm)
2	45	36	9	9	1.25	1.00	4.0	0.42	0	4.98	17.63
4	52	30	8	10	1.72	0.79	4.0	0.43	10	7.47	9.67
6	54	29	9	8	1.87	1.10	5.0	0.54	24	6.42	10.97
16	33	50	6	11	0.65	0.53	6.0	0.56	30	6.82	11.17
22	41	34	8	17	1.22	0.46	4.5	0.62	42	6.86	12.26
26	42	37	9	11	1.12	0.82	5.0	0.36	50	7.83	10.60
34	41	48	3	8	0.85	0.41	5.0	0.57	64	7.07	11.00
48	38	48	4	10	0.80	0.37	10.0	0.34	90	7.26	10.63
61	15	66	8	11	0.23	0.70	4.5	0.69	98	8.40	9.38
68	25	53	7	15	0.46	0.47	5.0	0.54	120	9.80	8.11
74	23	52	8	16	0.44	0.52	4.0	0.46	134	10.40	8.37
84	24	56	7	12	0.43	0.61	5.5	0.25	160	7.91	9.95
94	2	72	12	13	0.03	0.92	6.0	0.45	184	6.96	11.28
104	32	53	6	9	0.61	0.64	6.0	0.83	200	7.82	10.21
114	36	48	7	9	0.76	0.78	10.0	0.72	250	7.59	10.26
124	37	44	6	13	0.85	0.44	4.5	0.19	290	8.41	9.55
134	31	49	7	13	0.64	0.59	7.0	1.17	300	9.48	8.16
154	34	48	5	13	0.71	0.38	5.0	0.37	340	8.66	8.89
164	30	52	5	12	0.58	0.44	5.5	0.33	350	8.17	8.89
174	35	47	6	12	0.75	0.49	5.0	0.43	390	8.77	8.83
178	37	46	5	12	0.81	0.41	5.0	0.40	420	9.10	8.28
188	27	49	8	16	0.55	0.48	5.0	0.45	440	9.07	8.44
194	30	51	6	13	0.59	0.43	6.0	0.41	460	10.70	7.84
200	36	45	6	13	0.81	0.50	5.5	0.41	480	8.79	8.78
215	26	52	7	15	0.50	0.46	5.0	0.47	520	8.23	8.94
240	33	46	7	14	0.72	0.52	6.0	0.56	540	10.54	7.06
250	38	42	6	14	0.92	0.43	5.5	0.53	580	10.27	8.09
300	25	54	7	14	0.45	0.48	5.0	0.52	--	--	--
									--	--	--

Table 6.3. Down-core distribution of major clay minerals (S-smectite, I-illite, K- kaolinite, Ch- chlorite), half height width of illite peak (HHW), illite 5Å/10Å ratio, clay content and median grain size of terrigenous mud in GC-5

Depth (cm)	S (%)	I (%)	K (%)	Ch (%)	S/I	K/Ch	HHW	Illite 5Å/10Å	Depth (cm)	Clay (%)	Median (μm)
0	51	31	8	10	1.7	0.8	7	0.36	6	4.17	17.47
4	58	28	6	7	2.1	0.9	6	0.38	12	2.09	27.85
12	43	42	8	8	1.0	1.0	6	0.32	22	3.80	19.30
18	44	35	12	10	1.3	1.2	7	0.45	38	4.32	16.74
26	47	37	7	8	1.3	0.9	5	0.37	44	3.90	20.43
44	43	43	5	9	1.0	0.6	6	0.65	50	3.88	17.19
56	36	48	5	10	0.8	0.5	3.5	0.92	60	3.58	18.94
64	42	41	8	8	1.0	1.0	7	0.26	66	4.02	19.36
72	37	45	9	8	0.8	1.1	8	0.33	80	4.19	16.49
78	29	48	11	11	0.6	0.9	6	0.45	92	4.09	15.76
88	42	43	7	7	1.0	1.0	7	0.45	104	5.29	12.29
96	37	48	6	10	0.8	0.6	5	0.50	120	7.32	9.95
108	41	38	8	13	1.1	0.7	5	0.31	132	11.04	7.59
124	29	52	7	11	0.6	0.7	4.5	0.31	144	10.22	8.47
140	12	69	5	14	0.2	0.4	3.5	0.27	172	8.51	9.87
156	5	79	3	13	0.1	0.3	4	0.32	180	6.50	12.02
176	15	60	6	20	0.3	0.3	3.5	0.41	210	5.57	13.63
188	10	71	6	14	0.1	0.4	3.5	0.45	250	5.24	15.87
210	29	51	10	10	0.6	1.0	6	0.31	270	4.77	18.09
250	8	71	7	15	0.1	0.5	6	0.25	290	6.23	16.51
300	32	54	5	9	0.6	0.5	3	0.43	300	5.09	18.08
340	13	68	5	15	0.2	0.3	3.5	0.50	330	6.93	15.26
380	12	75	6	7	0.2	0.8	4	0.50	350	6.08	17.99
420	10	77	4	10	0.1	0.4	3.5	0.64	370	5.82	16.47
500	7	85	3	5	0.1	0.7	--	--	390	5.74	17.80
540	10	80	4	6	0.1	0.8	4	0.55	410	5.55	17.71
									430	5.44	17.74
									450	5.72	17.89
									470	5.56	17.85
									490	5.18	17.10
									520	5.35	17.22
									545	6.16	17.12

Table 6.4. Down-core distribution of major clay minerals (S-smectite, I-illite, K- kaolinite, Ch- chlorite), half height width of illite peak (HHW), illite 5Å/10Å ratio, clay content and median grain size of terrigenous mud in GC-6

Depth (cm)	S (%)	I (%)	K (%)	Ch (%)	S/I	K/Ch	HHW	Illite 5Å/10Å	Depth (cm)	Clay (%)	Median (μm)
0	22	60	10	8	0.38	1.38	5.0	0.52	0	8.57	9.12
8	22	57	10	11	0.38	0.92	8.0	0.48	10	7.05	11.24
16	32	52	7	9	0.62	0.81	5.0	0.38	20	7.00	10.19
24	22	61	8	9	0.36	0.85	5.0	0.44	30	7.55	12.18
32	23	63	7	8	0.36	0.88	6.0	0.35	40	7.17	12.77
40	31	51	9	9	0.61	0.94	5.0	0.35	50	7.14	12.82
48	34	54	5	6	0.63	0.78	4.0	0.38	60	5.93	16.15
60	25	54	7	14	0.47	0.52	5.0	0.43	70	7.69	10.87
68	36	44	8	12	0.83	0.73	6.0	0.33	80	7.18	11.03
76	54	32	5	9	1.70	0.62	8.0	0.32	90	7.77	10.16
84	39	42	11	8	0.94	1.50	6.0	0.54	100	7.05	10.17
92	40	42	9	10	0.94	0.89	6.0	0.33	120	6.94	11.05
100	22	57	9	12	0.39	0.79	9.0	0.39	140	6.11	14.78
120	59	29	6	6	2.07	1.04	6.5	0.42	160	6.34	10.92
140	54	30	7	9	1.84	0.72	9.0	0.23	180	6.14	10.88
160	54	32	6	9	1.68	0.64	6.0	0.23	200	5.96	10.30
180	47	40	6	8	1.18	0.76	5.0	0.47	220	5.98	11.84
200	33	42	14	11	0.80	1.23	5.0	0.23	240	6.68	10.78
230	20	64	7	10	0.30	0.68	4.0	0.29	260	6.83	10.88
240	17	63	8	12	0.27	0.67	4.5	0.25	280	9.53	8.58
260	15	61	7	17	0.25	0.44	6.5	0.24	300	10.60	7.96
280	22	59	8	10	0.37	0.80	5.0	0.32	320	11.77	7.14
300	17	64	4	14	0.27	0.31	3.5	0.22	340	11.71	7.18
320	17	62	6	15	0.28	0.42	3.0	0.33	360	11.22	7.29
340	16	63	5	16	0.26	0.32	3.0	0.44	380	10.76	7.10
370	10	72	6	12	0.14	0.46	2.5	0.28	400	12.08	6.78
420	17	68	5	10	0.25	0.50	3.5	0.32	420	13.32	6.22
440	11	66	5	18	0.17	0.28	5.0	0.30	440	11.82	6.72
470	12	69	4	15	0.18	0.28	4.0	0.34	460	12.90	6.27
500	13	69	5	13	0.19	0.37	4.0	0.25	480	12.95	6.12
									500	11.96	5.99

Table 6.5. Down-core distribution of major clay minerals (S-smectite, I-illite, K- kaolinite, Ch- chlorite), half height width of illite peak (HHW), illite 5Å/10Å ratio, clay content and median grain size of terrigenous mud in GC-7

Depth (cm)	S (%)	I (%)	K (%)	Ch (%)	S/I	K/Ch	HHW	Illite 5Å/10Å	Depth (cm)	Clay (%)	Median (μm)
0	7	68	6	19	0.1	0.30	5.0	0.36	0	7.11	7.70
8	15	67	6	12	0.22	0.47	4.0	0.38	10	11.92	7.52
16	8	70	7	15	0.12	0.46	5.5	0.23	20	12.53	7.02
24	9	73	5	13	0.13	0.42	4.5	0.44	30	11.36	7.97
36	10	69	6	15	0.14	0.40	5.0	0.29	40	11.05	8.18
44	7	68	8	16	0.11	0.53	5.0	0.34	50	11.17	8.26
52	10	70	5	15	0.14	0.33	4.0	0.32	60	11.21	7.84
70	9	76	4	11	0.13	0.41	4.0	0.22	62	8.90	11.67
76	8	72	7	13	0.11	0.52	4.0	0.26	66	9.40	9.65
84	9	72	6	14	0.12	0.42	4.0	0.33	70	8.32	10.51
92	7	74	6	13	0.1	0.45	5.5	0.25	80	5.80	13.47
100	7	73	7	14	0.09	0.50	4.0	0.28	90	7.29	11.60
130	5	76	7	12	0.06	0.56	4.0	0.34	100	7.01	11.61
140	8	76	3	14	0.1	0.23	5.0	0.21	120	6.67	12.59
160	5	81	4	10	0.06	0.44	4.5	0.36	140	6.88	12.17
170	6	76	6	12	0.08	0.50	5.0	0.20	160	8.45	11.06
200	9	74	4	13	0.12	0.32	4.0	0.16	180	7.25	11.88
220	6	74	6	14	0.08	0.44	3.0	0.22	200	6.89	12.42
250	9	73	4	11	0.16	0.37	4.0	0.25	220	7.80	11.67
280	8	70	7	16	0.11	0.41	4.0	0.26	240	6.49	13.46
310	9	68	5	17	0.14	0.32	4.0	0.36	260	7.04	11.78
350	7	78	4	11	0.1	0.31	3.0	0.28	280	7.40	11.47
380	6	74	6	15	0.08	0.38	4.0	0.21	300	6.30	12.27
410	9	79	3	9	0.11	0.28	3.5	0.32	320	6.36	12.47
440	10	80	1	9	0.13	0.16	5.0	0.24	340	6.29	11.74
470	8	77	4	11	0.1	0.40	4.0	0.50	360	7.77	11.08
500	9	71	4	16	0.13	0.27	4.0	0.31	380	6.83	11.40
									400	7.16	11.35
									420	6.27	12.26
									440	7.52	10.88
									460	8.28	10.14
									480	7.60	10.46
									500	7.64	10.50
									520	8.01	9.97
									540	7.22	11.40
									560	6.71	11.41

Chapter 7

Chapter 7

SUMMARY AND CONCLUSIONS

Fifteen sediment gravity cores collected along from the western margin of India at depths between 31m and 1940 m were investigated to better understand the palaeoclimatic and palaeoceanographic conditions during the late Quaternary. Of these, eleven cores are from the northwestern (NW) margin of India between the Gulf of Kachchh and Ratnagiri and four cores are from the southwestern (SW) margin between Mangalore and Cape Comorin.

The terrigenous sediments along the western margin of India are from diverse sources. The composition of the terrigenous sediments and their rate of deposition vary from north to south. The major sediment contributors are 1) The Indus, one of the largest rivers of the world, supplying sediments largely from the Himalayas, 2) Narmada and Tapti, discharged though the Gulf of Khambat, 3) moderate and seasonal rivers of the central and southwestern India and 4) aeolian dust from the alluvial soils of Pakistan and arid land masses of Iran-Makran-Thar regions. Although broad understanding has been achieved on the provenance of the sediments based on mineralogy of surficial sediments and Sr-Nd isotopes, palaeoclimatic studies using exclusively terrigenous sediments have not been attempted. In chapter 3 of the thesis, **the rock-magnetic properties** (magnetic concentration, magnetic grain size and magnetic mineralogy) of the sediments were investigated in detail and analysed these parameters in relation to other sedimentological properties in order to better understand the past climatic and provenance variations. The major conclusions are as follows:

- The magnetic susceptibility of the sediments is largely controlled by the detrital magnetite content. Regional variations in magnetic susceptibility are in accord with the mineralogical provinces.

- The highest MS values correspond to the sediments derived from the Deccan Traps, followed by the sediments from the Indus and least in the sediments off southern India.

- Intense chemical weathering in the Precambrian rocks of southern India results in leaching of iron from the source rocks and thereby reducing the MS value of the associated sediments.

- Authigenic green grains (Fe-rich clays) and biogenic magnetite at certain intervals in the cores enhance the total MS signal.

- Reductive diagenesis in organic-rich near surface sediments reduces the MS signal due to the dissolution of fine-grained magnetite.

- The MS contribution from the paramagnetic minerals (ilmenite, garnet, chlorite, smectite, glauconite, olivine, amphiboles, pyroxene) is much greater than that of dia-magnetic minerals (quartz, feldspar, calcite). The MS variations caused by varying carbonate content are minor.

- The glacial sediments in a core off the Indus exhibit low S-ratio% corresponding to high acid-insoluble residue. This implies the presence of high coercivity minerals like hematite and goethite and probable aeolian contribution from Pakistan and Indus drainage basin.

- The glacial sediments of the SW margin of India are characterised by low MS / high S-ratio% associated with low AIR and high OC and carbonate content, implying low terrigenous supply from the hinterland.

- The early Holocene sediments of both the NW and SW margin of India contain high MS / S-ratio% associated with high AIR and decreased $\delta^{18}O$ values. This implies enhanced supply of terrigenous material through fresh water, perhaps due to the intensified monsoonal activity at about this time.

- During the late Holocene, fine-grained magnetite on the continental slope is minor, may be due to stabilized sea levels and deposition of more terrigenous sediment on the shallow shelf.

- The late Holocene organic-rich sediments of the SW margin of India were subjected to reductive diagenesis and rock-magnetic properties were modified. Therefore, a caution needs to be exercised in interpreting the regional climatic signal through sediment magnetic properties.

Lime muds are abundant in the geological past but their Modern occurrences are confined to the Bahamas and Persian Gulf. Although extensive studies have been carried out on lime muds, their origin is still a subject of debate. The two popular theories exist for the origin of lime muds: a) inorganic precipitation of aragonite needles in hyper-saline, carbonate saturated shallow marine conditions and b) organic origin, whereby the aragonite needles are formed from the disintegration of codiacean algae. Lime muds in late Quaternary sediments of the northwestern margin of India have not been studied in detail and provide an opportunity to investigate and better understand their genesis. In chapter 4 of the thesis systematic studies carried out on lime muds in five gravity cores collected at depths between 56 m and 121 m. of the northwestern margin of India were presented. The studies include sedimentology (grain size, acid-insoluble residue, carbonate mineralogy, carbonate content, morphology), geochemistry (Sr content) and isotope (oxygen and carbon) chemistry and radiocarbon dates of the lime muds. The properties of the lime muds were

compared with that of the modern ones and following conclusions have been arrived.

- Gravity cores studied here contain abundant lime muds in the lower section and terrigenous-dominated sediments in the upper section.

- Lime muds are largely aragonitic in composition and are admixed with 30% to 50% terrigenous sediments on the shelf and <5% terrigenous material at the shelf break / slope.

- The grain size of the lime muds varies from 5 to 27 μm. The larger grain size in the shelf break/slope cores was due to aggregation of lime muds into ovoid and/or spheroidal grains.

- The Sr values of the lime muds in the shelf cores (0.18-0.61%) are much less than that of the shelf break/slope cores (0.10-0.83%).

- The Sr values of the slope cores are less than that of the inorganically formed aragonite needles from other regions and oolites.

- Depleted stable isotope ratios of the lime muds of the continental shelf indicate that the muds were formed either in water masses of different characteristic or altered after their formation.

- The lime muds at the shelf may have formed initially from the aragonite-producing plants and subsequently reworked and admixed with terrigenous sediments. .

- The age of the lime muds on the shelf ranges ~17-12 BP, implying submergence of the Gulf of Kachchh during early deglaciation and neo-tectonic activity in the Gulf region.

- The Sr values, stable isotopes and morphology of the aragonite needles at the shelf break/slope indicate that the lime muds were of organic origin and largely decomposed from codiacean algae.

- The organic matter associated with the muds may have facilitated cementation of individual needles into aggregates during early diagenesis and/or transportation at the sea floor.

- The age of the lime muds in the shelf break/slope varies from ~16-12 ka BP in shelf break / slope cores.

- Younger radiocarbon ages of lime muds between older ones in the slope cores indicate that the lime muds were reworked from the shelf or carbonate platform.

- The lime muds ceased to deposit after 14 ka in deeper water cores may be due to the global event (rapid rise in sea level)- associated with Melt Water Pulse (MWP)1A at 14 ka BP.

- The lime muds-dominated sediments gradually grade into terrigenous-dominated sediments after 12 ka BP. This change in depositional environment may be due to the combined influence of changes in regional climatic conditions, the Younger Dryas event and MWP1B.

Arabian Sea experiences seasonal reversal of monsoon wind patterns that result in **variations in upwelling and related primary productivity**. The

increased productivity in the water column resulted in permanent oxygen minimum zone on the continental slope at depths between 150 m and 1200 m and high organic carbon (OC) in the underlying sediments. The factors controlling the enrichment of organic carbon in sediments along the continental margin are a matter of debate for the last two decades. 'Productivity' and 'Preservation' models exist. In chapter 5 of the thesis, six sediment cores recovered from the northwestern margin of India at water depths between 56 m and 1900 m were investigated for organic carbon, calcium carbonate, organic carbon/total nitrogen ratio, acid-insoluble residue, grain size, sand content, planktonic and benthic foraminiferal content. Organic carbon data from the northwestern margin of India was also compared with that of the southwestern margin of India. The factors controlling the spatial and temporal distribution of organic carbon were identified. The summary and conclusions drawn from the study are:

- The organic carbon in the sediments of the shelf cores range from 0.18% to 0.47% and largely supplied from continental sources. In the late Pleistocene sediments of these cores OC was mostly reworked and associated with lime muds.

- The sediment texture, sedimentation rate and oxic water column at shallow shelf have influenced the OC content in the sediments.

- The late Pleistocene sediments of the upper slope also contain abundant lime muds.

- Within the continental slope, the cores from the oxygen minimum contain more OC (1.02%-4.83%) than those above (0.06%-1.14%) and below the oxygen minimum (0.28%-0.88%).

- The early deglacial sediments of the NW margin of India, in general, contain low OC content and agree well with that of the Pakistan margin.

- A distinct change in sedimentary environment occurs at ~12–11 ka BP in the early Holocene sediments.

- OC content increases progressively from 12-11 ka BP to until 7-6 ka BP and remains high in mid and late Holocene sediments. This implies high OC production was after 7-6 ka BP.

- The record of high OC content in the Holocene sediments mismatches with the past monsoon intensity record, which suggests that monsoon intensity was maximum at ~ 9-8 ka BP. This implies that factors other than productivity also play a major role in OC enrichment.

- Intervals of high OC also coincide with high sedimentation rate and finer grain size.

- The abundant aeolian transported material in the glacial sediments of the core off Indus may be responsible for low OC content.

- The glacial sediments of the northwestern margin of India contain low OC than that of the southwestern margin of India. This implies OC variations are controlled by localized hydrographic conditions.

- Comparison of the OC data between NW and SW margin of India suggests that high OC is not always associated with high productivity areas.

- It appears that a combination of several factors influences the special and temporal distribution of organic carbon.

As detailed in chapter 3 the northwestern margin of India receives terrigenous sediments, both from fluvial and aeolian sources. These are largely derived from the Himalayas, arid and alluvial soils of Pakistan and north India and Deccan Traps of the northwestern India. As climatic conditions have changed from arid to humid during the late Quaternary one would expect the sediments contributed by the fluvial and aeolian processes vary at different times in the Quaternary. Similarly, the northwestern margin of India was subjected to late Quaternary neo-tectonic activity. The tidal currents at the Gulf of Kachchh and Gulf of Khambat become operative as the sea level rose to the present position and influence the distribution of fine-grained sediments. In other words, the changing climatic and physiographic conditions on the northwestern margin of India influence the composition and transport of the fine-grained sediments. In chapter 6 of the thesis, clay mineralogy of the <2 μm fraction of the sediments together with illite crystallinity and illite chemistry, clay content and median grain size of the terrigenous mud were investigated in five gravity cores recovered at depths between 56 m and 420 m. The studies were undertaken to better understand the **provenance and transport pathways of the fine-grained sediments and hydrodynamic conditions in the depositional environment during the late Quaternary.** The conclusions drawn are summarized below

- Reworked sediments are present in the late Pleistocene sediments of the shelf core collected off the Gulf of Kachchh. Abundant illite and chlorite in these sediments represent the Indus-derived material.

- The late Pleistocene sediments on the continental shelf off Saurashtra contain an admixture of clay minerals derived from the Indus and hinterland.

- Increased smectite in the early and mid-Holocene sediments of both the shelf cores suggests larger supply of hinterland flux. The influence of tides operating at the Gulf of Kachchh acting as a barrier to the long shore sediment transport can be seen only in the late Holocene sediments.

- Increased clay content in the late Pleistocene sediments of the cores on the continental slope indicates direct supply of terrigenous material on to the continental slope during the lowered sea levels.

- Abundant illite and chlorite in the late Pleistocene sediments of all the continental slope cores suggest their derivation from the Himalayas by the River Indus and transported to the margin during the lowered sea levels.

- Illite, chlorite-rich sediments in the late Pleistocene change over to smectite and kaolinite-rich sediments in the Holocene. This reflects changing sedimentary environment at the core site from Indus-dominated to hinterland-dominated clays.

- The progressive increase in smectite content during the Holocene in a core off Saurashtra suggests increased cross shelf transport of clays from the hinterland.

- Continuous increase in median grain size despite decrease in clay content in the sediment cores suggests winnowing of fine-grained material is effective in the upper slope sediments, most probably due to gravity currents operating at the shelf edge.

- Intensified monsoon conditions during the early and mid-Holocene are evident from the increased concentrations of smectite in the slope cores.

- Illite crystallinity and illite chemistry measured from the X-ray diffractograms reveal crystallinity of illite responds much faster for the changing weathering conditions than illite chemistry.

- Contribution of aeolian dust to the study area is insignificant, except in a core off Indus. Low S-ratio% and illite dominance at LGM indicate arid conditions. If aeolian is present in other intervals, it must be <5% of the sediment that cannot be identified by X-ray diffraction studies.

- Sr-Nd isotopes are very much essential to characterize specific sources of illites off Saurashtra.

---xx---

References

REFERENCES

Agnihotri, R., Dutta, K., Bhushan, R. and Somayajulu, B.L.K., 2002. Evidence for solar forcing on the Indian monsoon during the last millennium. *Earth and Planetary Science Letters*, 198: 521-527

Agnihotri, R., Sarin, M.M., Somayajulu, B.L.K., Jull, A.J.T. and Burr, G.S., 2003. Late Quaternary biogenic productivity and organic carbon deposition in the eastern Arabian Sea. *Palaeogeography, Palaeoclimatology, Palaeoecology*, 197: 43-60.

Anderson, J.B. and Kurtz, D., 1985. The use of silt grain size parameters as a paleovelocity Gauge: A critical review and case study. *Geo-Marine Letters*, 5: 55-59.

Anonymous, 1965. Gazetteer of India, Publication division, Ministry of Information and Broadcasting, Government of India: 1652

Aston, S.R., Chester, R., Johnson, L.R. and Padgham, R.C., 1972. Eolian dust from the lower atmosphere of the eastern Atlantic and Indian Oceans, China Sea of Japan. *Marine Geology*, 14: 15-28.

Babu, M.T., Vethamony, P. and Desa, E., 2005. Modelling tide-driven currents and residual eddies in the Gulf of Kachchh and their seasonal variability: A marine environmental planning perspective. *Ecological Modelling*, 184: 299-312.

Babu, P.C., Brumsack, H.J. and Schnetger, B., 1999. Distribution of organic carbon in surface sediments along the eastern Arabian Sea: a revisit. *Marine Geology*, 162: 91-103.

Banse, K., 1987. Seasonality of phytoplankton chlorophyll in the central and northern Arabian Sea. *Deep-Sea Research*, 34: 713-723.

Baskaran, M., Rajagopalan, G. and Somayajulu, B.L.K., 1989. $^{230}Th/^{234}U$ and ^{14}C dating of the Quaternary carbonate deposits of Saurashtra, India. *Chemical Geology*, Isotope geoscience section, 79: 65-82.

Basu, D.N., Banerjee, A. and Tamhane, D.M., 1980. Source areas and migration trends of oil and gas in Bombay offshore Basin, India. *American Association of Petroleum Geologists Bulletin*, 64: 209-220.

Bathurst, R.G.C., 1971. Carbonate Sediments and their diagenesis. *Elsevier*, Amsterdam: 658pp.

Bauer, S., Hitchcock, G.L. and Olson, D.B., 1991. Influence of monsoonally-forced Ekman dynamics upon surface layer depth and plankton biomass

distribution in the Arabian Sea. *Deep-Sea Research*, 38: 531-553.

Berner, R.A., 1984. Sedimentary pyrite formation: an update. *Geochimica et Cosmochimica Acta*, 48: 606-616.

Bhattacharya, G.C. and Subrahmanyam, V., 1986. Extension of the Narmada-Son lineament on the continental margin off Saurashtra, western India as obtained from magnetic measurements. *Marine Geophysical Research*, 8: 329-344.

Bhattacharya, N., 1984. Provenance control of diagenesis in clayey sediments in the northern part of western continental shelf of India. *Journal of Geological Society of India*, 25: 427-436.

Bhushan, R., Dutta, K. and Somayajulu, B.L.K., 2001. Concentrations and burial fluxes of organic and inorganic carbon on the eastern margins of the Arabian Sea. *Marine Geology*, 178: 98-113.

Biscaye, P.E., 1965. Mineralogy and sedimentation of deep-sea clay in the Atlantic Ocean and adjacent sea oceans. *Bulletin of Geological Society of America*, 76: 803-832.

Biswas, S.K., 1987. Regional tectonic framework, structure and evolution of western marginal basins of India. *Tectonophysics*, 135: 307-327.

Biswas, S.K., 1988, Structure of the western continental margin of India and related igneous activity in Deccan flood basalts, Memoirs of Geological Society of India, 10: 371-393.

Bloemendal, J. and de Menocal, P., 1989. Evidence for a change in the periodicity of tropical climate cycles at 2.4 Myr from whole core magnetic susceptibility measurement. *Nature*, 342: 897-900.

Bloemendal, J., King, J.W., Hall, F.R., and Doh, S.J., 1992. Rock magnetism of Late Neogene and Pleistocene deep sediments: Relationship to sediment source, diagenetic processes and sediment lithology. *Journal of Geophysical Research*, 97: 4361-4375.

Bloemendal, J., King, J.W., Hunt, A., de Menocal, P.B. and Hayashida, A., 1993. Origin of sedimentary magnetic record at Ocean Drilling Program sites on the Owen Ridge, western Arabian Sea. *Journal of Geophysical Research (Solid Earth)*, 98: 4199-4219.

Bloemendal, J., Lamb, B. and King, J., 1988. Paleoenvironmental implications of rock-magnetic properties of late Quaternary sediment cores from the eastern Equatorial Atlantic. *Paleoceanography*, 3: 61-87

Bloemendal, J., Liu, J. X-M. and Rolph, T.C., 1995. Correlation of the magnetic susceptibility stratigraphy of Chinese loess and the marine oxygen isotope

record: chronological and palaeoclimatic implications. *Earth and Planetary Science Letters*, 131: 371-380.

Boardman, M.R. and Carney, C., 1991. Origin and accumulation of lime mud in ooid tidal channels, Bahamas. *Journal of Sedimentary Petrology*, 61: 661-680.

Bordovskiy, O.K., 1965. Sources of organic matter in marine basins. *Marine Geology*, 3: 5-37.

Brachfeld, S. and Banerjee, S.K., 2000. Rock magnetic carriers of century scale susceptibility cycles in glacial marine sediments from the Palmer Deep, Antarctic peninsula. *Earth and Planetary Science Letters*, 176: 443-455.

Broecker, W.S. and Takahashi. T., 1966. Calcium carbonate precipitation on the Bahama Bank. *Journal of Geophysical Research*, 71: 1575-1602.

Bryson, R.A. and Swain, A.M., 1981. Holocene variations of monsoon rainfall in Rajastan. *Quaternary Research*, 16: 135-145.

Calvert, S.E. and Pederson, T.F., 1992. Organic carbon accumulation and preservation in marine sediments: How important is anoxia? *In*: J.K. Whelan and J.W. Farrington (Editors), Productivity, Accumulation and Preservation of Organic Matter in Recent and Ancient Sediments. *Columbia University Press*, New York:: 231-263.

Calvert, S.E., Pederson, T.F., Naidu, P.D. and von Stackelberg, U., 1995. On the organic carbon maximum on the continental slope of the eastern Arabian Sea. *Journal of Marine Research*, 53: 269-296.

Canfield, D.E., 1989. Reactive iron in marine sediments. *Geochimica et Cosmochimica Acta*, 53: 619-632.

Canfield, D.C. and Berner, R.A., 1987. Dissolution and pyritization of magnetite in anoxic marine sediments. *Geochimica et Cosmochimica Acta*, 51: 645-660.

Chamley, H., 1989. Clay Sedimentology. *Springer-Velag*, Berlin: 425pp

Chamyal, L.S., Maurya, D.M. and Rachna Raj, 2003. Fluvial systems of the dry lands of western India: a synthesis of Late Quaternary environmental and tectonic changes. *Quaternary International*, 104: 69-86.

Chauhan, O.S., 1994. Influence of macro-tidal environment on shelf sedimentation, Gulf of Kachchh, India. *Continental shelf Research*, 14:

1477-1493.

Chester, R., Sharples, E.J. and Sanders, G.S., 1985. The concentration of particulate aluminium and clay minerals in aerosols from the northern Arabian Sea. *Journal of Sedimentary Petrology*, 55: 37-41.

Chivas, A.R., De Deckker, P., Wang, S. X. and Cali, J. A., 2002. Oxygen isotope systematics of the nektic ostracod *Australocypris robusta*. *In*: The Ostracoda: Applications in Quaternary Research. *American Geophysical Union*, Geophysical Monograph, 131: 310-313.

Cho, Y.G., Lee, C.B. and Choi, M.S., 1999. Geochemistry of surface sediments off the southern and western coasts of Korea. *Marine Geology*, 159: 111-129.

Clemens, S., Prell, W.L., Murray, D., Shimmield, G.B. and Weedon, G., 1991. Forcing mechanism of the Indian Ocean monsoon. *Nature*, 353: 720-725.

Cloud, P.E.J., 1962. Environment of calcium carbonate deposition west of Andros Island, Bahamas. *USGS*. Professional Paper, 350: 138.

Cowie, G.L., Calvert, S.E., Pederson, T.F., Schulz, H. and von-Rad, U., 1999. Organic content and preservational controls in surficial shelf and slope sediments from the Arabian Sea (Pakistan Margin). *Marine Geology*, 161: 23-38.

Cronan, D.D., Damiani, V.V., Kinsman, D.J.J. and Theide, J., 1974. Sediments from the Gulf of Aden and western Indian Ocean. *Deep Sea Drilling Project, Initial report*, 24: 1047-1110.

Darwin, C., 1846. An account of the fine dust which falls on vessels in the Atlantic Ocean. *Quarterly Journal of Geological Society (London)*, 2: 26pp.

De Groot, K., 1965. Inorganic precipitation of calcium carbonate from seawater. *Nature*, 207: 404-405.

Dearing, J.A., Dann, R.J.L., Hay, K., Lees, J.A., Loveland, P.J., Maher, B.A. and O'Grady, K., 1996. Frequency-dependent susceptibility measurements of environmental materials. *Geophysical Journal International*, 124: 228-240.

Demaison, G., 1991. Anoxia vs. productivity: what controls the formation o organic carbon rich sediments and sedimentary rocks?: Discussior *American Association of Petroleum Geologists Bulletin*, 75: 499.

Demaison, G.J. and Moore, G.T., 1980. Anoxic environments and oil source b

genesis. *Organic Geochemistry*, 2: 9-31.

den Dulk, M., Reichart, G.J. , Memon, G.M. , Roelofs, E.M.P. , Zachariasse, W.J. and van-der-zwaan, G.J., 1998. Benthic foraminiferal response to variations in surface water productivity and oxygenation in the northern Arabian Sea. *Marine Micropalaeontology*, 35: 43-66.

Deuser, W.G. and Degens, E.T., 1967. Carbon isotope fractionation in the system CO_2 gas-CO_2 (aqueous)-HCO_3 (aqueous). *Nature*, 215: 1033-1035.

Dietrich, G., W. Duing, K. Grasshoff and Koske, P.H., 1966. Physicalische und chemische Daten nach Beobachtungen des Forschungsschiffes Meteor im Indischen Ozean 1964/65. *Meteor Forschungsergebnisse*, A2: 1-5.

Dix, G. R. 2001. Origin of Sr-rich magnesian calcite mud in a Holocene pond basin (Lee Stocking Island, Bahamas). *Journal of Sedimentary Research*, 71: 167-175.

Duplessy, J.C., 1982. Glacial to interglacial contrast in the northern Indian Ocean. *Nature*, 295: 494-498.

Dutta, K., Bhushan, R. and Somayajulu, B.L.K., 2001. ΔR correction values for the northern Indian Ocean. *Radiocarbon*, 43: 483-488.

el Wakeel, S.K. and Riley, J.P., 1957. Determination of organic matter in marine muds. *Journal du Conseil International pour l' Exploration de la Mer*, 22: 180-183.

Ellwood, B.B. and Ledbetter, M.T., 1977. Antarctic Bottom water fluctuations in the Vema channel: Effects of velocity changes on particle alignment and size. *Earth and Planetary Science Letters*, 35: 189-198.

Ellwood, B.B., Crick, R.E., Hassani, A.E., Benoist, S.L. and Young, R.H., 2000. Magnetosusceptibility event and cyclostratigraphy method applied to marine rocks: Detrital input versus carbonate productivity. *Geology*, 28: 1135-1138.

Fairbanks, R.G., 1989. A 17,000 year glacio-eustatic sea-level record: influence of glacial melting rates on Younger Dryas event and deep ocean circulation. *Nature*, 342: 637-642.

Folk, R.L. and Lynch, F.L., 2001. Organic matter, putative nannobacteria and the formation of ooids and hardgrounds. *Sedimentology*, 48: 215-229.

Fontugne, M.R. and Duplessy, J.C., 1986. Variations of the monsoon regime during the upper Quaternary: evidence from carbon isotopic record of organic matter in north Indian Ocean sediment cores. *Palaeogeography, Palaeoclimatology, Palaeoecology*, 56: 69-88.

Gasse, F. and Van Campo, E., 1994. Abrupt post-glacial climate events in west Asia and north Africa monsoon domains. *Earth and Planetary Science Letters*, 126: 435-456.

Gasse, F., Arnold, M., Fontes, J.C., Fort, M., Gibert, E., Huc, A., Bingyan, L., Yuanfang, L., Qing, L., Melieres, F., Van Campo, E., Fubao, W. and Qingsong, Z., 1991. A 13,000 -year climate record from western Tibet. *Nature*, 353: 742-745.

Gibbs, R.J., 1972. Clay mineral segregation in the marine environment. *Journal of Sedimentary Petrology*, 47: 237-243.

Gingele, F.X., 1996. Holocene climatic optimum in Southwest Africa- evidence from the marine clay mineral record. *Palaeogeography, Palaeoclimatology, Palaeoecology*, 122: 77-87.

Ginsburg, R.N., 1956. Environmental relationships of grain size and constituent particles in some south Florida carbonate sediments. *American Association of Petroleum Geologists Bulletin*, 40: 2384-2427.

Gischler, E. and Lomando, A., 1999. Recent sedimentary facies of isolated carbonate platforms, Belize-Yucatan system, Central America. *Journal of Sedimentary Research*, 69: 747-763.

Goldberg, E.D. and Griffin, J.J., 1970. The sediments of the northern Indian Ocean. *Deep-Sea Research*, 17: 513-537.

Gorbunova, Z.N., 1966. Clay mineral distribution in Indian Ocean Sediments. *Oceanology*, 6: 215-221.

Griffin, J.J., Windom, H. and Goldberg, E.D., 1968. The distribution of clay minerals in the world Ocean. *Deep-Sea Research*, 15: 433-459.

GSI, 1975. A preliminary report on the clay mineralogy and other chemical parameters of western shelf sediments. *Progress report on Oceanavex-I* (1973-1974): 46-50.

Gupta, A.K. and Anderson, D.M., 2005. Mysteries of the Indian Ocean monsoor system. *Journal of Geological Society of India*, 65: 54-60.

Gupta, M.V.S. and Hashimi, N.H., 1985. Fluctuation in Glacial & interglacial sediment discharge of the River Indus as seen in a core from the Arabian Sea. *Indian Journal of Marine Sciences*, 14: 66-70.

Hashimi, N.H., Nair, R.R. and Kidwai, R.M., 1978. sediments of the Gulf of Kutch- A high energy tide dominated environment. *Indian Journal of Marine Sciences*, 7: 1-7.

Herrin, E., Hicks, H.S. and Robertson, H., 1958. A rapid volumetric analysis for carbonate in rocks. *Field and Laboratory*, 26: 139-144.

Hounslow, M.W. and Maher, B.A., 1999. Source of the climate signal recorded by magnetic susceptibility variations in Indian Ocean Sediment. *Journal of Geophysical Research*, 104: 5047-5061.

Ivanova, E., Scheibel, R., Singh, A.D., Schmidt, G., Niebler, H.S. and Hemleben, C., 2003. Primary Productivity in the Arabian Sea during last 135000 years. *Palaeogeography, Palaeoclimatology, Palaeoecology*, 197: 61-82.

Iyengar, R.N. and Radhakrishna, B.P., 2005. Evolution of the coastline of India and the probable location of Dwārakā of Kṛṣṇa: Geological prospective. *Journal of Geological Society of India*, 66: 285-292.

James, N.P., Bone, Y., Collins, L.B. and Kyser, T.K., 2001. Surficial sediment of the Great Australian Bight: facies dynamics and oceanography on a vast cool-water carbonate shelf. *Journal of Sedimentary Research*, 71: 549-567.

James, N.P., Bone, Y., Kyser, T.K., Dix, G.R. and Collins, L.B., 2004. The importance of changing oceanography in controlling late Quaternary carbonate sedimentation on a high-energy, tropical oceanic ramp: Northwestern Australia. *Sedimentology*, 51: 1179-1205.

James, N.P., Collins, L. B. Bone, Y. and Hallock, P., 1999. Subtropical carbonates in a temperate realeam : Modern sediments on the southwes Australian shelf. *Journal of Sedimentary Research*, 69: 1297-1321.

Jayakumar, D.A., 1999. Biogeochemical cycling of Methane and Nitrous oxide in the Northern Indian Ocean. *Ph. D. Thesis*, Goa University: 157pp.

Karbassi, A.R. and Shankar, R., 1994. Magnetic susceptibility of bottom sediments and suspended particulates from Mulki-Panaje river, estuary, and adjoining shelf, west coast of India. *Journal of Geophysical Research*, 99: 10207-10220.

Karlin, R. and Levi, S., 1983. Diagenesis of marine magnetic minerals in recent hemipelagic sediments. *Nature*, 303: 327-330.

Kessarkar, P.M., 2003. Investigations on the sediment cores of the Bengal fan: Inferences on the provenance of sediments during the late Quaternary. *Ph.D. Thesis*, Goa University: 160pp.

Kessarkar, P.M., Rao, V.P., Ahmed, S.M. and Anil Babu, G., 2003. Clay mineral and Sr-Nd isotope of the sediments along the western margin of India and their implications for sediment provenance. *Marine Geology*, 202: 55-69.

Kessarkar, P.M., Rao, V.P., Ahmad, S.M., Patil, S.K., Kumar, A.A., Babu, A.G., Chakraborty, S. and Rajan, R.S., 2005. Changing sedimentary environment during the Late Quaternary: Sedimentological and isotopic evidence from the distal Bengal Fan. *Deep-Sea Research Part 1*, 52: 1591-1615.

Kidwai, R.M. and Nair, R.R., 1972. Distribution of organic matter on the continental shelf off Bombay: a terrigenous carbonate depositional environment. *Indian Journal of Marine Sciences*, 1: 116-118.

Keil, R.G. and Cowie, G.L., 1999. Organic matter preservation through the oxygen deficient zone of the NE Arabian Sea as discerned by organic carbon:mineral surface area ratios. *Marine Geology*, 161: 13-22.

King, J., Banerjee, S.K., Marvin, J. and Ozdemir, O., 1982. A comparison of different magnetic methods for determining the relative grain size of magnetite in natural materials: some results from lake sediments. *Earth and Planetary Science Letters*, 59: 404-419.

Kirschvink, J.L. and Chang, S.B.R., 1984. Ultrafine- grained magnetite in deep-sea sediments: possible bacterial magnetofossils. *Geology*,12: 559-562.

Kolla, V., Henderson, L. and Biscaye, P.E., 1976. Clay mineralogy and sedimentation in the western Indian Ocean. *Deep- Sea Research*, 23: 949-961.

Kolla, V., Kostecki, J.A., Robinson, F., Biscaye, P.E. and Ray, P.K., 1981a. Distribution and origin of clay minerals and quartz in the surface sediments of the Arabian Sea. *Journal of Sedimentary Petrology*, 51: 563-569.

Kolla, V., Ray, P.K. and Kostecki, J.A., 1981b. Surficial sediments of the Arabian Sea. *Marine Geology*, 41: 183-204.

Konta, J., 1985, Mineralogy and chemical maturity of suspended matter in major river sampled under the SCOPE/UNEP project. *In*: T. Digens and S. Kempe (Editors), *Transport of carbon and minerals in major world river Part III,* Mitteilunga aus dem Geologisch-Palaontologischen Institut dcr Universit~it Hamburg: 569-592

Krishnan, M.S., 1982. Geology of India and Burma. *CBS Publishers*, New Delhi: 536pp.

Kunte, P.D., Zhao, C., Osawa, T. and Sugimori, Y., 2005. Sediment distribution study in the Gulf of Kachchh, India, from 3D hydrodynamic model simulation and satellite data. *Journal of Marine Systems*, 55: 139-153.

Kutzbach, J.E., 1981. Monsoon climate of the Early Holocene: Climate experiment with the Earth's orbital parameters for 9000 years ago. *Science*, 214: 59-61.

Labeyrie, L.D., Duplessy, J.C. and Blank, P.L., 1987. Variations in mode of formation and temperature of oceanic deep waters over the past 125,000 years. *Nature*, 327: 477-482.

Lamy, F., Hebbeln, D. and Wefer, G., 1998. Late Quaternary precessional cycles of terrigenous sediment input off the Norte Chico, Chile (27.5 S) and palaeoclimatic implications. *Palaeogeography, Palaeoclimatology, Palaeoecology*, 141: 233-251.

Lange, H., 1982. Distribution of chlorite and kaolinite in the northern Atlantic sediments off North Africa. *Sedimentology*, 29: 427-431.

Lee, K.E., Bahk, J.J. and Narita, H., 2003. Temporal variation in productivity and planktonic ecological structure in the East Sea (Japan Sea) since the last glaciation. *Geo- Marine Letters*, 23: 125-129.

Lepland, A. and Stevens, R.L., 1996. Mineral Magnetic and textural interpretation of sedimentation in the Skagerrak, eastern North Sea. *Marine Geology*, 135: 51-64.

Lisitzin, A.P., 1972. Sedimentation in the World Ocean. *Society of Economic Paleontologists and Mineralogists,* Special Publication, 17: 1-218.

Liu, J.P. and Milliman, J.D., 2002. Post- Glacial step-like sea level changes in the western Pacific: significance of the rapid Melt Water Pulses (1A, 1B, 1C and 1D). Abstracts, *2nd conference of the IGCP-464 project*: 55-57.

Loreau, J.-P., 1982. Sédiments aragonitiques et leur genèse. *Mémoires du*

Museum National d'Histoire Naturelle. Nouvelle série, c 47: 312pp.

Lowenstam, H.A.and Epstein, S., 1957. On the origin of sedimentary aragonite needles of the Great Bahama Bank. *Journal of Geology*, 65: 364-375.

Macintyre, I.G. and Reid, R.P., 1992. Comment on the origin of Bahamian aragonitic mud: a picture is worth a thousand words. *Journal of Sedimentary Petrology* ,67: 1095-1097.

Macintyre, I.G. and Reid, R.P., 1995. Crystal alteration in a living calcareous Alga (*Halimeda*): Implications for studies in skeletal diagenesis. *Journal of Sedimentary Research*, A65: 143-153.

Mahadevan, T.M., 1994. Deep continental structure of India: A review. *Geological Society of India Memoir*, 28: 309pp.

Maher, B.A. and Taylor, R.M., 1988. Formation of ultrafine-grained magnetite in soils. *Nature*, 366: 368-370.

Marshall, J.F. and Davies, P. J., 1988. *Halimeda* bioherms of the northern Great Barrier Reef. *Coral Reefs*, 6: 139-148.

Mattait, B., Peters, J.and Fokhardt, F.J., 1973. Results of petrographic analysis on sediments from the Indian Pakistan continental margin (Arabian Sea) (German). *"Meteor"* Forsch Ergebrisse Reiche no.14: 1-70.

Matthews, R.K., 1966. Genesis of recent lime mud in Southern British Honduras. *Journal of Sedimentary Petrology*, 36: 428-454.

Mc Cave, I.N., 1985. Sedimentology and stratigraphy of box cores from the HEBBLE site on the Nova Scotian Continental Rise. *Marine Geology*, 66: 59-89.

Mc Cave, I.N., Manighetti, B. and Robinson, S.G., 1995. Sortable silt and fine sediment size/composition slicing: Parameters for palaeocurrent speed and paleoceanography. *Paleoceanography*, 10: 593-610.

Merh, S.S., 2005. The great Rann of Kachchh: Perceptions of a field geologist. *Journal of Geological Society of India*, 65: 9-25.

Meynadier, L., Valet, J.P. and Grousset, F.E., 1995. Magnetic properties and origin of upper Quaternary sediments in the Somali basin, Indian Ocean. *Paleoceanography*, 10: 459-472.

Milliman, J.D., 1974. Marine Carbonates. *Springer-Verlag*, Heidelberg: 375pp.

Milliman, J.D., Freile, D. Steinen, R.P. and Wilber. R.J., 1993. Great Bahama Bank aragonitic muds: mostly inorganically precipitated, mostly exported. *Journal of Sedimentary Petrology*, 63: 589-595.

Milliman, J.D., Quraishee, G.S. and Beg, M.A.A., 1984. Sediment discharge from the Indus river to the ocean: past, present and future. *In*:.Haq, B.U. and Milliman, J.D. (Editors), *Marine geology and oceanography of Arabian Sea and coastal Pakistan,*. Van Nostrand and Reinhold: 65-70.

Mitterer, R.M., 1972. Biogeochemistry of aragonite mud and ooids. *Geochimica et Cosmochimica Acta*, 36: 1407-1422.

Morse, J.W. and Mackenzie, F.T., 1990. Geochemistry of Sedimentary Carbonates. Developments in Sedimentology 48, *Elsevier*, New York: 707pp

Morse, J.W., Millero, F.J., Thurmond, V., Brown, E. and Ostlund, H.G., 1984. Carbonate chemistry of Grand Bahama Bank waters: after 18 years another look. *Journal Geophysical Research*, 89: 3604-3614.

Moskowitz, B.M., Frankel, R.B. and Bazylinski, D.A., 1993. Rock-magnetic criteria for the detection of biogenic magnetite. *Earth and Planetary Science Letters*, 120: 283-300.

Muller, P.J. and Suess, E., 1979. Productivity, sedimentation rate and sedimentary organic matter in the oceans-I. Organic carbon preservation. *Deep- Sea Research*, 26: 1347-1362.

Mullins, C.E. and Titt, M.S., 1973. Magnetic viscosity, quadrature susceptibility and frequency dependence of susceptibility in single-domain assemblies of magnetite and maghemite. *Journal of Geophysical Research*, 78: 804-809.

Murty, P.S.N., Reddy, C.V.G. and Varadachari, V.V.R., 1969. Distribution of organic matter in the marine sediments off the west coast of India. *Proceedings of the National Institute of sciences of India*, 35: 377-384.

Muxworthy, A.R., 2001. Effect of grain interactions on the frequency dependence of magnetic susceptibility. *Geophysical Journal International*, 144: 441-447.

Naidu, A.S. and Shankar, R., 1999. Palaeomonsoon history during the Late Quaternary: Results of a pilot study on sediments from the Laccadive Trough, southeastern Arabian Sea. *Journal of Geological Society of India*,

53: 401-406.

Naidu, A.S., Mowatt, T.C., Somayajulu, B.L.K. and Rao, K.S., 1985. Characteristics of clay minerals in the bed loads of major rivers of India. Milleiuagen Aus dem geologisch-Paleontologischen Institute, *University of Hamburg*: 559-568.

Naidu, P.D., 1996. Onset of an arid climate at 3.5 ka in the tropics: Evidence from monsoon upwelling record. *Current Science*, 71: 715-718.

Naidu, P.D., Babu, P.C. and Rao, Ch.M., 1992. The upwelling record in the sediments of the western continental margin of India. *Deep-Sea Research*, 39: 715-723.

Nair, R.R., 1971. Beach rock and associated carbonate sediments on the fifty fathom flat, a submarine terrace on the outer continental shelf off Bombay. *Proceedings of Indian Academy of Sciences*, 73B: 148-154.

Nair, R.R., Hashimi, N.H. and Guptha, M.V.S., 1979. Holocene limestones of part of the western continental shelf of India. *Journal of Geological Society of India*, 20: 17-23.

Nair, R.R., Hashimi, N.H. and Rao, V.P., 1982a. Distribution and dispersal of clay minerals on the western continetal shelf of India. *Marine Geology*, 50: M1-M9.

Nair, R.R., Hashimi, N.H. and Rao, V.P., 1982b. On the possibility of high velocity tidal stream as dynamic barriers to longshore sediment transport: Evidence from the continental shelf off the Gulf of Kutch, India. *Marine Geology*, 47: 77-86.

Naqvi, S.W.A., Jayakumar, D.A., Narvekar, P.V., Naik, H., Sarma, V.V.S.S., DeSouza, W., Joseph, S., and George, M.D., 2000. Increased marine production of N_2O due to intensifying anoxia on the Indian continental shelf. *Nature*, 408 (6810): 346-349.

Nath, B.N., Bau, M., Rao, B.R. and Rao, Ch, M. 1997. Trace and rare earth elemental variation in Arabian Sea sediments through a transect across the oxygen minimum zone. *Geochimica et Cosmochimica Acta*, 61: 2375-2388.

Nayak, S.R. and Sahai, B., 1983. Morphological changes in the Mahi estuary. In.Proceedings of Natl. Conf. Application of Remote Sensing to Natural Resources, Environment, Land use and problems relating to Training and Education, *IIT Bombay*: 152-154.

Neuman, A.C. and Land, L.S., 1975. Lime mud deposition and calcareous algae in the Bight of Abaco, Bahamas: a budget. *Journal of Sedimentary Petrology*, 45: 763-786.

Odin, G.S., 1988. Green Marine clays. Developments in Sedimentology, 45. *Elsevier*, Amstredam: 445pp.

Oser, R.K., 1972. Sedimentary components of northwest Pacific pelagic sediments. *Journal of Sedimentary Petrology*, 42: 461-467.

Overpeck, J., Anderson, D., Trumbore, S. and Prell, W.L., 1996. The Southwest Indian Monsoon over the last 18,000 years. *Climate Dynamics*, 12: 213-225.

Paropkari, A.L., 1979. Distribution of organic carbon in sediments of the northwestern continental shelf of India. *Indian Journal of Marne Sciences*, 8: 127-129.

Paropkari, A.L., Babu, P.C. and Mascarenhas, A., 1992. A critical evaluation of depositional parameters controlling the variability of organic carbon in Arabian Sea sediments. *Marine Geology*, 107: 213-227.

Paropkari, A.L., Babu, P.C. and Mascarenhas, A., 1993. New evidence for enhanced preservation of organic carbon in contact with oxygen minimum zone on the western continental slope of India. *Marine Geology*, 111: 7-13

Paropkari, A.L., Iyer, S.D., Chauhan, O.S. and Babu, P.C., 1991. Depositional environments inferred from variations of calcium carbonate, organic carbon and sulfide sulfur: A core from southwestern Arabian Sea. *Geo-Marine Letters*, 11: 96-102.

Pattan, J.N., Masuzawa, T., Naidu, P.D., Parthiban, G. and Yamamoto, M., 2003. Productivity fluctuations in the southeastern Arabian Sea during the last 140 ka. *Palaeogeography, Palaeoclimatology, Palaeoecology*, 193: 575-590

Peck, J.A., King. J.W., Colman, S.M., and Kravchinsky, V.A., 1994. A rock-magnetic record from lake Baikal, Siberia: Evidence for Late Quaternary climate change. *Earth and Planetary Science Letters*, 12: 221-238.

Pederson, T.F. and Calvert, S.E., 1990. Anoxia vs. productivity: What controls the formation of organic carbon rich sediments and sedimentary rocks? *American Association of Petroleum Geologists Bulletin*, 74: 454-466.

Pederson. T.F., Shimmield, G.B. and Price, N.B., 1992. Lack of enhanced preservation of organic matter in sediments under the oxygen minima in the Oman margin. *Geochimica et Cosmochimica Acta*, 56: 545-551.

Petermann, H.B., U., 1993. Detection of live magnetotactic bacteria in South Atlantic deep-sea sediments. *Earth and Planetary Science Letters*, 117: 223-228.

Peters, C. and Dekkers, M.J., 2003. Selected room temperature magnetic parameters as a function of mineralogy, concentration and grain size. *Physics and Chemistry of the Earth*, 28: 659-667.

Peterson, N. and Von Dobeneck, T., 1986. Fossil bacterial magnetite in deep-sea sediments from the South Atlantic Ocean. *Nature*, 320: 611-615.

Popov, V.P. and Gershanovich, D.Ye., 1978. Terrigenous-Mineralogical provinces of recent bottom sediments on the continental margin in the Arabian Sea and the Gulf of Aden. *Oceanology*, 18: 177-180.

Powers, M.C., 1959. Adjustment of clays to chemical change and the concept of the equivalence level. Clays and Clay Minerals, 6th National Conference *Pergamon*, Oxford, New York: 309-326.

Prabhu, C.N. and Shankar, R., 2005. Palaeoproductivity of the eastern Arabian Sea during the past 200ka: A multi-proxy investigation. *Deep Sea Research-II*, 52: 1994-2002.

Prabhu, C.N., Shankar, R., Anupama, K., Taieb, M., Bonnefille, R., Vidal, L., and Prasad, S., 2004. A 200-ka palaeoclimatic reecord deduced from pollen and oxygen isotopic analyses of sediment cores from eastern Arabian Sea. *Palaeogeography, Palaeoclimatology, Palaeoecology*, 214: 309-321.

Prell, W.L., 1984, Variations of monsoon upwelling: A response to changing solar radiation. *Geophysical Monograph Series*, American Geophysical Union, Washington DC: 48-57.

Prell, W.L. and Hutson, W.H., 1979. Zonal temperature anomaly maps of Indian Ocean surface waters: modern and ice age patterns. *Science*, 206: 454-456.

Prell, W.L. and Kutzbach, J.E., 1987. Monsoon variability over the past 150,000 years. *Journal of Geophysical Research*, 92: 8411-8425.

Prell, W.L., Hutson, W.H., Williams, D.F., Be, A.W.H., Geitrenaner, K. and Molfino, B., 1980. Surface circulation of the Indian Ocean during the last Glacial Maximum, approximately 18,000 yr B.P. *Quaternary Research*, 14: 309-336.

Prell, W.L., Marvil, R.E. and Luther, M.E., 1990. Variability in upwelling fields in the northwestern Indian Ocean 2. data model comparison at 9000 years BP. *Paleoceanography*, 5: 447-457.

Prins, -.M.A., Postma,-G., Cleveringa,-J., Cramp,-A. and Kenyon,-N.H., 2000. Controls on terrigenous sediment supply to the Arabian Sea during the late Quaternary: the Indus Fan. *Marine Geology*, 169: 327-349.

Qasim, S.Z., 1977. Biological productivity of the Indian Ocean. *Indian Journal of Marine Sciences*, 6: 122-137.

Radhakrishnamurty, C., Likhite, S.D., Amin, B.S. and Somayajulu, B.L.K., 1968. Magnetic susceptibility stratigraphy in ocean sediment cores. *Earth and Planetary Science Letters*, 4: 464-468.

Radczewski, O.E., 1939. Eolian deposits in marine sediments. *In*: Trask, P.D (Editor), Recent Marine Sediments (Symposium): Tulsa, Okla, *American Association of Petroleum Geologists*: 736pp.

Rajamanickam, G.V. and Setty, M.G.A.P., 1973. Distribution of Phosphorus and Organic Carbon in the Nearshore Sediments off Goa. *Indian Journal of Marine Sciences*, 2: 84-89.

Ramamurty, M. and Murty, P.S.N., 1989. Distribution of organic carbon in the surficial sediments off Bombay, Ratnagiri and Calicut in the Arabian Sea. Recent Geo-scientific studies in the Arabian Sea off India. *Geological Survey of India, Special Publication*, 24: 173-182.

Ramaswamy, V. and Nair, R.R., 1989. Lack of cross shelf transport of sediments on the western margin of India: evidence from clay mineralogy. *Journal of Coastal Research*, 5: 541-546.

Rao, B.R. and Rao, K.S., 1989. Continental slope off Bombay and Ratnagiri: its morphology and sedimentation. Recent Geo-scientific studies in the Arabian Sea off India. *Geological Survey of India. Special Publication*, 24: 3-20.

Rao, B.R. and Veerayya, M., 2000. Influence of marginal highs on the accumulation of organic carbon along the continental slope off western India. *Deep -Sea Research 2, Topical Studies in Oceanography* , 47: 303-327.

Rao, K.L., 1975. India's water wealth, *Orient Longman*, New Delhi: 255pp.

Rao, V.P., 1991. Clay mineral distribution in the continental shelf and slope off Saurashtra, west coast of India. *Indian Journal of Maine Sciences*, 20: 1-6.

Rao, V.P. and Rao, B.R., 1995. Provenance and distribution of clay mineral in the sediments of the western continental shelf and slope of India. *Continental Shelf Research*, 15: 1757-1771.

Rao, V.P. and Veerayya, M., 1996. Submarine terrace limestones from the continental slope off Saurashtra-Bombay: Evidence of Late Quaternary neotectonic activity. *Current Science*, 71: 36-41.

Rao, V.P. and Wagle, B.G., 1997. Geomorphology and Geology of the western continental margin of India: a review. *Current Science*, 73: 330-350.

Rao, V.P., Kessarkar, P.M., Krumbein, W.E., Krajewski, K.P. and Schnider, R.J., 2003b. Microbial dolomite crust from the carbonate platform off western India. *Sedimentology*, 50: 819-830.

Rao, V.P., Kumar, A.A., Naqvi, S.W.A., Chivas, A.R. and Sekar, B., 2005. Limemuds and their genesis off Northwestern India during the late Quaternary. (*Marine Geology- communicated*).

Rao, V.P., Nair, R.R. and Hashimi, N.H., 1983. Clay mineral distribution on the Kerala continental shelf and slope. *Journal of Geological Society of India*, 24: 540-546.

Rao, V.P., Rajagopalan, G., Vora, K. H. and Almeida, F., 2003a. Late Quaternary sea level and environmental changes from relic carbonate deposits of the western margin of India. *Proceedings of Indian Academy of Sciences (Earth and Planetary Science)*, 112: 1-25.

Rao, V.P., Veerayya, M., Nair, R.R., Dupeuble, P.A. and Lamboy, M., 1994. Late Quaternary *Halimeda* bioherms and aragonitic faecal pellet-dominated sediments on the carbonate platform of the western continental shelf of India. *Marine Geology*, 121: 293-315.

Rao, V.P., Veerayya, M., Thamban, M. and Wagle, B.G. 1996. Evidences of late Quaternary neo-tectonic activity and sea level changes along the western continental margin of India. *Current Science*, 71: 213-219.

Rateev, M.A., Gorbunova, Z.N., Lisitzyn, A.P. and Nosov, G.L., 1969. The distribution of clay minerals in Oceans. *Sedimentology,* 13: 21-43.

Reichart, G.J., den Dulk, M., Visser, H.J., van der Weijden, C.H. and Zachariasse, W.J., 1997. A 225 kyr record of dust supply, paleoproductivity and the oxygen minimum zone from the Murray Ridge (northern Arabian Sea). *Palaeogeography, Palaeoclimatology, Palaeoecology*, 134: 149-169.

Reichart, G.J., Lourens, L.J. and Zachariasse, W.J., 1998. Temporal variability i the northern Arabian Sea oxygen minimum (OMZ) during the last 225,00

years. *Paleoceanography,* 13: 607-621.

Reid, R.P. and Macintyre, I.G., 1998. Carbonate recrystallization in shallow marine environments: A wide spread diagenetic process forming micritized grains. *Journal of Sedimentary Petrology*, 68: 928-946.

Reid, R.P., Macintyre, I.G. and Post, J.E., 1992. Micritized skeletal grains in northern Belize lagoon: a major source of Mg-calcite mud. *Journal of Sedimentary Petrology*, 62: 145-156.

Rex, R.W. and Goldberg, E.D., 1958. Quartz content of pelagic sediments of Pacific Ocean. *Tellus*, 10: 153-159.

Rixen, T., Haake, B. and Ittekkot, V., 2000a. Sedimentation in the western Arabian sea: the role of coastal and open-ocean upwelling. *Deep- Sea Research II*, 47: 2155-2178.

Rixen, T., Ittekot, V., Haake, G.B. and Schaefer, P., 2000b. The influence of the SW monsoon on the deep-sea organic carbon cycle in the Holocene. *Deep- Sea Research II*, 47: 2629-2651.

Robbins, L.L. and Blackwelder, P.L., 1992. Origin of whitings: a biologically induced non- skeletal phenomenon. *Geology*, 20: 464-467.

Robinson, S.G., 1986. The late Pleistocene palaeoclimatic record of North Atlantic deep-sea sediments revealed by mineral magnetic measurements. *Physics of the Earth and Planetary Interiors*, 42: 22-47.

Robinson, S.G., Maslin, M.A. and Mc Cave, I.N., 1995. Magnetic susceptibility variations in upper Pleistocene deep sea sediments of the NE Atlantic: Implications for ice-rafting and paleo-circulation at the last glacial maximum. *Paleoceanography*, 10: 221-250.

Rolph, T.C., Vigliotti, L. and Oldfield, F., 2004. Mineral magnetism and geomagnetic secular variation of marine and lacustrine sediments from central Italy: timing and nature of local and regional Holocene environmental change. *Quaternary Science Reviews*, 23: 1699-1722.

Rosteck, F., Bard, E., Beaufort, L., Sonzogni, C. and Ganssen, G., 1997. Sea-surface tempreture and productivity records for the past 240 kyr in the Arabian Sea. *Deep- Sea Research*, 44: 1461-1480.

Ruhlmann, C., Muller, P.J. and Schneider, R.R., 1999. Organic carbon and carbonate as productivity proxies: Examples from high and low productivity areas of the tropical Atlantic. *In*: Use of proxies in

Palaeoceanography: Examples from the South Atlantic (Eds. Fischer, G. and Wefer, G.). *Springer-Verlag*, Berlin Heidelberg: 316-344.

SAC, (ISRO), 2003. IRS-P4 OCM/Satcore project report, Vol III. Marine and water resources group, *SAC, (ISRO)*, Ahmedabad

Sarkar, A., Ramesh, R., Bhattacharya, S.K. and Rajagopalan, G., 1990. Oxygen isotope evidence for a stronger winter monsoon current during the last glaciation. *Nature*, 343: 549-551.

Sarupria, J.S. and Bhargava, R.M.S., 1993. Seasonal primary production in different sectors of the EEZ of India. *Mahasagar*, 26: 139-137.

Schenau, S.J., Passier, H.F., Reichart, G.J. and de Lange, G.J., 2002. Sedimentary pyrite formation in the Arabian Sea. *Marine Geology*, 185: 393-402.

Schmidt, A.M., Von Dobeneck, T. and Bleil, V., 1999. Magnetic characterization of Holocene sediment in the South Atlantic. *Paleoceanography*, 14: 465-481.

Schulte, S., Mangelsdorf, K. and Rullkoetter, J., 2000. Organic matter preservation on the Pakistan continental margin as revealed by biomarker geochemistry. *Organic Geochemistry*, 31: 1005-1022.

Setty, M.G.A.P. and Rao, C.M., 1972. Phosphate, carbonate and organic matter distribution in sediment cores off Bombay saurashtra coast, India. *24th International Geological Congress section*, 8: 182-191.

Sewell, R.B.S., 1935. The topography and bottom deposits of the Laccadive Sea. *Memoirs of Asiatic Society of Bengal*, IX: 425-450.

Shallow, J.C., 1984. Some aspects of the physical oceanography of the Indian Ocean. *Deep- Sea Research*, 31: 639-650.

Shankar, R., Subba Rao, K.V. and Kolla, V., 1994a. Magnetic susceptibility studies of surficial sediments from the deep Arabian Sea. *Journal of Geological Society of India*, 43: 159-167.

Shankar, R., Thompson, R. and Galloway, R.B., 1994b. Sediment source modelling: Unmixing of artificial magnetization and natural radioactivity measurements. *Earth and Planetary Science Letters*, 126: 411-420.

Shankar, R., Thompson, R. and Prakash, T.N., 1996. Estimation of heavy and opaque mineral contents of beach and offsore placers using rock

magnetic techniques. *Geo-Marine Letters*, 16: 313-318.

Sheu, D.D. and Huang, C.Y., 1989. Carbonate and organic carbon sedimentation on the continental margin off southwestern Taiwan. *Geo-Marine Letters*, 9: 45-51.

Shinn, E.A., Steinen, R.P., Lidz, B.H., Halley, R.B., 1985. Bahamian whitings- No fish story (abstract). *American Association of Petroleum Geologists Bulletin*, 69: 307.

Shinn, E.A., Steinen, R.P., Lidz, B.H., Swart, P.K., 1989. Whitings: a sedimentological dilemma. *Journal of Sedimentary Petrology*, 59: 147-161.

Singer, A., 1984. A palaeoclimatic interpretation of clay minerals in sediments- a review. *Earth Science Reviews*, 21: 251-293.

Singh, G., Joshi, R.D., Chopra, S.K. and Singh, A.B., 1974. Late Quaternary history of vegetation and climate of Rajastan desert, India. *Philosophical Transactions of the Royal Society of London*, 276B: 467-501.

Singh, G., Wasson, R.J. and Agrawal, D.P., 1990. Vegetational and seasonal climate changes since the last full Glacial in the Thar Desert, northwestern India. *Review of Paleobotony and Palynology*, 64: 354-361.

Sirocko, F. and Lange, H., 1991. Clay mineral accumulation rates in the Arabian Sea during the late Quaternary. *Marine Geology*, 97: 105-119.

Sirocko, F. and Sarnthein, M., 1989. Wind-borne deposits in the northwestern Indian Ocean: record of Holocene sediment versus modern satellite data. *In*: M. Linen and M. Sarnthein (Editors). Paleoclimatology and Paleometeorology: modern and past Patterns of Global Atmospheric Transport. (*NATO ASI Series C*, 282) Kluwer, Dordrecht: 401-433.

Sirocko, F., Sarnthein, M., Erleneuser, H., Lange, H., Arnold, M. and Duplessy, J.C., 1993. Century scale events in monsoon climate over the past 24000 years. *Nature*, 364: 322-324.

Sirocko, F., Sarnthein, M., Lange, H. and Erlenkreuser, H., 1991. Atmospheric summer circulation and coastal upwelling in the Arabian Sea during the Holocene and the Last Glaciation. *Quaternary Research*, 36: 72-93.

Sirocko, F., Schonberg, D.G. and Devey, C., 2000. Process controlling the trace element geochemistry of Arabian sediments during the last 25,000 yrs. *Global Planetary Change*, 26: 217-303.

Somayajulu, B.L.K., Walsh, T.J. and Radhakrishnamurty, C., 1975. Magnetic susceptibility stratigraphy of Pacific Pleistocene sediments. *Nature*, 253: 616-617.

Stanley, D.J. and Liyanage, A.N., 1986. Clay-mineral variations in the Northeastern Nile delta, as influenzed by depositional processes. *Marine Geology*, 73: 263-283.

Steinen, R.P., Swart, P.K., Shinn, E.A. and Lidz, B.H., 1988. Bahamian lime mud: the algae didn't do it (Abstract). *Geological Society of America, Abstract with Program*: 209.

Stewart, R.A., Pilkey, O.H. and Nelson, B.W., 1965. sediments of the northern Arabian Sea. *Marine Geology*, 3: 411-427.

Stieglitz, R.D., 1972. Scanning Electron Microscopy of the fine fraction of recent carbonate sediments from Bimini, Bahamas. *Journal of Sedimentary Petrology*, 42: 211-226.

Stockman, K.W., Ginsburg, R.N. and Shinn, E.A., 1967. The production of lime mud by algae in south Florida. *Journal of Sedimentary Petrology*, 37: 633-648.

Stolz, J.F., Chang, S-B.R., and Kirschoink, J.L., 1986. Magnetotactic bacteria and single domain magnetite in hemipelagic sediments. *Nature*, 321: 849-851.

Stuvier, M., Reimer, P.J., Bard, E., Beck, J.W., Burr, G.S., Houghen, K.A., Kromer, B., Mc Coremac, F.G., v.d. Plicht, J., and Spurk, M., 1998. INTCAL 98 radiocrbon age calibration, 24,000-0 cal BP. *Radiocarbon*, 40: 1041-1083.

Suthhof, A., Jennerjahn, T.C., Schaefer, P. and Ittekkot, V., 2000. Nature of organic matter in surface sediments from the Pakistan continental margin and the deep Arabian Sea: Amino acids. *Deep- Sea Research II*, Topical studies in Oceanography, 47: 329-351.

Swain, A.M., Kutzbach, J.E. and Hastenrath, S., 1983. Estimates of Holocene precipitation for Rajastan, India based on pollen and lake level data. *Quaternary Research*, 19: 1-17.

Sykes, T.J.S. and Kidd, R.B., 1994. Volcanogenic sediment distribution in the Indian Ocean through Cretaceous and Cenozoic and their Paleoenvironmental implications. *Marine Geology*, 116: 267-291.

Thamban, M., 1998. Sedimentological investigations on sediments from the western continental margin of India: inferences on the palaeoceanography during late Quaternary. *Ph.D. Thesis*, Goa University: 155pp.

Thamban, M. and Rao, V.P. 2000. Distribution and composition of verdine and glaucony facies from the sediments of the western continental margin of India, *SEPM (Society for Sedimentary Geology) Special Publication* no. 66: 233-244.

Thamban, M., Rao, V.P. and Raju, S.V., 1997. Controls of organic carbon distribution in sediments from the eastern Arabian Sea margin. *Geo-Marine Letters*, 17: 220-227.

Thamban, M., Rao, V.P. and Schneider, R.R., 2002. Reconstruction of Late Quaternary monsoon oscillations based on clay mineral proxies using sediment cores from the western margin of India. *Marine Geology*, 186: 527-539.

Thamban, M., Rao, V.P., Schneider, R.R. and Grootes, P.M., 2001. Glacial to Holocene fluctuations in the hydrography and productivity along the southwestern continental margin of India. *Palaeogeography, Palaeoclimatology, Palaeoecology*, 165: 113-127.

Thompson, R. and Oldfield, F., 1986, Environmental magnetism, *Allen & Unwin Publishers Ltd*, U.K.: 227pp.

Thompson, R., Bloemendal, J., Dearing, J.A., Oldfield, F., Rummery, T.A., Stober, J.C. and Turner, G.M., 1980. Environmental applications of magnetic measurements. *Science*, 207: 481-486.

Thompson, L.G., Yao, T., Davis, M.E., Henderson, K.A., Mosley-Thompson, E., Lin, P.N., Beer, J., Synal, H.A., Cole-Dai, J. and Bolzan, J.F., 1997. Tropical climate instability: The last glacial cycle from a Quinghai-Tibetan Ice core. *Science*, 276: 1821-1825.

Tissot, B.P. and Welte, D.H., 1978. Petroleum formation and Occurrence. *Springer*, Berlin: 538pp.

Vallier, T.L., 1974. Volcanogenic sediments and their relation to landmass volcanism and sea-floor continent movements, western Indian Ocean. Leg 25, *Deep- Sea Drilling Project*, Initial report, 25: 515-542.

van Andel, T.H., 1973. Texture and dispersal of sediments in the Panama Basin. *Journal of Geology*, 81: 434-457.

van Campo, E., 1986. Monsoon fluctuations in two 20,000 year B.P. oxygen isotope/ pollen records off south west of India. *Quaternary Research*, 26: 376-388.

van Campo, E., Duplessy, J.C. and Rossignolstrick, M., 1982. Climatic conditions deduced from a 150,000 year oxygen isotope – pollen record from the Arabian Sea. *Nature*, 296: 56-59.

Vaz, G., Misra, V.S., Biswas, N.R., Jayakumar, P.V., Krishna Rao, J.V., Sankar J. and Faruque, B.M., 1993. Lime mud in continental shelf edge and slope off Katchchh. *Indian Journal of Marine Sciences*, 22: 209-215.

von Rad, U., Schaaf, M., Michels, K.H., Schulz, H., Berger, W.H. and Sirocko, F., 1998. A 5000-yr record of climate change in varved sediments from the Oxygen Minimum Zone off Pakistan, Northern Arabian Sea. *Quaternary Research*, 51: 39-53.

von Rad, U., Schulz, H. and SONNE 90 Scientific Party, 1995. Sampling the oxygen minimum zone off Pakistan: glacial-interglacial variations of anoxia and productivity (preliminary results, Sonne 90 cruise). *Marine Geology*, 125: 7-19.

von Rad, V., Schulz, H., Riech, V., Den-Dulk, M., Berner, V. and Sirocko, F., 1999. Multiple monsoon controlled breakdown of oxygen minimum conditions during the past 30,000 years documented in laminated sediments off Pakistan. *Palaeogeography, Palaeoclimatology, Palaeoecology*, 152: 129-161.

von Stackelberg, U.V., 1972. Faziesverteilung in sedimentendes Indich-Pakistanischen Kontinental-Randes (Arabisches Meer). *Meteor Forschunsergebrisse*, Reiche, C9: 1-73.

Wagle, B.G., Vora, K.H., Karisiddaiah, S.M., Veerayya, M. and Almeida, F., 1994. Holocene submarine terraces on the western continental shelf of India; Implications for se level changes. *Marine Geology*, 117: 207-225.

Wasson, R.J., Smith, G.I. and Agrawal, D.P., 1984. Late Quaternary sediments, minerals and inferred geochemical history of Didwana Lake, Thar Desert, India. *Palaeogeography, Palaeoclimatology, Palaeoecology*, 46: 345-372.

Weaver, C.E., 1989. Clays, Muds and Shales. *Elsevier*, New York: 810pp.

Webster, P.J., 1987. The elementary monsoon. J.S. Fein and P.L. Stephens (Editors), *John Wiley*, New York: 3-32.

Wells, A.J. and Illing, L.V., 1964. Present day precipitation of calcium carbonate in the Persian Gulf. In: Deltaic and shallow marine deposits. *Elsevier*, Amsterdam: 429-435.

Whitehouse, U.G. and Mc Carter, R.S., 1958. Diagenetic modification of clay mineral types in artificial sea water. *Clays and Clay Minerals*. 7th National Conference: 1-80.

Windom, H.L., 1975. Eolian contribution to marine sediments. *Journal of Sedimentary Petrology*, 45: 520-529.

Wiseman, J.D.H. and Bennett, H., 1940. The distribution of organic carbon and nitrogen in sediments of the Arabian Sea. *John Murray Expedition 1933-34, Scientific Report*, 3: 193-221.

Worm, H.U. and Jackson, M.J., 1999. The Superparamagnetism of Yucca Mountain tuff. *Journal of Geophysical Research*, 104: 25415-25425.

Wyrtki, K., 1971. Oceanographic atlas of International Indian Ocean Expedition. *National Science Foundation*, Washington DC: 531pp

Wyrtki, K., 1973. Physical oceanography of the Indian Ocean. In: Zeitschel, B. (Ed.), The Biology of the Indian Ocean. *Springer*, New York: 18-36.

Yamazaki, T. and Katsura, I., 1990. Magnetic grain size and viscous remnant magnetization of pelagic clay. *Journal of Geophysical Research*, 95: 4373-4382.

Yamazaki, T. and Loka, N., 1997. Environmental rock magnetism of pelagic clay: Implications for Asian eolian input to the North Pacific since the Pliocene. *Paleoceanography*, 12: 111-124.